UNIVERSITY OF SURREY

STRUCTURAL CHARACTERISTICS OF ALIGNED FIBRE/MATRIX SPACE STRUCTURES

By:

M.A. RUSTUM

A Thesis Submitted for the
Degree of Doctor of Philosophy in the
Department of Civil Engineering.

SEPTEMBER 1984

ProQuest LLC.
789 East Eisenhower Parkway
P.O. Box 1346
Ann Arbor, MI 48106 – 1346

ABSTRACT

An investigation was undertaken into the structural behaviour of skeletal systems, manufactured from pultruded fibre reinforced polyester (f.r.p.), also into the structural characteristics of pultruded f.r.p. and into the reliability of the material and structural systems. The study applied theoretical and experimental methods to single member elements and to the main classes of skeletal space structures. The testing of single members was undertaken to determine the properties of the material and to assess its degree of variability. A computer program was developed for the non-linear analysis of skeletal structures manufactured from pultruded f.r.p. members. The program was used for the analysis of full scale models, and in addition, was used to undertake a theoretical parameter investigation to study the methods of improving the performance of these skeletal systems. The experimental testing of the various models was carried out to study the structural performance up to failure, in both the pre and post-buckling states, to assess the validity of the non-linear analysis program developed for this research, and also to compare the linear and non-linear methods of analysis of the various systems.

The need for the non-linear method of analysis for the f.r.p. skeletal structures, especially for the flexible type is shown when the experimental behaviour of a skeletal dome is compared with the theoretical computer linear and non-linear analyses. The cases in which the linear method of analysis can be utilized and its limitation for the skeletal f.r.p. structures are clearly pointed out.

Various aspects of the behaviour of the f.r.p. members and structural assemblies such as the deformability, recovery and mode of failure are obtained. The importance of the combination of more than one type of f.r.p. members on the structural efficiency is shown.

To My Wife Gabriella
and My Parents

ACKNOWLEDGEMENTS

I would like to express my gratitude to Dr L Hollaway for his guidance, advice and encouragement throughout the period of the research.

Thanks are due to Dr P Mullord and Mr A I Tarzi for their advice on various aspects of the non-linear method of analysis.

Thanks are also due to my friends, Dr A Pickett, Dr V G Iskatian and Mr G Mallin for the invaluable discussions and advice during the course of this research.

Special thanks are due to my colleagues and friends in room 6 AA 19, namely Eric, Colin, Hana, Hashim, Robert, Simon and Steve.

I am indebted to the technicians of the Civil Engineering Workshop for their efficiency in the fabrication of components for some of the models.

I wish to thank Miss S Nicholls for the excellent typing of this thesis.

Finally, I wish to express my gratitude to the members of the Linguistics Department, in particular Mrs S M Gee, for their help in checking the manuscript of this thesis.

C O N T E N T S

NOTATION

X, Y, Z	Rectangular Coordinates
L, R, H	Cylindrical Coordinates
A	Cross Sectional Area
t	Thickness of Circular Hollow Section Members
J	Polar Moment of Inertia of a Cross Section
σ	Normal Stress
τ	Shearing Stress
ε	Unit Elongation
θ	Angle of Twist Per Unit Length
M	Bending Moment
T	Torque
E_{TL}, E_{TH}, E_{TR}	Tensile Elastic Moduli in L, R and H Directions
E_{CL}, E_{CH}, E_{CR}	Compressive Elastic Moduli in L, R and H directions
$\nu_{LH}, \nu_{LR}, \nu_{HR}$	Poisson's Ratios in Cylindrical Coordinates
G_{LH}, G_{LR}, G_{HR}	Shear Moduli in Cylindrical Coordinates
V	Potential Energy
$\bar{P}$	Load Vector
$\bar{q}$	Generalised Coordinates Vector
q_i^E	Generalised Coordinate i at Equilibrium Position E
λ	Load Factor
u, v, w	Components of Displacement
$k_T, k_E, k_\sigma, k_\delta$	Tangent, Elastic Linear, Initial Stress and Initial Displacement Matrices for a Member
$K_T, K_E, K_\sigma, K_\delta$	Tangent, Elastic Linear, Initial Stress and Initial Displacement Matrices for a Structure

SUPERSCRIPTS

1	A Quantity Relevant to G.R.P.
2	A Quantity Relevant to C.G.R.P.

CHAPTER ONE

INTRODUCTION

1.1 GENERAL

During the last few years many radical changes have taken place in the manufacturing techniques of fibre reinforced polyesters (f.r.p.). In the past, it has been a labour intensive industry and consequently has been somewhat unpopular with engineers because of the slow, laborious hand lay-up technque, with quality control problems where the final product is operator sensitive.

With more advanced technology in the form of new mechanics and with the introduction of resin formulation, fibre reinforced polyester products are becoming more efficient and reliable and the material property variability is being reduced to a minimum.

The pultrusion technique is one of the fully automated methods of production. It is a mechanised process for producing f.r.p. sections by the closed mould system. There are no physical limits to the size of sections that can be produced, but for the tubular sections, for the reasons of economy, they generally vary from 25mm diameter with a wall thickness of 2mm up to 150mm diameter and wall thickness of 5mm. The fibre/matrix percentage ratio by weight can have a wide range of values with an upper limit of about 70/30. The pultruded tube is an ideal unit with which to manufacture skeletal systems. The modulus of elasticity for the upper limit of the fibre glass reinforced polyester would be of the order of 25000 N/mm^2. This value is relatively low compared with that of steel but if members, which are highly loaded in a skeletal system, require greater stiffness to prevent buckling, a hybrid composite of carbon and glass fibre in a polyester matrix, or even a higher stiffness fibre, could be used. An acceptable carbon fibre/glass fibre/polyester resin ratio from an economic view point would be 30/30/40% by weight and the modulus of elasticity would be of the order of 70000 N/mm^2.

The use of fibre reinforced polyester (f.r.p.) composites in construction, although not widespread, is now well established. One of the principal uses of the material in this field has been in the form of repeatable units of both load bearing and infill type that can be assembled to form a structure. The technique for jointing these units is also well established. F.r.p. in the form of rods and tubes has not yet been seriously used; this is due, mainly, to the difficulty of jointing tubular members at nodal points. Recently the crimped and bonded joint technique [1] has been presented by the Fulmer Research Institute and The Royal Aircraft Establishment and has been used in this investigation to make end connections to f.r.p. pultruded members which may then be screwed into an aluminium nodal joint. This invention has opened up a whole new field in skeletal structural systems which can be manufactured from fibre matrix componenets and pultruded members, in particular.

1.2 THE PULTRUSION TECHNIQUE

The pultrusion describes the process which uses a pulling action to draw and shape the composite material. Historically pultrusion techniques date back to 1946. However, great technological improvements have taken place since then whereby a large variety of shapes and profiles with excellent surface finishes can now be produced. Although the process was at first limited to produce g.r.p., nowadays various types of fibres and resins are combined to produce a high performance material such as carbon fibre reinforced epoxy.

A schematic representation of the process is shown in Figure (1.1) where continuous fibre roving reinforcements are drawn from creels through a bath containing the resin mixture; the resin impregnated reinforcement passes through a heated die having the shape and dimensions of the required section. The surplus resin and air are squeezed from the reinforcement in the cold part and on passing through the hot part of the die the setting of the resin commences. The proceed section is pulled by a hydraulically driven puller which provides the motive force for the operation. A diamond tipped flying saw cuts the profiles to the required length. In certain variations, the resin is injected under pressure to impregnate the reinforcement within the die. Often radio frequency curing is used for fast production (up to 7m/min).

Glass fibre makes up the bulk of reinforcement used in pultrusion, although any fibre compatible with the resin and the processing method can be used. Pultrusion sections which have exclusively unidirectional reinforcement are anisotropic with extremely high axial and flexural strength but relatively low transverse strength, but incorporating hooped strands along a reinforcement core can improve the cross strength. Mats, especially continuous fibre mat (c.f.m.), can also be used for the transverse reinforcement.

Generally the role of the resin in any composite is to bind the fibres together, to distribute and to transfer stresses to the reinforcements. The polyester resin, the major resin used in the pultrusion process, is normally a combination of polybasic acid and polyhydric alcohol, to which the minimum of styrene is added to enable some cross linking of the polymers to take place and also to improve the physical properties; a curing agent and possibly a flame retardant should be added. It is thermosetting material, thus, when exposed to a flame, localised charring takes place as opposed to the melting which is associated with thermoplastic polymers.

The main properties of the pultruded composite which gives it a special significance are:

i) <u>High Strength/Weight Ratio</u>

Considering a pultruded g.r.p. element of unit length and unit cross sectional area (of fibre/matrix ratio by weight of 60/40), and a mild steel element of unit length and of the same weight as the g.r.p. element, the ratio of the tensile strengths of these two elements (g.r.p./steel) would be of 3.7/1.

ii) <u>Dimensional Stability</u>

As the material is of a thermosetting type it maintains its physical properties over a wide temperature range and, unlike thermoplastics, does not soften or melt at temperatures in excess of 300° C (the melting point of high technology thermoplastic polymers).

iii) Low Finishing

Pultruded members generally do not require any surface finish. However, pigments can be added to the resin at the time of fabrication of the sections.

iv) Corrosion Resistance

Examples of the use of pultruded g.r.p., where corrosion is a major problem, will be given in the next section.

Other properties, such as a relatively low thermal coefficient of expansion, a high electrical resistance and an electromagnetic permeability to radio waves make the material suitable for particular applications.

1.3 THE USE OF COMPOSITES IN SKELETAL STRUCTURES

During the last decade skeletal structures in fibre reinforced polymers started to gain credibility; however, applications were limited to simple experimental types of structures; some examples of these applications in various fields are given below.

Collings and Steinlen [2, 1970] presented a paper, in which potential applications of composite tubes to VTOL aircraft structure components were demonstrated by the design and fabrication of a composite tail skid brace. Model studies of a possible redundant truss structure for the tail section of a large crane helicopter where made.

Baker et al [3, 1974] presented a study of experimental bipod legs, which could be used in place of a standard non-adjustable metal bipod leg for 81mm mortar (gun) unit. They were manufactured from carbon fibre reinforced polyester tubes with bonded metal ends. The composite units performed successfully under practical firing conditions. The saving in weight in the tubular sections, by replacing the aluminium alloy with composite material, was about 45%. This value indicated the significant potential for the application of carbon fibre reinforced polyester to

items of service equipment where such weight saving can be shown to be cost effective.

Fager [4, 1976] presented a paper on the use of light weight graphite composites for large autenna systems for communication satellites. The material was described as ideal for its high rigidity and near zero coefficient of thermal expansion and in addition a 40 to 60% weight reduction when compared to existing metal systems could be achieved. The study included the development of an 8-ft graphite composite reflector. The truss element, rings and radial stiffeners were all made from unidirectional graphite composites. Another aspect discussed was the significant improvement that can be made in using the graphite composite material in erectable autenna.

Hollaway and Ishakian [5, 1977] illustrated the superior mechanical characteristics that a fibre/matrix composite skeletal structure has over the one that has been manufactured from a ductile material. A model of rigidly jointed cantilever space structures, made from pultruded carbon fibre reinforced epoxy resin rods of 8mm diameter, was used in this investigation. Further study, by the same authors [61, 1981] was undertaken into the first buckling characteristics of a skeletal continuum structure made from pultruded g.r.p. members and chopped strand mat fibre glass reinforced plate elements.

In 1980, an exhibition in association with the third conference on composite materials in Paris was arranged. A walkway, of overall span 4.3 metres and total weight of 35kg, made from pultruded g.r.p. elements was presented. This structure was built by Fulmer Research Laboratories Limited in collaboration with BTR Permali RP Limited. However, the structure was very crude.

In April 1981, a BP technical report [6] was published describing a high strength/light weight composite structure; the manufacturing technique is known as 'Mathweb', and was invented and patented in 1977 by BP. The structures, in this technique, are manufactured from continuous filaments in which the materials used are the continuous fibre and the polyemerised struts and frames. The open-lattice structures are fabricated in a jig. Fixing lugs, bushes, bobbings, etc, can be incorporated in the structure during manufacture.

Morrison [7, 1981] presented an interesting discussion on a long span, single piece girder structure manufactured from glass reinforced polyester resin and used for special applications in the chemical and wastewater treatment fields. A second structure discussed was a roof beam system composed entirely of f.r.p; this installation was used as a roof to mercury-cell chlorine plant. No information about the structural system, design, analysis or behaviour was given.

Opinger et al [8, 1983] published a paper on structural analysis, design and testing of a framework made of pultruded glass reinforced polyester which was developed to replace a metallic frame system for large tent applications. The frame was tested and a simplified non-linear analysis was undertaken. The study showed that the non-linear effects (geometric) were considerable in such structures.

Various papers of a more general character were published. An example of such work was given in a paper by Makowski [9, 1981]. It contains a review of the development in structural and semi-structural applications of plastics within the last decade. A more general paper, dealing with the application of glass reinforced polyester in buildings was given by Einsfeld [10, 1982].

1.4 OBJECTIVES AND APPROACH TO THE CURRENT INVESTIGATION

In the previous section various examples, showing the wide fields of application of the skeletal fibres reinforced polymer structures, were given. The application in the field of structural engineering is generally limited to cases with particular requirements, such as the resistance to chemical corrosion. The structures built tend to be over-designed and of the traditional style, mainly because of the limited knowledge of the material potential and design procedures.

Although pultruded f.r.p. is one of the most promising skeletal structural elements, it has never been fully investigated. Therefore, the main objectives of the present study were to determine the viability for using the pultruded fibre/matrix composite materials as component members in light weight structural systems. The investigation, which

included experimental procedures and theoretical analysis, was undertaken on single elements, as well as large scale assemblies representing the main classes of skeletal space structures. The development of a practical technique of non-linear analysis, applicable to the pultruded f.r.p. skeletal structures, was required to achieve the objectives. This technique had to be general and had to include the pre and post-buckling states. Constructing the full curve of the structural behaviour was considered an important part of the study as the first buckling does not always imply collapse.

The material used in the investigation was limited to the pultruded glass reinforced polyester (g.r.p.) and the pultruded hybrid, carbon and glass, reinforced polyester (c.g.r.p.). The material mechanical properties were determined and an investigation on member behaviour was undertaken. These investigations and a full discussion of the results are included in Chapter Two. The non-linear analysis technique was based on the findings obtained from this investigation. Some important aspects of the concepts of stability and a review of the main practical non-linear analysis techniques for skeletal systems were included in Chapter Three. The method of non-linear analysis adopted and the computer program implementation were given in the same chapter.

The first class of structures considered, and manufactured from g.r.p. and c.g.r.p., was of the stiff type. Two double-layer grid models (short span and long span) were analysed and tested to enable a study of the behaviour in the pre and post-buckling states to be made. In addition, the mode of failure and amount of deformation that occur in the structure prior to failure were also investigated. The effect of replacing the critical g.r.p. members with c.g.r.p. ones on the performance of the structure was also considered. The comparison of the experimental results and those obtained analytically by the computer program developed here offered the possibility of assessing the program's performance. A further parameter study on three types of double-layer grid systems was undertaken; this completed the study on the stiff type of structures.

The second class of structures to be considered was of the flexible type. A shallow three-way skeletal dome was analysed and tested. Also a theoretical parameter study of a braced barrel vault was undertaken. The objectives were to obtain full information on the structural behaviour and to investigate methods of improving their performance.

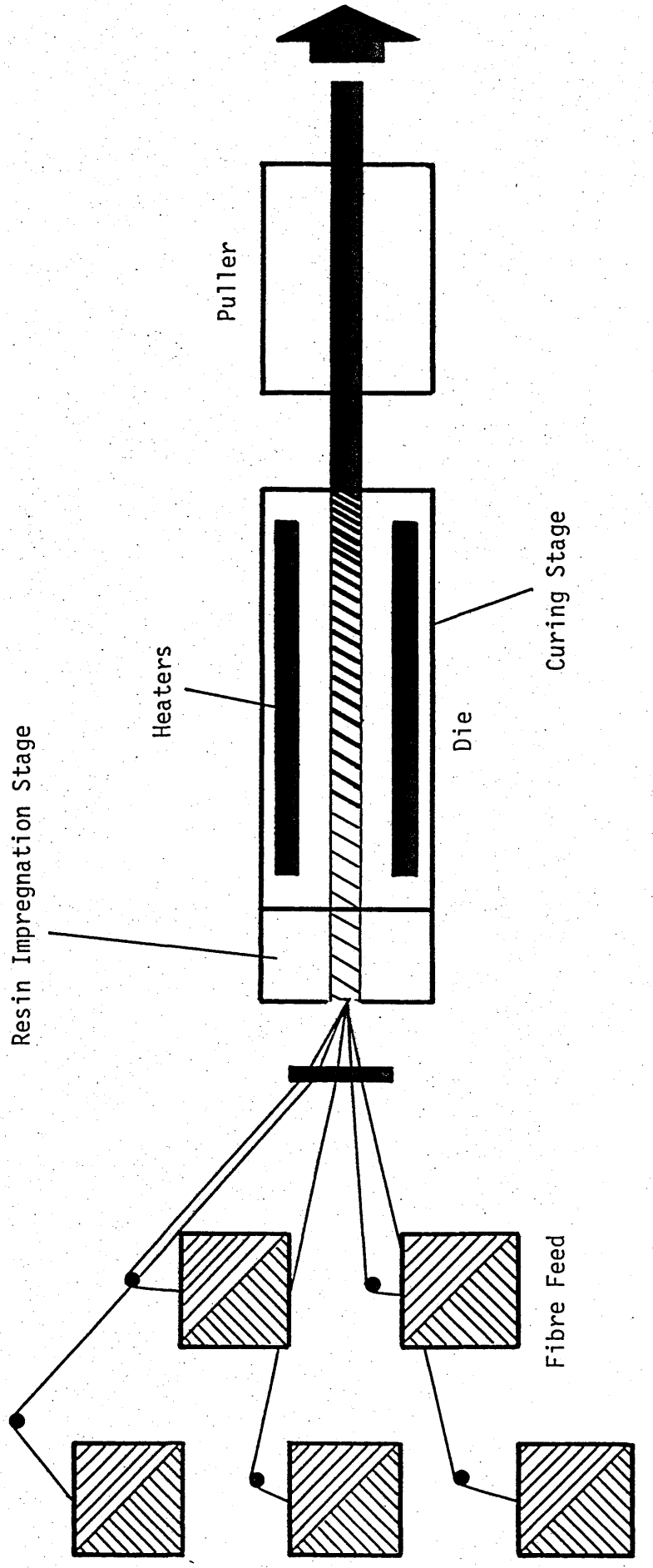

Fig (1.1) Schematic representation of the Pultrusion Process

CHAPTER TWO

PULTRUDED F.R.P. MEMBERS

2.1 INTRODUCTION

The investigation into the use of fibre reinforced polyester pultruded sections as structural members in skeletal systems has been undertaken by experimental and theoretical techniques. The experimental testing of the pultruded sections alone was required in order to determine its behaviour under load as well as to obtain data on its mechanical properties for use in the theoretical analysis. The study carried out on the tubular sections also included a theoretical finite element analysis to determine the stress distribution in the member subjected to axial force.

The investigation was limited to two fibre reinforced polyester composite sections; the first was a pultruded glass fibre reinforced polyester (g.r.p.) with fibre to matrix weight ratio of 60/40 percent and the second was a hybrid composite of carbon and glass fibre reinforced polyester (c.g.r.p.) with a carbon/glass/resin weight ratio of 30/30/40 percent. These values were obtained by burning various specimens in a furnace at a temperature of 430^{0}C. Only one size of pultruded hollow sections was considered.

2.2 MECHANICAL PROPERTIES

A series of tests were undertaken to determine the mechanical properties of g.r.p. and c.g.r.p. pultruded circular hollow section members of external diameter of 25.4mm and wall thickness of 2mm. The members were tested in axial tension, axial compression, torsion about their longitudinal axis and hoop tension. Only a limited number of c.g.r.p. specimens were tested due to the cost of producing the experimental material.

2.2.1 TENSILE TESTING

(a) Specimens and Testing Arrangement

All of the g.r.p. specimens were obtained from different batches of commercially produced pultruded tubes purchased from B.T.R. Permali and the c.g.r.p. specimens were obtained from experimental production.

Six specimens of g.r.p. and three specimens of c.g.r.p., each 250mm long, were tested in tension. To enable the samples to be set up in an Instron testing machine, crimped and bonded aluminium tubes were secured on to each end of the tensile specimens. The preparation for the crimped bonded procedure involved thorough cleaning of the ends of the specimens by means of sandpaper and solvent. To remove grease and foreign matter, the inner surface of the aluminium sleeve was treated in a similar manner to the outer surface of the g.r.p. tube before crimping. The aluminium sleeves of internal diameter of 27mm and 130mm long were then crimped on to allow an overlap of 60mm. An epoxy adhesive was applied to the inner surface of the sleeves and to the outer surface of the pultruded tube. Prior to crimping, the aluminium sleeves were heat treated up to 530° C and then quenched to anneal the material. The softening prevented the aluminium cracking when crimped. The crimping tool used was manufactured from mild steel and consisted of two blocks each with a channel shaped cavity. When the two blocks were brought together the two cavities were of cylindrical form with a gap between the two halves to allow the permanently deformed aluminium tube to enter the space. As a result of the crimping, a uniform thin glue line formed between the outer surface of the specimen and the inner surface of the aluminium tube. The 70mm lengths of aluminium tube outside the overlap were flattened to enable the specimen to be set up in the jaws of the Instron machine. The specimen was allowed to cure in a furnace at 60° C.

This type of crimped and bonded end grip was proposed by Green and Philips [1]. As the crimped and bonded joint was weaker than the pultruded tube, an aluminium tube bonded to the inside of the

pultruded member was required in order to produce an increase in the bonded surface and, hence, an increase in the strength of the joint so that the specimen could be loaded to failure. The inner aluminium tubewas surface prepared exactly in the same way as the outer aluminium tube; also the inner surface of the f.r.p. tube was roughened. The application of adhesive and the insertion of the inner tube took place immediately before crimping. A diagram of the cross-section of the pultruded tube and aluminium end fittings is shown in Figure (2.1)A.

The specimens were tested in tension in an Instron testing machine of type No. TTD TTDM. The moving crosshead was operated by two vertical driven screws from a servo controlled drive system. The chart of the recorder was driven synchronously at a variety of speed ratios with respect to the crosshead. The crosshead speed used in this testing was of 1mm/min.

In some of the specimens the strain was measured by means of 8mm electrical metal oil strain gauges, with a resistance of 120 Ohms and gauge factor of 2.09. The strain gauges were stuck on the external surface midway along the specimens, in both the longitudinal and hoop directions. Three strain gauges were equally spaced around the specimens and were connected to a data logging system. For the other specimens the testing machine chart recorder was used to obtain the load against displacements of the crosshead.

(b) The Results

Figure (2.2) shows that the average values of the readings of the three strain gauges varies linearly with the average stress applied to the specimens. The average stress is equal to the applied tensile load divided by the specimen cross-sectional area. The graph shows only small discrepancies in the linear behaviour between the various specimens tested. The elastic modulus, obtained by averaging the results of all tested specimens, was

found to be equal to 21061 N/mm^2 for the g.r.p. (E^1_{TL}) and 71428 N/mm^2 for the c.g.r.p. (E^2_{TL}). It is necessary to emphasise that these two values were based on the assumption of a uniform distribution of the stresses. A value of 0.2534 was obtained for the Poisson's ratio of g.r.p. (ν^1_{LH}) which is defined as the ratio of the average strain in the hoop direction and the average strain in the longitudinal direction.

To obtain the ultimate tensile stress, tests were carried out using a Saetec machine and, since there was no data logging system available, the testing machine chart recorder was used. A linear behaviour, up to failure, of the load against crosshead displacement was observed. The ultimate loads of the g.r.p. specimens tested were 42.0 kN. 44.9 kN and 46.0 kN. The average value divided by the cross-sectional area of 147mm^2 gave an ultimate tensile stress of 301 N/mm^2. This may have involved bending strains which were unavoidable due to eccentricity in the loading arangement. It was not possible to fail the c.g.r.p. specimen due to the premature failure of the crimped and bonded ends on this composite.

The failure of the g.r.p. specimens involved complete destruction of the tube, characterised by the debonding of the fibres as plate (2.1) shows. In order to explain the reasons for this mode of failure, further investigation was required to determine the state of internal stresses and their possible effect.

2.2.2 COMPRESSIVE TESTING

(a) Specimens and Testing Arrangement

The specimens for this test were short and the ends were cut perfectly square to the axis. The ends of the specimens were encapsulated into a tight fitting inner steel plug with an outer steel ring and an end cap, as shown in Figure (2.1)B. The inner plug and outer ring were used to protect the edge of the specimens

and to prevent local splitting. Three g.r.p. specimens and three c.g.r.p., specimens each of length 100mm, were strain gauged and tested in compression in an Instron machine. In addition, using a crosshead speed of 1mm/min, 10 g.r.p. specimens and 5 c.g.r.p. specimens, all 100mm long, were tested but without measuring strains.

(b) The Results

Figure (2.3) shows the relationship between stress and strain for the compressive specimens and it will be seen that the three sets of results are very close. The relationship is linear, as confirmed by the testing of the monitor Instron chart specimens and as shown in Figure (2.4). The elastic modulus of the g.r.p. (E^1_{CL}), obtained by averaging the results from the tested specimens, was found to be equal to 22058 N/mm^2, whilst the corresponding test results of the c.g.r.p. (E^2_{CL}) was 70994 N/mm^2. The averaged results of both compressive and tensile tests of g.r.p. and c.g.r.p. were plotted on the same graph shown in Figure (2.5); this allows a direct comparison of the material behaviour. The results indicate that the material has the same stress/strain behaviour under compression and tension and that the ultimate compressive strength obtained lies between 31 and 36 kN. The ultimate loads obtained from the testing of the 10 g.r.p. and 5 c.g.r.p. specimens are shown in Table (2.1). The mode of failure of the compressive specimens clearly showed that the longitudinal fibres underwent local microbuckling and local matrix crushing. It is unlikely that local shell buckling took place as the ratio of wall thickness to the tube radius is high; this aspect will be discussed in Section 2.3. The testing of the 5 c.g.r.p. specimens showed a similar mode of failure. The minimum, maximum and average values of the ultimate compressive load obtained were 23.75 kN, 37.5 kN and 32.55 kN respectively. The average ultimate stresses obtained were 229 N/mm^2 and 221 N/mm^2 for g.r.p. and c.g.r.p. respectively.

2.2.3 TORSIONAL TESTING

(a) Specimens and Testing Arrangement

Three specimens of g.r.p. and two specimens of c.g.r.p., of identical dimensions to those described in Section 2.1, were tested by means of a 'Tecquipment' torsion testing machine. The test specimens were fitted with two machined steel end blocks to allow them to be mounted into the testing machine. Each end consisted of a steel block A with a cylindrical hole, to accomodate the specimen, at one side and a pin of hexagonal cross-section B to be fixed on to the testing machine at the opposite side; Figure (2.6) shows the arrangement. The end blocks were machined to a high precision, with the centre of the hole coinciding with the axis of the pins. Epoxy resin was used to fix the specimen to the end blocks. A special jig was used to bond the components and to give the specimen an effective length of 250mm. During testing,the applied torsional moment and the corresponding deflections, d_1 and d_2, (of two marked positions on the two rods) were recorded. The two deflections were measured by means of dial gauges in a direction perpendicular to the plane containing the rod and the axis of the specimen.

(b) The Results

The value of the shear modulus (G_{LH}) was obtained from the displacements d_1 and d_2, the applied torque, and the geometrical dimensions of the tested specimens.

The values of J x θ (Polar moment x angle of twist per unit length) were plotted against the applied torque T for all tests as shown in Figure (2.7). The value G_{LH} was obtained by averaging the results of all the specimens tested. These latter results for both g.r.p. and c.g.r.p. were plotted on the same graph of Figure (2.7). The tangent to the initial section of these last two curves gave a value of 4490 N/mm^2 for G^1_{LH} of g.r.p. and 5960 N/mm^2 for G^2_{LH} of c.g.r.p.

2.2.4 PRESSURE TESTING FOR HOOP CHARACTERISTICS

(a) Specimens and Testing Arrangement

The g.r.p. specimen tested was 1 metre long with four metal foil strain gauges bonded to the external surface midway along its length, two circumferential and two longitudinal. At the two ends of the g.r.p. tube an aluminium sleeve 70mm long was crimped and bonded following the same procedure described in Section 2.1.1. A thread was then cut onto the aluminium sleeve and two steel caps were fitted. The two steel caps were drilled and tapped to allow for influx of hydraulic fluid and bleeding. To prevent seepage leaks due to porosity, a polythene inner tube was used. The internal pressure loads were applied hydraulically by a small hand operated jack as shown in Plate (2.1).

(b) The Results

The results are summarized in the two curves shown in Figures (2.8) and (2.9). The stress values used in Figure (2.8) were obtained from the internal pressure by simple equilibrium considerations. The tensile elastic modulus (E^1_H) in the hoop direction was obtained from the best fit to the experimental points in Figure (2.8). The Poisson's ratio ν^1_{HL} was obtained from the curve of Figure (2.9). In order to obtain the elastic modulus in compression, the specimen should have been subjected to external pressure. However, as the modulus of elasticity in tension and compression in the longitudinal direction were of similar value, it was not felt necessary to undertake a compressive test in the hoop direction and the two hoop moduli values were assumed equal. As the value ν'_{HL} obtained experimentally was very close to the theoretical value obtained from the relationship

$$\nu_{HL} = \frac{EL}{EH} \times \nu_{LH},$$

it was felt that only one hoop tensile test was required. The

values obtained for E_H and ν_{HL} were 10666 N/mm^2 and 0.118 respectively.

2.2.5 DISCUSSION

The material mechanical properties required for the theoretical analysis of skeletal systems made of g.r.p. and c.g.r.p. were obtained by experiment. It has been shown that the differences, under compressive and tensile force, in the values obtained were insignificant, with the exception of the ultimate strengths. Consequently, for the theoretical analysis, the properties were assumed equal and no testing under bending was required.

Full material mechanical properties, required for the finite element analysis assuming the element to have orthotropic material properties, were obtained for the g.r.p. only. However, the results of this analysis could be extended to the c.g.r.p. material. The mechanical properties obtained experimentally are summarised in Table (2.2).

It must be mentioned that the variability of the results from the testing of g.r.p. specimens, which were obtained from the supplier from different batches, was a minimum, as the small scatter indicates. The number of c.g.r.p. specimens tested was limited and, although the variability of results were small, no conclusion can be drawn.

2.3 AXISYMMETRIC FINITE ELEMENT ANALYSIS

2.3.1 THE ANALYSIS

The mechanical properties obtained as a result of subjecting f.r.p. specimens to axial loading were based on the assumption that a uniform stress distribution in the cross-section existed and that the effect of end constraints was negligible. To verify this assumption and to provide a greater understanding of the material

behaviour, a theoretical analysis was undertaken on axially loaded members under two different boundary conditions. This analysis did not include the stress concentration in the region of end constraints as this has been fully investigated by Pickett [11].

For this analysis, the LUSAS finite element program, written by Finite Element Analysis Ltd., was used. A 50mm long g.r.p. pultruded circular hollow section member, with an external diameter of 25.4mm and a wall thickness of 2mm was analysed. The member was subjected to a uniform axial force and with boundary condition symmetric about the axis of the tube. The discretisation of the tube and the constraints is shown in Figure (2.10). In this linear analysis, with orthotropic material properties, an eight node quadrilateral axisymmetric element was chosen. This high order 'quadratic' element allows stress and strain variation across the element. The mechanical properties required for the analysis were E_L, E_R, E_H, G_{RL}, ν_{RL}, ν_{LH} and ν_{RH}, where suffices L, R and H indicate the principal material directions in the longitudinal, radial and circumferential or hoop directions respectively, as shown in Figure (2.10). Symmetry of the material properties in the plane RH was assumed as the reinforcement was mainly in the axial direction. Consequently, $E_H = E_R$ and $\nu_{LR} = \nu_{LH}$. From the material testing, all the properties required for the analysis were available, except for ν_{RH} which was difficult to determine and for this reason two trial analyses were undertaken using different values of ν_{RH}. The first was equal to the cured polyester resin value and the second was smaller. Since the difference in the results of the two trial analyses was negligible (less than 1%) it was concluded that it was possible, without affecting the outcome of the analysis, to use either of the two values.

Although the results were for tensile loading, as the analysis was linear it could also represent a compressive loading by simply changing the sign of the results.

The two boundary conditions assumed for the analysis were:

(a) A set of rollers which provided the constraint for all end nodes in the longitudinal direction. The constrained nodes, however, were free to move in the RH plane.

(b) The same boundary conditions mentioned in (a) were applied but with an additional roller to prevent movement of the outer constrained end node in the radial direction. This boundary condition simulates, with a fair degree of accuracy, the end arrangement of the specimens under compression. This is an extreme condition in the case of the tensile specimens, as the crimped aluminium end cap had a certain amount of flexibility and the constraint in the radial direction should have been represented by a spring.

2.3.2 THE RESULTS OF ANALYSIS

The results obtained from the finite element analysis were:

(a) The longitudinal and transverse displacements.
(b) The stress in the three principal directions.
(c) The shear stress.

The results are displayed in isometric projection graphs. In these graphs the X-axis represents the radial direction, the Y-axis the longitudinal direction and the Z-axis contains the results from the finite element analysis. The two graphs representing the same results relative to the two boundary conditions are displayed in the same figure to allow a direct comparison. This representation gives a clear, general view of the distribution of the results.

Since the area of interest was limited to the stress distribution in the pultruded members, and the stress concentration in the region of the constraints was not of particular interest, a fine mesh was not used and the elements with constrained nodes were omitted from the results.

Of the two graphs displayed in each figure, the top graph relates to the boundary condition (b) whilst the bottom one relates to the boundary condition (a). The above results are for an externally applied tensile load of 1508N.

The longitudinal displacement graphs, shown in Figure (2.11), indicate that the extra constraint resulted, in general, in a reduction of the displacements. The graph for boundary condition (a) showed that near the constrained end the displacements were uniform across the section and at the far end the displacements were larger towards the external surface. The top graph showed that with boundary condition (b) displacements near the external surface were generally higher than those near to the internal surface and the nearer the position was to the constrained nodes the larger the difference. The radial displacements, as shown in Figure (2.12), were all negative which meant that all nodal points moved towards the centre of the tube. However, the values were very small (of the order of 10^{-2}mm). The results for boundary condition (a) indicated a uniform displacement, with values ranging between -0.93×10^{-2} and -0.83×10^{-2}, and the introduction of the extra radial constraint reduced the displacements locally near the constrained end.

The axial stresses are shown in Figure (2.13) where boundary condition (a) produced a linearly variable stress with a value of 11.1 N/mm^2 near the external surface of the tube and a value of 9.7 N/mm^2 near the inside surface. This distribution was altered near the loaded nodes. The top graph of this figure shows the effects produced by the extra radial constraint which resulted in reducing the stresses locally and in the vicinity of the constrained end. The situation was similar to the constrained end region of the bottom graph. The stresses in the radial direction are shown in Figure (2.14) where the bottom graph shows the stresses varying between zero, at both surfaces and a maximum value, at mid wall thickness, of approximately -0.018 N/mm^2. This maximum value is very small compared to the longitudinal stresses. Although the extra radial constraint increased the stresses locally, elsewhere they maintained values similar to those of boundary condition (a).

The local effect was only limited to approximately 15mm from the constrained end. The hoop stresses were nearly non-existent with boundary condition (a), whilst boundary condition (b) produced local hoop stresses with values varying across the wall thickness of the tube. These stresses were positive near the external surface, negative at mid wall thickness, nearly zero near the internal surface, and with parabolic shape as shown in Figure (2.15).

As the geometry, loading condition and boundary conditions were axisymmetric, the only shear stress present was τ_{LR}. The two graphs of Figure (2.16) show its distribution for boundary conditions (a) and (b). With boundary condition (a), the shear varies linearly across the wall thickness of the tube, with two extreme values of approximately 0.4 N/mm^2 and -0.4 N/mm^2. Such a distribution of shear was compatible with the stress distribution shown in Figure (2.13). The extra constraint added to boundary condition (b) increased the shear locally.

2.3.3 DISCUSSION

The results of the finite element analysis reveal some important points. Firstly, they show the effect which is produced by the radial constraints (which represent the end mountings). The region affected was limited to a small zone approximately 20mm from the boundary at which point this effect becomes negligible as is shown in Figures (2.12) to (2.16). Secondly, the geometry of the specimen tested had some influence on the stress distribution. The longitudinal stress varied linearly across the wall thickness with the higher value close to the internal surface. Consequently, the elastic modulus, which was determined experimentally by strain gauges bonded to the external surface, should be factorised by a quantity equal to the ratio of the stress in the external surface to the average stress. It was also shown that the values of the other stresses, such as the hoop stresses, were very small when stress concentration near the constrained ends were not taken into account.

The stress distribution obtained may explain the mode of failure of specimens tested in tension. As the longitudinal stress varies linearly, with higher stress near the external surface, some of the external fibres reach their failure load. The load is redistributed to neighbouring fibres, resulting in the eventual failure of the composite. It appears that the shear in the matrix around the failed fibre or group of fibres, increases considerably causing longitudinal interface shear failure and the debonding of fibres. A dynamic factor must be involved as the release of stresses, after a fibre has failed, occurs dynamically. The eccentricity, which is always present, and the bending moment associated with it, increases the stresses at one extreme of the tube's cross-section and causes a premature failure. Plate (2.2) shows the mode of failure of two specimens, where debonded fibres can be seen.

2.4 BUCKLING OF PULTRUDED C.H.S., G.R.P. AND C.G.R.P.

2.4.1 INTRODUCTION

Circular hollow section members are extensively used in skeletal structures in which the load is carried by axial force action. From a design point of view, local or general instability often represents the limiting force that the member can carry.

Although a considerable amount of theoretical and experimental information is available for isotropic material, this is not the case for anisotropic material. With the introduction of fibre reinforced polymers in the field of structural engineering and its use in reticulated type structures, extensive theoretical work was undertaken to extend the classical theory to cover the new material. Experimental work to back-up the theoretical work and to provide data for various types of composite material was also carried out. A review of the static buckling theory for anisotropic composite circular cylinders was presented by Tennyson, R C [12] in 1975. In this review, geometric imperfection and combination of loading tests were discussed.

In this section, the buckling behaviour of c.g.r.p. pultruded circular hollow sectioned members, of the same dimensions as considered in the previous sections, is considered only from a theoretical viewpoint, whilst the g.r.p. members are analysed both from a theoretical and an experimental consideration. The testing of g.r.p. was carried out to permit a comparison with theory and to determine the buckling load, the amount of deformation before failure, the recovery, the mode of failure and the reliability of the material.

2.4.2 THEORETICAL BACKGROUND AND APPLICATION TO G.R.P. AND C.G.R.P. MEMBERS

(a) Local Instability

The critical load of a strut may be improved by increasing the cross-sectional inertia. This may be achieved without extra material by simply distributing the material as far as possible from the principle axis of the cross-section by reducing the wall thickness and increasing the transverse dimensions. There is a limit, however, beyond which the wall itself could become unstable and the local instability could occur before the column instability.

The stress failure by local instability (local crippling) for anisotropic composite materials as given by Baker et al [2] and Norris and Rosen [13] is:

$$\sigma_{Li} = \frac{\gamma K \sqrt{E_L E_T}}{2} \cdot \frac{t}{R} \cdot \Phi$$

where

$$K = \frac{2}{\sqrt{3(1-\nu_{TL}\nu_{LT})}}$$

Φ is the smallest of the following two values:

$$\Phi = 1$$

$$\Phi = \frac{2G_{LT}}{\sqrt{E_L E_T}} (1+\nu_{TL}.\nu_{LT})$$

γ is a buckling coefficient, and its value is less than or equal to unity depending on the material.

t is the wall thickness.

R is the radius to the middle plane of the tube's wall.

When the geometrical dimensions and the mechanical properties of the g.r.p. which were obtained experimentally were substituted in the formule, the value of K became equal to 1.17, of $\Phi = 0.74$ and $\sigma_{Li} = \gamma \times 1140\ N/mm^2$.

(b) Column Buckling

When a perfect pin ended elastic column, of elastic modulus E, ultimate compressive stress σ_{uc} and a slenderness ratio of $\frac{L}{r}$ is subjected to compressive axial force then the Euler buckling stress σ_E, as given by Timoshenko [14], is:

$$\sigma_E = \pi^2 E/(L/r)^2$$

The limiting value $(\frac{L}{r})^*$, below which the Euler stress is not applicable because the member reaches its ultimate strength σ_{uc}, before the Euler stress σ_E is:

$$(\frac{L}{r})^* = \pi\sqrt{\frac{E}{\sigma_{uc}}}$$

In the case of a member with fixed ends the critical Euler stress is equal to:

$$\sigma_E = \frac{4\pi^2 E}{(\frac{L}{r})^2}$$

For a composite material, the elastic modulus E is replaced by the longitudinal elastic E_L and a shear correction term, which is significant for high anisotropic material, is introduced to give a critical stress equal to:

$$\sigma_c = \frac{\sigma_E}{(1+2\sigma_E/G_{LT})}$$

2.4.3 TESTING OF G.R.P. MEMBERS

(a) Specimens and Testing Arrangement

The experimental investigation, as mentioned previously, was limited to 25.4mm diameter g.r.p. tubes and only column buckling was considered as local buckling stress was much higher than the ultimate compressive strength of the material. The testing of 24 members, of lengths varying between 200mm and 1000mm, was undertaken. All members were fixed ended and had the same identical end support arrangements for the Instron testing machine, as has been discussed in Section 2.2.2 and shown in Figure (2.1)B. Great care was exercised in cutting the member, fixing the ends into their supports and ensuring minimum eccentricity. A low crosshead testing speed (1mm/min) was selected. The load-crosshead displacement curves were plotted by the machine chart recorder.

In order to study the member deformation two, one metre long members were tested. The members were pin ended in order to have a low buckling load and large measureable lateral deformations. The end arrangements in this case were similar to the fixed ends with the exception that the end caps had a smaller outer diameter and a ball bearing with seating. The length of the members were measured between the centres of the two ball bearings. The members were subjected to more than one non-destructive buckling test and they were allowed to recover between two successive tests; eventually they were failed. Plates (2.3) and (2.4) show the column before and after buckling.

(b) The Results

The results obtained from the testing of the 24 g.r.p. specimens are plotted on a graph that includes the two theoretical curves of P_E and P_C against the length of members. For practical reasons, the graph, shown in Figure (2.17), was plotted in the form of load against member lengths and not in the standard non-dimensional form. The same graph also includes the theoretical curves for the c.g.r.p.

Comparisons of the deflections, due to repeated buckling loads on the above mentioned two specimens, were recorded on the Instron chart. After the fourth loading cycle, the average value, just prior to failure, of the maximum central deflection for the two specimens was recorded and was approximately equal to 98mm.

2.4.4 Discussion

The theoretical and experimental results of g.r.p. indicated good agreement, with a maximum difference in the order of 25%. The difference between the two theoretical curves of P_E and P_C was very small. The results were consistent but where a variability of buckling loads did occur it did not exceed 20% and, therefore, the critical loads for this material could be predicted with a good degree of accuracy.

The g.r.p. members, after a small number of cycles, showed perfect recovery after non-destructive buckling. Quasi-statically applied loading and a recovery period of three hours between two successive loadings prevented the test specimens being subjected to fatigue or dynamic loading.

The amount of deformation at failure was relatively small. However, the value obtained when compared with the local deformation of certain types of structures was considerable and could allow for redistribution of forces before failure in a prototype structure system. The load against crosshead displacement was linear except for the last section where the

non-linearity was caused by the change of geometry. Failure of members was always sudden.

It is important to mention that the local buckling stress was very high compared with the ulimate compressive stress of the material which indicates that this tube size was not very efficient.

Ultimate load in kN

Specimen No.	g.r.p.	c.g.r.p.
1	3.350	2.975
2	3.200	3.300
3	3.525	3.150
4	3.600	3.100
5	3.350	3.750
6	3.150	-
7	3.350	-
8	3.100	-
9	3.550	-
10	3.500	-
Average	3.3675	3.255

Table (2.1): Ultimate Compressive Strength of 100mm long pultruded g.r.p. and c.g.r.p. specimens

Mechanical Property	g.r.p.	c.g.r.p.
Elastic Modulus in L direction	21600 N/mm²	71210 N/mm²
Elastic Modulus in R+H direction	10666 N/mm²	-
Shear Modulus G_{LR}	4490 N/mm²	5960 N/mm²
Poisson's Ration ν_{LH}	0.2534	-
Poisson's Ratio ν_{HL}	0.1176	-
Tensile Strength	301 N/mm²	-
Compressive Strength	229 N/mm²	221 N/mm²

Table (2.2) Mechanical properties obtained experimentally for g.r.p. and c.g.r.p.

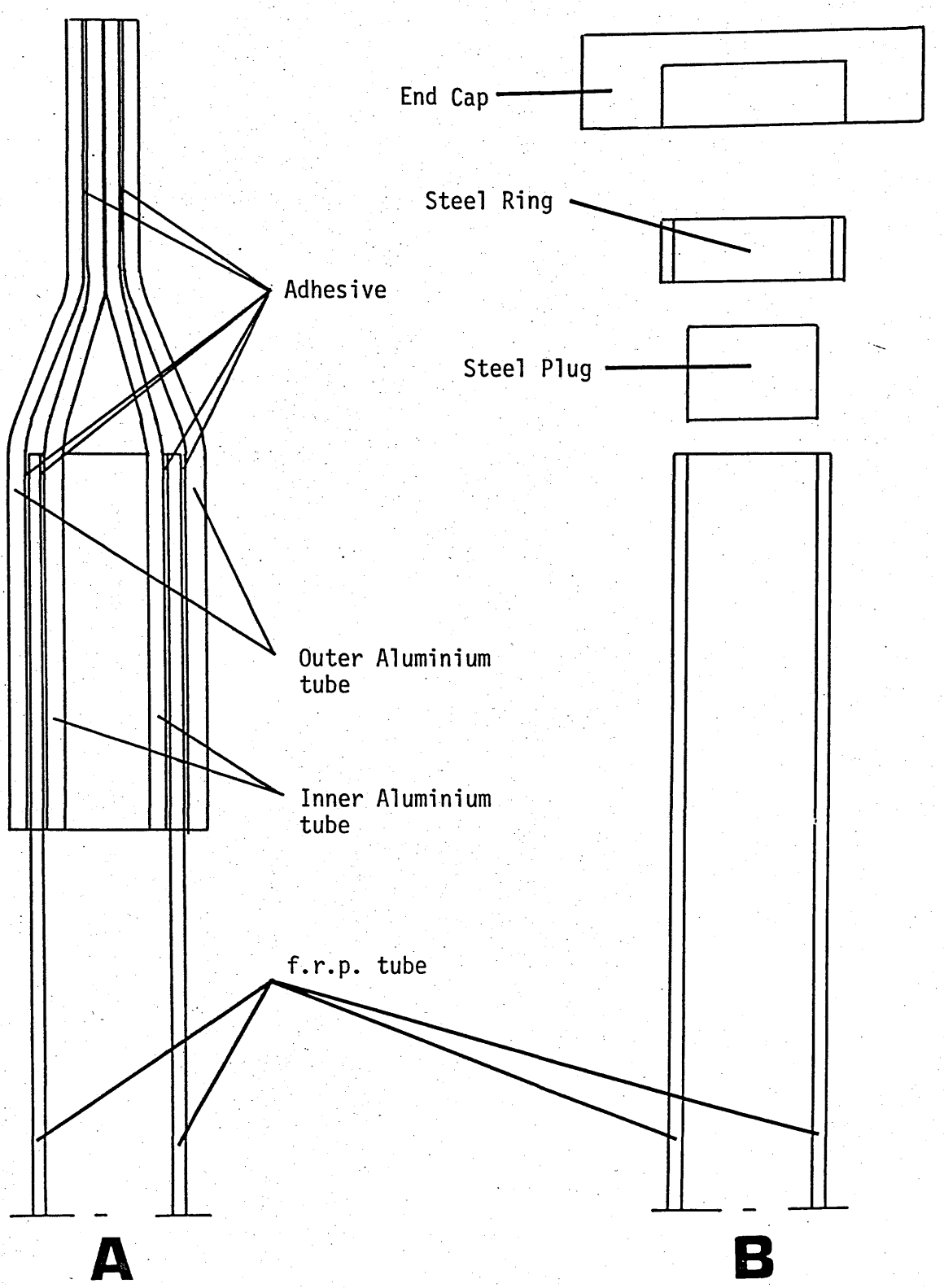

Fig (2.1) End Arrangement for Tensile and Compressive Testing of f.r.p. Specimens

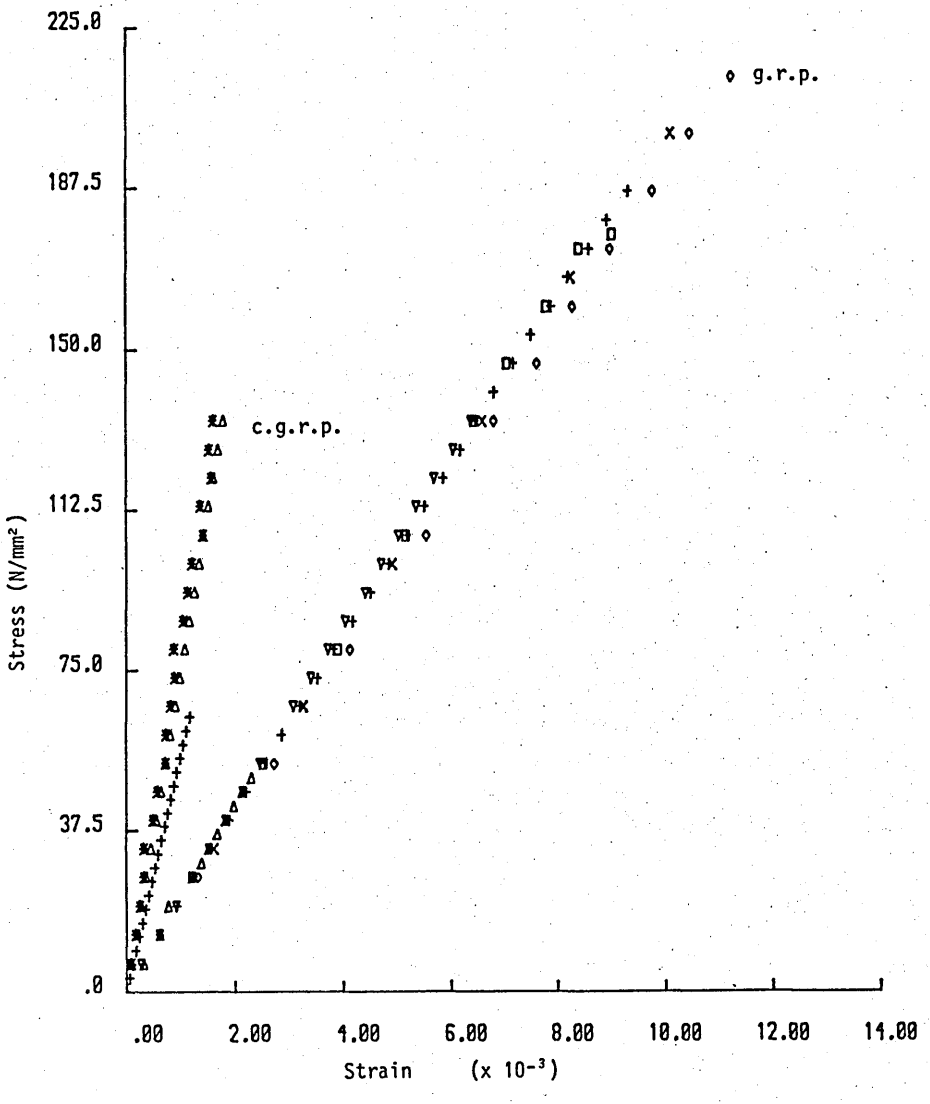

Fig (2.2) Stress-Strain Results of Tensile Testing

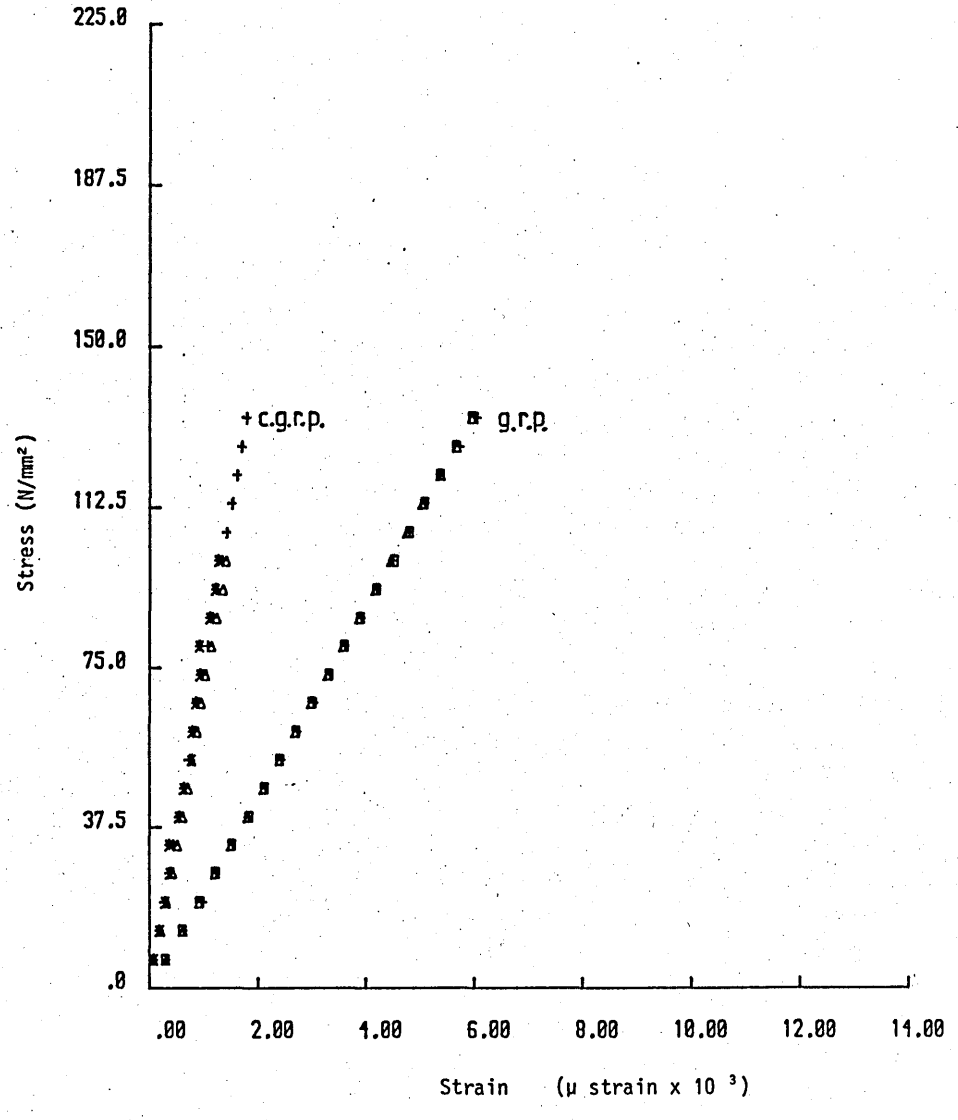

Fig (2.3) Stress-Strain Relationship for g.r.p. and c.g.r.p. specimens

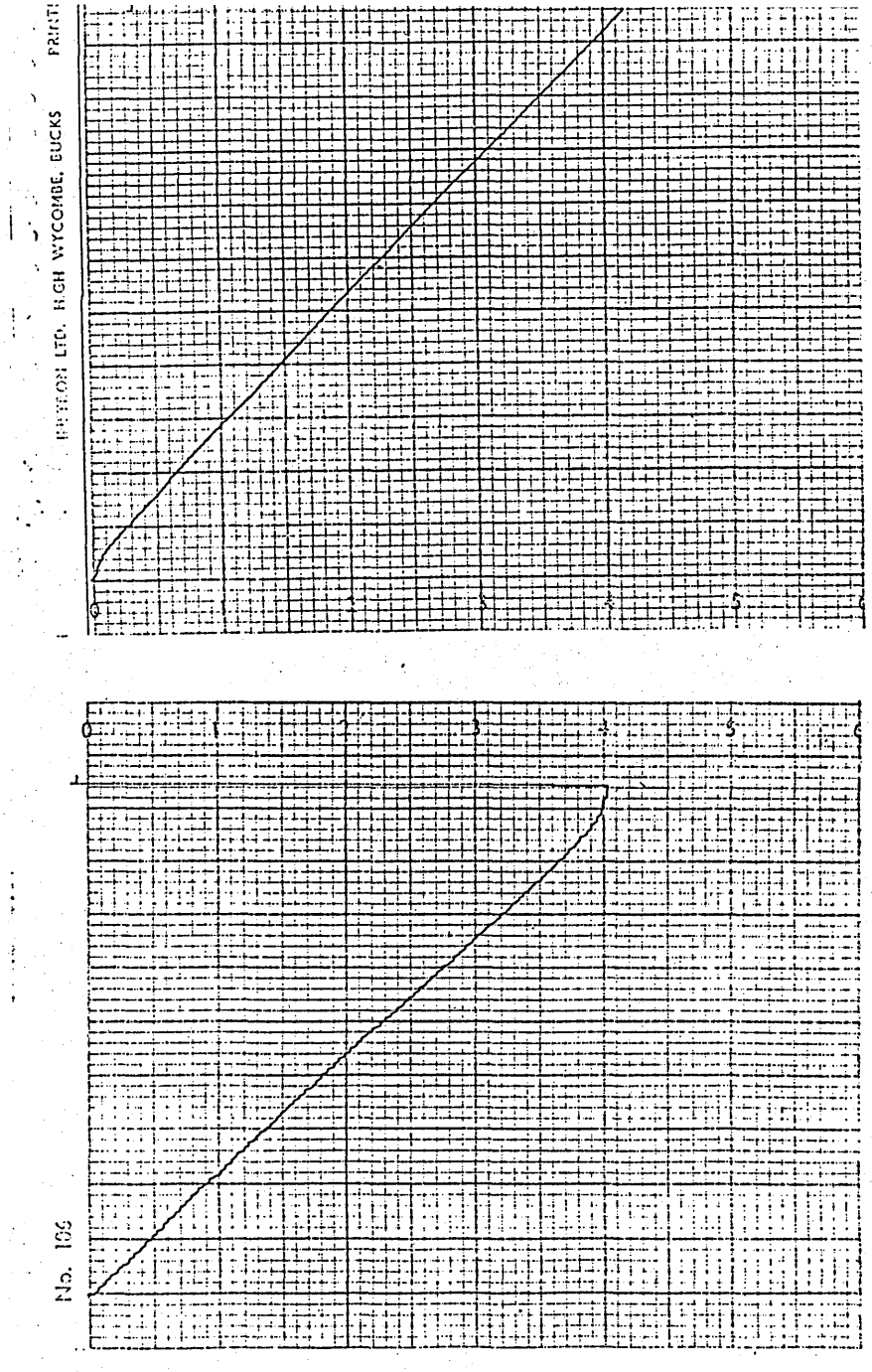

Fig (2.4) Examples of the Load Crosshead Displacement Plotted by the Instron Chart Recorder

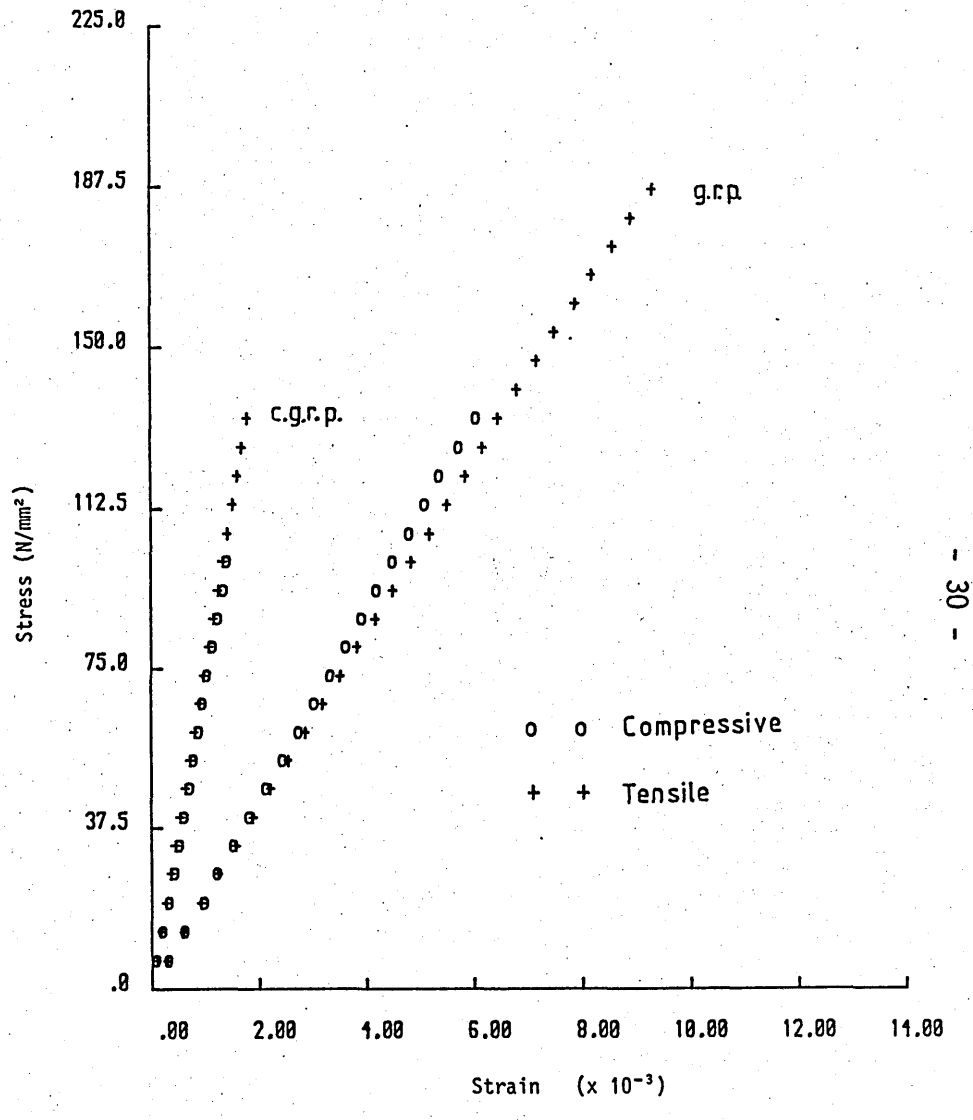

Fig (2.5) Comparison of the average of the results of compressive and tensile testing of pultruded g.r.p. and c.g.r.p.

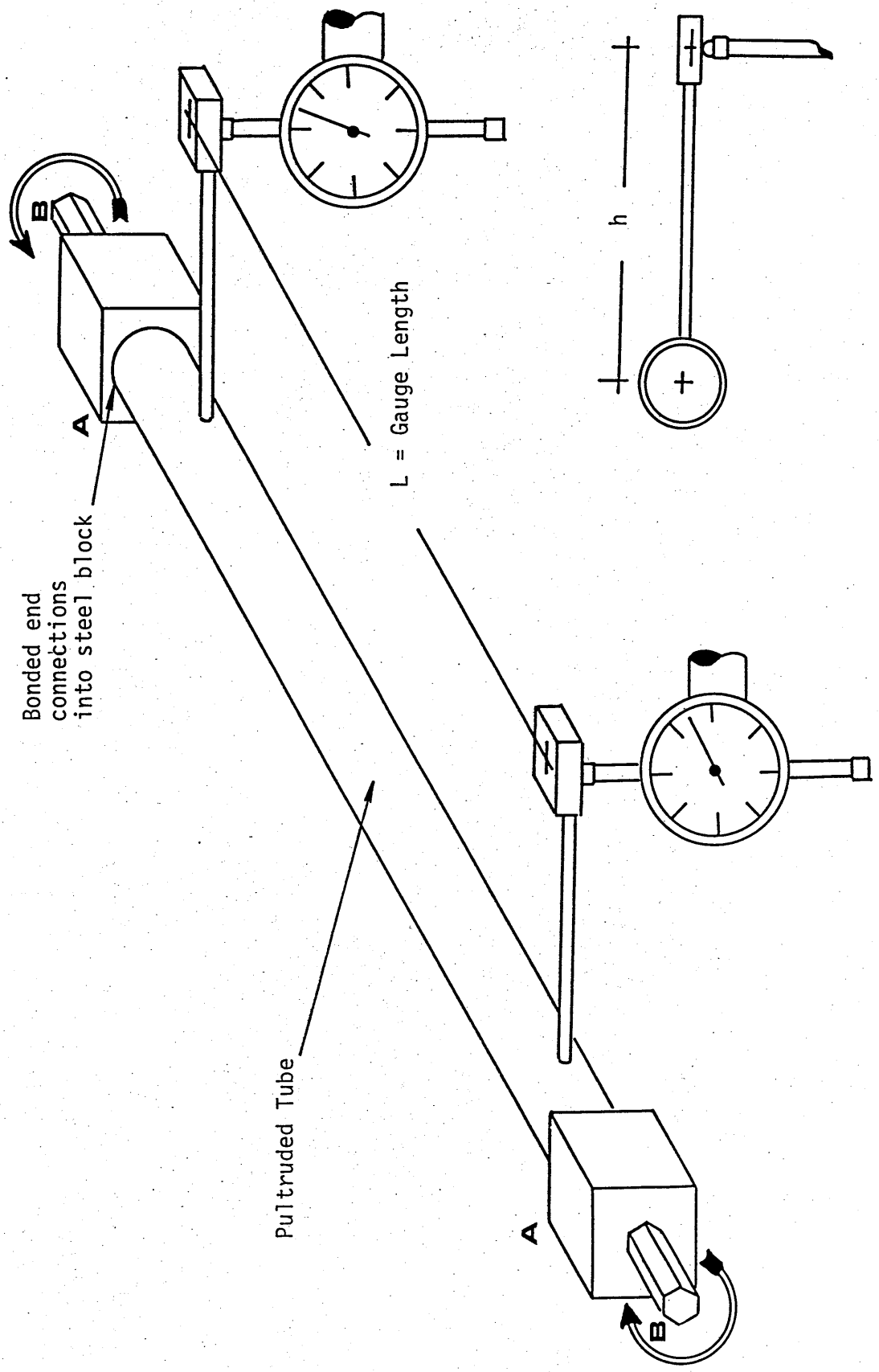

Fig (2.6) Torsional Testing Arrangement of g.r.p. and c.g.r.p.

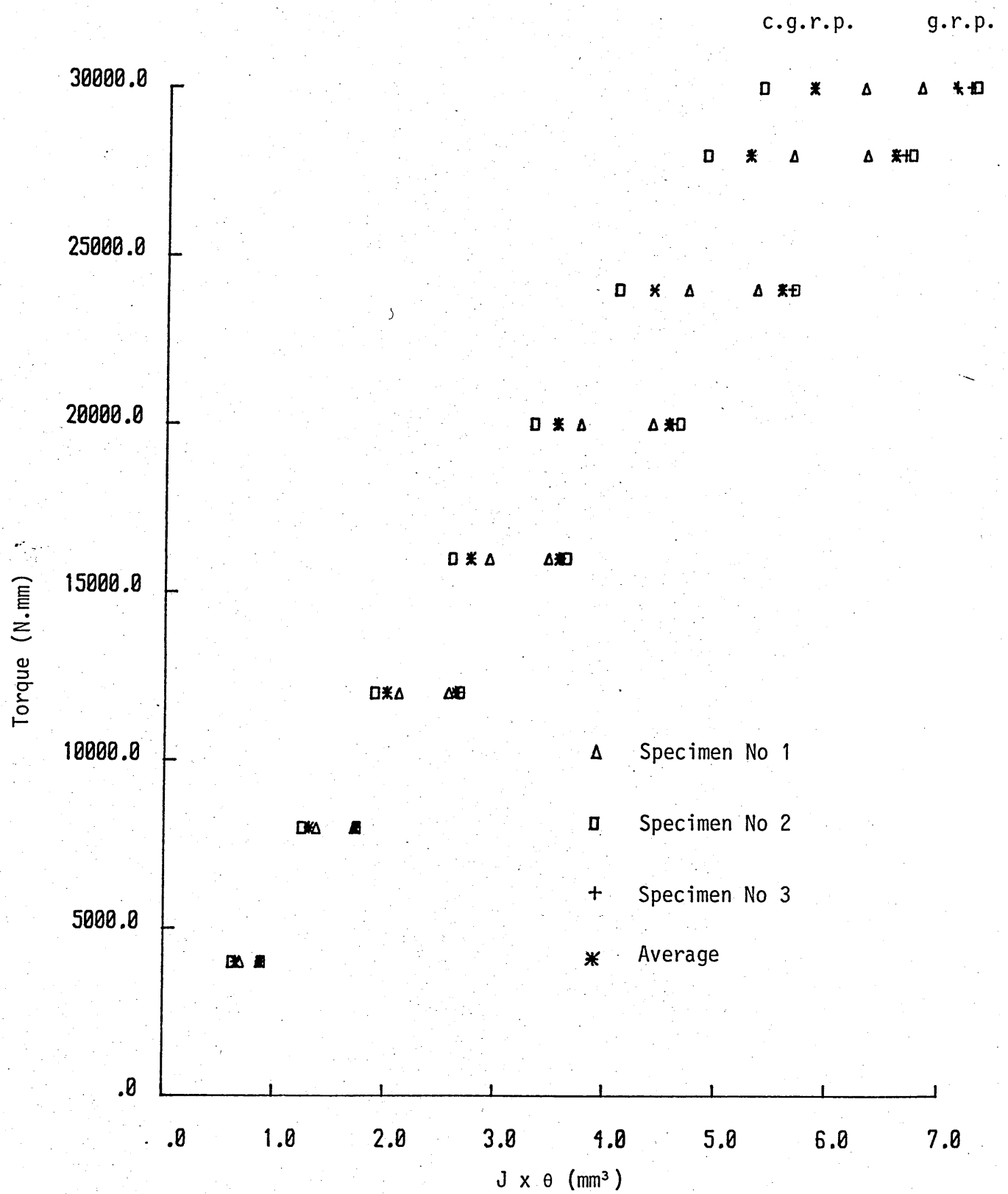

Fig (2.7) Torque - (polar moment x unit angular distortion) for torsional testing of pultruded g.r.p. and c.g.r.p.

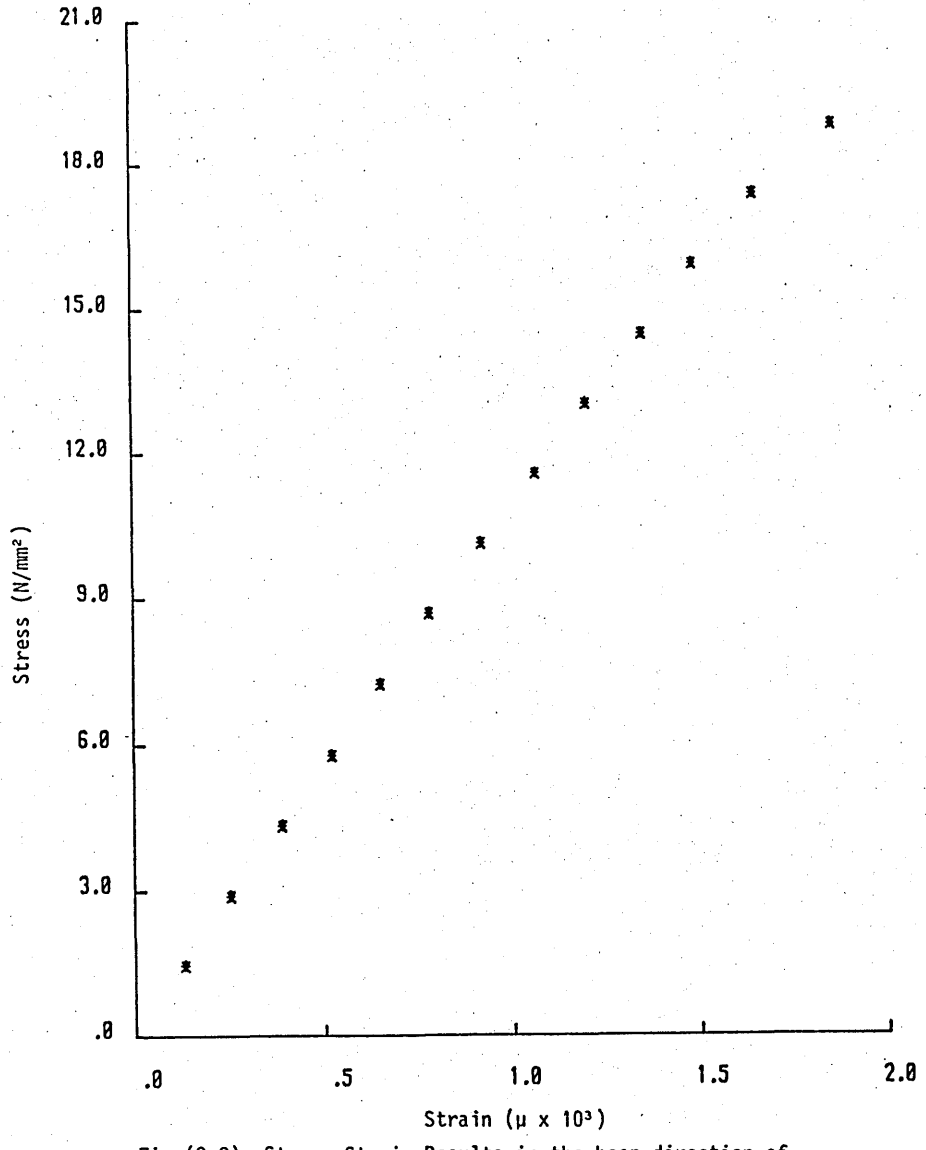

Fig (2.8) Stress-Strain Results in the hoop direction of Pultruded g.r.p. tube specimen subjected to internal Pressure

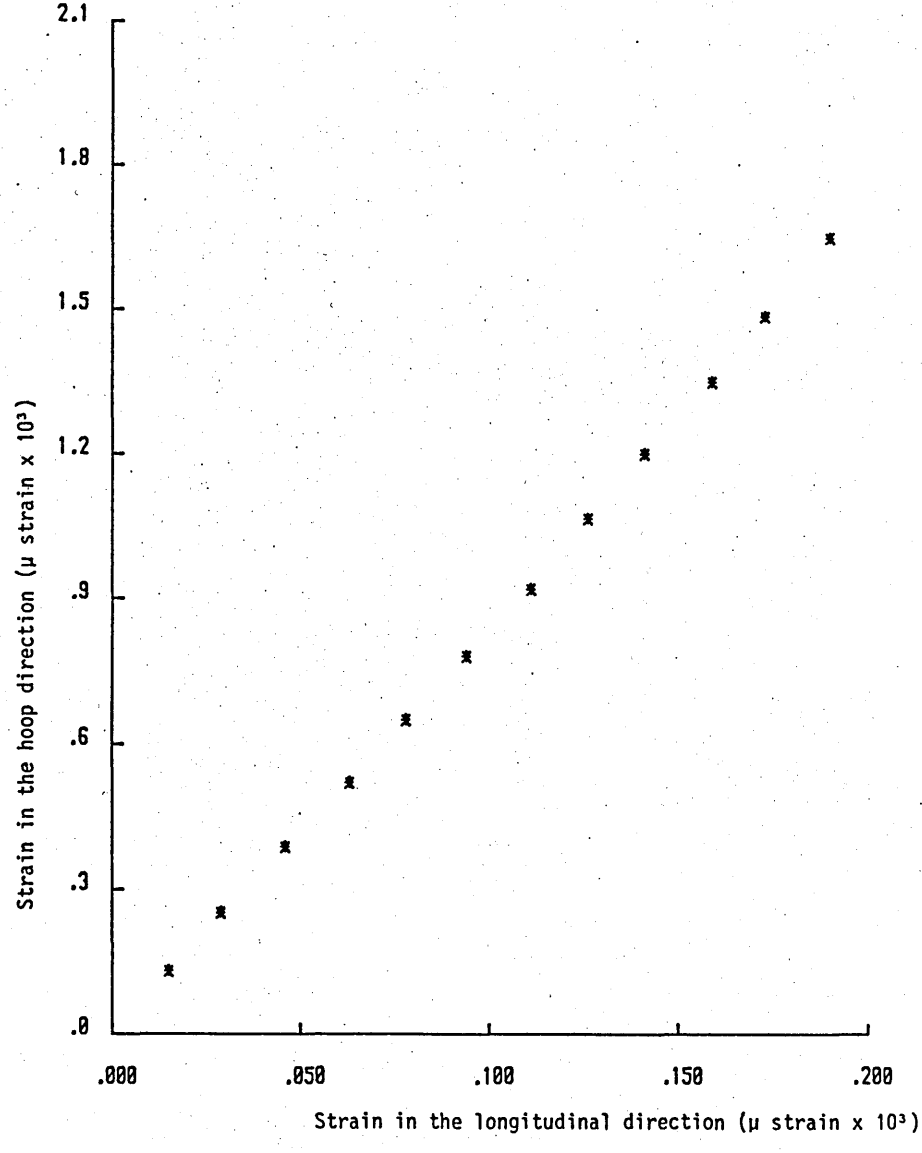

Fig (2.9) Hoop strain - longitudinal strain for the pultruded g.r.p. tube specimen subjected to internal pressure

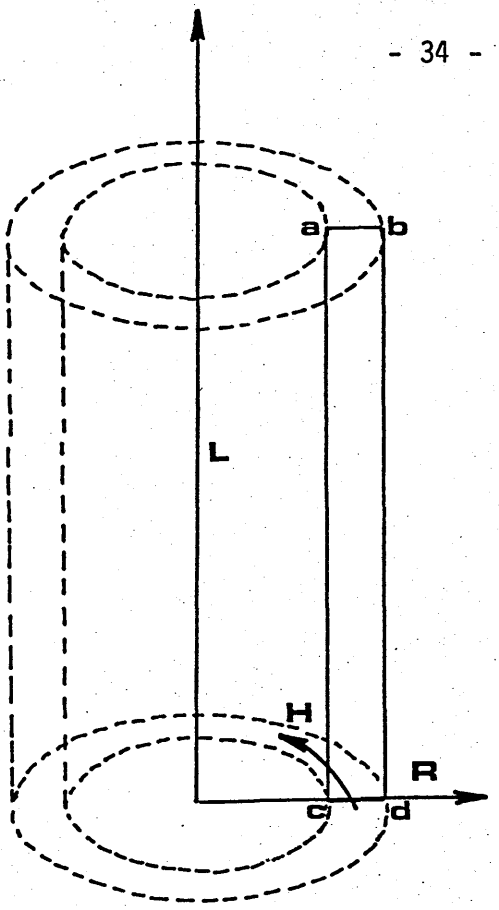

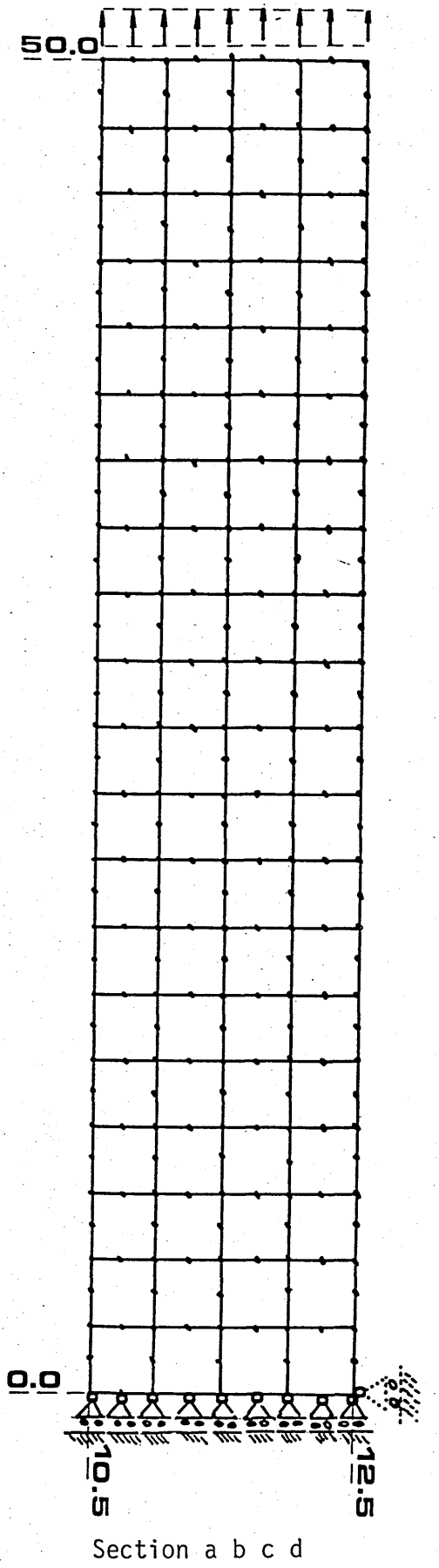

Fig (2.10) The pultruded tube finite element discretization arrangement, load and boundary condition

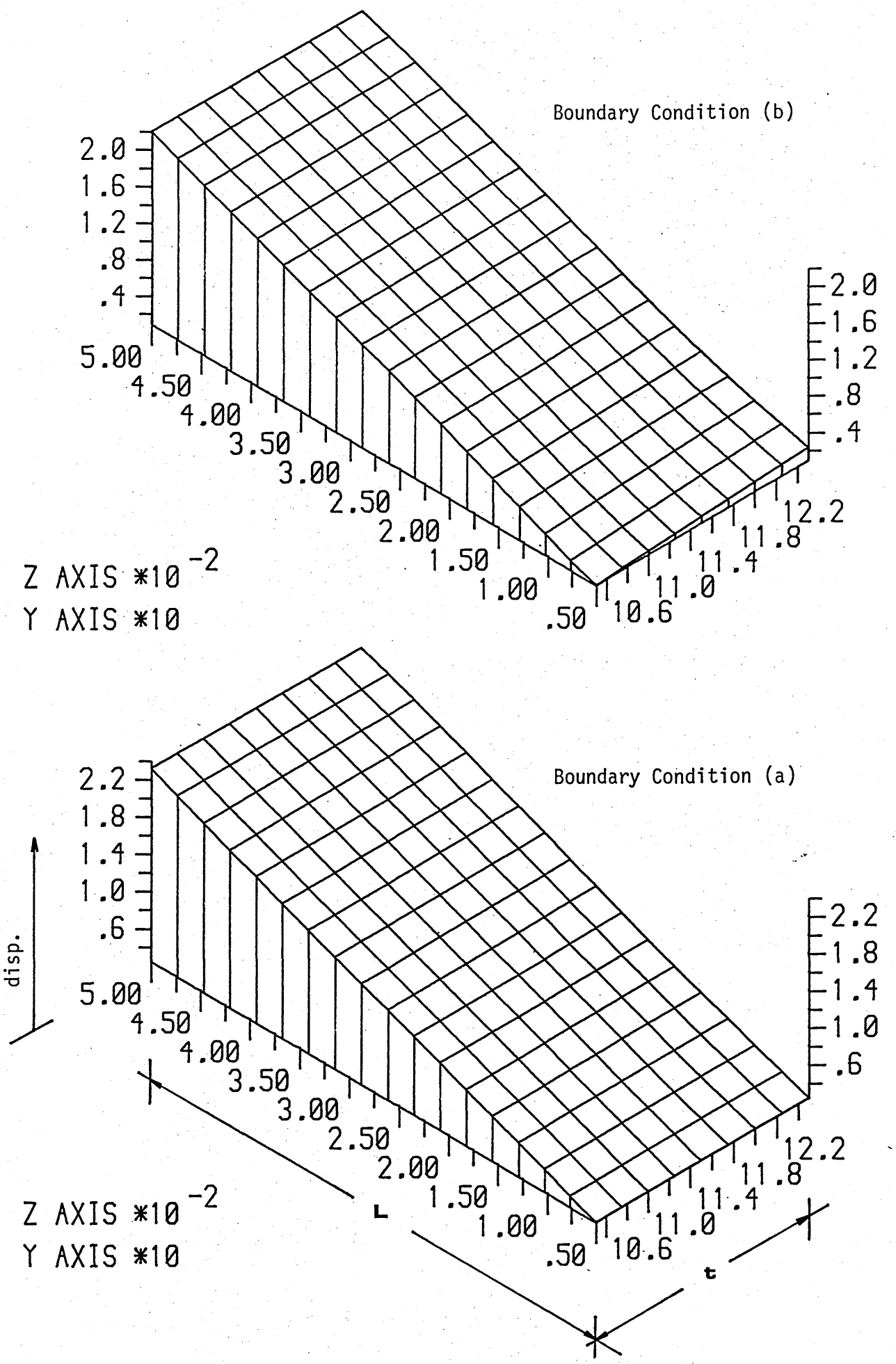

Fig (2.11) The isometric projection graph of distances (L and R) against displacements in the L direction

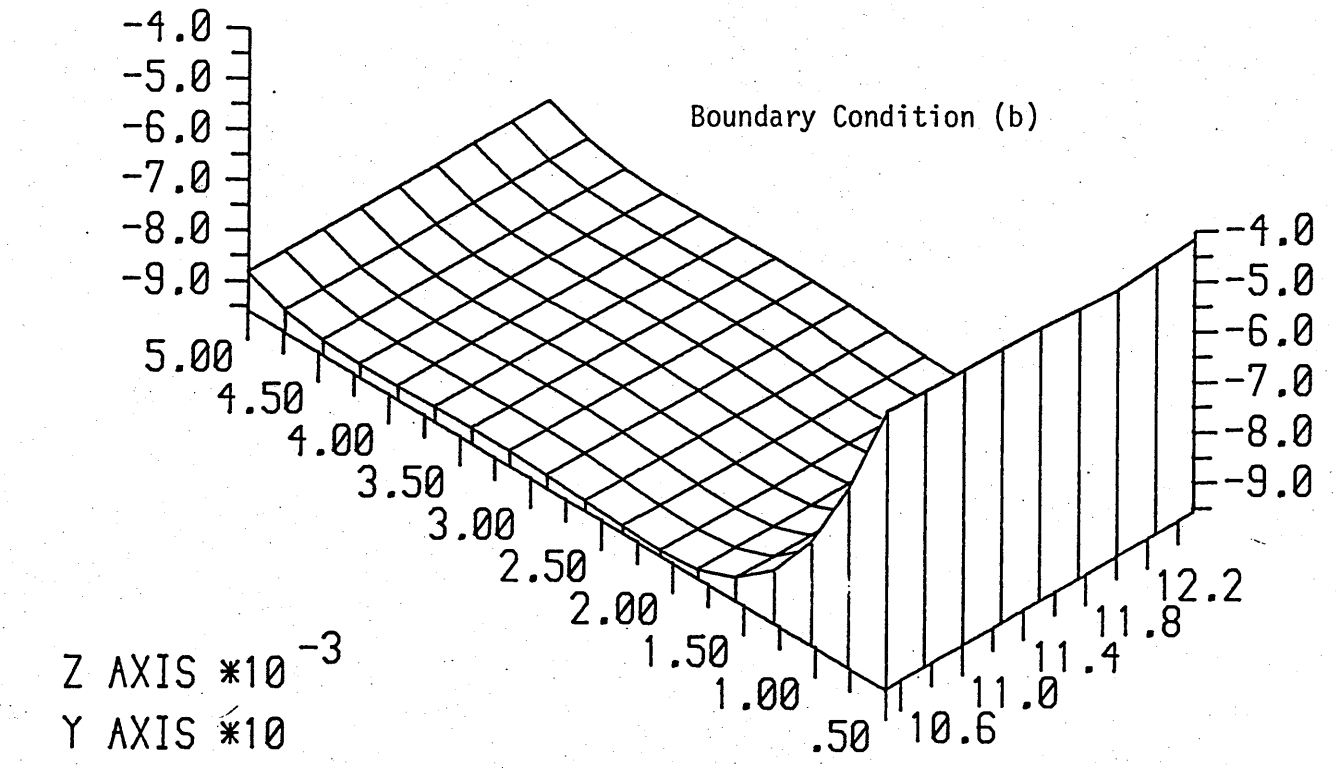

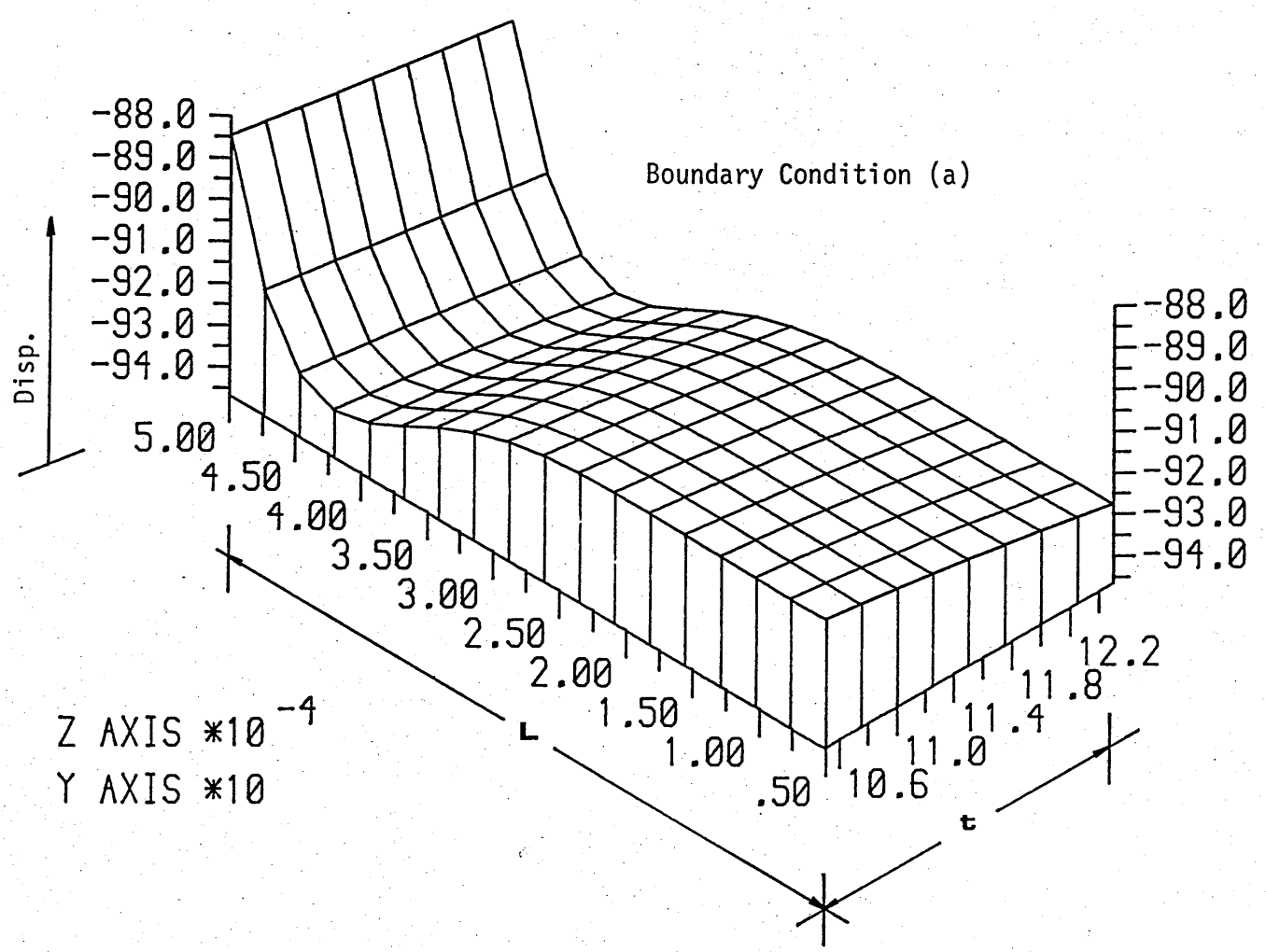

Fig (2.12) The isometric projection graph of distances (L and R) against displacement in the R direction

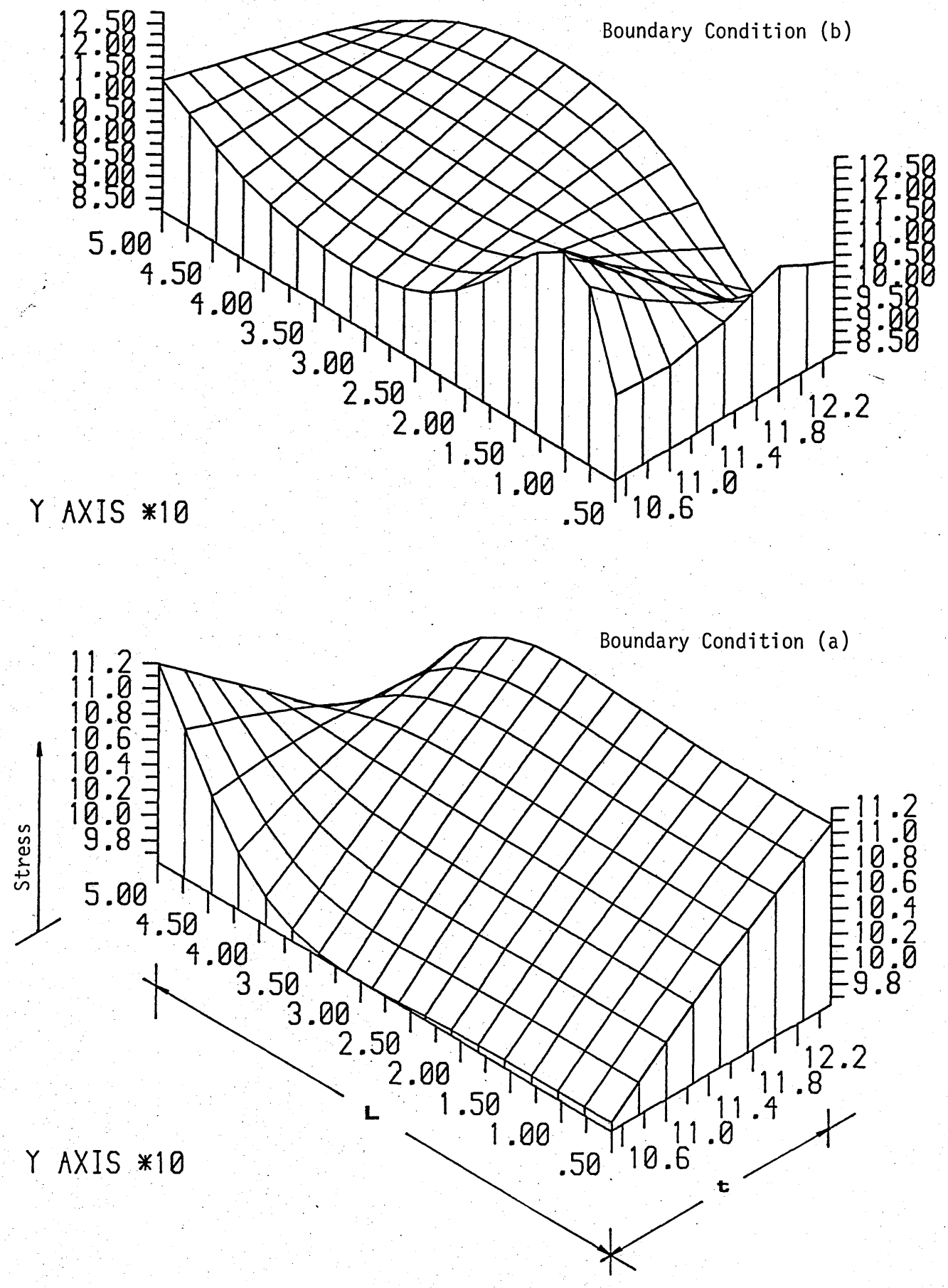

Fig (2.13) The isometric projection graph of distances (L and R) against stresses in the L direction

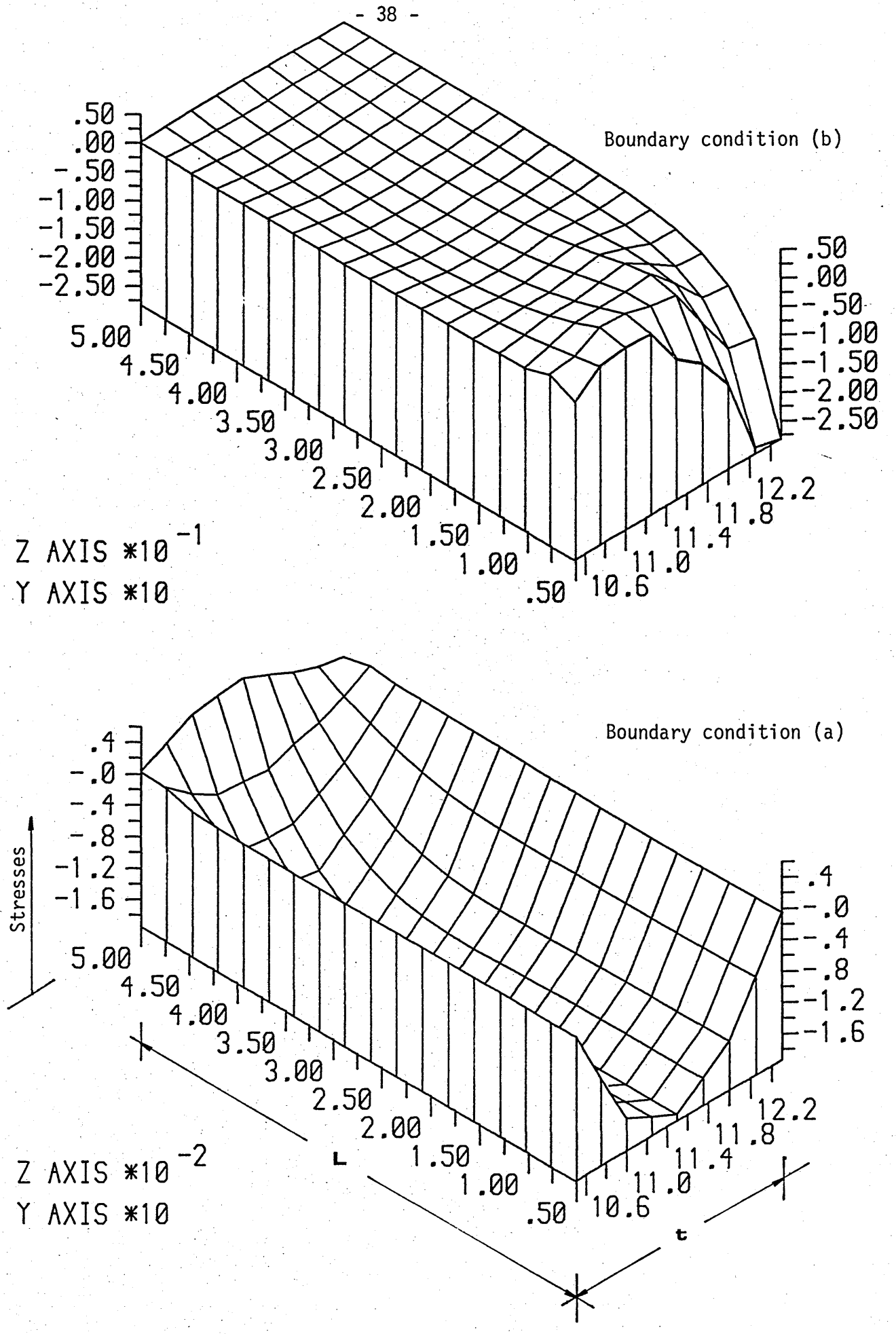

Fig (2.14) The isometric projection graph of distances (L and R) against stresses in the R direction

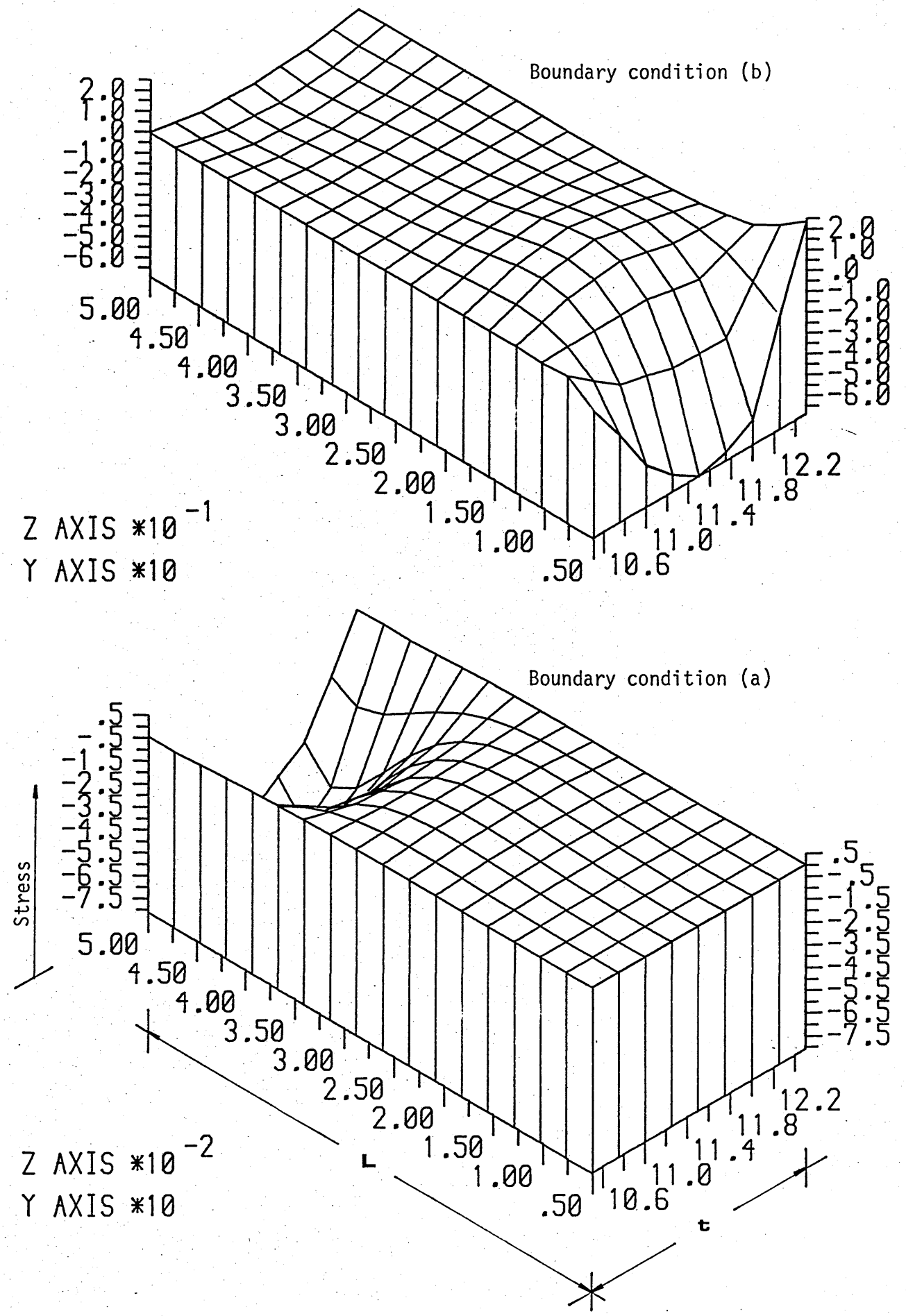

Fig (2.15) The isometric projection graph of distances (L and R) against stresses in the H direction

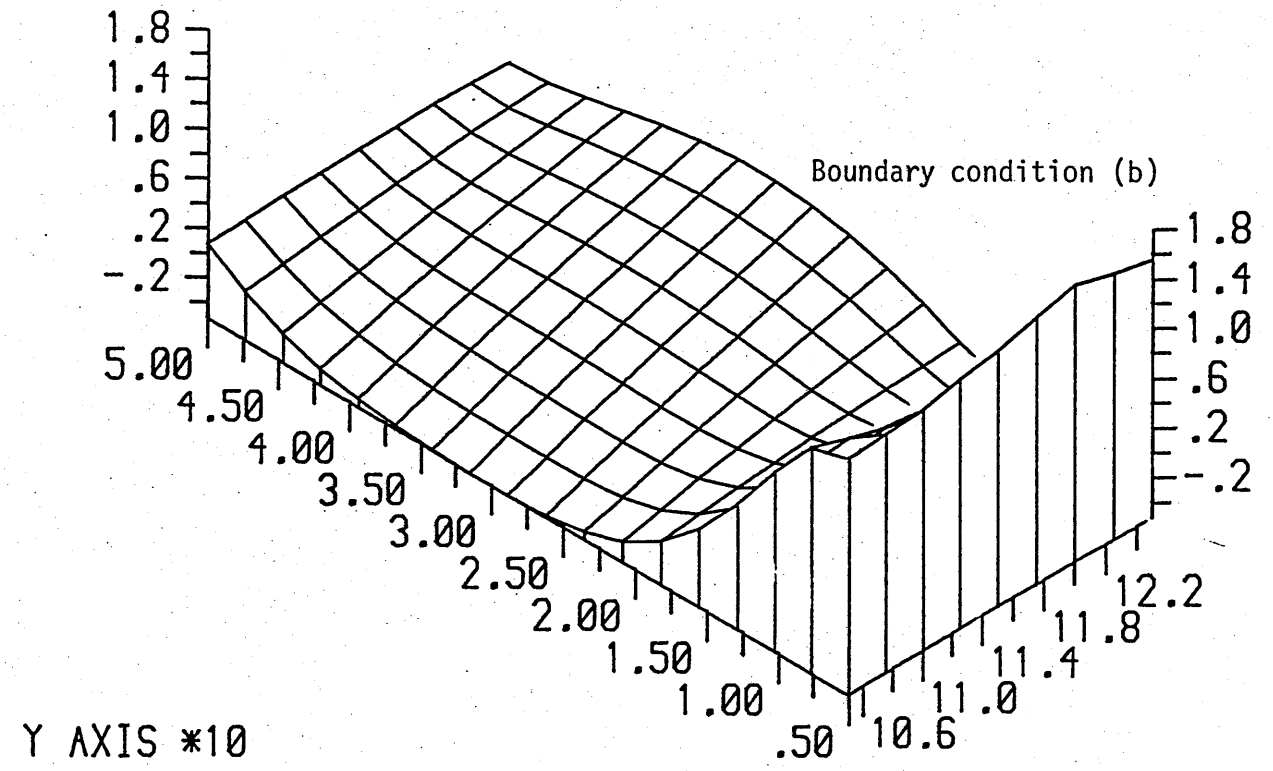

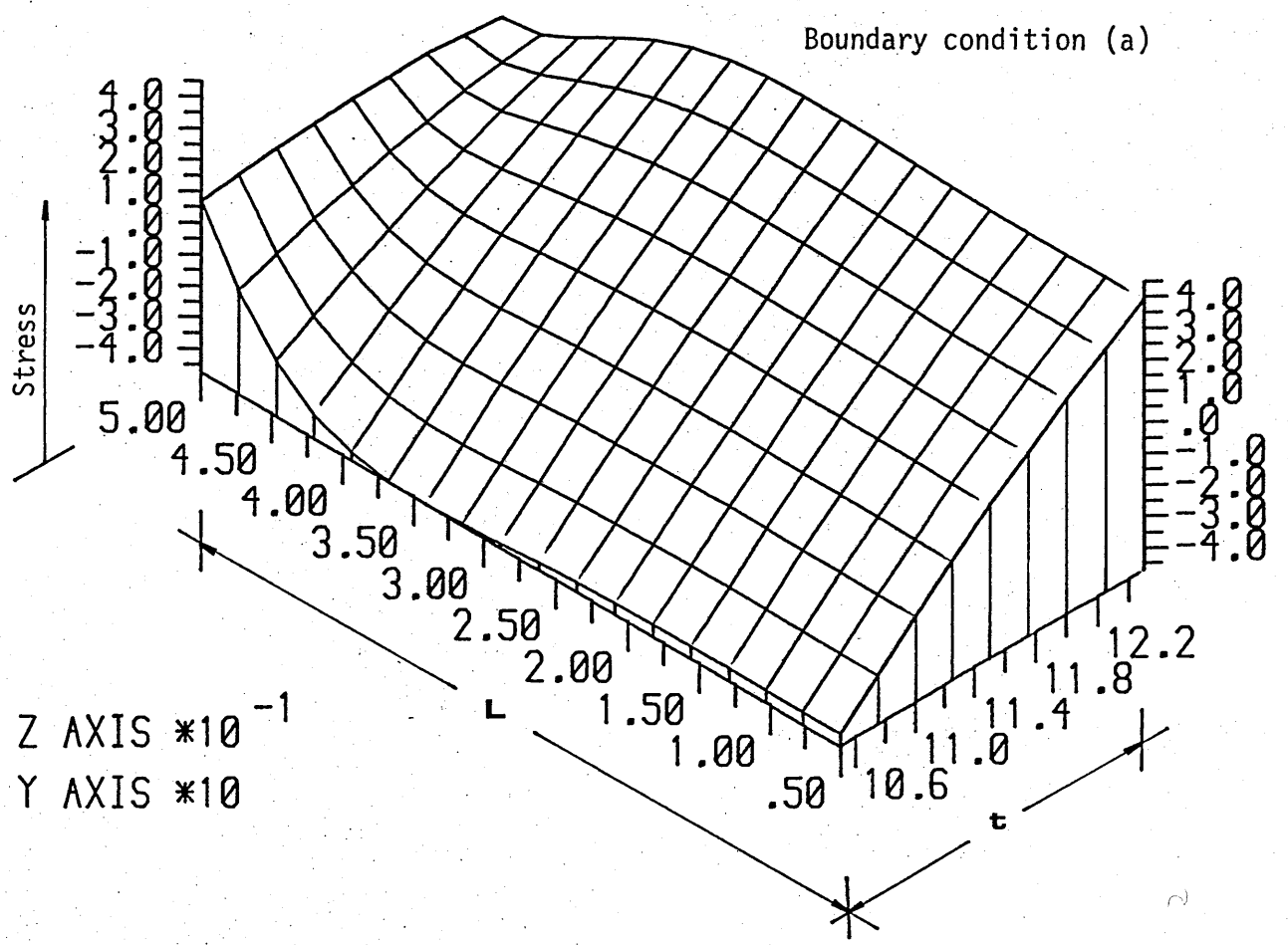

Fig (2.16) The isometric projection graph of distances (L and R) against shear stress

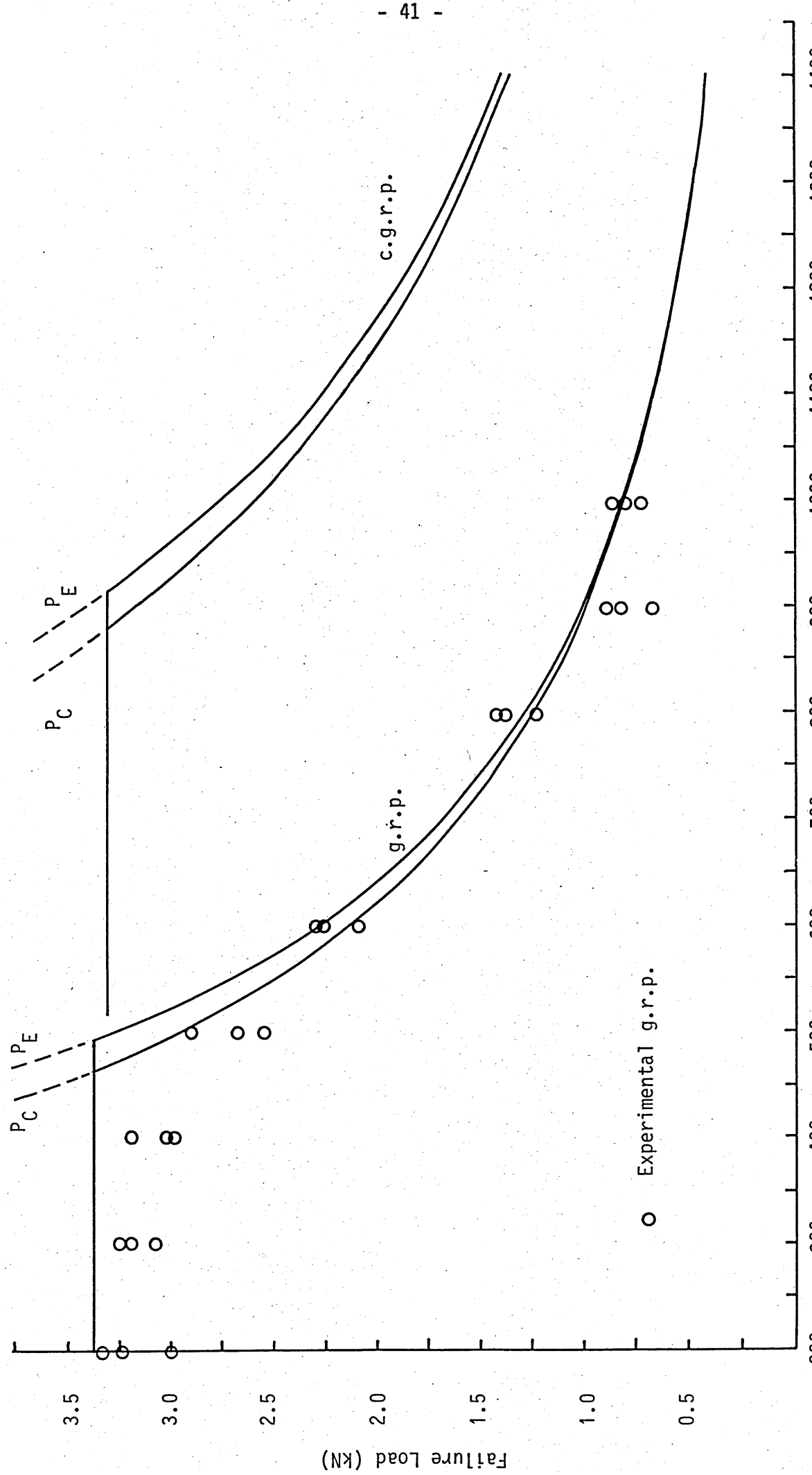

Fig (2.17) Experimental and theoretical values for failure load - f.r.p. tube length

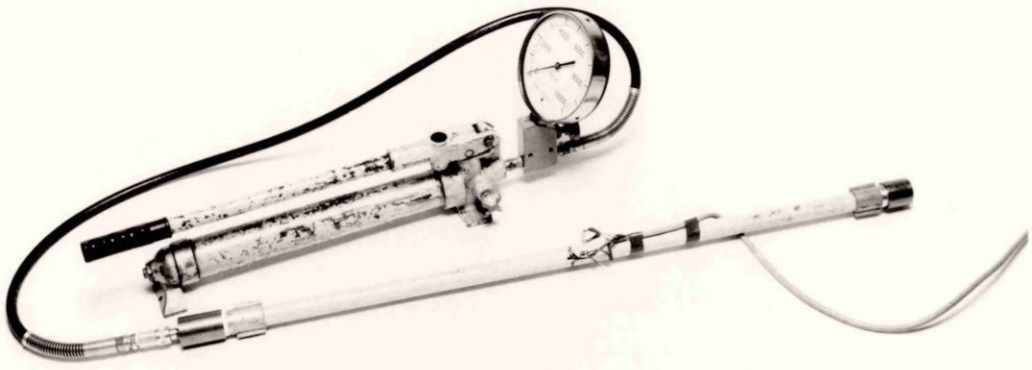

Plate (2.1) Testing arrangement for g.r.p. specimen subjected to internal pressure

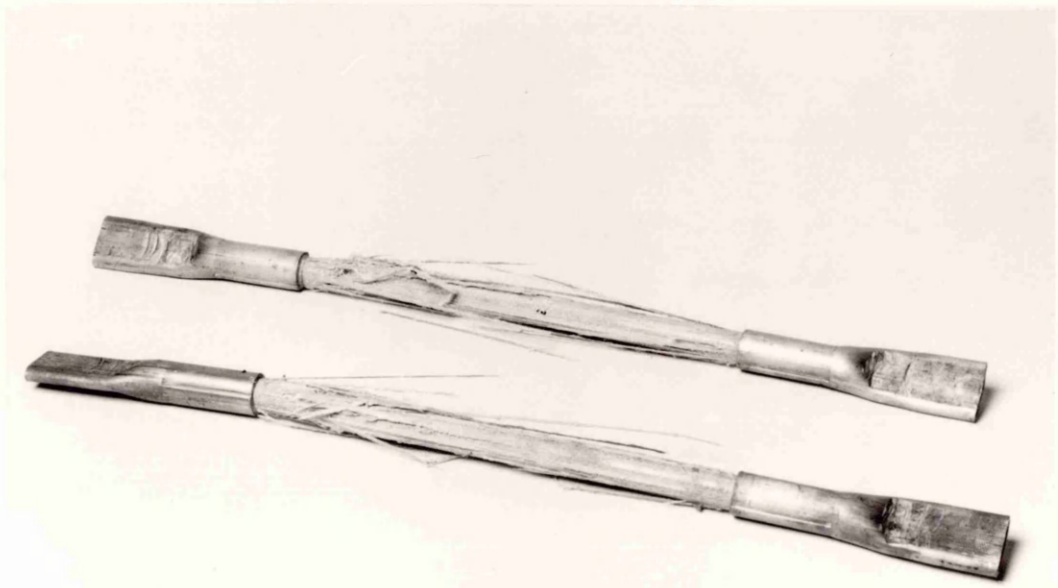

Plate (2.2) Typical failure of tensile g.r.p. specimens

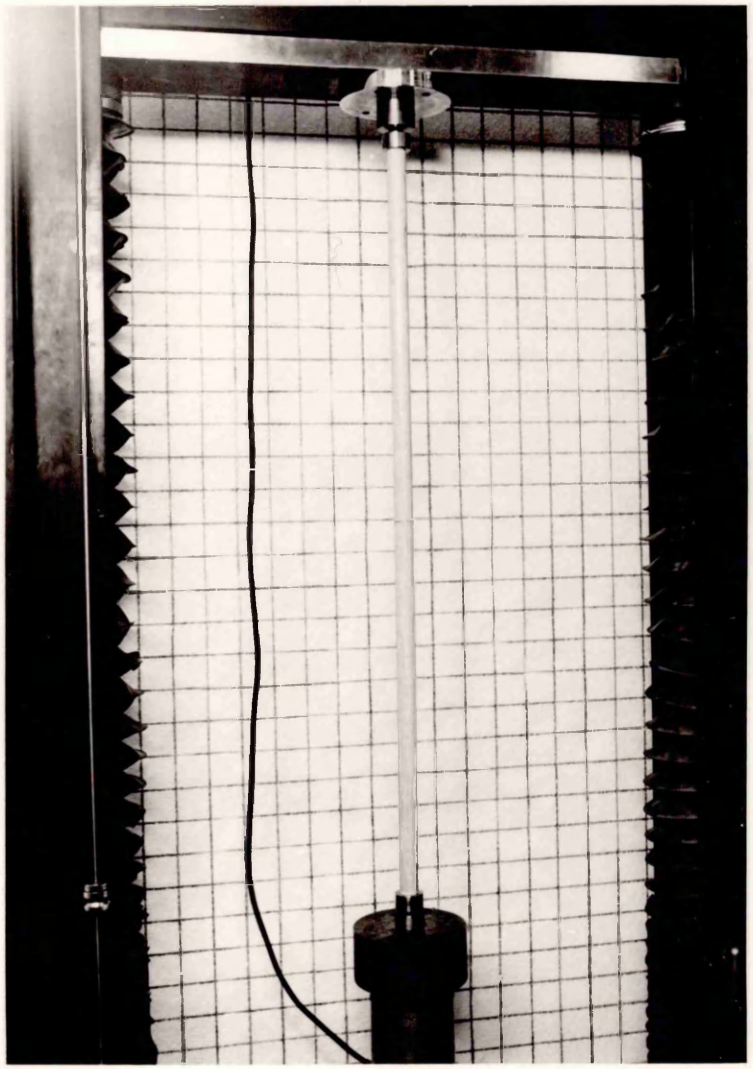

Plate (2.3) Member before loading

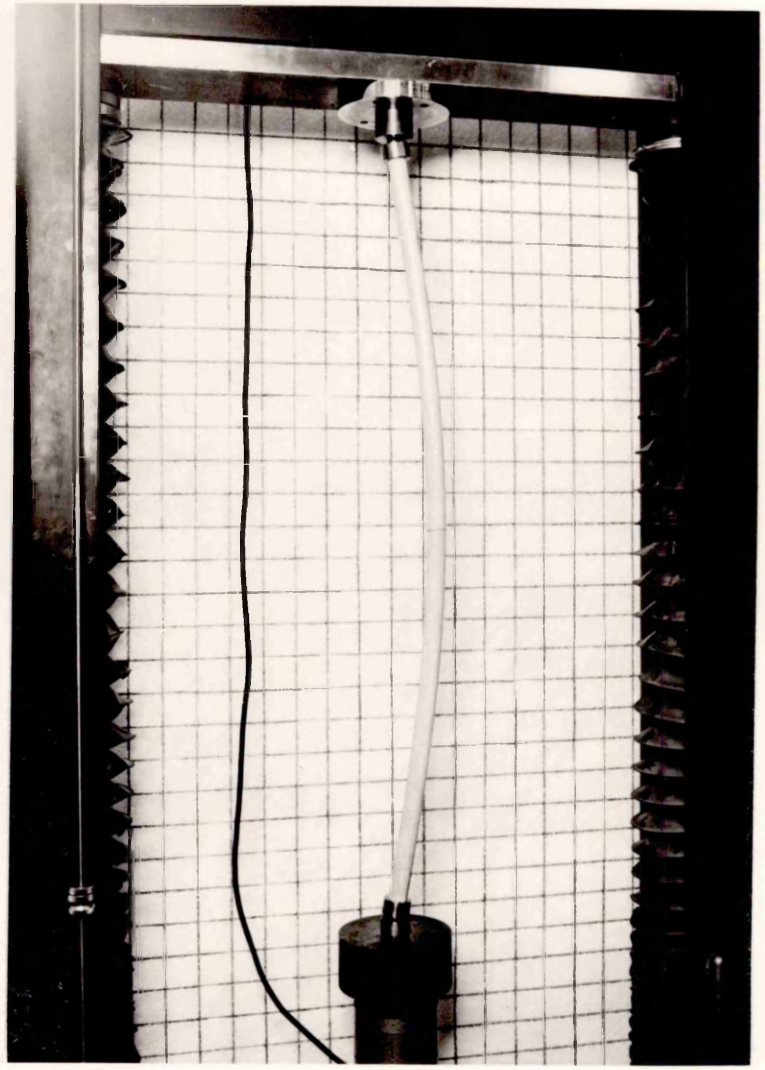

Plate (2.4) Buckled member under axial loading

CHAPTER THREE

NON-LINEAR ANALYSIS OF SKELETAL STRUCTURES

3.1 INTRODUCTION

One of the results of the technological developments achieved over the last few decades is the introduction of high quality structural material, such as light weight high strength alloys and fibre reinforced polymers; the use of which produced very efficient light structures. However, these types of structures bring new problems, especially in the area of analysis and design. The response of these structures is generally non-linear with high risk of instability and the consequences of this can be disasterous. The analysis empoyed for such structures must guarantee the prediction of the response to the design loads which may occur during the lifetime of the structure.

A large amount of work has been carried out on the subject of instability of structures. Many investigators have studied the phenomena, analysed the instability process and laid the foundations for the practical methods of analysis. The basic principles of the general theory of elastic stability associated with conservative systems are now well established; the notable pioneers in this field have been Koiter, Ziegler, Chilver, Britvec, Thompson, Sewell, Budianski and Hutchinson. The literature is extensive and consequently, the discussion will be limited to discrete elastic conservative systems which apply to skeletal structures.

Only the basic concepts of elastic stability will be discussed here. The concepts are important for the development and the understanding of the practical methods of analysis and the problems associated with the loss of stability and the post-buckling behaviour.

The stability of an arbitrary equilibrium state of a discrete elastic conservative system is discussed. It is based on the energy criterion with particular importance given to the points of transition between the prebuckling and post-buckling state. These points are known as the critical points.

The practical methods of non-linear analysis based on the finite element method are discussed and relevant previous work is presented.

A description of a method of analysis for skeletal systems and the computer implementation is presented. This method is used for the analysis of various skeletal configurations made of fibre reinforced polyester.

3.2 SOME RELEVANT BASIC PRINCIPLES OF ELASTIC STABILITY

3.2.1 EQUILIBRIUM OF STRUCTURES

The class of problem discussed in this section relate to discrete elastic systems under conservative loading condition. It is well known that the potential energy function of these systems contains information relevant to equilibrium and stability. The equilibrium configuration of these systems is defined by a set of N generalised coordinates,

$$\bar{q} = q_1, q_2, \ldots, q_N. \qquad \ldots\ldots 3.1$$

In addition to the generalised coordinate external load parameters are introduced. The simplest and most common case is the one parametric load (the loading of a structure is dependent upon a single intensity parameter λ). In such a case, the analysis is limited to proportional loads.

$$\bar{P} = \lambda P \qquad \ldots\ldots 3.2$$

where P is the load vector and λ is a scaler multiplier. The potential energy is given as a function of N+1 variables

$$V = V(\bar{q},\lambda) \qquad \ldots\ldots 3.3$$

The equilibrium equations are obtained by:

$$\frac{\partial V(\bar{q},\lambda)}{\partial qi} = 0 \quad \text{For } i = 1, \ldots, N \qquad \ldots\ldots 3.4$$

For practical reasons repeated subscripted notations are used, where subscripts on V represent differentiation with respect to the corresponding generalised coordinate and repeated subscript within an expression implies summation from 1 to N. The previous equations will be written as follows:

$$V_i(q_i,\lambda) = 0 \qquad \ldots\ldots 3.5$$

The N equations in the N+1 unknowns are generally Nonlinear in q and λ. The solution of this system describes what is known as the equilibrium path with all points on the path satisfying equilibrium. The undeformed state is assumed to be the reference state with q_i and λ equal to zero. The configuration (q_i,λ) can be visualised as a point in N+1 dimensional Euclidian space. The solution of the equilibrium equations can be expressed in parametric form by:

$$q = q(\eta) \qquad \lambda = \lambda(\eta) \qquad \ldots\ldots 3.6$$

where η is a path parameter. The parameter may be taken as λ and the parametric expression takes the form

$$q = q(\lambda) \qquad \lambda = \lambda \qquad \ldots\ldots 3.7$$

3.2.2 THE STABILITY OF EQUILIBRIUM

In order to investigate the stability of an equilibrium state the quadratic form is formulated

$$V_{ij}\delta q_i \delta q_j$$

The stability of the equilibrium is ensured if this form is positive definite.

Consider now an equilibrium state E and introduce the transformation

$$q_i = q_i^E + \Delta q_i \qquad \text{..... 3.9}$$

and

$$\Delta q_i = \alpha_{ij} U_j \quad \text{with} \quad |\alpha_{ij}| \neq 0 \qquad \text{..... 3.10}$$

where this last equation diagonalizes the quadratic form of the energy function; note that the matrix $[\alpha_{ij}]$ is not in general unique, and to ensure a unique transformation at a given equilibrium state an orthogonal transformation matrix $[\alpha_{ij}]$ is specified.

$$H(u_i,\lambda) = V(q_i^E + \alpha_{ij} u_j, \lambda) \qquad \text{..... 3.11}$$

with the properties

$$H_{ij} = 0 \qquad \text{For } i \neq j \qquad \text{..... 3.12}$$

Here we assume that complete relative minimum of the potential energy is necessary and sufficient for stability. Analytically, this corresponds to the positive conditions of the second variation of the energy function. Thus, if all poincaries coefficients H_{ii} $(i = 1, \ldots, N)$ are positive then the state is stable. However, if at least one coefficient is negative then the state is unstable. The equilibrium state is called critical in the case of one or more zero coefficients. Such a state is unstable if any of the other coefficients are negative, and are truly critical if none of the other coefficients are negative and it is usual to refer to the latter as primary critical. A decision regarding the stability of this state cannot be made at this stage, as the second variation of energy does not give enough information so that higher order variations are needed. A necessary condition of a critical state is the zero value of the stability determinant

$$V_{ij}(q,\lambda) = H_{ij}(u,\lambda) = H_{11} \times H_{22} \times \ldots \times H_{NN}$$

..... 3.13

3.2.3 THE CRITICAL POINTS

The stability of a structural system is usually terminated in one of two ways:

(a) snap through (limit point);
(b) bifurcation.

The bifurcation is categorized in three forms,

(a) asymmetric;
(b) stable symmetric;
(c) unstable symmetric,

as shown in Fig (3.1), for a single degree of freedom system. These geometrical concepts follow from the analysis of the solution of equilibrium equations, expressed in parametric form, in the neighbourhood of the critical points. Only limit points are considered in more detail.

Expressing the generalised coordinates u_j as a function of an arbitrary parameter η which defines progress along the path; it could be either of the generalised coordinates or the load parameters λ

$$u_j = u_j(\eta)$$
$$\lambda = \lambda(\eta) \qquad \text{..... 3.14}$$

The equation expressing equilibrium:

$$H_i[u_j(\eta), \lambda(\eta)] = 0 \qquad \text{..... 3.15}$$

differentiating with respect to η

$$H_{ij}\dot{u}_j + H'_i\dot{\lambda} = 0 \qquad \text{..... 3.16}$$

note that dots denote differentiation with respect to η and primes with respect to λ.

A further differentiation gives

$$H_{ijk}\dot{u}_j\dot{u}_k + 2\acute{H}_{ij}\dot{u}_j\dot{\lambda} + H_{ij}\ddot{u}_j + \acute{\acute{H}}_i\dot{\lambda}^2 + \acute{H}_i\ddot{\lambda} = 0 \qquad \ldots\ldots 3.17$$

It is usual to refer to these equations as first and second order equilibrium equations.

The way in which the fundamental stable path loses its stability depends on the properties of the structural system as reflected in the various derivatives of the total potential energy function. However, the behaviour at loss of stability must fall into one of two categories; these are either limit point or bifurcation.

3.2.4 LIMIT POINT BEHAVIOUR

The limit point behaviour is characterised by a loss of stability coinciding with a local maximum of the load parameter λ.

The important coefficient that differentiates limit point from bifurcation is $\acute{H}_i$. At point E, $\acute{H}_i$ must not vanish.

In the first order equation, putting $i = 1$ and $n = u_1$ and evaluating at the critical point E gives:

$$\frac{\partial\lambda}{\partial u_1}\Big|_E = \dot{\lambda}^E = \frac{H_{11}}{\acute{H}_i}\Big|_E \qquad \ldots\ldots 3.18$$

since $H_{11} = 0$ $\qquad \ldots\ldots 3.19$

$\dot{\lambda}^E = 0$ $\qquad \ldots\ldots 3.20$

Thus it is clear that the path slope is zero.

If, instead of $i = 1$, $i = r \neq 1$, the first order equilibrium equation gives,

$$H_{rr}\, u_{r1} \Big|_E = 0 \qquad \ldots\ldots 3.21$$

since $H_{rr} \neq 0$ for $r \neq 1$ we get 3.21

$$u^E_{r1} = 0 \qquad \ldots\ldots 3.22$$

which shows that the tangent to the equilibrium path is parallel to u_1.

For i = 1 and exluding the zero terms from the second order equilibrium equation when evaluated at the critical point E.

$$H_{111} + H'_1\, \ddot{\lambda}^E \Big|_E = 0 \qquad \ldots\ldots 3.23$$

Therefore,

$$\ddot{\lambda}^E = - \frac{H_{111}}{H'_1} \Big|_E \qquad \ldots\ldots 3.24$$

Having maximum load at E means that $\ddot{\lambda}^E \neq 0$ and consequently H_{111} should not vanish.

3.3 GEOMETRIC NONLINEARITY OF SKELETAL SYSTEMS BY THE FINITE ELEMENT METHOD

3.3.1 GENERAL

The direct stiffness method of finite element analysis is by now well established and widely used for the solution of elastic linear problems [15]. A wide variety of elements have been developed, and several general purpose computer programs with the capability of dealing with any linear elastic structural problems are now in use [16].

Since the establishment of the finite element method, there has been a great deal of interest in extending the method to nonlinear analysis and various approaches have become available, including several computer programs. However, these approaches are still under development.

The nonlinearity arises from two sources:

(a) geometric nonlinearity, and
(b) material nonlinearity.

The former is divided in two classes, the large deformation small strain condition, and the large deformation large strain condition. Each class is usually treated separately as the large strain condition greatly complicates the theoretical formulation of the problem. Regarding the material nonlinearity, the most commonly used nonlinear material is the elastic-plastic material for which a linearized incremental method is usually adopted. However, the material nonlinearity is not of interest here and, therefore, will not be discussed further.

Nonlinear theory is inevitably more complex than the linear theory because of the mathematical problems which are usually intractable. Similar difficulties may occur even in connection with certain linear problems. It was the complexities of theoretical stress analysis that lead to the development and spread of the finite element method. The extreme mathematical complexity involved in obtaining quantitative solutions to nonlinear problems in finite elasticity resulted in a finite number of solutions to the problems being dealt with in the literature. The solutions available pertain to structures with a very simple geometry. Moreover, even in the case of simple geometries, approximate numerical techniques are often introduced in the final steps of the solution. At the present time the finite element method represents the most practical method for solving complex nonlinear problems, since the fundamentals for dealing with nonlinear problems, using the finite element methods, are by now well established.

Geometric nonlinearity results in two classes of problems that are well known to the structural engineer; the large deformation and the structural stability. The term 'large deformation' is misleading as not all problems falling within this category have large deformations. However, the deformed configuration of the structure must be used when writing the equilibrium for the large deformation problem. In addition, the strain displacement equations must include the higher order nonlinear terms; the problem of instability of a structure is generally considered separately from the basic analysis. There are several matrix methods at present available which allow the critical load of skeletal structures to be determined. The main methods usually fall into one of the two following groups:

(a) Those using a single standard matrix K_0 with certain stability correction factors.

(b) Those using the combination of a standard stiffness matrix K_0 and the so called Geometric matrix.

In the second method the application of the direct stiffness method is associated with the derivation of the geometric (an initial stress) stiffness matrix that takes into account some of the higher order terms of the strain displacement relationship. Using these matrices an eigenvalue problem is established from which critical loads can be evaluated. This approach is well suited to problems in which the intensity of the internal forces varies linearly with the applied load. Furthermore, only eigenvector (buckling mode shape) could be predicted and no knowledge of the post-buckling behaviour could be obtained. However, with the right mathematical model that includes the effects of the change of geometry, and with the advantage of digital computers, a full analysis could be carried out with the construction of the whole load deflection curve, including the detection of any instability that may occur.

It was felt that the stiffness (displacement) method was generally more suitable than the flexibility (force) method for an analysis

involving the change of geometry. One reason was that the effects of change of geometry could be more readily evaluated if the deformations rather than the forces were defined. This resulted in the use of the stiffness method in most of the developments.

The nonlinear finite element method of analysis may be considered to have two basic components. These are an element mathematical model and a solution procedure to determine the equilibrium conditions.

There are two basic classes of methods that utilize the finite element technique; these are the asymptotic methods and the direct methods. The asymptotic methods build the equilibrium path in the vicinity of a known equilibrium state by using the power series expansion. The coefficients of the power series are the derivatives of the total potential energy function of the structural system. The asymptotic methods are considered as application and extension to Koiters perturbation method. The general nonlinear theory developed by Thompson [17] and Sewell [18] represents an example of this method.

The direct finite element methods are utilized more than other methods and are generally accepted as more powerful. The energy search method is an example of the direct method, in which the potential energy function is used as the mathematical model and the solution is obtained by mathematical search techniques for the stationary values. The simplicity of this method exists in the fact that the potential energy of a structure is equal to the sum of the energy contribution of each element which, in the finite element method, is constructed with relative ease, but care should be taken in the selection of the displacement mode to avoid excessive artificial stiffness. The major drawback of this method is the computational effort required for the unconstrained minimization of a function of many variables.

The direct solution of the nonlinear equilibrium equations which represent the relationship between displacements and the applied

load, to provide the equilibrium configuration, is used more frequently but, the cost of performing the solution is often considerable. More effective methods of solving the nonlinear systems of equations can be of significance both in reducing the cost of analysis and improving the solution.

3.3.2 HISTORICAL REVIEW

The literature on the nonlinear analysis is vast and several publications reviewing the work done on nonlinear analysis have appeared. For example, Martin [19] reviews some of the methods dealing with geometric nonlinearities and Stricklin et al [20] reviews solution procedures. As there is a considerable volume of literature on this topic, most of the work discussed in this section is concerned with the finite element geometric nonlinear analysis of skeletal systems, which is closely related to the topic of this research work.

The initial paper treating geometric nonlinearity by finite elements was published by Turner et al in 1960 [21]. An incremental technique was used in which the load was applied in small increments; during each increment the response of the structure was assumed linear. Displacements and internal stresses were evaluated at the end of each increment and used to form various corrective stiffness matrices. These matrices account for higher order terms in the strain displacement relationship and are essential for investigating large deflection and stability problems. The updated stiffness matrices were then used for the successive increment. In this paper matrices for pin-jointed bar and triangular plane stress elements were derived.

Renton [22] in 1962 presented a formulation as an extension to the three dimensional case of a previous work by Livesly and Chandler [23] in which the latter calculated the stability functions that take into account nonlinearity. The stability correction factors used by Renton took account of the gusset plates and the difference between the centroidal axis and the shear centre.

Gallagher and Padlog [24] in 1963 presented a consistent procedure based on the principle of minimum potential energy for introducing geometric nonlinearity in the finite element stiffness method. This formulation was limited to a linearized stability analysis. As an example, the stiffness matrix for a beam column was developed. Linearized stability analyses are convenient from a mathematical point of view but quite restrictive and could be applied to a special class of structures. Also in 1963, Saafan [25] presented a nonlinear formulation for rigid-jointed or pin-jointed frames considering the effects of axial load, finite deflection and bowing of the deformed members. An important point illustrated by Saafan's examples was that end shortening due to bowing may be of the same order of magnitude as the linear extension term.

Real progress in the application of the finite elements to geometric nonlinear analysis began in 1964 when Argyris [26] discussed a step-by-step linearized technique to determine the approximate nonlinear load deflection behaviour of rigid-jointed space frames. The tangent stiffness matrix used is evaluated at the initial position of each increment. In forming the tangent stiffness matrix the above author neglected the effect of axial force on the member flexibility. Martin [27] developed stiffness matrices for beam element and triangular plate element in plane stress. Oden [28] in 1966 presented a general formulation for evaluating the geometric stiffness matrices for the stability analysis of discrete systems. The development falls within the framework of the classical theory of elastic stability.

In 1966 Mallett and Berke [29] presented a computer program for the geometric nonlinear analysis of three dimensional truss and frame assemblies. The solution was based on the direct minimization of the total potential energy with respect to displacements. The same principle of minimizing the total potential energy to determine the equilibrium configuration was used in the theoretical formulation presented by Mallett and Schmit [30] in 1967. In this paper the function minimization techniques wer discussed in more detail and a

few examples of structural configurations with truss element werepresented. Oden [31] in the same year extended the finite element method to the analysis of elastic bodies that experience large deformation and finite strain. Another application of the minimization of the potential energy method for the analysis of three dimensional bar structures was also presented, in 1967 by Berke and Mallett [32].

In 1968 Connor et al [33] presented a nonlinear formulation for a rigid-jointed space frame with prismatic linear elastic members loaded only at the joints. This derivation was restricted to small rotations, ie, cases in which the squares of the rotation angles are negligeable with respect to unity, torsion flexure coupling was neglected to simplify the formulation. A Newton-Raphson iterative technique of solution was used. Also, in 1968 Mallett and Marcal [34] presented three different solution procedures, an incremental, an iterative, and an energy minimization, all based on the same formulation. In this formulation, higher order terms, which were previously neglected, were included. New element matrices were obtained and a heirarchy of nonlinearity was identified. This formulation was in Lagrangian-SR coordinates. In the same year Euler coordinates were used by Jennings [35] in a method which incorporated the effect of change in geometry into a displacement transformation for members of plane frames. This method includes flexure shortening in the formulation, and it can also be adopted in the case of large deformation.

Powell [36] in 1969, presented a consistent derivation of stiffness matrices. The effects of the various types of nonlinearities were illustrated by separating the nonlinear transformation. The matrices of beam column element were given. However, the formulation is general and could be applied to derive the matrices of various elements. In 1970, Hibbitt et al [37] proposed a large strain large displacement formulation which may be implemented in a computer program. In this approach the author adopted the incremental approach and the development was made in a Lagrangian frame reference.

A unified formulation of large deformation finite strain, and material plasticity problems were given by Zienkiewicz and Nyak [38] in 1971. Both Lagrangian and Eulerian formulations were discussed. Striklin et al [39] proposed a self-correcting initial value formulation as an alternative to the incremental approach. This formulation was proposed to reduce computing time, especially for large systems. Another paper by Striklin et al [40] also presented in 1971, described three different formulations for the analysis of geometrically nonlinear problems by the direct stiffness method. The direct energy formulation was compared with that of Turner et al [21] and Argyris [26] for simple truss members. The comparison showed the equivalence of the two formulations. Another relevant conclusion was that the initial value approach was inferior to the modified Newton-Raphson approach and the incremental approach as well. Haisler et al [41, (1971)] presented a review and a comparative study of the solution technique of nonlinear equations characterizing geometric nonlinear structural problems. A simple truss-spring problem was one of the examples used for the applications.

In 1972 an extensive list of references on reticulated shells was compiled by the ASCE subcommittee on latticed structures [42]. These references have been categorized according to analysis, stability, design, etc. Ebner and Ucciferro [43, (1972)] presented a theoretical and numerical comparison of five finite element formulations used for the nonlinear elastic analysis of planar skeletal structures. The nonlinear force displacement equations associated with these formulations were derived from a common starting point. Iterative, load increment and displacement increment solution procedures were used with a group of problems that cover a wide range of types of nonlinearity. The authors concluded that Jenning's direct formulation [35] yielded excellent results for all classes of nonlinear problems. Powell's direct formulation [36] yielded good results only for problems of relatively small displacements whereas with large deformation problems more elements were required. The Mallett-Marcal formulation [34] produced good results for small displacement but

could not be used for large displacement problems. Both Martin's [27] and Argyris's [26] appear to give excellent results and, in addition, the use of displacement incrementation yielded the whole load-displacement curve for snap through buckling problems.

In 1973 Striklin et al [44] presented an assessment of the solution procedures available for the analysis of nonlinear systems. Attention was focused on computational and solution techniques. The accuracy and economy of each solution technique was evaluated as a result of applying solution procedures to circular plates and shells of revolution. Oran [45, (1973)] developed a tangent stiffness matrix for the analysis of geometrically nonlinear space frames based on the assumption of small strain but large rotations. The approach was based on the beam column theory.

Noor [46, (1974)] presented a mixed method (stiffness and flexibility) for the analysis of pin-jointed trusses with both geometric and material nonlinearities. The formulation involved member forces and joint displacements. The resulting nonlinear algebraic equations were solved by means of iterative techniques. Numerical examples of plane and space trusses with geometric and material nonlinearities helped to prove the reliability and simplicity of applications.

In 1975 Jagannathan et al [47] presented a nonlinear finite element method based on a Lagrangian formulation in which linearly elastic truss elements were considered and the importance of the higher order terms in the strain displacement relationship was stressed. A Newton-Raphson method was used to solve the system of nonlinear equations with convergence criteria based on the displacements. An approximate method to derive the critical snap-through load was also considered.

The computational capabilities of a general type method, which was previously developed by Oran [45] was the subject of investigation by Oran and Kassimali [48, (1976)]. The method could use either Eulerian or Lagrangian coordinate systems. Extensive numerical studies were carried out on a group of simple structural systems. The method was claimed to be practical and accurate.

In 1977 Wood and Zienkiewicz [49] presented a geometrically nonlinear analysis of elastic inplane skeletal structures in a Lagrangian coordinate system. A continuum approach was adopted with paralinear isoparametric element. Displacements and rotations were unrestricted in magnitude. A Newton-Raphson iterative method was used for the solution of the nonlinear equilibrium equations and some examples were given. The derivation was extended to include axisymmetric structures.

The paper by Kiciman and Popov [50] in 1978 considered, first, the problem of the calculation of the critical loads and second, the problem of overcoming the singularity of the critical point to trace the post-buckling path. Eigenvalue and determinant approaches were discussed for the first problem, and a perturbation technique, where the Eigenvector of the singular tangent stiffness matrix could be used as perturbation on the displacement vector, was suggested for the second. Numerical examples were given of cylindrical shells. Another much more efficient approach for overcoming the point of singularity where an incremental approach was adopted, was given by Riks [51, (1979)]. A major characteristic of this method was the use of the length of equilibrium path as control parameter. A modified version of the Riks approach was given later by Crisfield [52, (1981)] and this was applied in conjunction with a Newton-Raphson method in both the original and accelerated forms. The modified method is more suitable for use with the finite element method. Mohr and Milner [53, (1981)] compared the fictitious load approach developed for prismatic beam elements by Kohnk with the general procedure outlined by Zienkiewicz. The two methods produced identical results with problems involving only axial strain, but with problems involving flexural effects the general method performed poorly. A means by which large displacements may be taken into account in the evaluation of flexural strains, was proposed in this paper; this was required to enable an improvement to be made in the performance of the general procedure.

In the same year, Papadrakakis [54] presented a study on the application of the large deflection behaviour of space structures.

The dynamic relaxation and the first order conjugate gradient do not require the computation of a tangent stiffness matrix. It was shown that these methods, combined with the basic element force deformation relations based on the conventional beam column theory, provided a reliable method in studying the post-buckling behaviour of space structures. Numerical examples were used for the comparison with previous results.

Although the above listing is not complete, it can be seen that methods of analysis of geometrically nonlinear problems are numerous and the trend is that the latest publications were more concerned with efficiency in storage requirements and computer time.

3.3.3 SOLUTION OF NONLINEAR EQUATIONS

The two basic types of techniques used to solve the system of nonlinear load-displacement equations are incremental and iterative. A combination of the two techniques is also used where at each load increment iterations are carried out to ensure equilibrium.

A. Incremental Techniques

(a) **Load Increment.** In this technique the load is applied in small increments and the resulting displacement is obtained. Each increment is considered linear with the stiffness coefficients evaluated at the beginning of each load increment. An example of one degree of freedom is shown in Fig (3.2)A.

(b) **Displacement Increment.** This technique is used mainly to overcome problems associated with limit points (snap buckling) or where the load displacement curves have a flat section with multiple equilibrium states corresponding to a prescribed load level. The load increment technique does not yield a solution in these conditions. A solution represented a single degree of freedom is shown in Fig (3.2)B.

When utilizing this method, the solution tends to drift away from the real curve, and to reduce this drift, smaller load or displacement increments have to be used.

B. Iterative Techniques

(a) **Newton-Raphson.** This is a direct solution of the nonlinear equilibrium equations where at a prescribed load level iterations are carried out. To explain this technique a single degree of freedom is considered, Fig (3.2)C. Suppose that the load applied is P_A. The solution sought is the displacement D_A. The tangent stiffness matrix is evaluated at the origin K_0 and the following equation is solved:

$$K_0 \ (\Delta D_1) = P_A \qquad \ldots\ldots 3.25$$

The first solution estimate is $D_1 = \Delta D_1$. The next iteration uses the tangent stiffness matrix K_1 evaluated at point 1 to enable a solution ΔD_2 to be obtained for the out of balance force $P_A - P_1$,

$$K_1 \ (\Delta D_2) = P_A - P_1 \qquad \ldots\ldots 3.26$$

The second estimate of the solution $D_2 = D_1 + \Delta D_2$. The iterations are repeated until convergence is achieved.

(b) **Modified Newton-Raphson.** This method is similar to the previous method except that the tangent stiffness matrix is not formed during the iterations; Fig (3.2)D illustrates the technique for a single degree of freedom system. It will be seen that this method requires more iterations to enable convergence to be achieved, but the expensive operation of forming and triangulaizing the stiffness matrix in each step is avoided. It is important to mention that there are various techniques to improve and accelerate convergence.

(c) **Riks and Modified Riks (arch length).** This method is used in conjunction with Newton-Raphson and Modified Newton-Raphson methods and it is characterized by having an extra constraining equation.

This extra constraint prevents the iterations from diverging at limit points.

Fig (3.2)E & F illustrate the application of this procedure to the solution of a one dimensional problem. Riks used the normal to the tangent whilst in the modified version presented by Crisfield [29], the circular path was used for a problem with N displacement variables. The following constraint equation is added to the usual N equilibrium equations:

$$\Delta P^T.\Delta P + \Delta\lambda^2\ qq^T = \Delta l^2 \qquad \ldots\ldots\ 3.27$$

ΔP is the incremental displacement vector and q is the total applied loading vector. The scalar λ is the loading parameter while Δl fixes the length of the increment in the N+1 dimensional space. In this method a load increment is applied and during the iterations the value of load increment is altered to satisfy the constraining equation. The dotted line in Figs (3.2)E & F represent the constraining equation.

3.4 COMPUTER PROGRAMS FOR THE GEOMETRICALLY NONLINEAR ANALYSIS OF SKELETAL SYSTEMS

3.4.1 THE COMPUTER PROGRAMS

The linear and nonlinear static analysis program for skeletal systems was developed to enable a research program to be undertaken into the response to loading of skeletal structures manufactured from pultruded tubular fibre reinforced polyester members. In this program the following assumptions are made:

(1) A perfectly linear elastic material behaviour up to failure.
(2) Small strains but large displacements.
(3) Constant cross section with double symmetry about the principle axis.
(4) Torsional stiffness completely uncoupled to bending and axial stiffness.

(5) Shear deformations are neglected.
(6) Only limit point instability is dealt with.

As the whole load deflection curve is of interest, an incremental solution scheme with iterations at each load step was required, thus avoiding drifting from the real equilibrium path and also enabling the critical point to be dealt with, the latter being of greater importance than the former. The modified Riks method in conjunction with modified Newton-Raphson method was used.

The nonlinear element stiffness matrix was derived analytically and took into account axial strain only. The stiffness matrix, the derivation of which will be discussed later, consists of three parts, which are:

(a) The elastic linear matrix K_E.
(b) The initial stress matrix K_σ which is dependent upon the element internal stresses.
(c) The initial displacement matrix K_δ which is a function of element nodal displacements.

In the case of structures in which the loss of stability occurs by bifurcation buckling, as is the case in double-layer grids, a set of imperfections are introduced to degenerate the behaviour to a limit point type behaviour. A multiple of the Eigenvectors of the singular tangent stiffness matrix is used to introduce imperfections and for this purpose another computer program was developed. This program is based on small displacements where K_E and K_σ were used to establish the Eigenvalue problem. The smallest Eigenvalue and the corresponding Eigenvector, which represent the first buckling mode of the structure, were usually derived and used. However, other Eigenvalues and Eigenvectors could also be considered. This second program can be used to determine the first buckling of stiff types of space structures. This program is very simple and there is no need to discuss it; however, a flow chart is shown in Fig (3.3). The flow chart of the main geometrically nonlinear analysis program is shown in Fig (3.4). The steps and methods of assembling the overall stiffness

matrix, implementing boundary conditions are standard and are described in many text books; Refs [55] and [56]. All load increments, other than the first, are obtained from the magnitude of the previous load increments and the number of iterations which are required to achieve convergence. The higher the number of iterations within a load increment the smaller the successive load increments. The convergence criterium in this program is based on the ratio of the norm of out of balance forces to the norm of the applied load. This value and the maximum number of iterations are specified according to the problem, degree of accuracy required, etc.

For the solution of the linearized system of equations the modified Chelosky method is used, where the factorization of the stiffness matrix takes the form

$$K = LDL^T \qquad \ldots\ldots 3.28$$

The sign of the elements of the diagonal matrix D shows when the stiffness matrix ceases to be positive definite, and in that case the load increment is applied with a negative sign.

The program deals only with conservative loadings applied to the nodal points. A discretization of the member is required for structures having highly nonlinear behaviour. The program makes use of the active column (skyline) storage technique, Ref [57] and [58], which minimizes storage requirements and it is possible to use fixed or updated Lagrangian-SR coordinate systems.

3.4.2 DERIVATION OF THE STIFFNESS MATRIX

The derivation of the element stiffness matrix is based on the following strain displacement relationship:

$$\varepsilon_x = \frac{du}{dx} + \frac{1}{2}\left[\left(\frac{dv}{dx}\right)^2 + \left(\frac{dw}{dx}\right)^2\right] - Y\frac{d^2v}{dx^2} - Z\frac{d^2w}{dx^2} \qquad \ldots\ldots 3.29$$

This represents the longitudinal strain at a coordinate point (X, Y, Z) where u, v and w are displacements in X, Y and Z directions of a generic point on the member axis.

A linear displacement function in X was chosen for u and a cubic function in X for both v and w, which means that loads can only be applied to the nodal points, since this assumption restricts the member to carrying only constant shear, and linearly variable bending moment.

$$u = a_0 + a_1 x$$

$$v = a_2 + a_3 x + a_4 x^2 + a_5 x^3$$

$$w = a_6 + a_7 + a_8 x^2 + a_9 x^3 \qquad \text{..... 3.30}$$

The above coefficients are derived from boundary conditions and are expressed as functions of nodal displacements. Substituting the expression for displacement in the strain displacement relationship, we obtain:

$$\varepsilon_x = F(U_A, V_A, \ldots, \theta_{BY}, \theta_{BZ}, X, Y, Z) \qquad \text{..... 3.31}$$

The strain energy of the element caused by a load increment is given by:

$$U = \iiint \left[\int_{\varepsilon_0}^{\varepsilon_0+\varepsilon_x} \sigma \, d\varepsilon \right] dx dy dz$$

$$= E \iiint \left[\int_{\varepsilon_0}^{\varepsilon_0+\varepsilon_x} \varepsilon d\varepsilon \right] dx dy dz$$

$$= E\,\varepsilon_0 \iiint \varepsilon_x \, dx dy dz + \frac{E}{2} \iiint \varepsilon_x^2 \, dx dy dz \qquad \text{..... 3.32}$$

where it is assumed that the member was in a deformed state, which is denoted by ε_0, before the load increment.

A substitution of ε_x from 3.31 in the strain energy expression 3.32, integrating and making use of Catiglian's theorem to derive the coefficients of the stiffness matrix leads to:

$$K_T = K_E + K_\sigma + K_\delta$$

A linear twist rate is assumed and the relation is added to the element stiffness matrix.

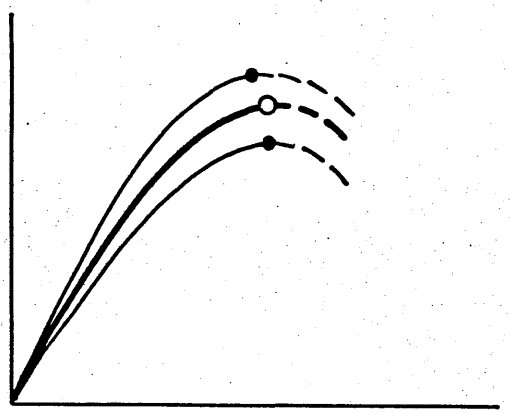

(a) Limit Point

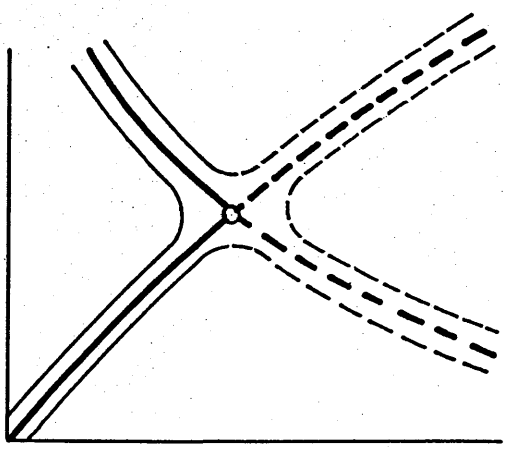

(b) Bifurcation asymmetric Point

——— Perfect stable system

– – – Perfect unstable system

——— Imperfect stable system

– – – Imperfect unstable system

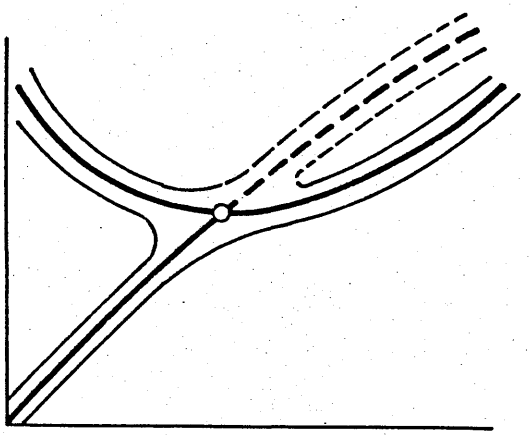

(c) Bifurcation stable-symmetric Point

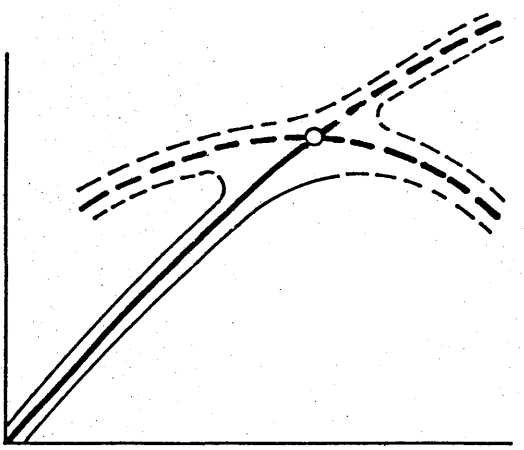

(d) Bifurcation unstable-symmetric Point

Fig (3.1) Equilibrium paths of perfect and corresponding imperfect systems in the vicinity of critical points

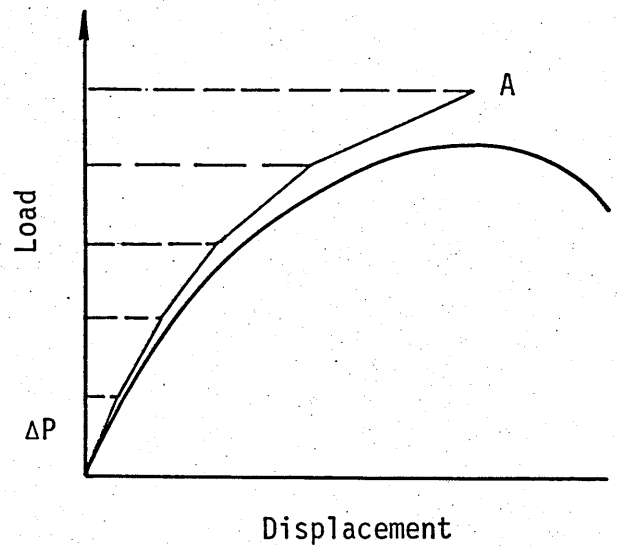

A - Load increment

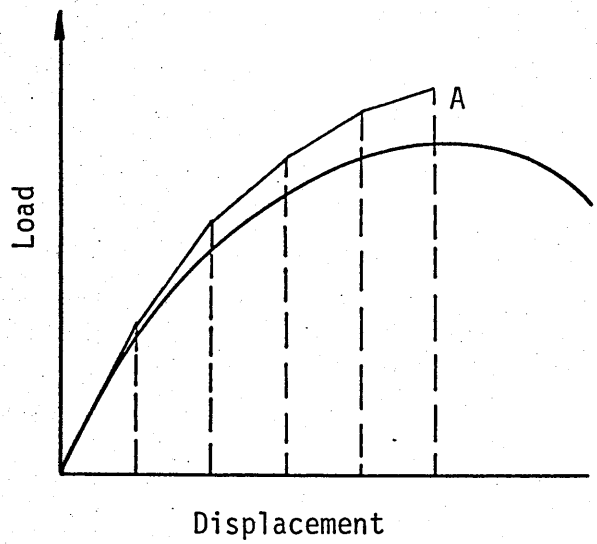

B - Displacement increment

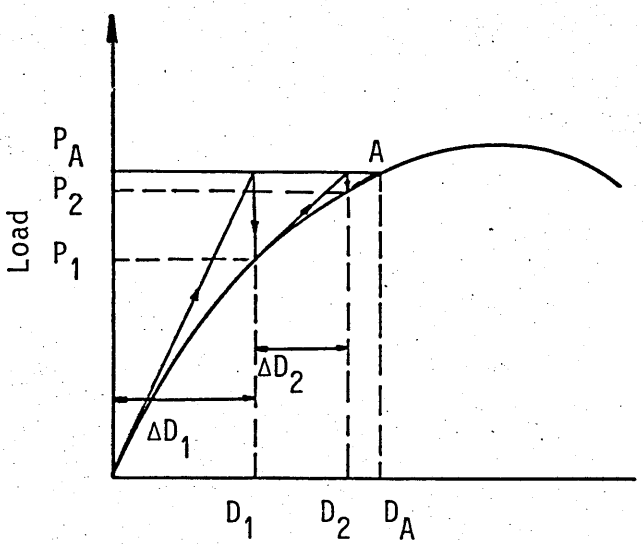

C - Newton Raphson

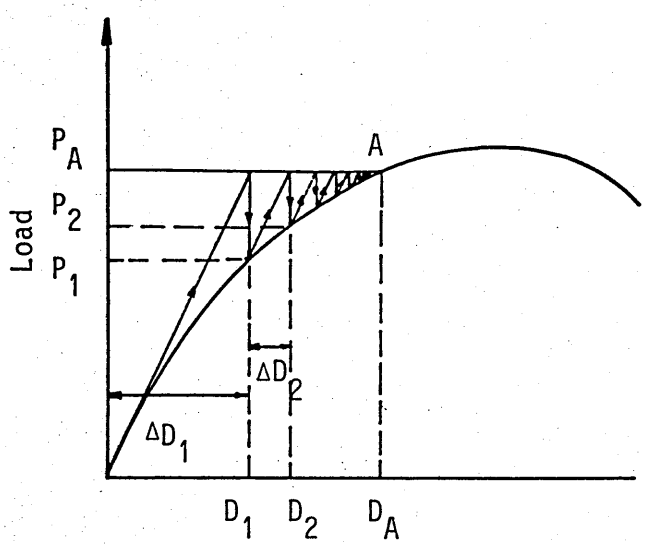

D - Modified Newton Raphson

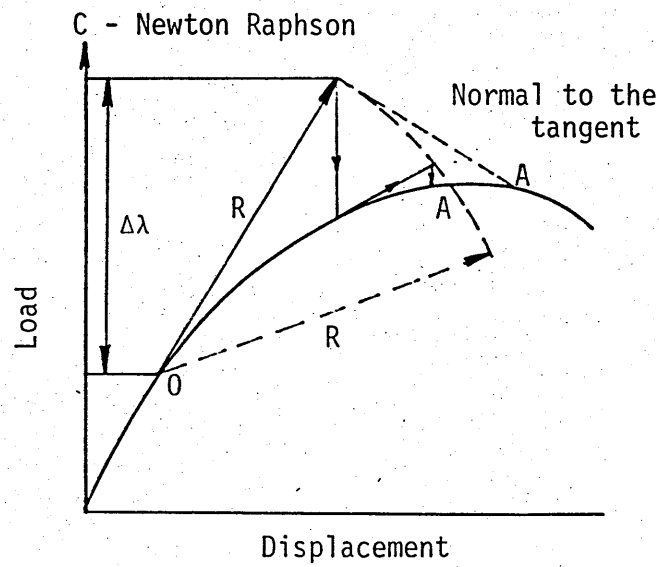

D - Arch length (with NR)

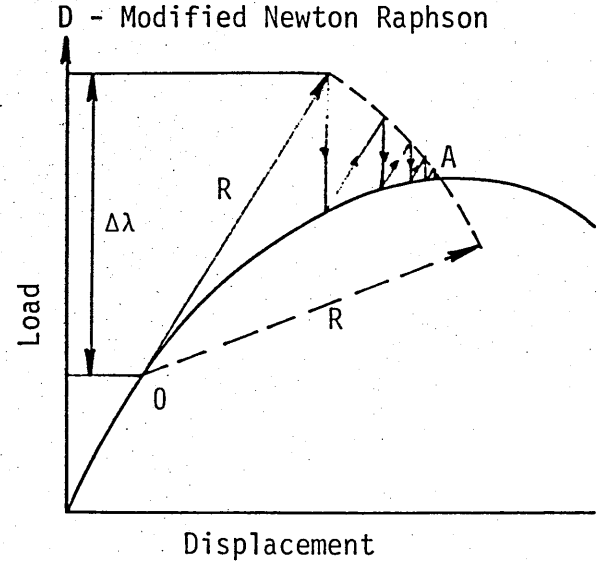

E - Arch length (with mNR)

Fig (3.2) Schematic representation of numerical solutions of nonlinear equations

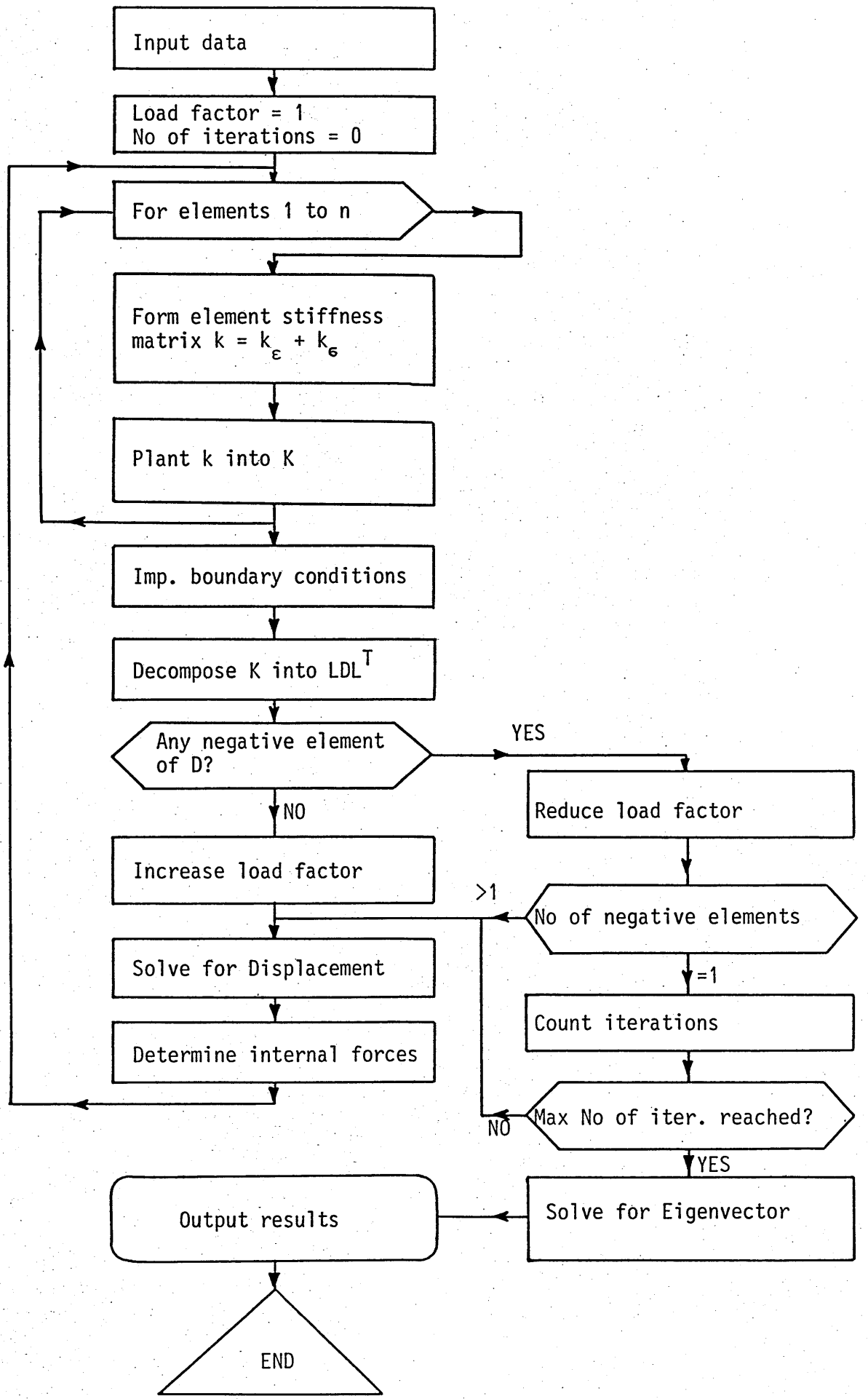

Fig (3.3) Flow chart of the first buckling analysis computer program

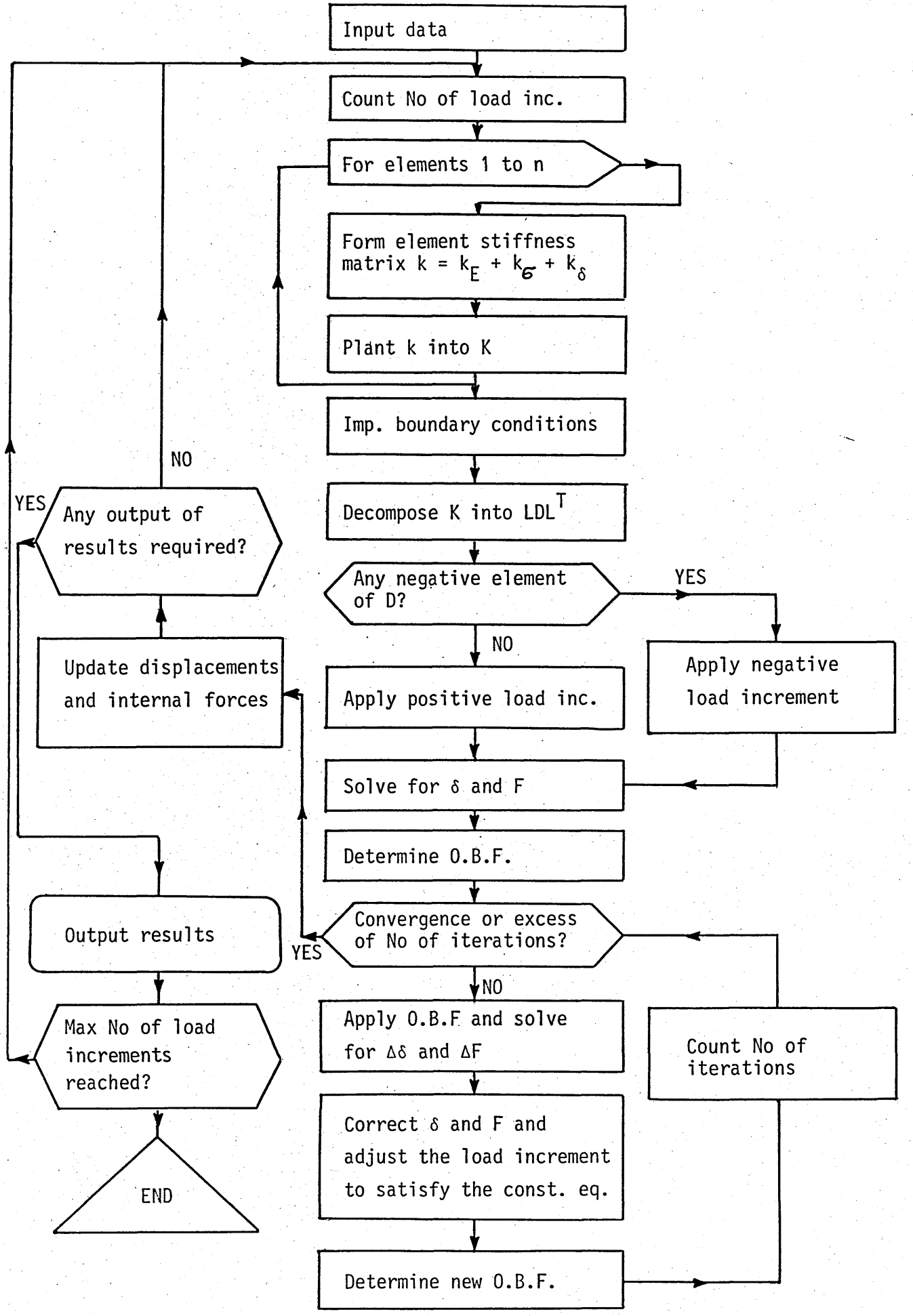

Fig (3.4) Flow chart of the nonlinear analysis computer program

CHAPTER FOUR

STIFF SKELETAL STRUCTURES IN PULTRUDED F.R.P.

4.1 INTRODUCTION

Double-layer grids are an example of stiff space structures which are characterised by small deflections and large internal stresses. The applied loads are carried mainly by axial force; shear, bending and torsion are very small in the members.

The systems have an international appeal and over the years many have been designed and constructed using a variety of configurations and joining methods [59]. The success achieved by these structures is due to several factors, such as their pleasing visual appearance, ease and fast production and erection, the characteristic of covering large spans with no internal supports and economy. The two factors that in the past affected the economy of such systems were the cost of analysis and the cost of the node joints. With the development of computers, the first factor does not now present a problem, and the second factor has been solved quite successfully for steel and aluminium structures.

The pultruded fibre/matrix composite tube material, although generally of lower modulus of elasticity than that of steel, is believed to be suitable for use in the manufacture of skeletal systems for medium to short span structures. One great advantage of this material is that the reinforcement fibres can be positioned in the composite to enable the most efficient use of the two component materials. There is, however, difficulty in the joining of pultruded tubes together at nodal points where the members meet at different angles. Just recently the development of two or three systems, Ref [1] and [44], have been reported and it is now possible to fabricate skeletal systems manufactured from pultruded tubes.

The structural performance of any pultruded member can be up-graded by the use of hybrid fibres and the percentage ratio of high to low modulus fibres can be varied to provide the required properties. One particular

type of these members, which have been discussed previously, will be discussed in connection with double-layer grids.

The use of pultruded fibre reinforced members manufactured in the form of double-layer grids is discussed in this chapter. The results obtained from the theoretical linear and nonlinear analysis and the testing of short and long span large scale experimental models are compared.

A further theoretical parameter study based on first buckling analysis is discussed to provide more information on the combination of more than one type of composite members.

4.2 SMALL SPAN MODELS

4.2.1 THE MODEL STRUCTURES

Two structures were analysed, one an all glass reinforced polyester system and the other a g.r.p./c.g.r.p. system.

The Glass Reinforced Plastics System (1A)

The model is a skeletal double-layer grid system of the type square on square and has rigid joints. The grid system consists of four basic pyramidal units each having a square base, with 1 metre length members manufactured from glass reinforced plastics (g.r.p.); the inclined members (diagonals) also are 1 metre in length. The apices of the four units are connected by similar pultruded members. Plate (4.1) shows a photograph of the model.

Figure (4.1) shows the member configuration, the member discretization and the joint numbering system. The thick full lines represent members adjacent to the nodal points which have increased stiffness parameters. This modification of the properties of the members enables the effect of the stiff nodes to be included in the computation.

The skeletal members have been manufactured from pultruded g.r.p. tubes with a fibre/matrix ratio by weight of 60%/40% respectively. The outside

diameter of the tubes was 25.4mm and the wall thickness was 2mm.

The nodal joints of the bottom members of the skeletal structure were made by crimping and bonding aluminium tube onto the ends of the g.r.p. tubes; the internal diameter of the aluminium tube was 29mm, the wall thickness was 3mm and the crimped length was 70mm. The aluminium ends were then threaded and finally screwed into the aluminium node joints. The nodal joints are made of aluminium block machined to sizes and shape and provided with the threaded holes in the right location with the required oreientation to accommodate the members. Plate (4.2) shows the eight skeletal members of the central aluminium nodal joint. The top nodes of the space structure were manufactured by means of a mould which was made from plaster and silicon rubber. It was formed in two halves round a prototype node made in the Department of Civil Engineering Workshop. Polyester resin and glass fibre were used to form the nodes. These nodes were spherical and hollow with openings moulded into them to receive the skeletal members. The spheres were then filled with epoxy resin to form the bonded joint. The manufacture of these nodes was undertaken so that any of the skeletal members could be replaced if they failed during a test. Plate (4.3) shows the detail of this joint.

The g.r.p./c.g.r.p. System (1B)

A geometrically similar model to the above was also tested. This structure had all members made from pultruded g.r.p. except for the four external corner diagonal members which were made from a hybrid composite (c.g.r.p.) of carbon fibre/glass fibre/polyester resin with percentage by weight of 30/30/40. The external diameter and wall thickness of the composite members were the same as the g.r.p. pultruded tubes but the stiffness of the former composite was three times that of the latter.

The double-layer grid was assembled by screwing the bottom layer members into their respective joints. In order to achieve this, three parallel adjacent members had a left handed screw thread at one end and a right handed screw thread at the other. The inclined members were then screwed into the bottom nodal joints and the other ends, together with the top horizontal grid members, were positioned in the top nodal points. Before

bonding, the internal surfaces of these nodes and the members entering them were separated by a polythene sheet; the sphere was then filled with epoxy resin.

4.2.2 TESTING OF THE MODELS

(a) Support Conditions

The two skeletal structural systems were supported at the bottom four extreme corner nodes on ball bearings in order to allow horizontal displacements and rotations about any axis at these nodes caused by deformations of the structures. Four steel plinths fixed to the floor were used to sustain the structures and to raise their level to allow for the displacement transducers to be placed, as well as providing space for deflection of the system to take place.

(b) Loading

The top four nodes were loaded by means of hydraulic jacks through a circular steel plate, in order to distribute the stresses evenly and prevent any local damage to the g.r.p. nodes, and spherical bearings in such a way that the loads were applied through the centre of the node joint. The hydraulic pressure was applied by means of an electric hydraulic pump and the magnitudes of loads were monitored by load cells in series with the hydraulic jacks.

(c) Instrumentation

Selected members of the skeletal structure were strain gauged, with metal foil strain gauges of 120 Ohms resistance and having a gauge factor of 2.09, to enable axial and bending strains to be measured. At each point three gauges were used and were spaced equally around the member. Certain symmetric members were gauged to enable checking of imperfections in the system which are unavoidably introduced during manufacturing and assembly of the various components of the model.

Stoke potentiometric transducers were used to measure the vertical displacements at nodal points 5, 26, 50 and 55 (Fig 4.1). The strain, displacements and load values (through load cells) were recorded by means of a data logging system.

(d) Testing Procedure

Initially structure 1A was loaded in the linear range in increments of 0.5kN per node up to a maximum load of 3kN, after which the load was removed. A final test was undertaken during which the structure was loaded beyond the linear range with smaller load increments until failure of one of the members occured; in this case it was one of the external corner diagonals. The failure of model 1A is shown in Plate (4.4) and a detail of the failed member is shown in Plate (4.5). After this test, the structure was dismantled and any member which had been subjected to high internal stresses was replaced and structure 1B was assembled.

The test of structure 1B followed the same cycle as structure 1A and the strains and displacements were recorded. As in the previous structure, failure occured in one of the corner diagonals.

(e) Possible Sources of Imperfections in the Models

Although a great deal of care had been taken in the fabrication and assembly of both the models, imperfections did exist and the experimental results verified this.

Some of the possible sources of imperfections are stated below:-

(i) Due to the method of fabrication a maximum of 0.5mm error in the nodes was possible.

(ii) A small variation of wall thickness in some pultruded tubes could have existed.

(iii) Some members may have had initial curvature.

(iv) In the fabrication of such skeletal structures it is

inevitable that some lack of fit in the system will occur.

(v) Due to frictional effects on the hydraulic jacks the load applied to the top four nodal joints were not exactly equal.

(f) Stiffening Effects of the Nodal Joints

In conventional steel space structures the effects of the nodal joints on the stiffness of members is usually negligible and the actual length of the member is taken as the distance between the centres of the nodes to which the member is joined. If the members are manufactured from a relatively low modulus material the joints and end fixings do have an effect on the flexibility of the structure and it should be taken into account in the analysis of such a skeletal system. The effects can be incorporated in the analysis by having short stiff members connecting the centre of the node to a nodal point where the member and node surface meet.

4.2.3 THE THEORETICAL ANALYSIS

A linear analysis and a nonlinear analysis were undertaken on the fibre/matrix space structures 1A and 1B. The two analyses were performed in order to compare them with the actual performance of the structures. Attention was focussed on the accuracy of the nonlinear analysis to predict the behaviour of both structures up to failure. In addition, the effects of certain imperfections on the behaviour and on the value of the ultimate load were investigated.

The nonlinear method, which was fully discussed in Chapter 3, takes only geometric nonlinearity into account. This is fully justified as the material from which the space structures were manufactured, has a linear stress-strain characteristic to failure.

This computer program has been written for the solution of structures which only have a limit point behaviour. Therefore, for these structures it is necessary to introduce imperfections in

order to degenerate their behaviour from a bifurcation mode to a limit point one. Any attempt in using the perfect geometry with this program will result in a breakdown of the computation at the first bifurcation point. The procedure here is to use a linear stability analysis in order to obtain the buckling mode (Eigenvector) corresponding to the smallest buckling load, and introduce geometric imperfections proportional to this buckling mode. Other buckling modes on random imperfections could be used to produce asymmetric behaviour. Another imperfection introduced in the analysis of these structures was eccentricity given to one of the top four nodes.

4.2.4 RESULTS AND DISCUSSION

In the following results, the load factor is a function of the load on any one nodal joint.

Figures (4.2), (4.3), (4.4) and (4.5) show the relationship between the load factor and deflection for the analytical and experimental solutions of models 1A and 1B for the four joints 5, 26, 50 and 55 respectively. The stiffening effect of the nodes was taken into account in the analysis. It will be seen that the behaviour is linear up to about 80% of the ultimate load. For external loads in excess of this value a nonlinear relationship exists to a point at which the structure is incapable of taking further load and commences to deflect excessively. Throughout the loading cycle the experimental and theoretical nonlinear analyse results compare favourably.

For both models, graphs have been drawn for different degrees of imperfections, two of which have been considered. The first, is an initial curvature compatable with the first buckling mode, as previously mentioned, and given to the members of the structure with variations in maximum deformation of 0.1 to 1.0mm and the second, is an eccentricity of 2mm at the top node of the system. The effects of these imperfections are clearly shown in Figures (4.2), (4.3), (4.4) and (4.5). It is noticeable that the former

imperfections did not have any appreciable effect on the results of the linear analysis and only the latter imperfection produced slightly different behaviour.

A point of interest, obtained from the theoretical nonlinear analysis, is the effect of imperfections on the ultimate load. For the most severe conditions considered in the present investigation (i.e. a type 1 imperfection of maximum deformation of the curved member equal to 1.0mm and a type 2 imperfection with eccentricity of 2mm at one of the top nodes) there is a reduction in ultimate load of about 3.9 and 3.6 per cent of the smallest imperfection considered (i.e. 0.1mm for models 1A and 1B respectively).

An investigation was undertaken into the accuracies caused by ignoring the stiffening effects of the nodes and end fixings. In order to do this the two models were analysed again, without considering the stiffening effects and using the same material properties and imperfections as far as the previous analyses. Figure (4.6) shows the load factor plotted against the central joint displacement where an ultimate load reduction for models 1A and 1B of 21.3 and 12.6 per cent respectively are obtained.

Although great care was exercised in the fabrication and assembly of the models, symmetric deformations, especially at high load levels, were not obtained. Figure (4.7) shows a plot of the load against vertical displacement of two symmetric nodes (viz 5 and 50) for model 1A. The difference between the two readings is in excess of 20% immediately before failure.

In double-layer grids it is well known that axial forces are the predominant member loadings and consequently, only axial forces are considered here. Figures (4.8) to (4.13) show relationships between the load factor and axial force in the most highly stressed members of models 1A and 1B; each plot contains the results of the linear and nonlinear analyses as well as the experimental solution. The latter results apply to symmetric members.

There is very little difference between the results of the linear and nonlinear theoretical analyses under the applied loads below 80 per cent of ultimate value, and indeed above 80 per cent of ultimate value of difference is small.

Imperfections had no noticeable effect on the internal forces of those members which were highly stressed but did have an effect on the members which were under low internal stresses. The reason for this is that only imperfection in the highly stressed members results in very small changes in their internal forces, but to balance these changes large relative forces are imposed on their neighbouring members which have only a small stress imposed by the external loads. One such example is shown in Figure (4.14) where the maximum axial force imposed by the external loads on the structure is less than 1 per cent of the highly stressed member meeting at the same node.

4.3 LARGE SPAN STRUCTURES

4.3.1 THE MODEL STRUCTURES

The decision to test longer span models was made for two reasons:

1) As the mode of failure of the two small span models was caused by shear effect, failure occured in diagonal members in both models. For practical double-layer grids, bending effects are usually predominant with the result of possible failure of top or bottom layer chord members for load acting vertically downwards and upwards respectively.

2) The small span might have magnified or minimized certain characteristics of the model tested.

Two large span structures were analysed in a similar way to the previous models. The first one was all glass reinforced polyester and the second a g.r.p./c.g.r.p. system.

The Glass Reinforcement System

The model is a rigid jointed double-layer grid of the type square on square. The basic pyramidal units are identical to those of the previous two models. All members are manufactured of g.r.p. and were 1 metre long. This structure is 4 metres long and 2 metres wide with 12 aluminium nodes at the bottom layer and 8 g.r.p. nodes at the top layer. A photograph of the model is shown in Plate (4.6).

Figure (4.15) shows the member discretization and joint numbering system. The full lines represent the bottom layer members, the dashed lines the top layer members and the dotted lines the diagonal members. The stiff members representing the nodal points are not shown for the sake of clarity but they are assumed to connect the centre of the node with the neighbouring nodal points.

The skeletal members, bottom nodes and top nodes, are all similar to those of the previous models 1A and 1B. Only top members entering the spherical top nodes were separated from the nodes by a polythene sheet to allow replacement, whilst the diagonal members were embedded in the epoxy resin after putting a pin through them to improve their bonding. This pin is an additional item to the arrangement adopted in models 1A and 1B because the preliminary analysis showed that some of the diagonals in this model will go into tension.

The g.r.p./c.g.r.p. System (2B)

This model is geometrically identical to model 2A with all members made from pultruded g.r.p. except for the two top central longitudinal members which were made from pultruded c.g.r.p. with carbon fibre/glass fibre/polyester resin with percentage by weight of 30%/30%/40%. The geometric properties of these members are identical to the g.r.p. pultruded members but, their axial stiffness is about three times that of the g.r.p.

The same procedure of assembly was adopted as used in the previous models. A left handed screw thread at one end of a member and a right handed thread at the other end were used for certain bottom layer members to allow the bottom layer grid to be formed. Top nodes were filled with epoxy resin after completing the assembly and checking the geometry of the structural system. Great care was taken to minimize imperfections and any possible lack of fit at this critical stage.

4.3.2 THE MODELS TESTING

(a) Support Conditions

The two large span models were supported at the bottom four extreme corner nodes (nodes no. 1, 9, 207 and 215). Four ball bearings were used to allow the rotation of the nodes about any axis. One of the nodes was position fixed, a second was fixed in two directions only and the other two were free in the horizontal plane. These constraints prevented any rigid body movement and allowed any displacement of the constrained nodes as a result of structural deformation caused by applied loading. Four steel plints bolted to the laboratory floor were used to support the two models.

(b) Loading

The same loading arrangement was used for the previous models 1A and 1B consisting of four hydraulic jacks, the electric hydraulic pump and the four load cells for load level monitoring was adopted. The top four central nodes were loaded through circular steel plates and ball bearings. Attention was given to the hydraulic system to ensure even pressure and avoid overloading any one of the four nodes. The load cells were carefully calibrated against a proving ring by loading the two in series in the Instron testing machine.

(c) Instrumentation

Fifteen members of each model were strain gauged. For each member three strain gauges were used and were spaced equally around the member. The strain gauges were electrical resistance metal foil ones with gauge factors of 2.09 and resistance of 120 Ohms. Out of the fifteen members strain gauged, four pairs were symmetric members.

The vertical displacements of nodes 5, 31, 55, 60, 84, 103, 108, 113 and 156 for both models were measured by means of stroke potentiometric transducers.

(d) Testing Procedure

Both structures were tested in the same identical manner. An initial testing under a relatively low load was necessary to check the instrumentation, to assess the behaviour of the model in the linear region and ensure that everything was in order before proceeding with the final testing of the structures up to failure. The theoretical analysis was carried out before testing, and here it is discussed subsequently to the experimental testing. It was found more convenient to perform the analytical analysis first so that the behaviour of the structure and its failure load could be predicted for the experimental model and hence, if necessary, to adjust the loading increments, especially near to the ultimate load.

The readings were recorded on a punch tape by means of a data logger. The instruments were connected to the channels of the data logging system such that the load cells readings were scanned first, those of displacements transducers second and finally, the readings of the various strain gauges were scanned. This arrangement was used so that in case of a sudden failure, which was expected with these types of structures, the important readings were recorded first.

The first model testing led to a sudden failure of one of the top central longitudinal members (member 84-137). Plate (4.7) shows the failure model (2A). The buckled member did not undergo large deformation before failure and the mode of failure of the member was similar to that of model 1A.

The same procedure used in testing model 2A was followed in testing model 2B. Failure in this model was sudden with two members failing simultaneously. These two members were member numbers 79-132 and 137-190, the former was made of c.g.r.p. and the latter of g.r.p. The failure of model 2B is shown in Plate (4.8).

The experimental results, obtained on the punch tape, were transfered to the University main computer (Prime 750) where a routine was written especially for processing the experimental data. This data was combined with the theoretical analysis results and two forms of output could be obtained: tables or graphic plots.

4.3.3 THE THEORETICAL ANALYSIS

The linear and nonlinear analyses of the models 2A and 2B were undertaken using the two programs developed for this research work; these are discussed in Chapter 3. The same steps as those used for the analysis of models 1A and 1B were followed here. Geometric imperfections proportional to the first buckling mode had to be introduced because of bifurcation buckling characteristic of these structures. No other imperfections were considered. The node stiffening effect was dealt with in the same way as discussed previously. Only three theoretical (linear and nonlinear) analyses were undertaken for each model. These correspond to three deformed shapes with factors of 0.5, 1.0 and 2.0 used with the first buckling mode.

4.3.4 RESULTS AND DISCUSSIONS

The load-deflection curves of the seven nodes 5, 31, 55, 60, 84, 108 and 113 are shown in Figures (4.16) to (4.19). The experimental and theoretical analyses results for both models 2A and 2B were plotted on the same graph so that direct comparison can be made. The results of the theoretical analysis, shown in these figures, are of the models with three degrees of imperfections. The imperfections being an initial member curvature compatable with the first buckling mode with a maximum member deformation of 0.5, 1.0 and 2.0mm. These imperfections had similar effects on both models. The linear analysis was hardly affected, as for the nonlinear analysis, it can be seen that the larger the imperfections the higher the degree of nonlinearity and, at the same time, the lower the ultimate load. The difference in the values of ultimate load between the smallest and largest imperfections considered here is of about 3.6% for model 2A and 3.5% for model 2B.

The behaviour of the two models was linear almost up to failure load where the nonlinear relationship starts to curve, becoming nearly horizontal. Due to the fact that any small increase of load in this region results in a large deformation, only a small number of experimental points were obtained before the sudden failure.

All figures show that the load-deflection nonlinear curves compare favourably with the experimental results, when the general behaviour and the ultimate level (flat horizontal section of the nonlinear curve) are predicted with good accuracy.

A point of interest here is that, although the model 2B varied from that of model 2A by the two hybrid members only, the former model had a much greater stiffness and a much increased failure load over that of the latter. The respective failure loads per node were 4.28kN and 3.2kN.

The experimental deflections of the two symmetric nodes 60 and 156 for both models are shown in Figure (4.20). It will be observed that, for both models, the deflections of node 60 are always greater than those of node 156, with a maximum difference of about 10%. Figure (4.21) shows the deflections of symmetric nodes 103 and 113, and it will be seen that the deflections of node 113 are greater than those of node 103. For the model 2A the difference consistently increased with the load, where the maximum difference, of about 17%, was reached just before failure. For the model 2B the difference increased with load up to about 3.2kN per node (76% of ultimate load) where a sudden jump occured in the displacements of node 103. The sudden increase in displacements of the node brought the value of displacements for those two symmetric nodes closer together until just before failure, at which point the difference reached a value of about 23%. The sudden increase in displacements had little effect on other displacements of nodes and internal forces of members.

The load-axial force relationship in the most highly stressed members of the double-layer grid models 2A and 2B are shown in Figures (4.22) to (4.27). The results of the theoretical linear analysis and nonlinear analysis as well as the experimental results of the models 2A and 2B are plotted on the same graph. As the axial forces of the theoretical analyses of the models with the different degree of imperfections are almost identical, only the graphs with maximum imperfections are plotted.

There is very little difference between the linear and nonlinear theoretical analyses results under the applied loads up to almost the failure load and only in the last section (of about 10% of the total length of the curve) was there any difference and there the maximum value did not exceed 10%. Furthermore, the difference between the axial forces of the two models, at any load level, was insignificant.

The results of the experimental and theoretical analyses compare favourably, with good agreement fo certain members (viz Figures

(4.22), member 60-84, Figure (4.23), member 9-31 and Figure (4.24) member 60-113), but for others the agreement is not as good. However, some of the experimental results of the symmetric members shown in Figures (4.28) and (4.29) may explain the reasons for the discrepancies in the results. These two figures show the axial forces at symmetric members. When the figures are observed in conjunction with Figures (4.20) and (4.21) a greater understanding of the imperfections within the models is obtained. These results show that the axial forces on the right-hand side of the longitudinal central axis of the model (containing node 113) were smaller than those on the left-hand side, whereas the deflections on the right-hand side were larger. This indicates a certain amount of twist in the model. All considered, it can be said that the results were satisfactory. Another important point to be mentioned is that in the nonlinear part of the load axial force, most of the experimental results tend to follow the theoretical nonlinear curves.

4.4 PARAMETER STUDY

4.4.1 INTRODUCTION

A simplified theoretical parameter study, based upon first buckling analysis was carried out on three skeletal configurations. The study which consisted of successive analyses of the three configurations involved two member types only, viz a pultruded g.r.p. and a pultruded c.g.r.p. (hybrid composite). The former consisted of 60/40 per cent weight of glass fibre/polyester resin and the latter contained 30/30/40 per cent by weight of carbon fibre/glass fibre/polyester resin. The mechanical properties of the two types of material were determined experimentally (Chapter 2). Both types of members had an external diameter of 50mm and wall thickness of 2mm. The three structural configurations analysed were initially assumed manufactured from g.r.p. members. The critical buckled members were determined and replaced by the stiffer c.g.r.p. members and the analysis was repeated.

Nonlinear analysis of the three structures of the square on square type was undertaken. The three structures consisted of the all g.r.p. and the two successive improved g.r.p/c.g.r.p. structures. The nonlinear analysis helped in assessing the validity of first buckling criteria used in this study as well as obtaining imformation about the post-buckling behaviour.

4.4.2 THE STRUCTURAL SYSTEMS

In the three double-layer grid systems which were investigated the bottom layer configuration and the height and spans of the structures were identical; they all had mansard edges and were simply supported along the edge of the bottom layer. The three configurations were:

(a) Square on square, system 1, which had a two-way top and bottom grid with diagonal bracings. All the members were 1 metre long and there were 144 and 188 members in the top and bottom layers respectively; there were 324 bracing members. The total length of the members in the structure was 698 metres. The configuration is shown in Figure (4.30).

(b) Diagonal on square, system 2, had an identical bottom layer and diagonal bracing configuration to that of type (a) but the top layer differed from that of system 1 in that it consisted of a diagonal configuration made up of 256 members, each of length $0.5\sqrt{2}$ metres. The total length of members for this structure was 717 metres. The configuration is shown in Figure (4.31).

(c) Three way on square, system 3, in which the top layer was a three way grid and consequently the diagonal bracing configurations differed from those of the previous two systems. The top layer consisted of 128 members of length $0.5\sqrt{5}$ metres, 84 members of length 1 metre and 8 members of length 0.5 metres. The total member length of the top layer was 231 metres and the total length of the members in the whole structure was 678.6 metres. The system is shown in Figure (4.32).

The type (a) system was chosen because of its simplistic configuration and ease of fabrication with all members having equal lengths. The choice of the other systems was based upon the first choice. The top layer of the first system was replaced, in the second system, by a higher density layer but the diagonals and bottom layers were unaltered. In the third system a high density layer was used compared with the second system but because of the difficulty in connecting the increased number of nodal joints in the top layer to the bottom, a modified diagonal arrangement had to be used. However, it must be stated that the geometry, the member lengths and the height of the grid systems, although practical, are not the optimum.

4.4.3 THE THEORETICAL ANALYSIS

The first buckling analysis program, details of which were given in Chapter 3, was used throughout this study to undertake successive analyses of the three systems. In these analyses, the smallest Eigenvalue is derived as is the corresponding Eigenvector, which represents the buckling mode of the structure. From this mode the critical members are readily obtained. These members are then replaced by stiffer c.g.r.p. ones and the process is repeated until buckling occurs in stiff members or for some other practical reasons.

Nonlinear analysis of three successively upgraded structures of type (a) was carried out. As has been mentioned previously, geometric imperfections are required to be introduced in order to be able to apply the nonlinear analysis computer program to these types of structures (Chapter 3). Eigenvectors associated with the first buckling analysis were used, where a maximum member deformation of 2mm was used. The relevant results of these analyses are displayed in a graph form.

All analyses assumed a uniformly distributed load acting over the whole area of the structure. The uniformly distributed load is converted to a system of loads which act on the nodes according to the area of influence around each node.

4.4.4 RESULTS AND DISCUSSION

Only a brief discussion of the results of the nonlinear analysis will be given as it is intended not to deviate from the main objective which is the improvement that could be achieved by combining the two types of members (g.r.p. and c.g.r.p.).

The load deflection curves of the nodes marked II to VIII of the first system, with all members assumed to be g.r.p. ones, are shown in Figure (4.33).

Three points may be observed:-

(1) The nonlinear load deflection curve is very close to the linear one up to buckling.

(2) The magnitude of the critical load obtained from the first buckling analysis is very close to the magnitude of load at which a change in stiffness occurs in the nonlinear analysis. At this point load increments become small as an indication of difficulty in convergence.

(3) The reduction in stiffness which has taken place after the first buckling indicates that buckled members were incapable of taking more load; however, the excess load was transmitted and distributed to adjacent members, thus making it possible for the structure to take more load.

Load factor-deflection curves for node II obtained from the nonlinear analysis of:

(a) system 1 with no c.g.r.p. members,
(b) system 1 with 8 c.g.r.p. members and,
(c) system 1 with 16 c.g.r.p. members,

is shown in Figure (4.34). These results confirm the points discussed above and indicate the increase in stiffness of the structure as a result of replacing the critical g.r.p. members with the stiffer c.g.r.p. The load factor in these two graphs represent the applied load/1.5kN per square metre.

The main discussion in this section is related to the first buckling loads in the three structures. For systems 1, 2 and 3 in which all members were assumed to be manufactured from g.r.p. pultruded tubes, the external loads applied to the structures to cause initial buckling were found to be 6.5kN/m^2, 9.4kN/m^2 and 9.8kN/m^2 respectively when these were applied vertically downwards. When, however, the external loads were applied upwards, the corresponding values for the three structures were 5.5kN/m^2, 5.4kN/m^2 and 4.58kN/m^2 respectively. These results indicate that, for a downward load, as the top member density increases the buckling resistance of the structure also increases but for an upward load the buckling load decreases. However, by replacing the critical g.r.p. member with a c.g.r.p. one the buckling resistance of the structural configuration is increased.

Structural System 1

(a)

(a) Vertically downward acting load

Figure (4.35) shows the relationship between the critical load and c.g.r.p. member length and it may be clearly seen that, as certain g.r.p. members buckle and are replaced by c.g.r.p. ones, the critical load increases. For system 1 four analyses were undertaken, the first three predicted the critical buckling in members which were manufactured from g.r.p. but during the fourth analysis the critical buckling took place in the first replacement c.g.r.p. members. Consequently, this investigation was terminated as it would have required a higher percentage of stiffness in these c.g.r.p. members to enable a higher external load to cause buckling of the new system. Figure (4.30) shows the sequence of buckling of the top members. Members α (eight in number) buckled during the second analysis and members γ (eight in number) during the third analysis. Finally, during the fourth analysis, members α, the first substituted c.g.r.p. member buckled.

Figures (4.36) and (4.37) show the relationship between deflection and total length of replaced c.g.r.p. members after successive analyses; for positions I, on the top grid, and II and VI, on the bottom grid of the configuration shown in Figure (4.30). The results of these curves are relative to a u.d.l. of $1.5kN/m^2$. Clearly the deflection of the structure will decrease as the stiffer c.g.r.p. members are increased in number; there is a 20 per cent decrease in deflection at position I for a total c.g.r.p. replacement length of 24.0 metres.

(b) Vertically upward acting load

Four analyses were undertaken with a vertically upward load applied to the structure. Figure (4.38) shows the relationship between the critical load and the total length of c.g.r.p. members which replace the g.r.p. members in the bottom layer configuration. The critical load was increased by 62 per cent by replacing 20 metres of g.r.p. pultruded tube with c.g.r.p. ones.

The sequence of buckling of the lower grid members is shown in Figure (4.30) where members δ (four in number) buckled during the second and members ω (eight in number) during the third analysis. During the fourth analysis the c.g.r.p. members in position δ buckled and the analysis was terminated.

Structural System 2

(a) Vertical downward acting load

Seven analyses were undertaken on this structure and Figure (4.35) also shows the relationship between the critical load factor of each successive analysis and the c.g.r.p. member lengths. It may be seen that even after the seventh analysis it would have been possible to improve upon the critical load value by replacing other g.r.p. members with c.g.r.p. ones, but the analysis was terminated at this point because of the excessive length of c.g.r.p. members being used.

The seventh, and ultimate, increment shows that a total of 67.58 metres of g.r.p. was replaced by c.g.r.p. members with an improvement in critical first buckling load of 79 per cent.

It is important to realise that the replacement of the critical g.r.p. members by c.g.r.p. ones does not always increase the critical buckling load of the structure. Referring to Figure (4.35) it can be seen that the third point on the curve related to the structural system under consideration shows a lower critical buckling load than the second one. A possible reason for this is that the replacement of the low elastic modulus members by higher stiffness c.g.r.p. ones causes changes in the force distribution in the structure and this replacement may have the undesirable effect of overstressing members already subjected to high forces which in turn causes a drop in the critical load of the structural system. From the curve it may be seen that, in the second analysis, a replacement of 11.3 metres of g.r.p. members in the top layer increases the external load values, applied to the structure to cause buckling, to 19.2kN/m^2 but a further replacement of 11.3 metres reduces this value to 12.6kN/m^2.

(b) Vertical upward acting load

Figure (4.38) shows that an improvement in the critical first buckling load value of 20 per cent was achieved by replacing 4 metres of g.r.p. members by c.g.r.p. ones in the bottom layer but no further improvement was possible because of the buckling of the c.g.r.p. members. It is important to point out that the increase of density of members in the top layer grid had the effect of reducing the buckling load for the upward condition of loading.

Structural System 3

(a) Vertically downward acting load

Ten successive analyses were undertaken on this structure and during the last analysis a diagonal member buckled. The analysis

was terminated at this stage because the investigation was limited to the buckling of top or bottom members resulting from bending moment action. The maximum length of g.r.p. top layer members replaced by hybrid ones was 35.3 metres and the corresponding increase in the critical load was 55.5 per cent. As was shown in structural system 2, the replacement of g.r.p. members by the stiffer c.g.r.p. members does not necessarily produce a structure with higher critical load.

(b) Vertical upwards acting load

Again only two solutions were possible for this structural system as during the second one the replacement of 4 g.r.p. members in the bottom layer increased the first buckling critical load value by 20 per cent.

It has been shown that it is possible to improve the stability of double-layer grid systems made of g.r.p. by either increasing the density of the layer under compressive action or by introducing stiffer composite members in the critical regions of the configurations. It is important to remember however, that for structures manufactured from relatively low modulus materials the deflections must also be investigated.

Consequently, the deflections at positions I, II and VI shown in Figures (4.30), (4.31) and (4.32) for the vertically downwards external load on the three structural systems were investigated and were plotted against the length of hybrid membrs which replaced the buckled g.r.p. members at each analysis.

The strains imposed upon double-layer grid systems by external loads applied at the nodal joints of the system are mainly axial and as deflections are caused by axial deformations of members, the replacement of the critical g.r.p. members by the high stiffness ones must reduce the deflections of the structure. Figure (4.36) shows the vertical deflections for the three systems at or near the centre of the doube-layer grid structure at positions I and II on the top and bottom grids respectively. It will be noticed that a

reduction in deflection takes place as g.r.p. members are replaced by the higher modulus c.g.r.p. members to enable a greater buckling load value to be obtained. The deflections of the lower grid point VI against replacement c.g.r.p. member lengths for all structures is shown in Figure (4.37) and it will be observed that the reduction in deflection is not a localised effect in the vicinity of the replaced members but one that is associated with all nodal points in the structure.

Similar deflection results were obtained for vertically upward applied loads and these are shown in Figure (4.39) and (4.4) for positions II and IV (as shown in Figures (4.30), (4.31) and (4.32)).

4.5 OBSERVATIONS

The behaviour of light-weight double-layer grid systems manufactured from g.r.p. and c.g.r.p. is linear for much of the load-deflection curve. The fact that their structural behaviour becomes highly nonlinear only after first buckling means that the linear eigenvalue method of analysis, which enables the first buckling to be obtained and also the corresponding mode of buckling to be determined, can be used to find the point at which linear analysis is acceptable (a margin of safety has to be taken into account as imperfections may lower the first buckling load).

If the structures post-buckling behaviour is required, nonlinear analysis must be used. This analysis used in the double-layer grid investigation proved to be a useful tool to predict accurately the behaviour of the system; this has been clearly shown in the solution to the model tests.

All double-layer grid structures analysed in this chapter showed a reduction in stiffness after the first buckling. This reduction in all models tested (Figures 4.1 and 4.15) was much more severe than that for the double-layer grids shown in Figures (4.30) to (4.32). This variation is stiffness was clearly caused by the geometry of the structural configurations. In the model analysis the loads in members were unable

to distribute their forces to adjacent members due to the small overall dimensions of the structure but in the latter case the structure had breadth and was able to distribute forces to a larger number of members.

In these types of structures the failure seemed to occur as a result of buckling of members subjected to compressive axial forces. To overcome this problem and to produce more efficient structures, two approaches were explored; these are either to increase the density of members in the area under the compressive action or to introduce member types of higher stiffness in the region of critical comnpressive forces. The latter method is usually more practical and the results appear to be good. However, the assembly of such structures becomes a critical operation where error in positioning any of the high stiffness members may have negative effects. Careful analysis and understanding of the structural problem is also required because replacing a highly stressed member by a stiffer one does not always improve the performance of the overall structure.

During the testing of the structures relatively small deformations of the buckled members were noted. The members failed suddenly by a brittle failure. The overall deflections of the structure are large when compared with metallic systems, but using high stiffness members in the region of high internal forces will tend to reduce the overall deflections considerably.

Imperfections can affect deflections and internal forces which in turn will affect critical load and mode of buckling. The effect of imperfections on structures can be readily incorporated in nonlinear analysis where their effects can be studied.

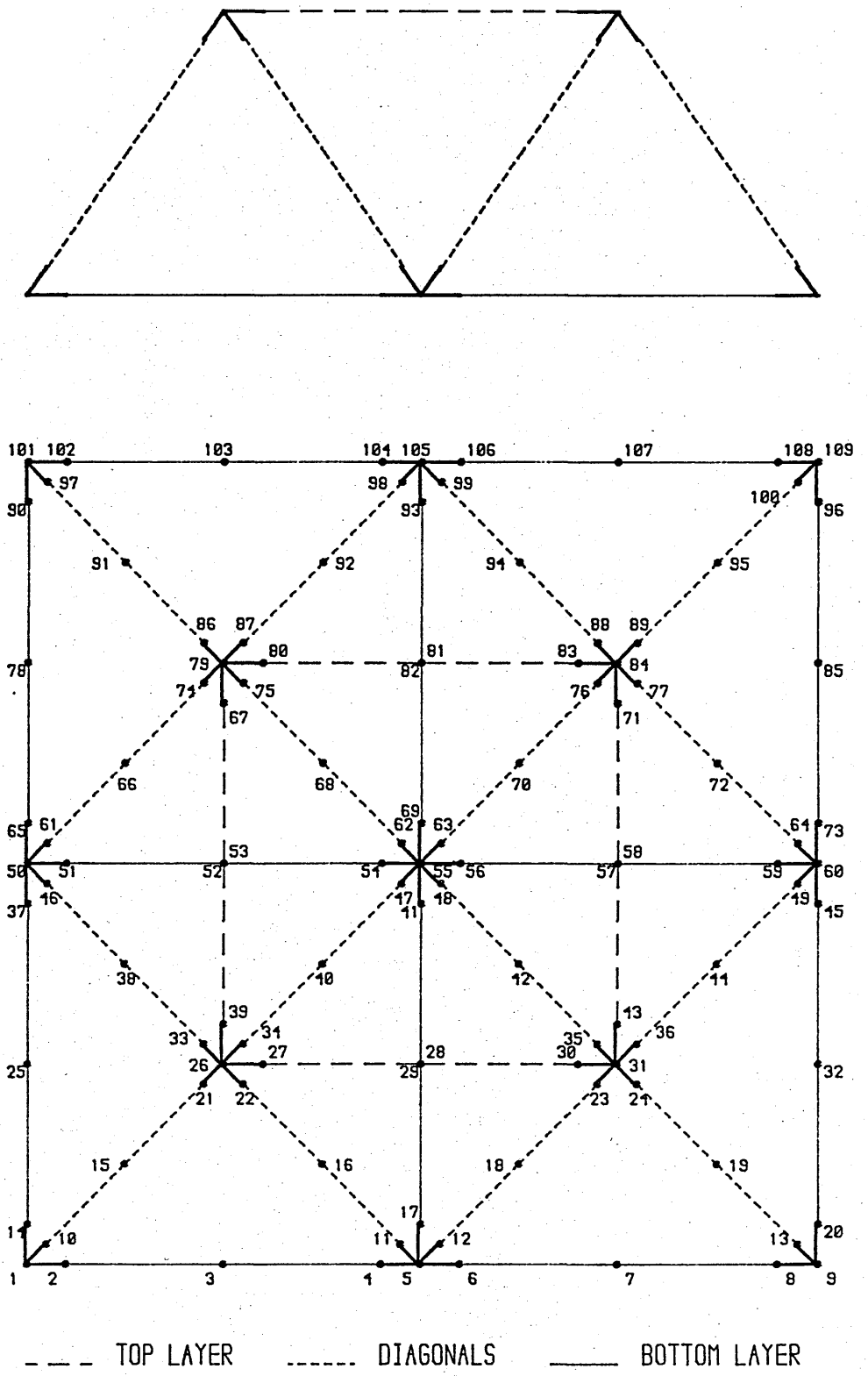

FIG 4.1 CONFIGURATION AND JOINT NUMBERING SYSTEM

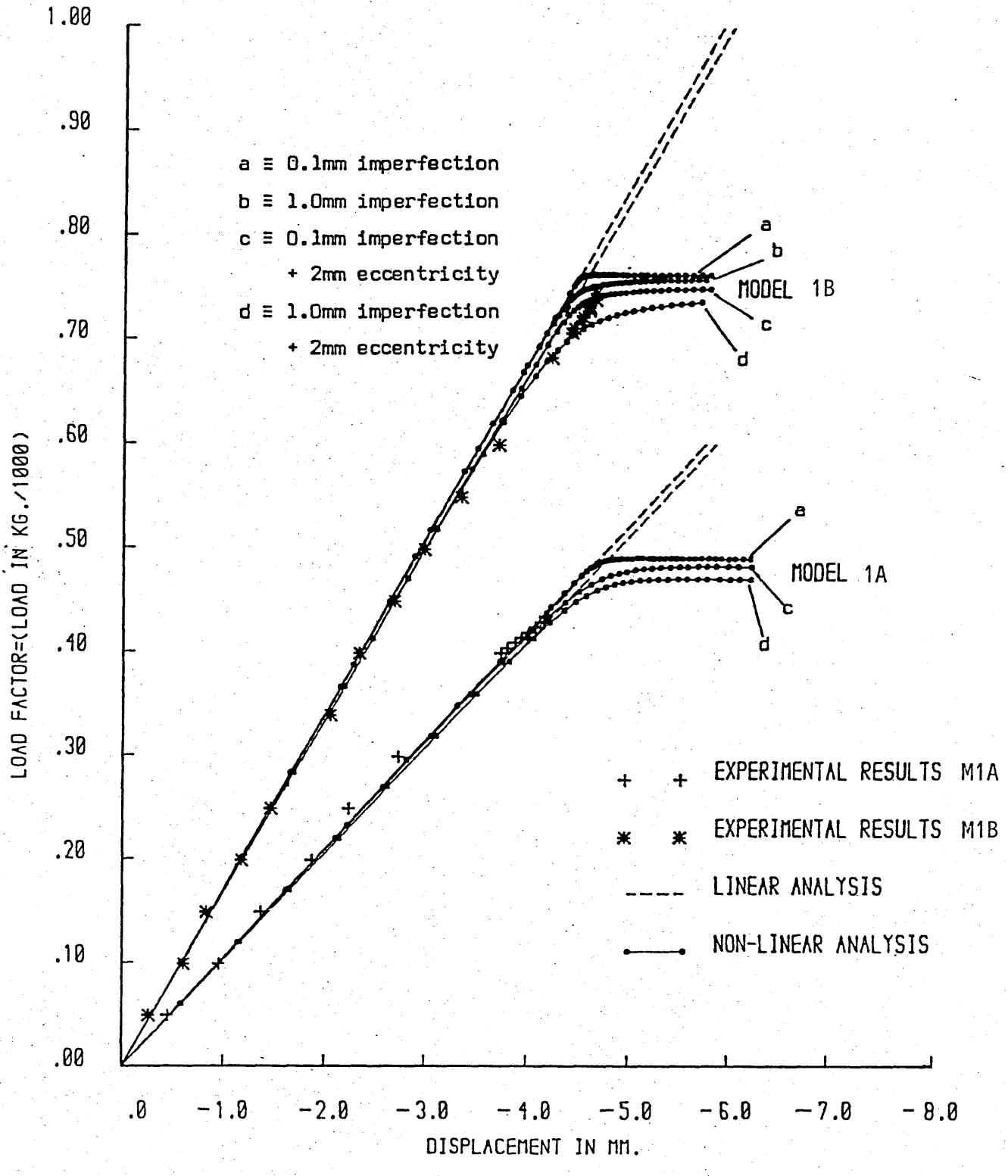

Fig (4.2) Load Factor - Z dispacement of joint No 5

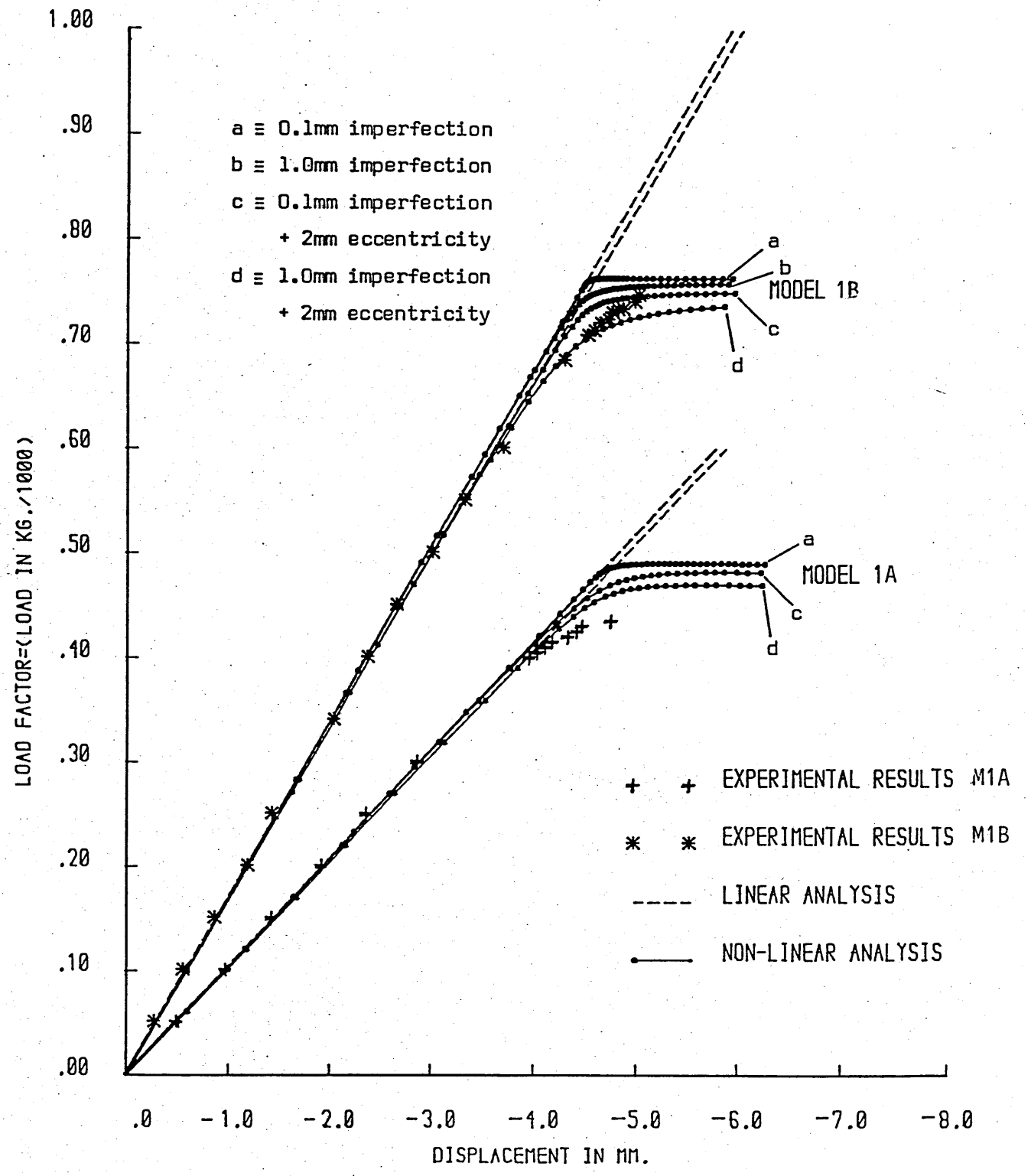

Fig (4.3) Load Factor - Z-displacement of joint No 26

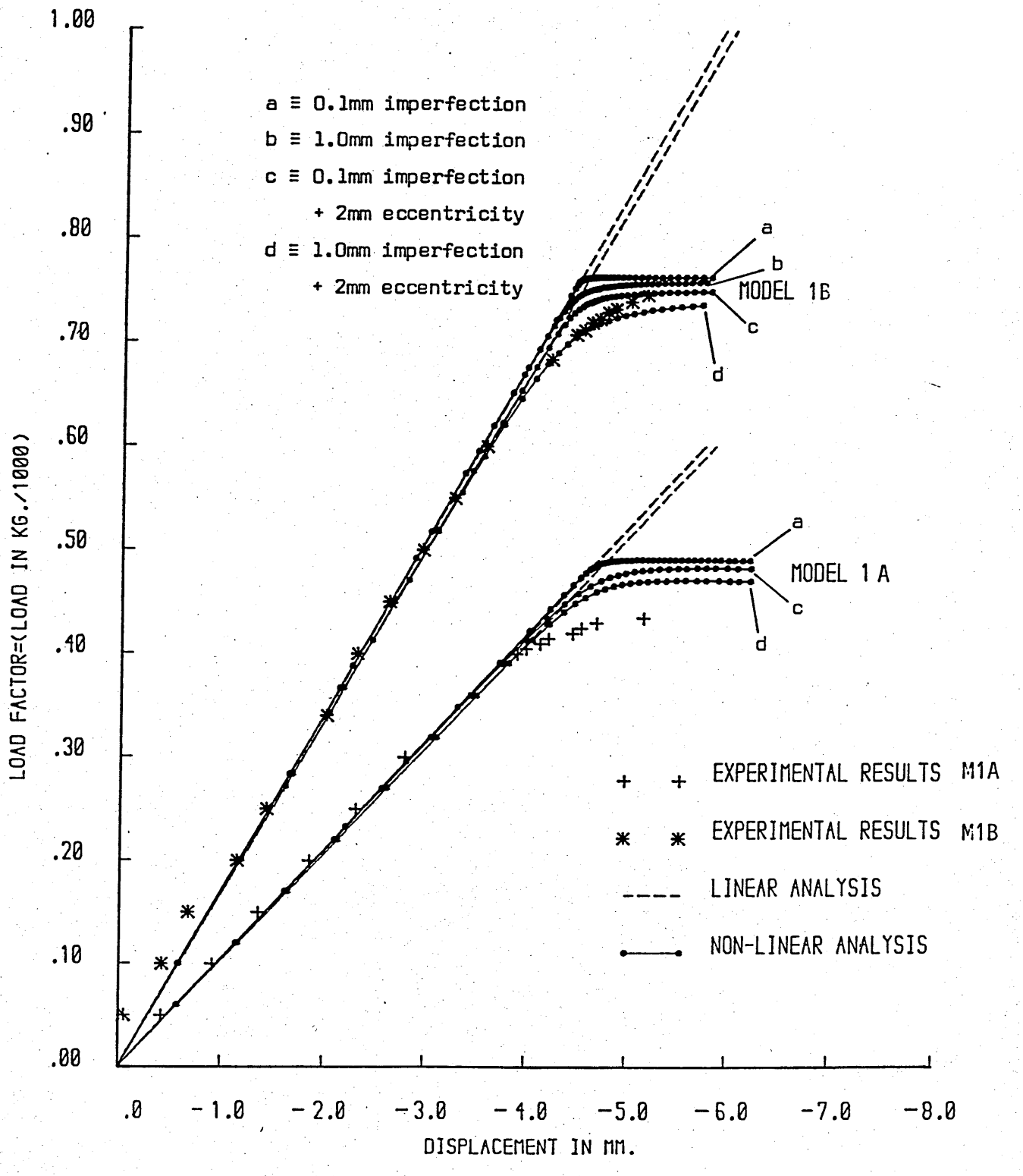

Fig (4.4) Load Factor - Z-displacement of joint No 50

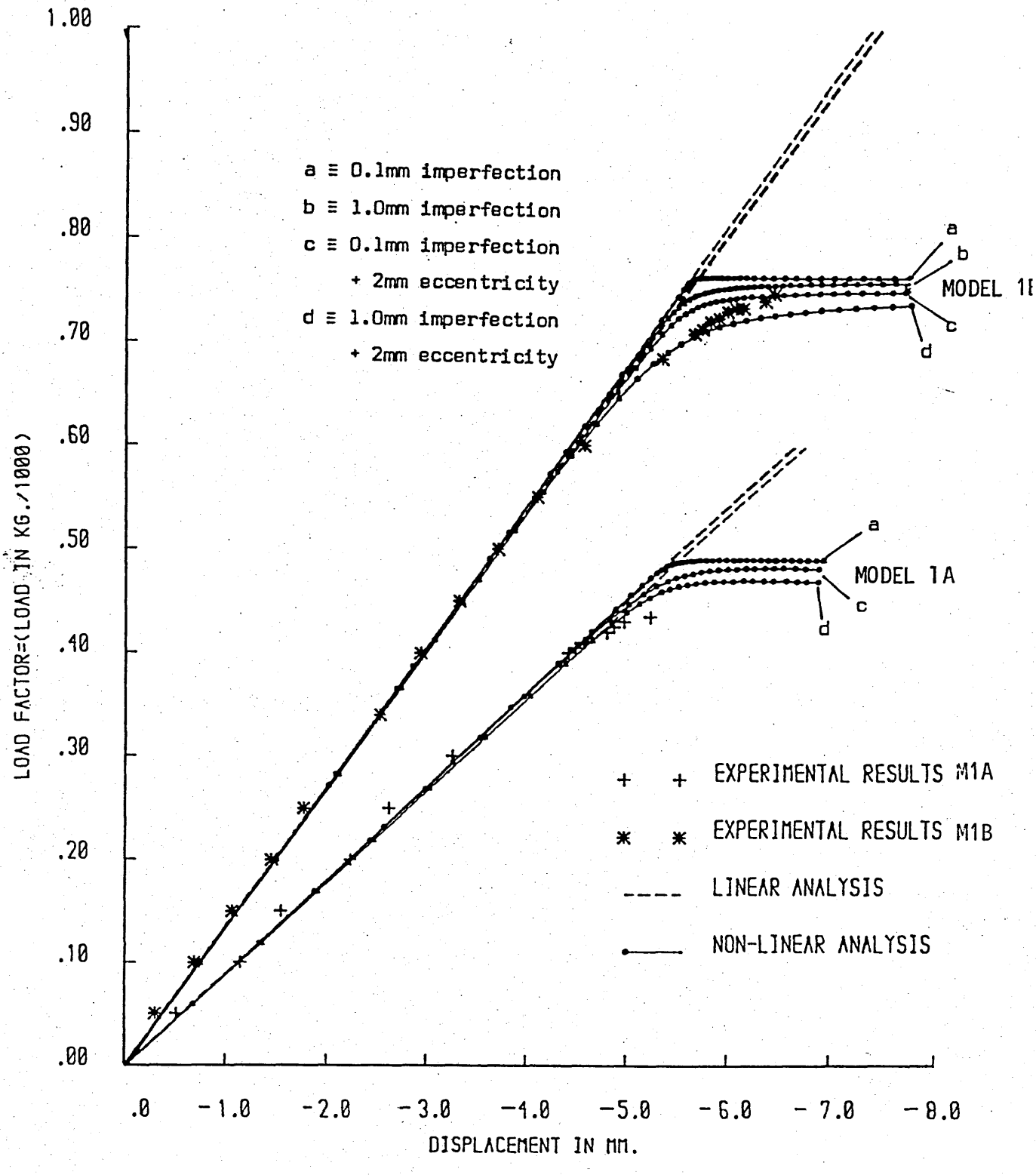

Fig (4.5) Load Factor - Z-displacement of joint No 55

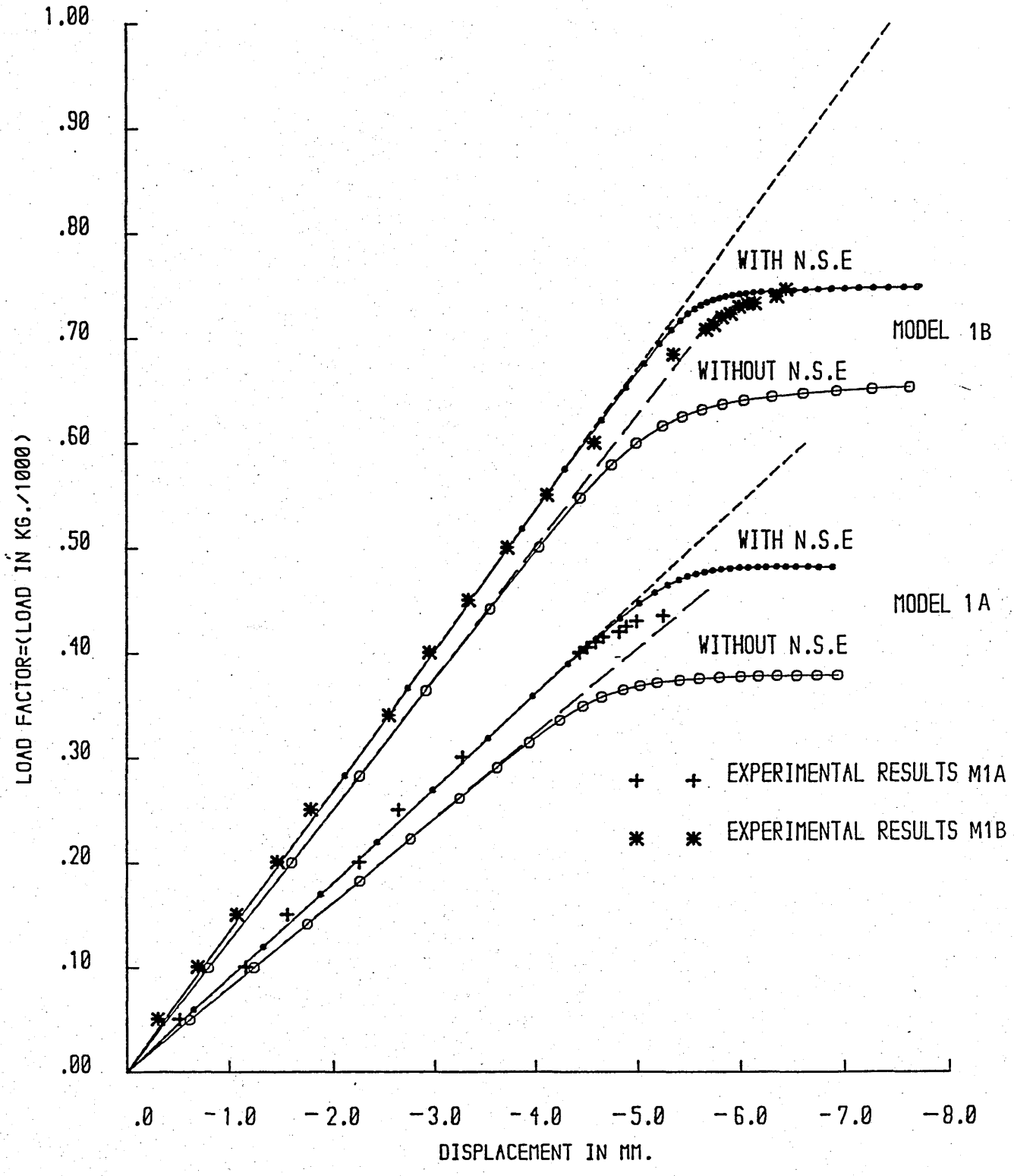

Fig (4.6) Load - Z-displacement of joint No 55 with and without N.S.E. (ie, Nodal Stiffening Effect)

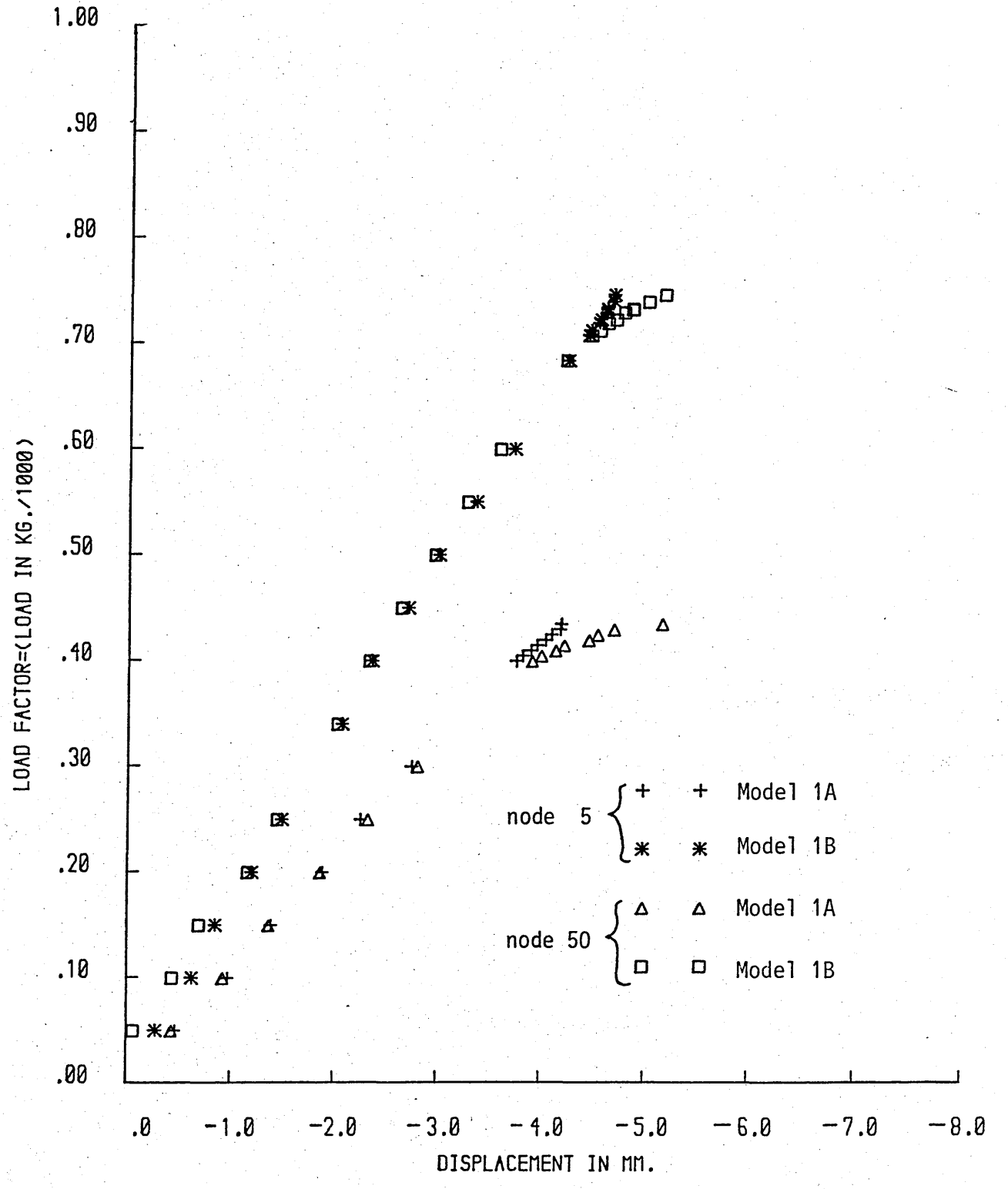

Fig (4.7) Load Factor - Displacement for two symmetric nodes (Viz 5 and 50)

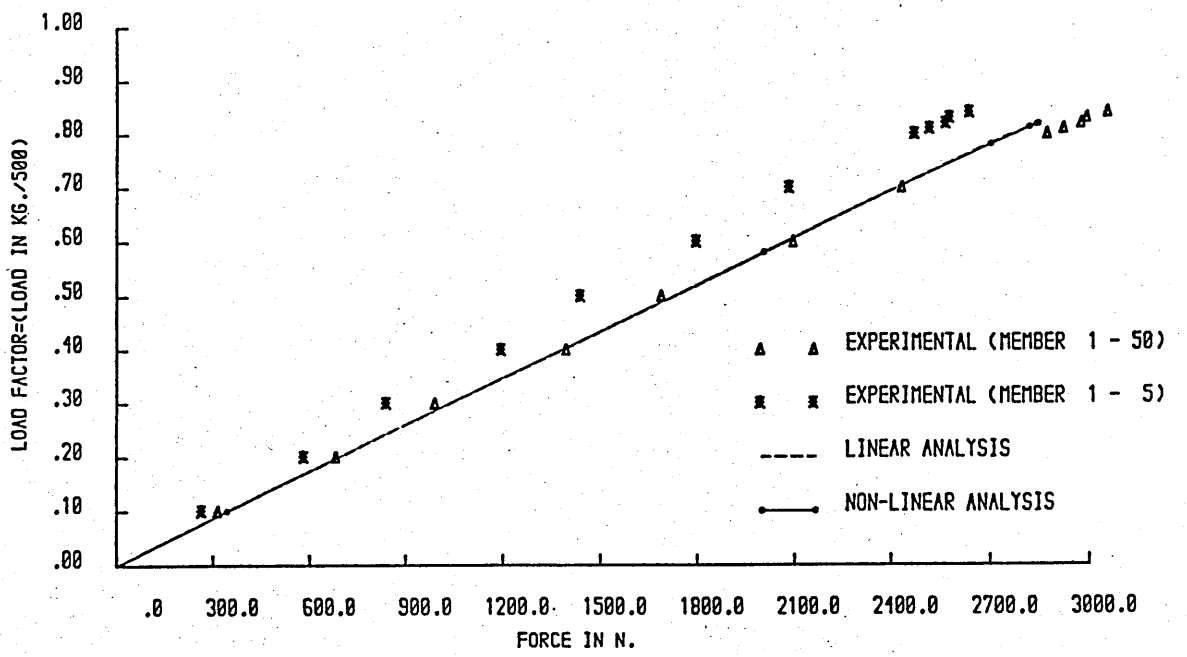

Fig (4.8) Load Factor - Axial force (model No 1A, members: 1-5 and 1-50)

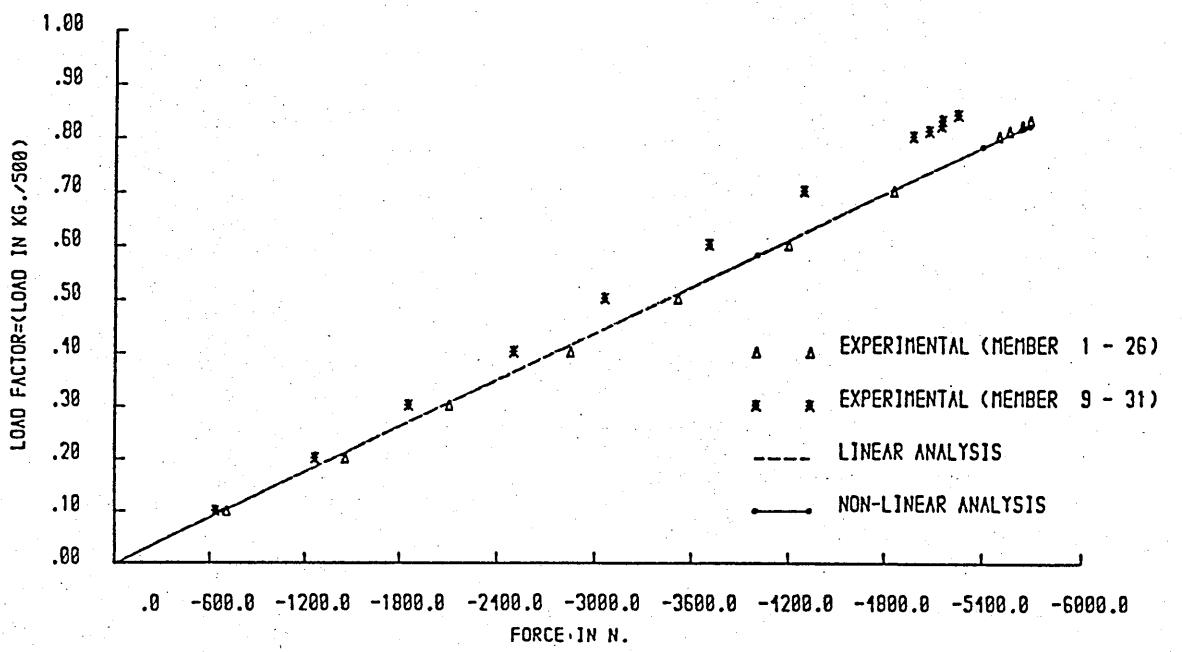

Fig (4.9) Load Factor - Axial force (model No 1A, members 9-31 and 1-26)

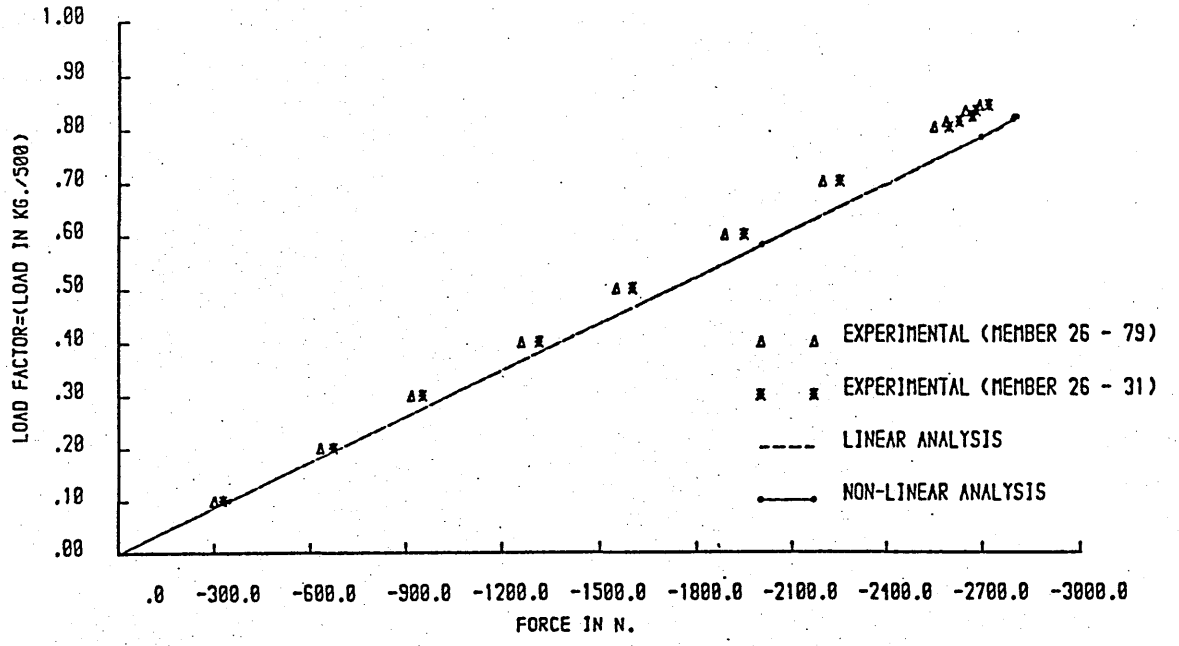

Fig (4.10) Load Factor - Axial force (model No 1A, members: 26-31 and 26-79)

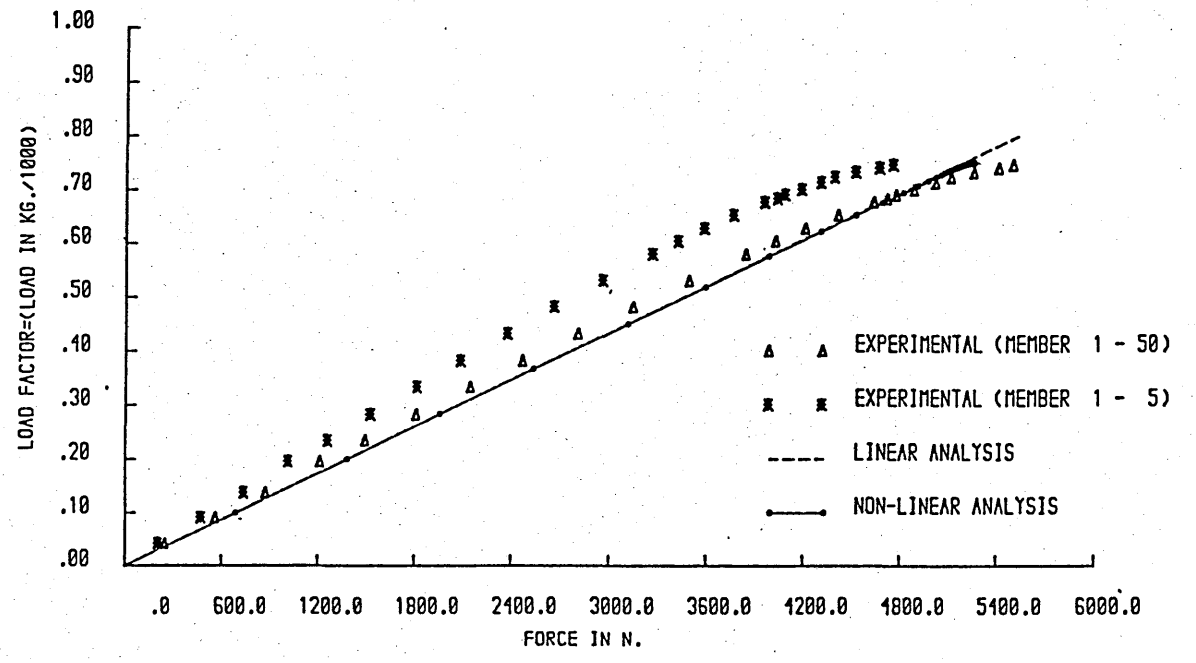

Fig (4.11) Load Factor - Axial force (model No 1B, members: 1-5 and 1-50)

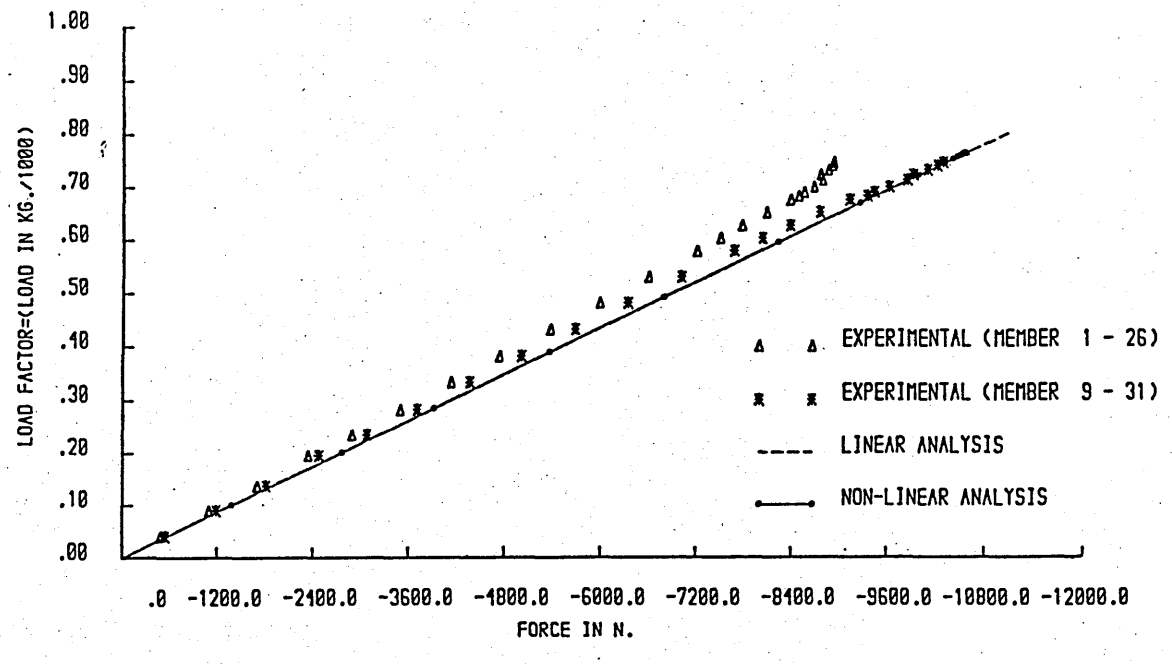

Fig (4.12) Load Factor - Axial force (model No 1B, members: 9-31 and 1-26)

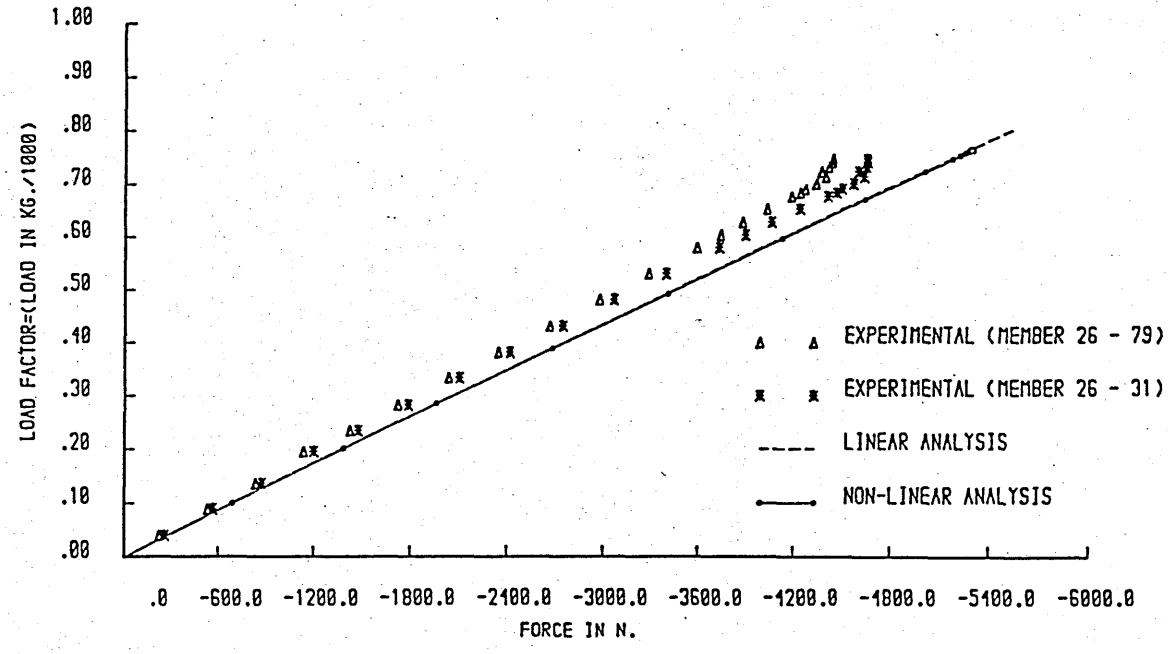

Fig (4.13) Load Factor - Axial force (model No 1B, members: 26-31 and 26-79)

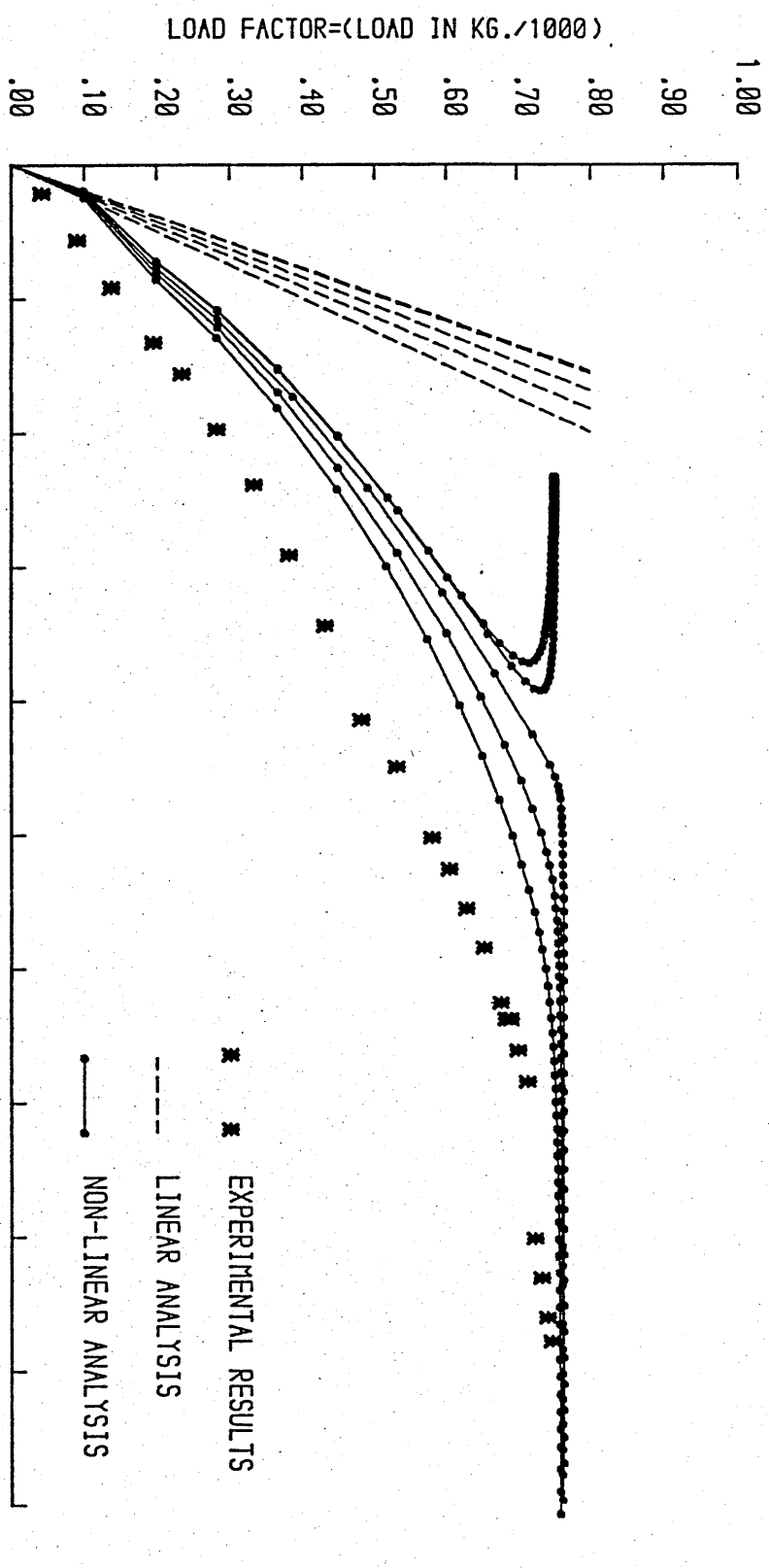

Fig (4.14) Load Factor - Axial force (model No 1B, member 50-55)

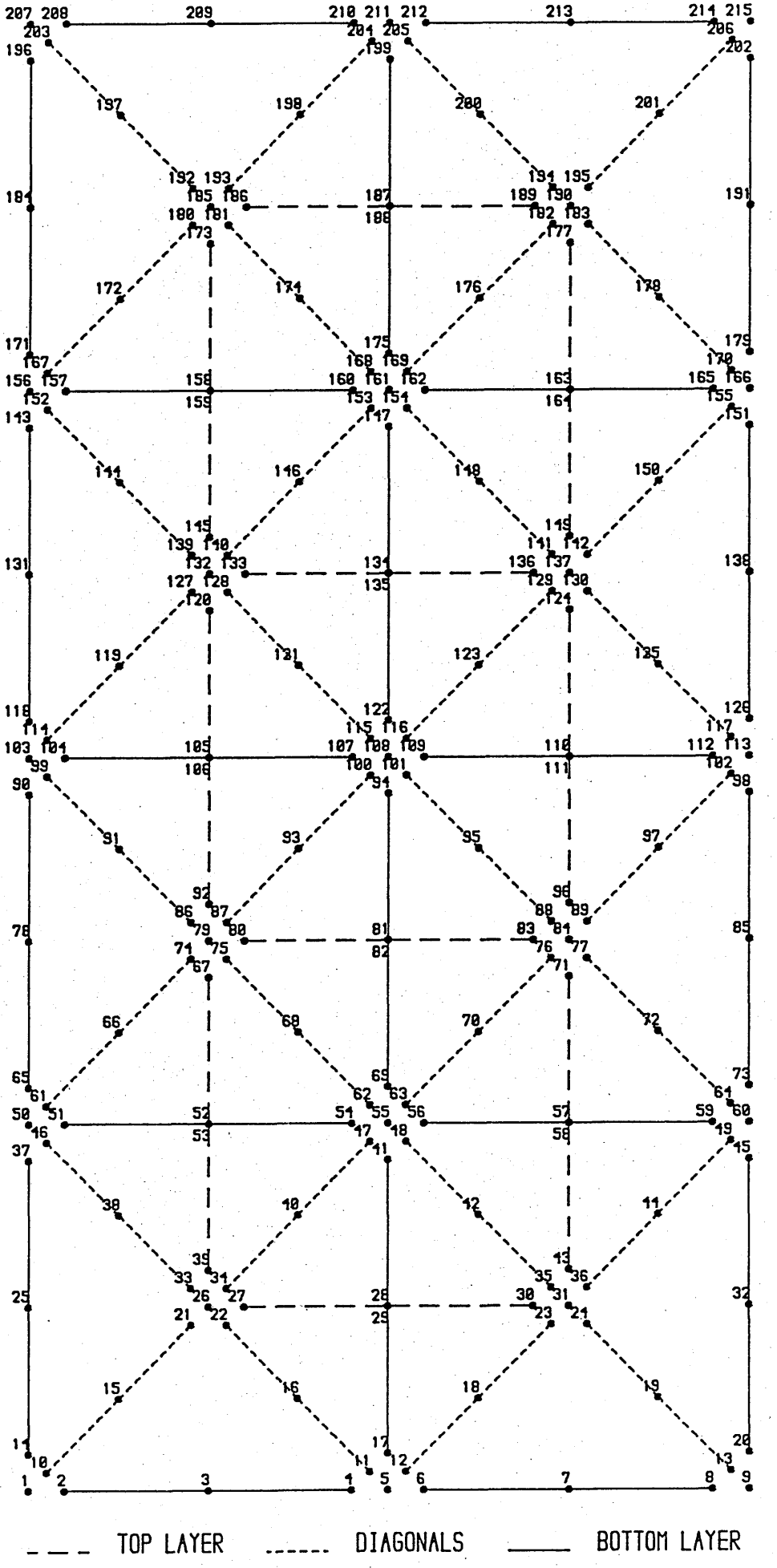

FIG 4.15 CONFIGURATION AND JOINT NUMBERING SYSTEM

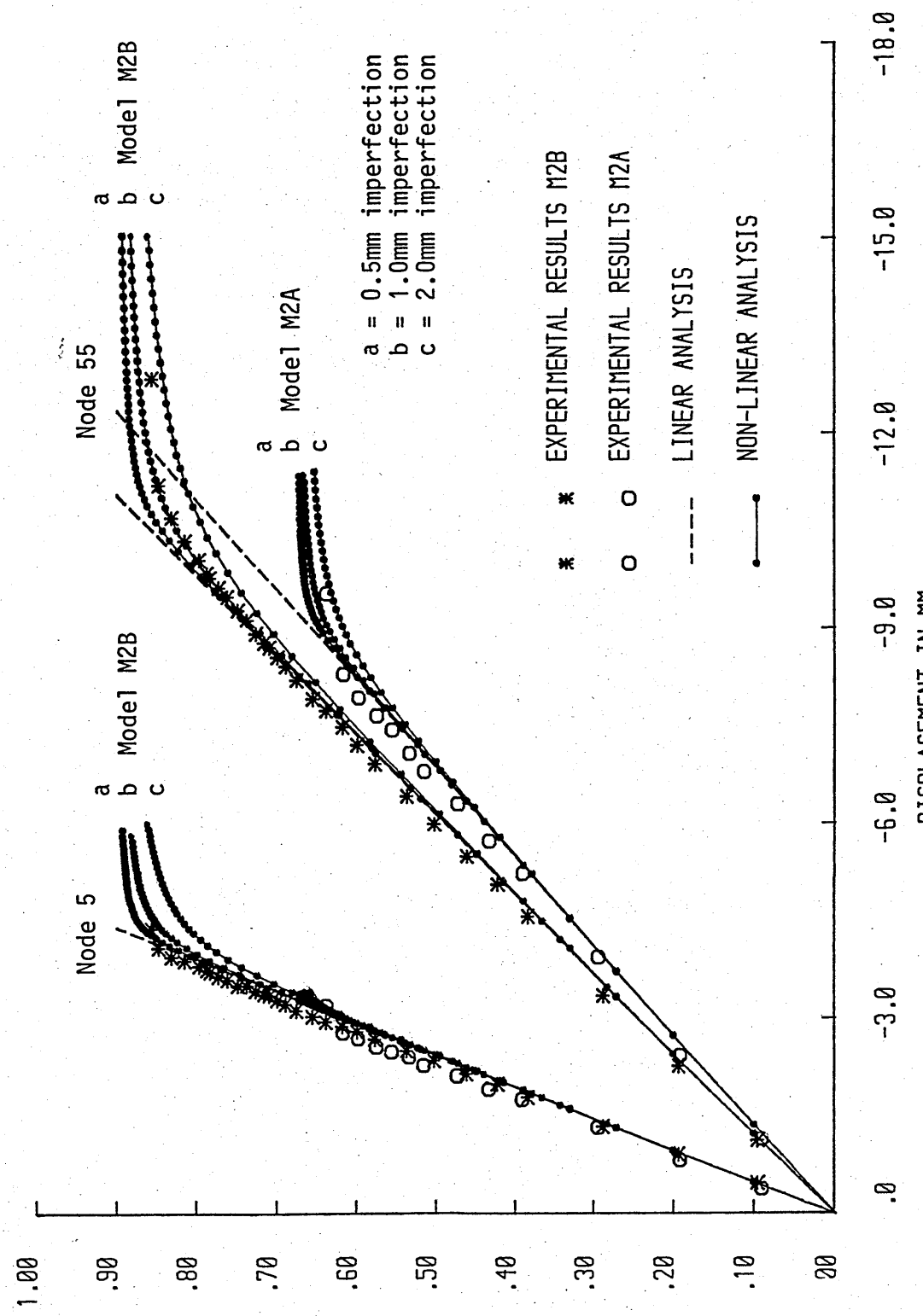

Fig (4.16) Load Factor - Z-displacement of joint Nos 5 and 55 for models M2A and M2B

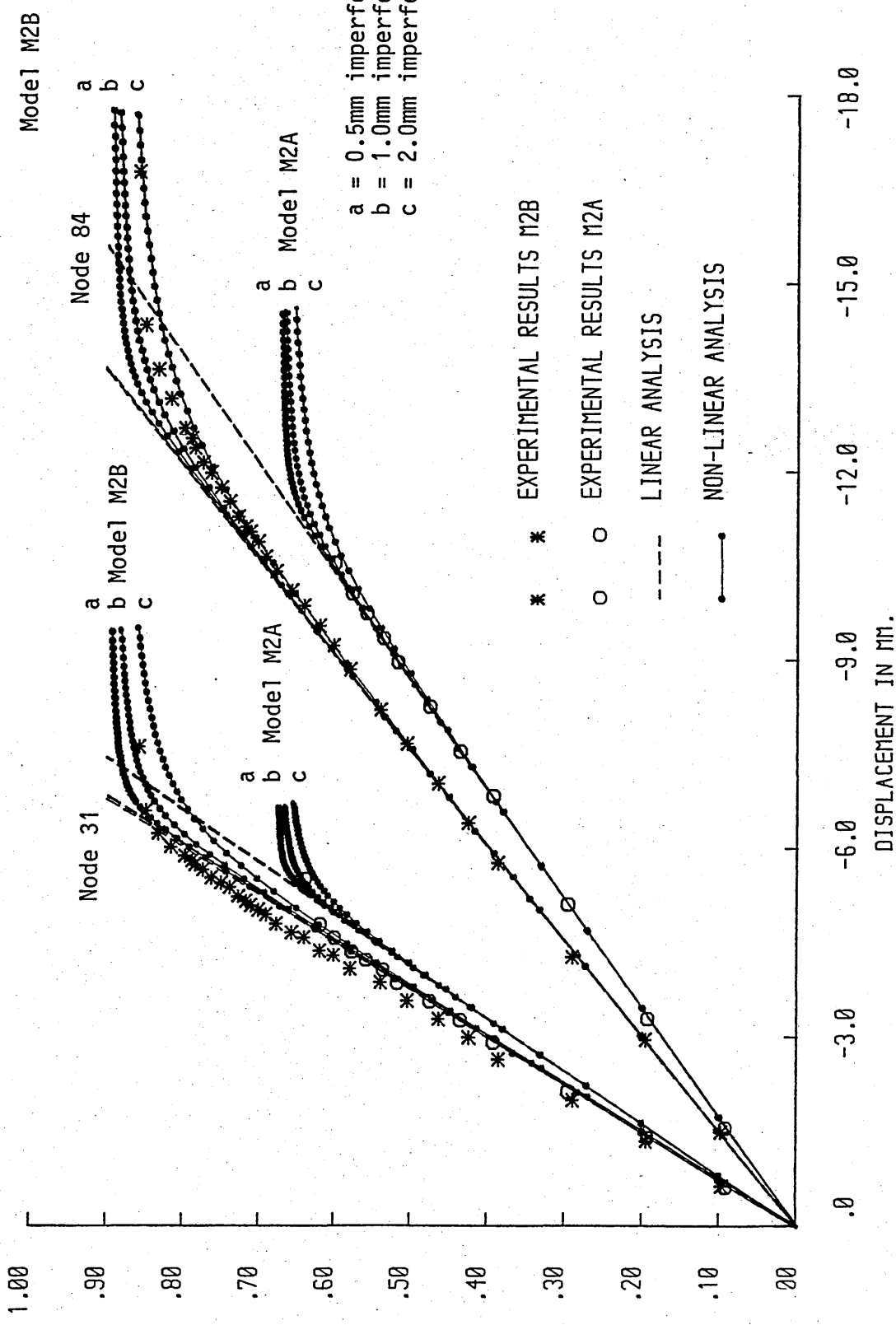

Fig (4.17) Load Factor - Z-displacement of joint Nos 31 and 84 for models M2A and M2B

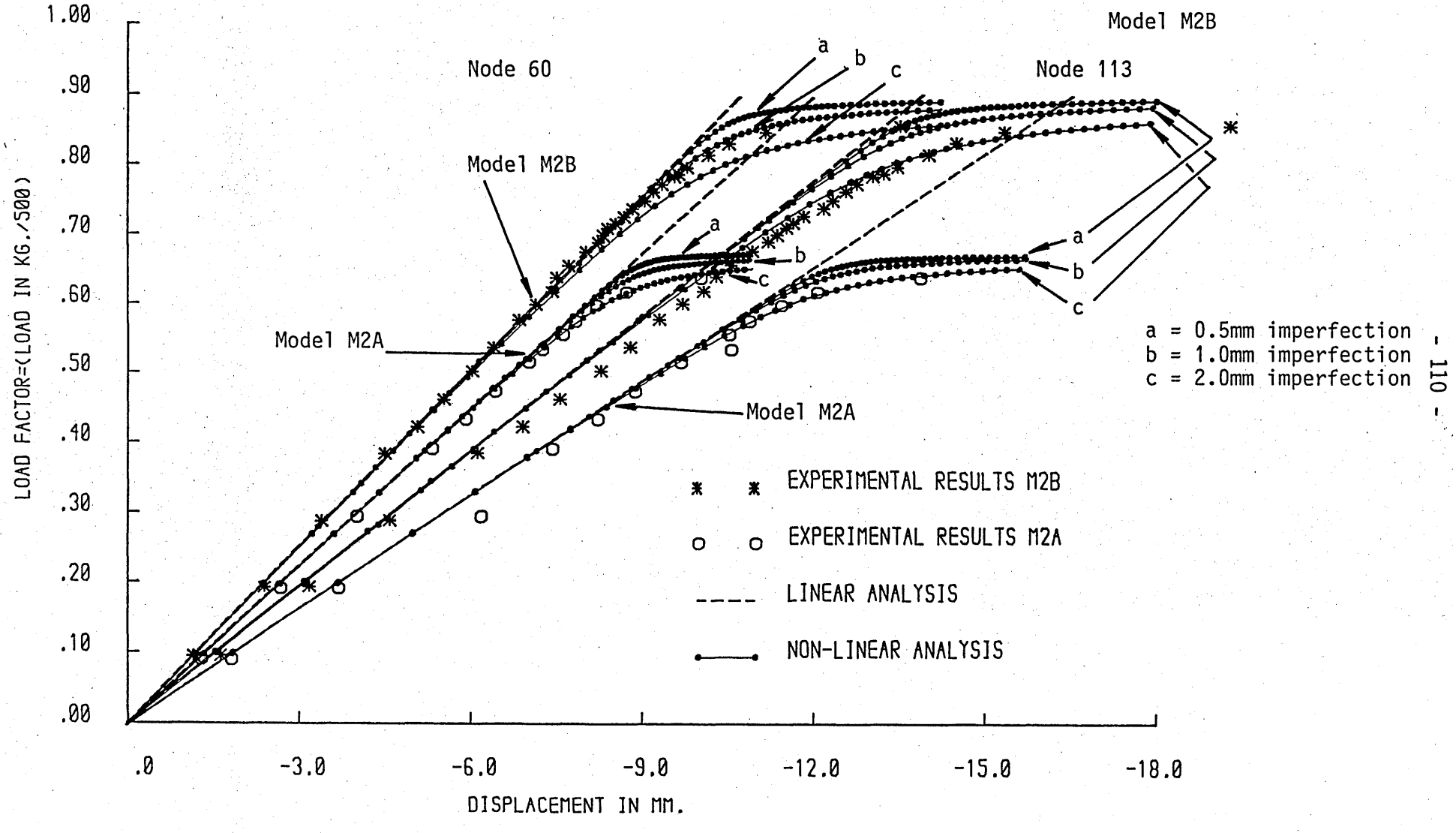

Fig (4.18) Load Factor - Z-displacement of joint Nos 60 and 113 for models M2A and M2B

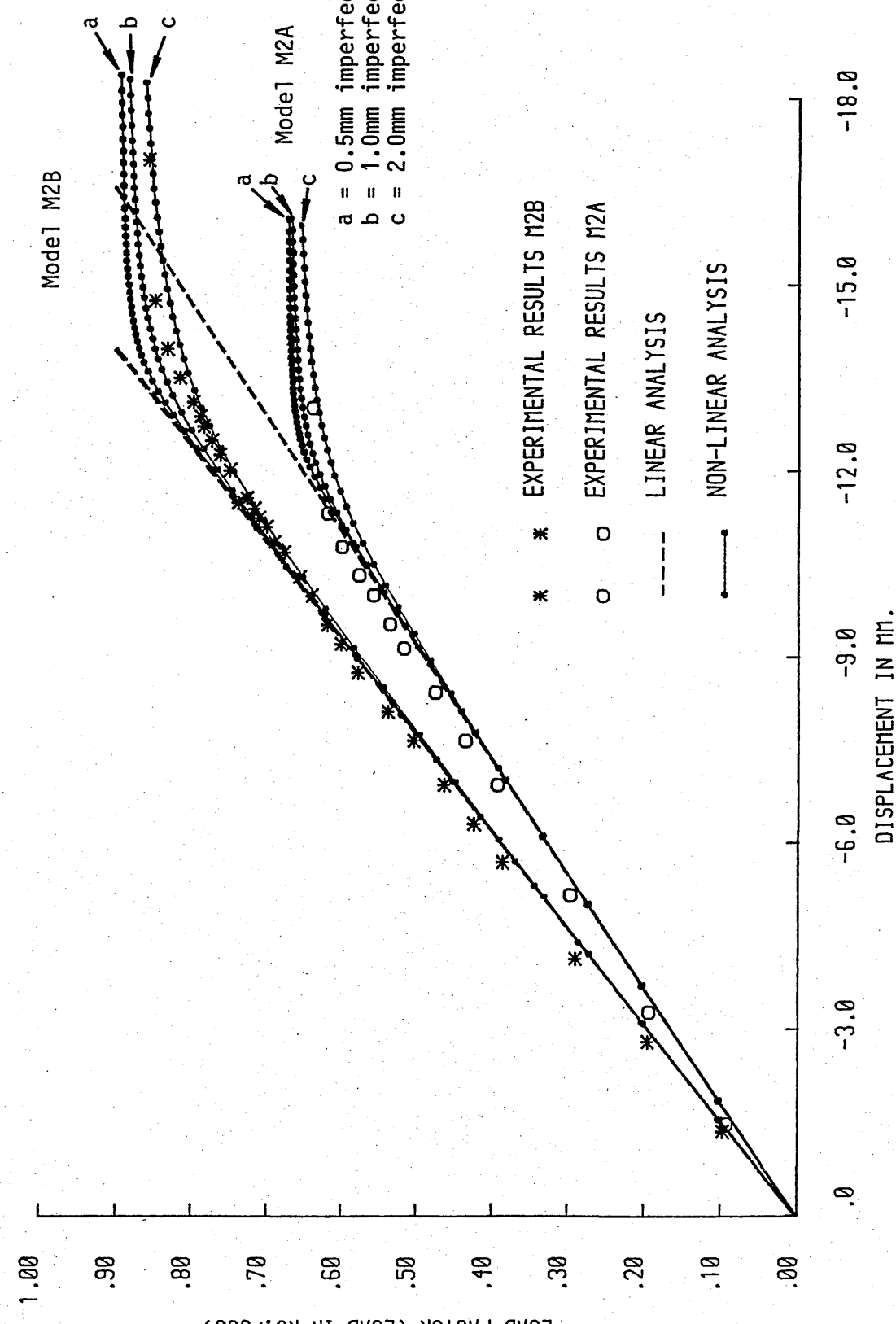

Fig (4.19) Load Factor - Z-displacement of joint No.108 for models M2A and M2B

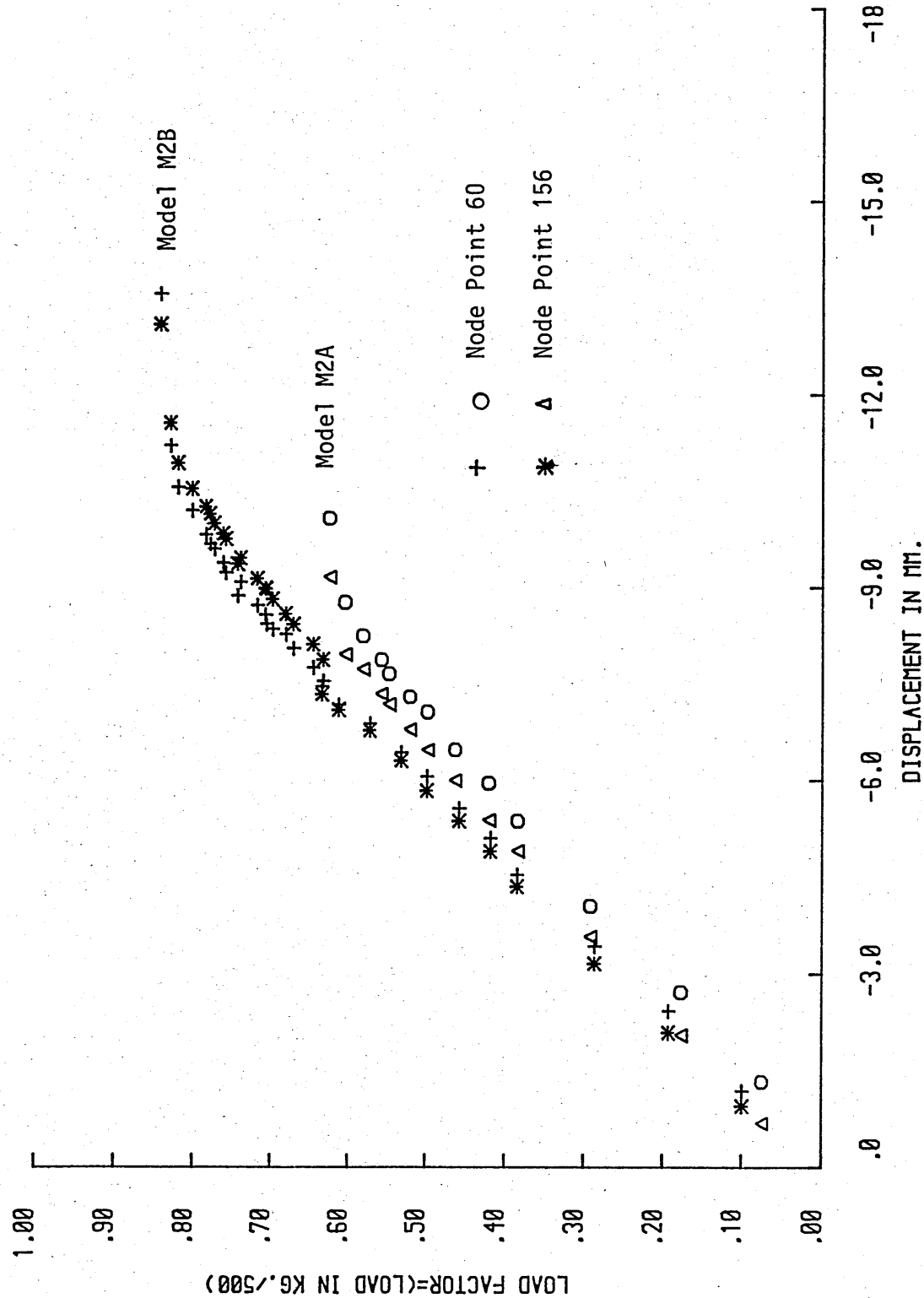

Fig (4.20) Load Factor - Z-displacement of four symmetrical nodal points for models M2A and M2B

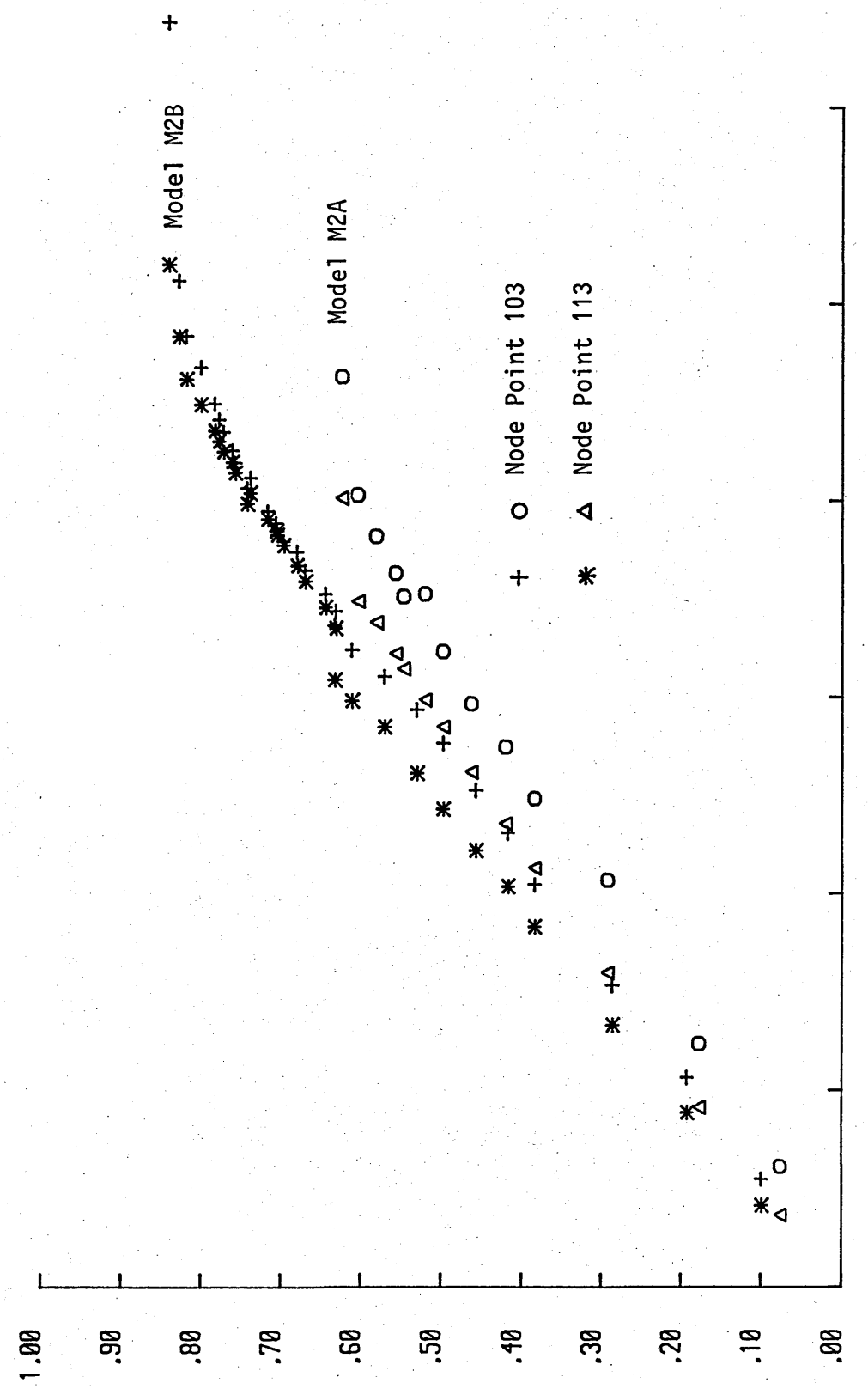

Fig (4.21) Load Factor - Z displacement of four symmetrical nodal points for models M2A and M2B

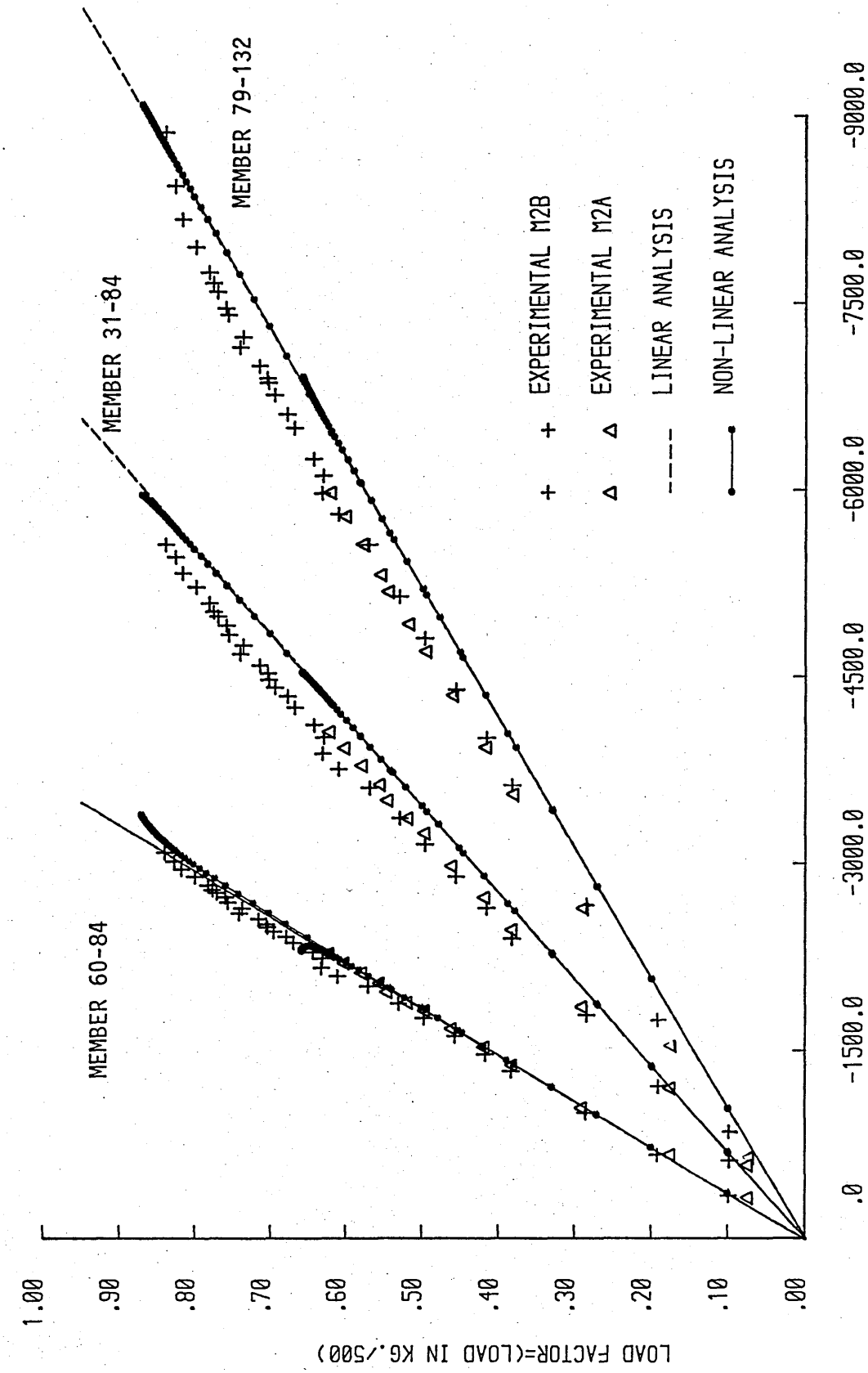

Fig (4.22) Load Factor - Axial force in members 60-84, 31-64 and 79-132 for models M2A and M2B

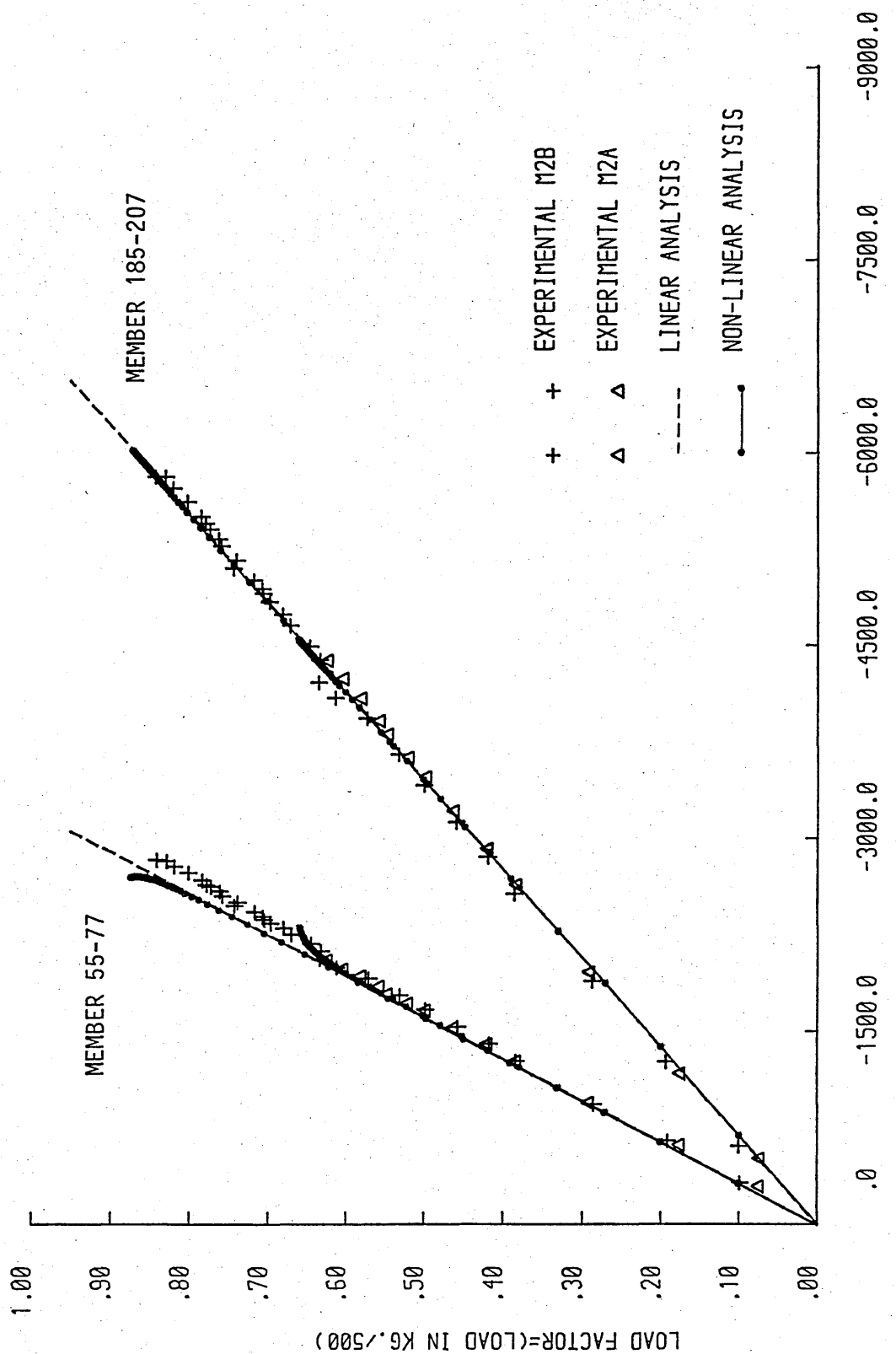

Fig (4.23) Load Factor - Axial force in members 55-77 and 185-207 for models M2A and M2B

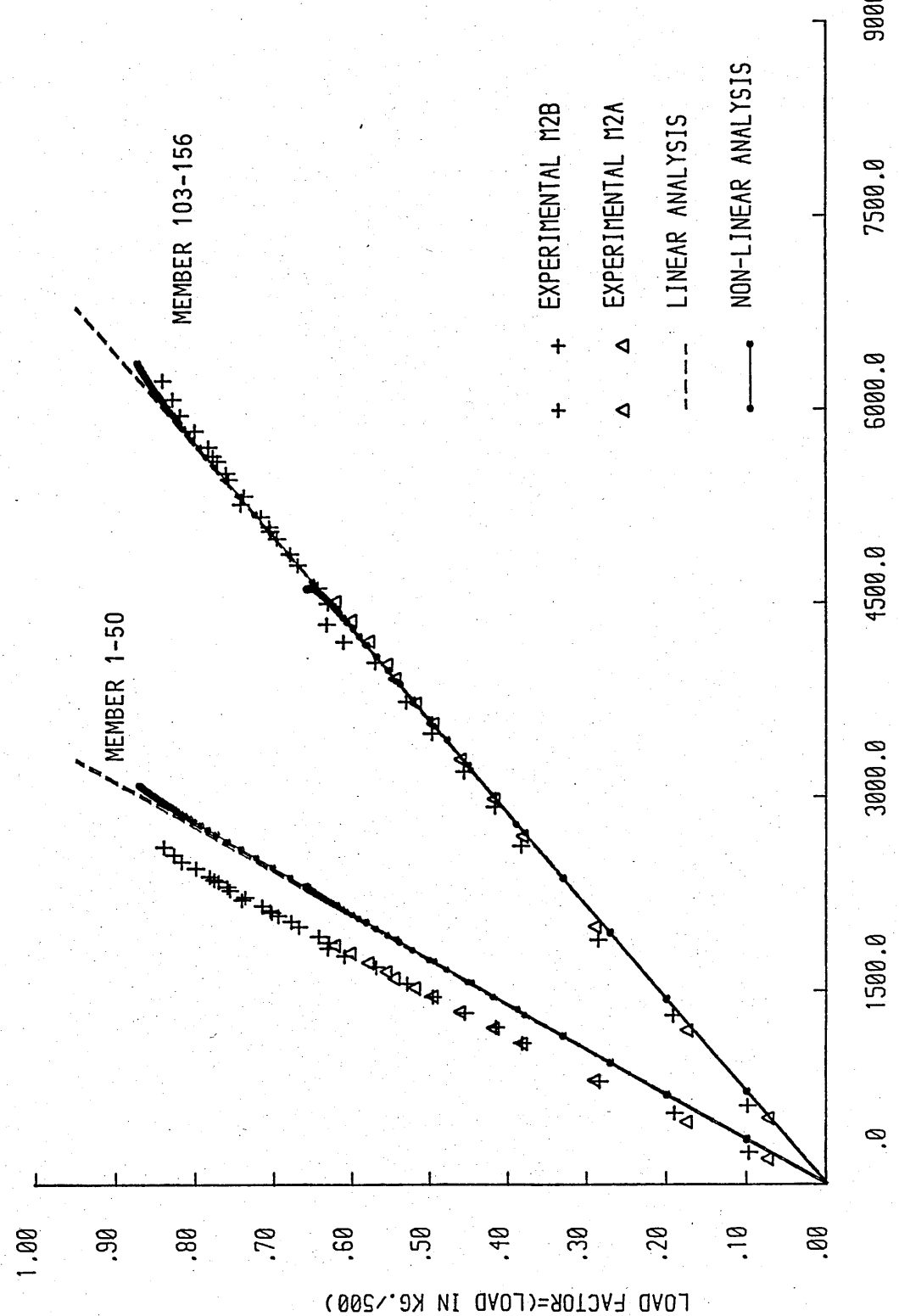

Fig (4.24) Load Factor - Axial force in members 1-50 and 103-156 for models M2A and M2B

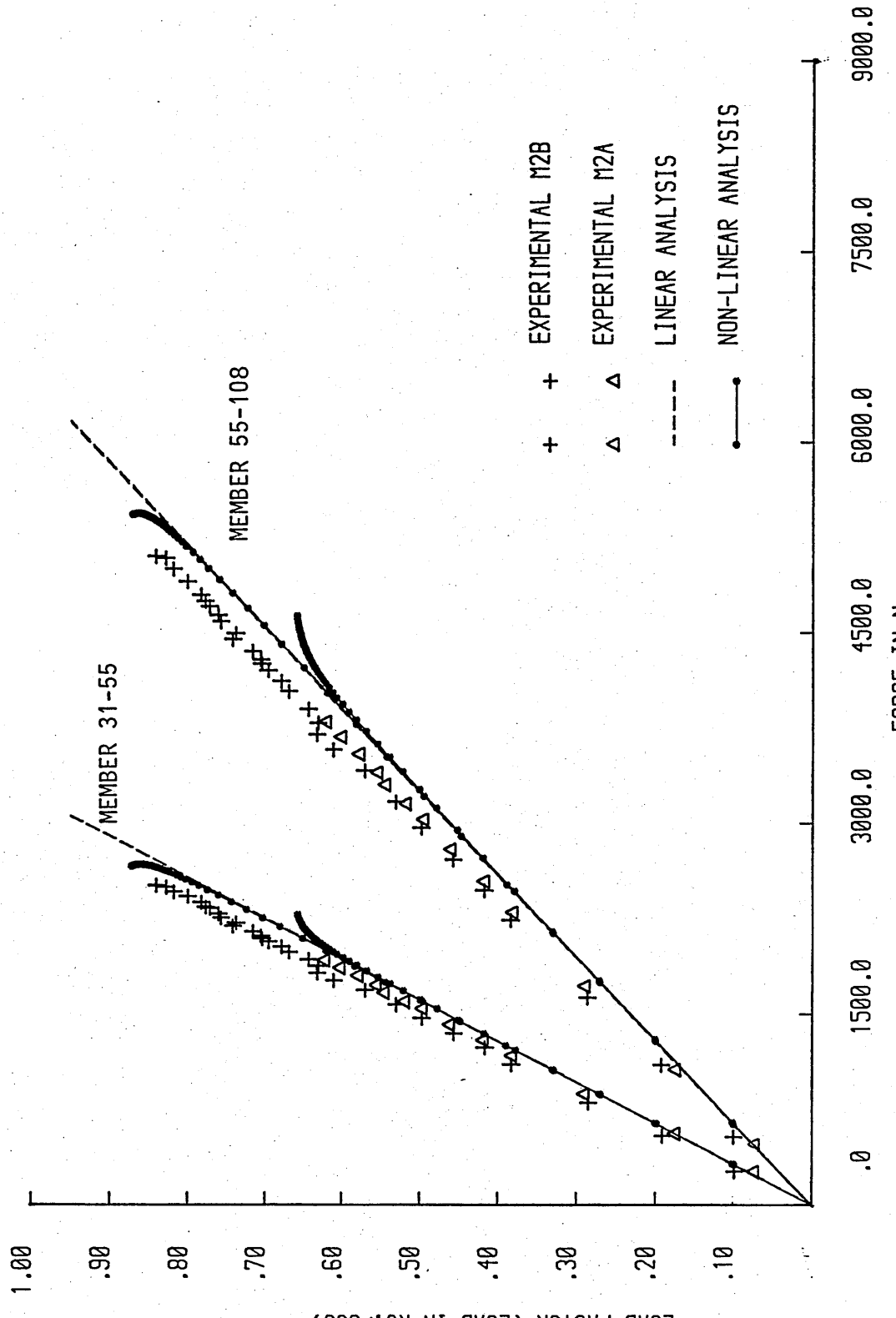

Fig (4.25) Load Factor - Axial force in members 31-55 and 55-108 for models M2A and M2B

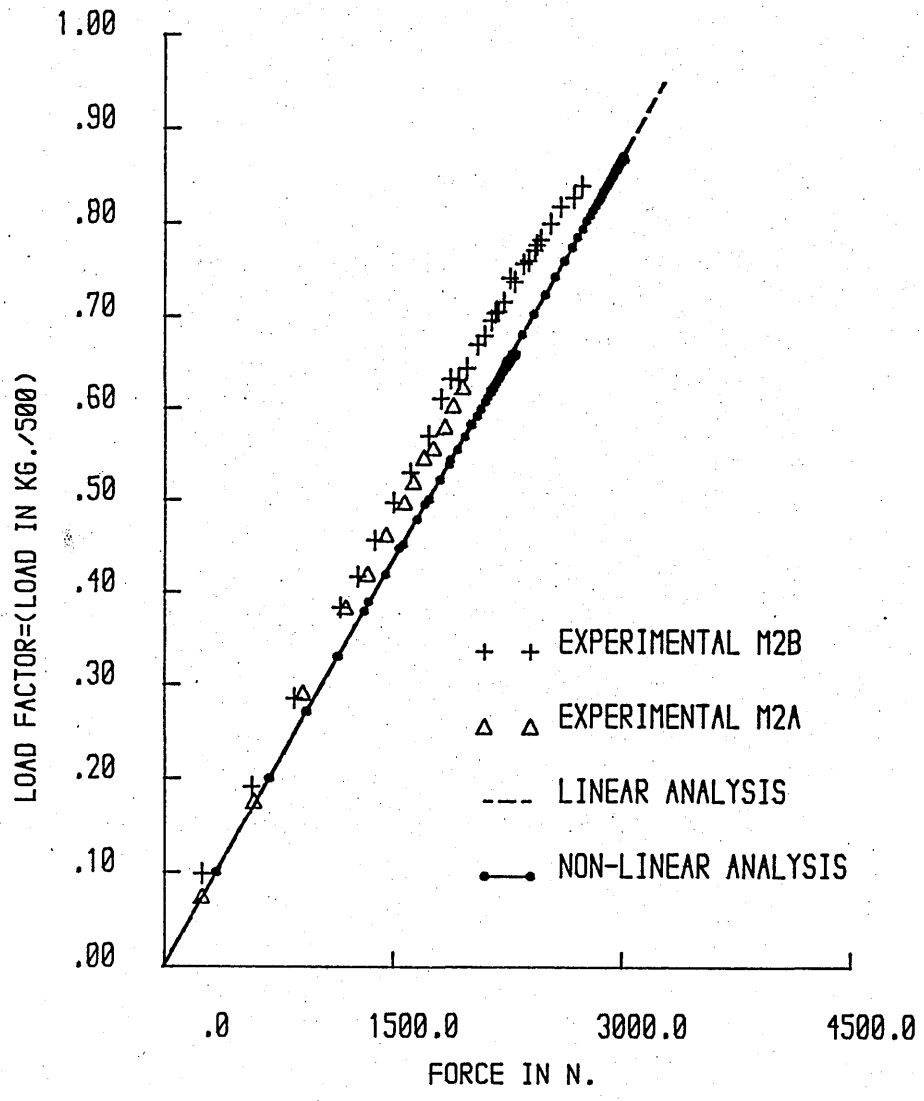

Fig (4.26) Load Factor - Axial force in member 5-9 for models M2A and M2B

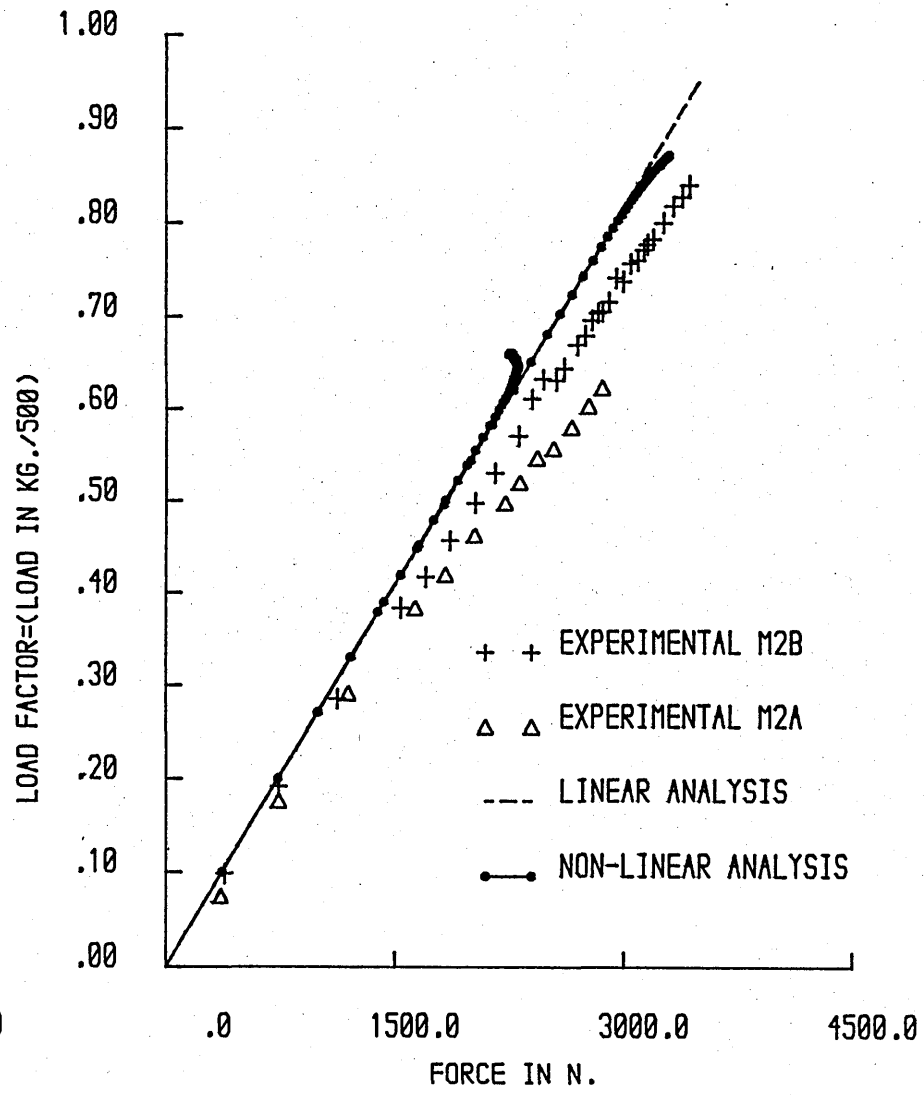

Fig (4.27) Load Factor - Axial force in member 31-60 for models M2A and M2B

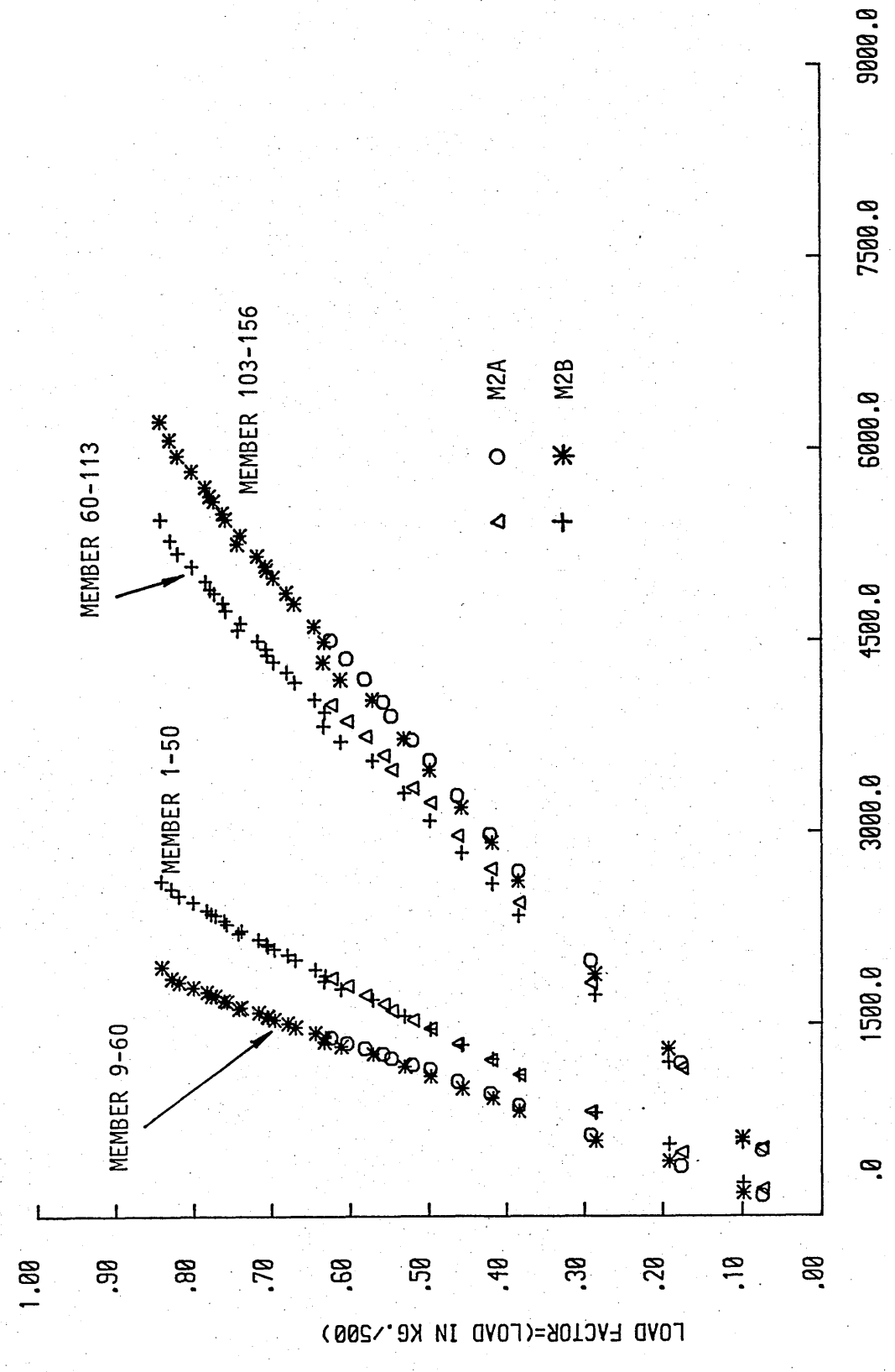

Fig (4.28) Load Factor - Axial force in members 9-60 and 1-50 and in members 10-113 and 103-156

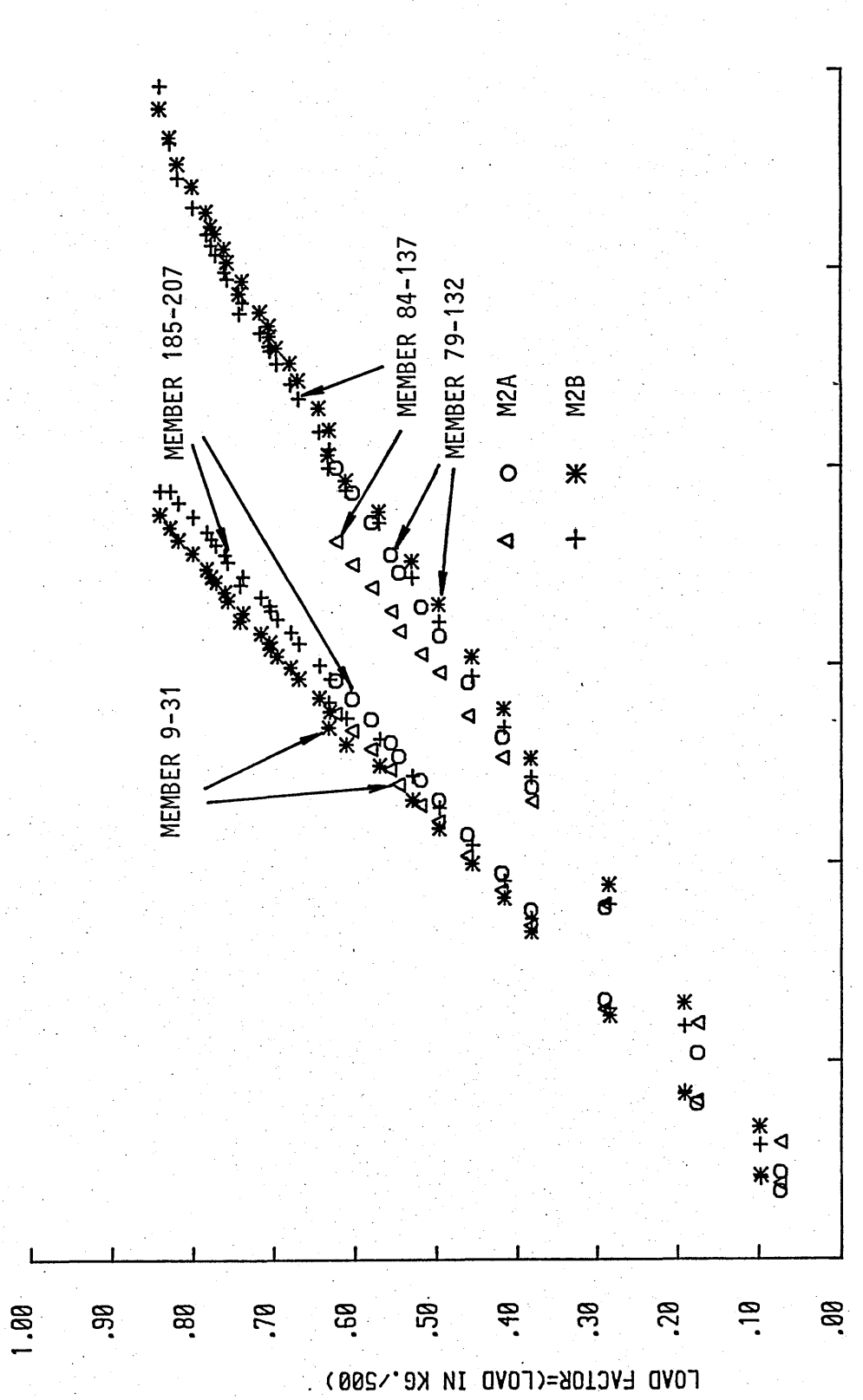

Fig (4.29) Load Factor - Axial force in members 9-31 and 185-207 and in members 84-137 and 79-132

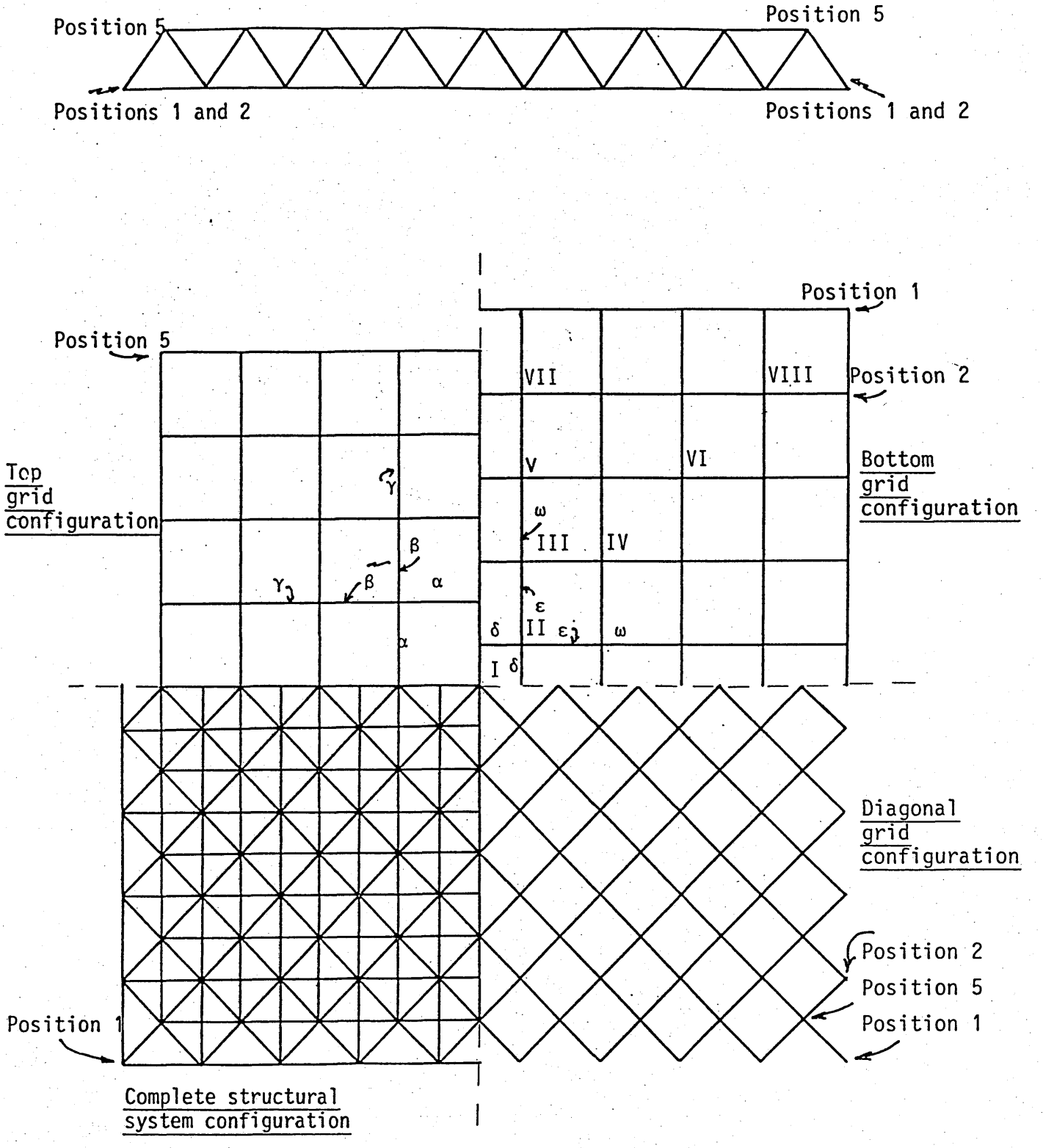

Fig (4.30) Skeletal Structural System 1. Plan showing the seperate layer configurations

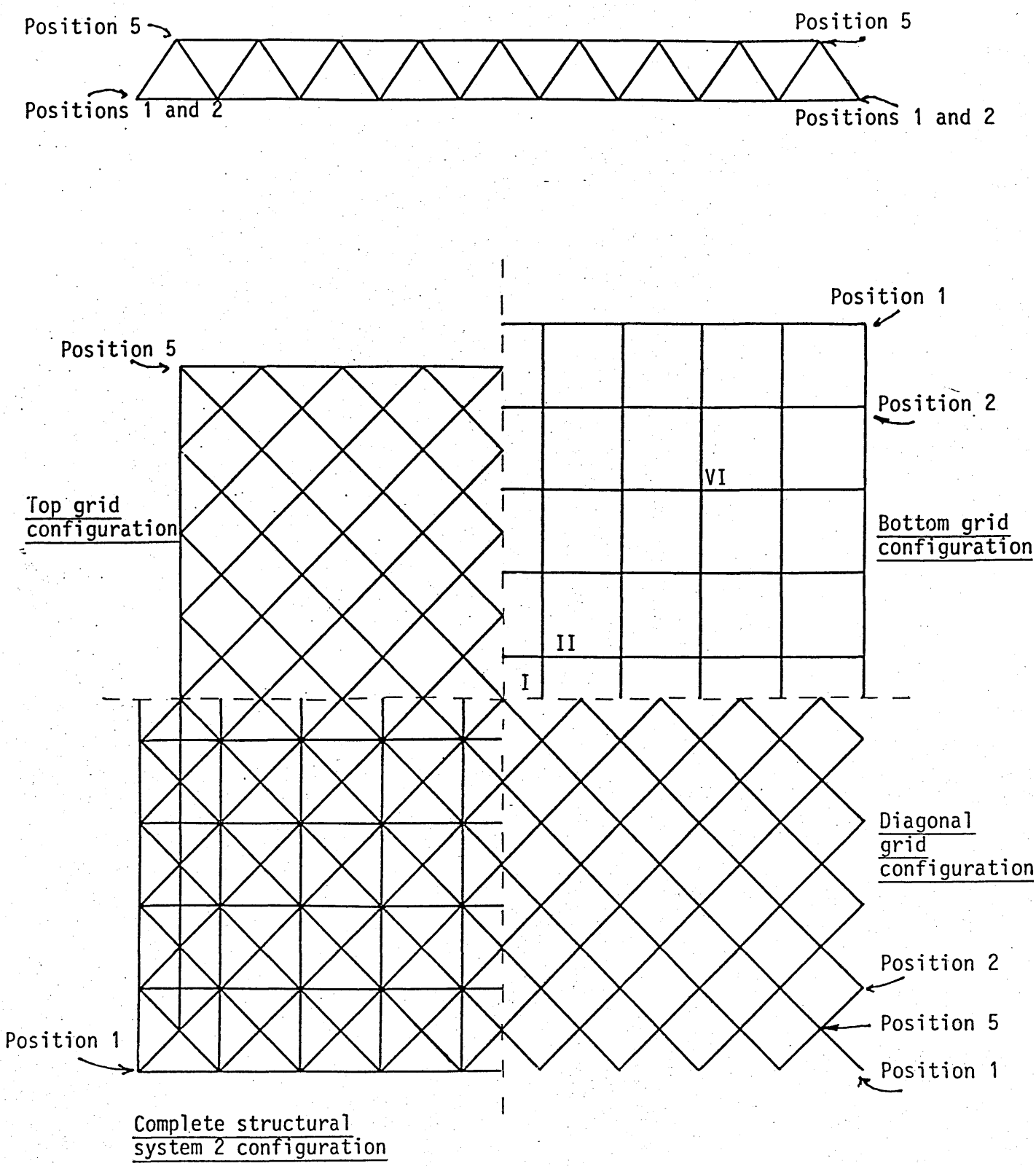

Fig (4.31) Skeletal Structural System 2. Plan showing the separate layer configurations

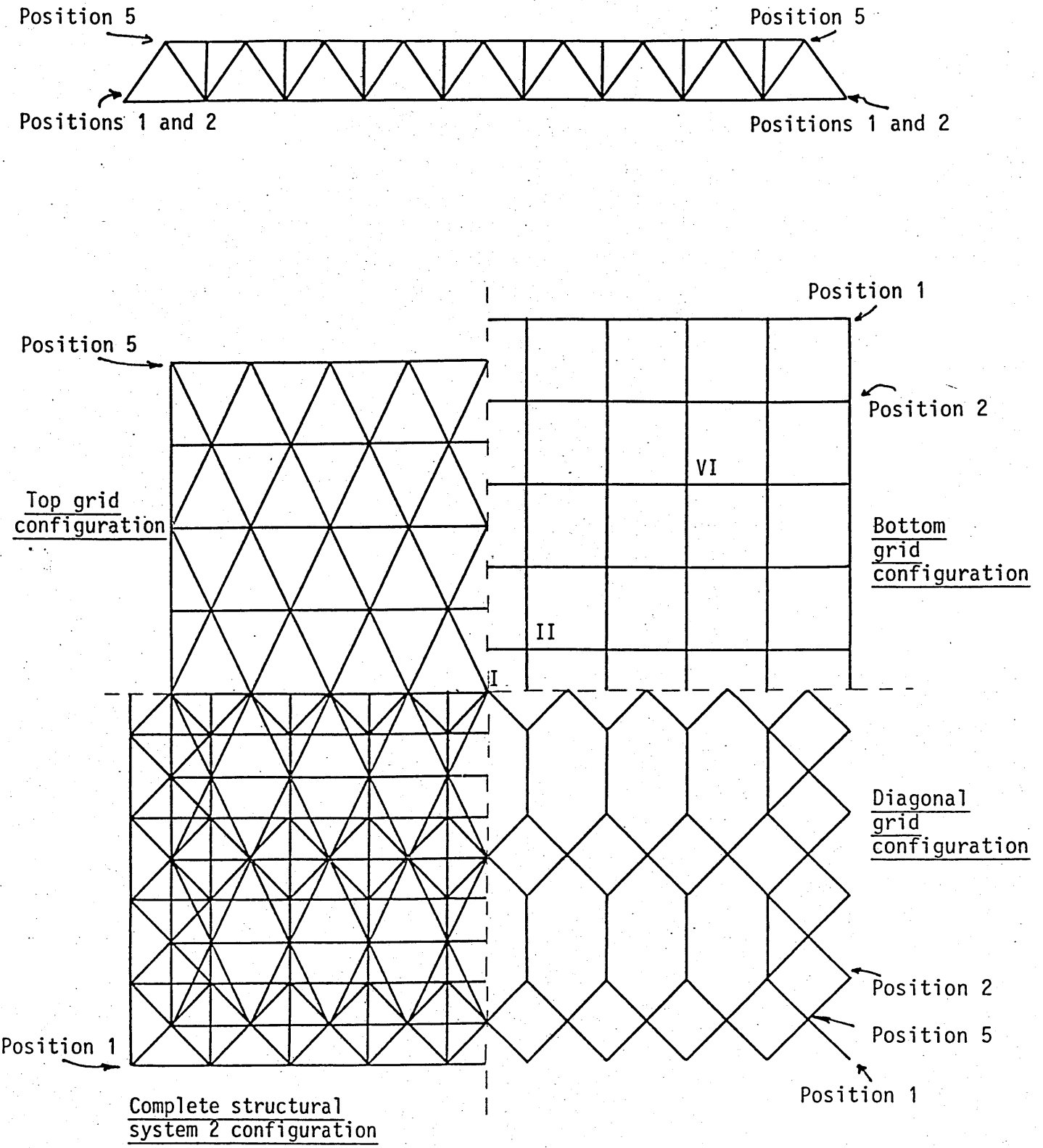

Fig (4.32) Skeletal Structural System 2. Plan showing the separate layer configurations

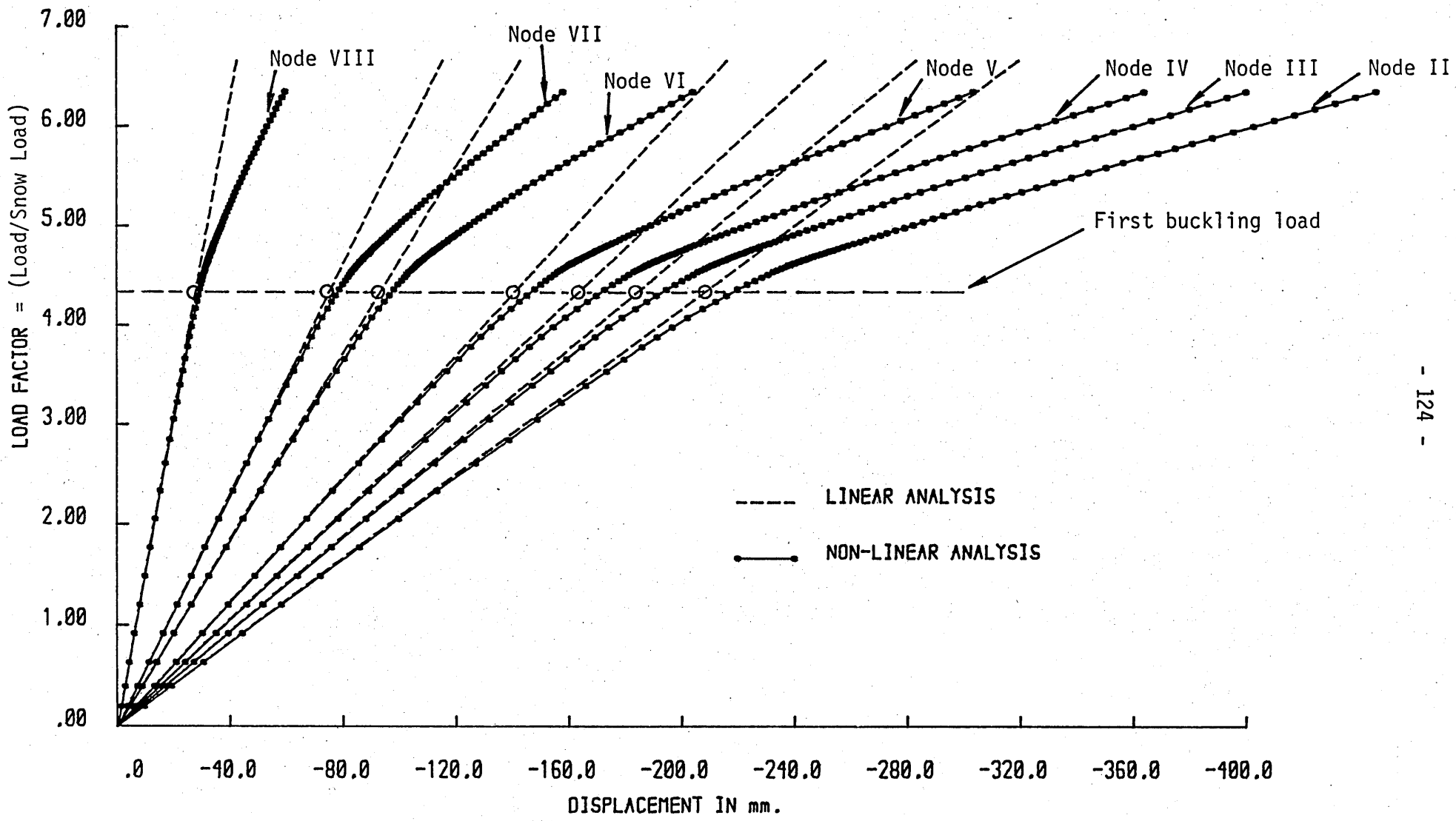

Fig (4.33) Load factor - deflection relationship for nodes II to VIII of all g.r.p. system 1

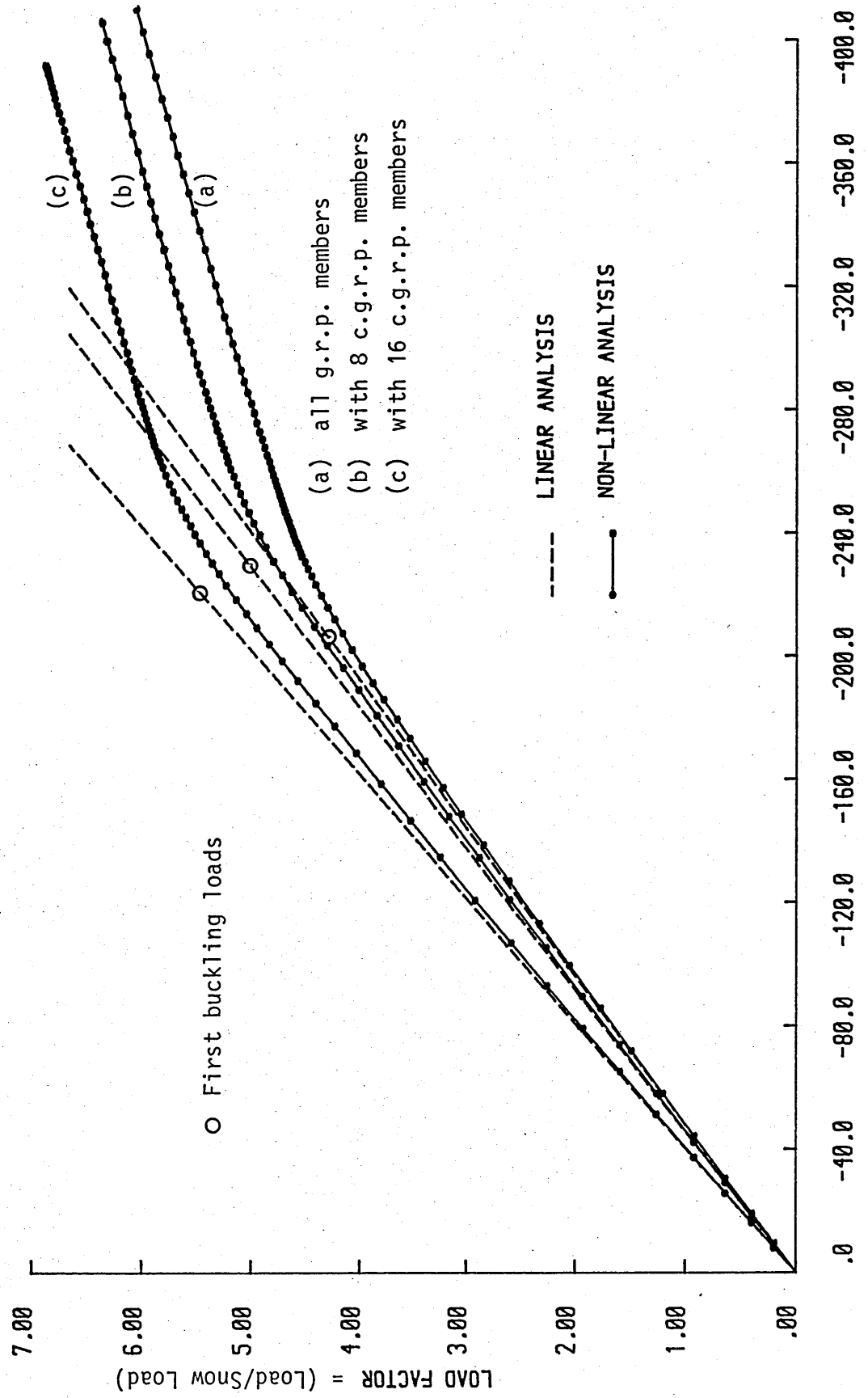

Fig (4.34) Load factor - deflection relationship for node II of system 1

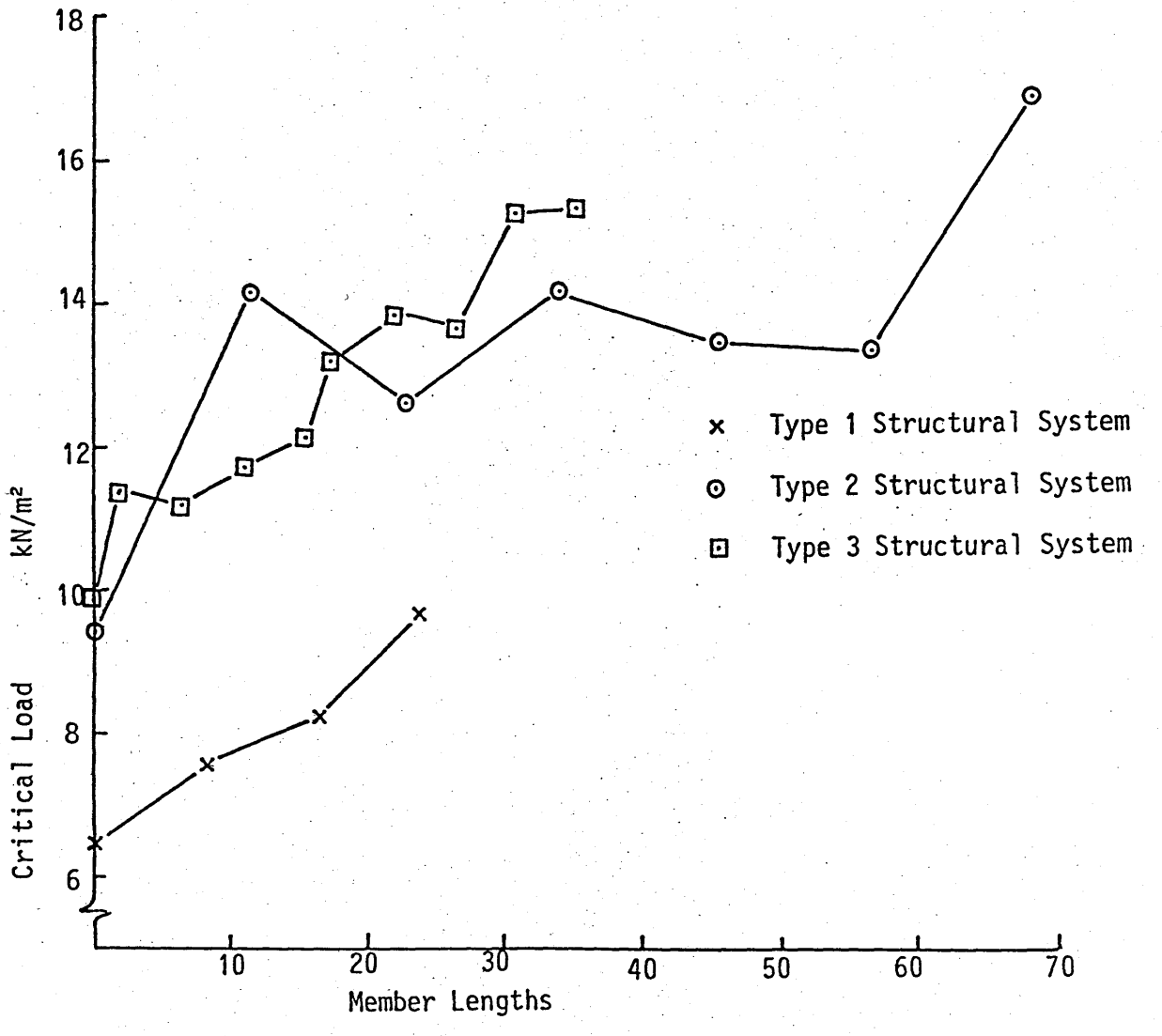

Fig (4.35) Relationship between critical load and c.g.r.p. member length

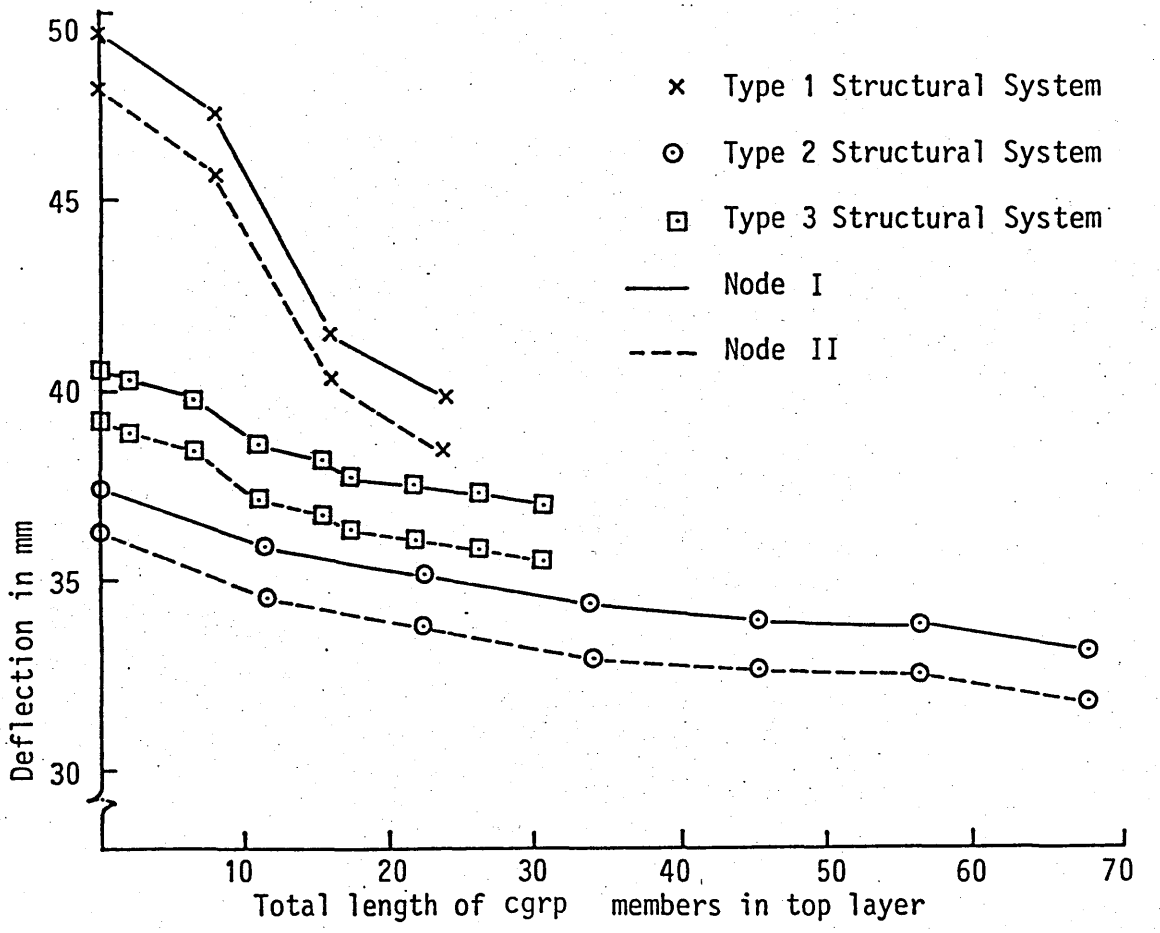

Fig (4.36) Relationship between downward deflection and total length of hybrid members at positions I and II

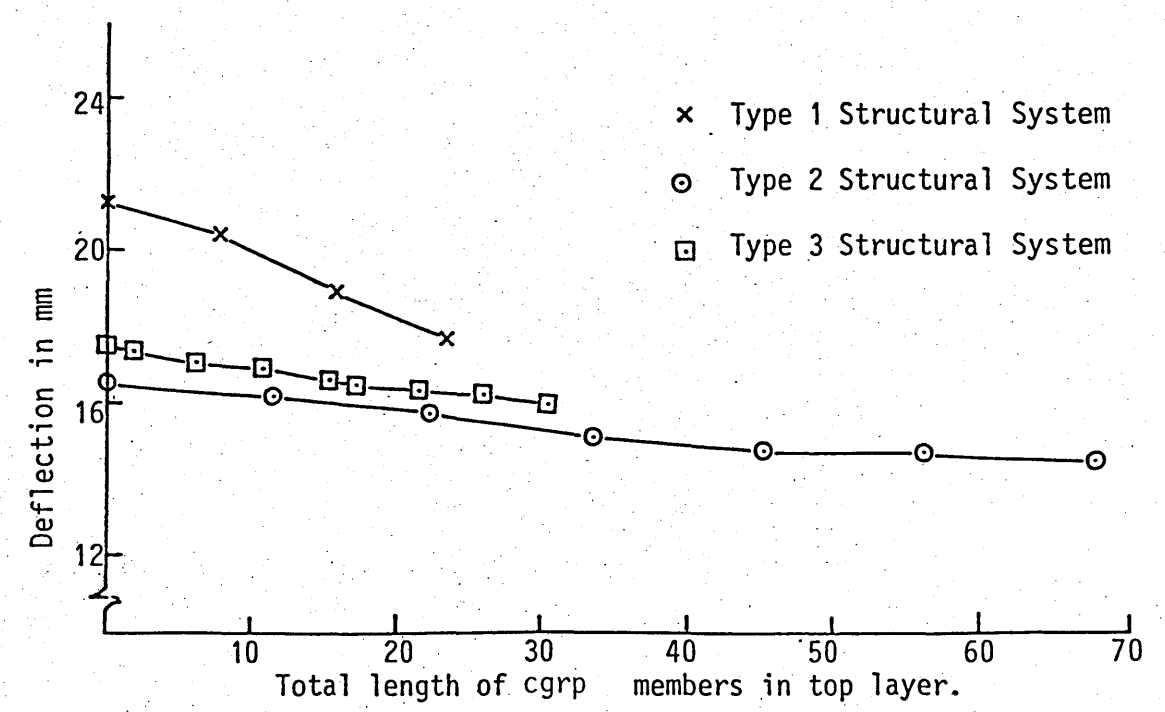

Fig (4.37) Relationship between downward deflection and total length of hybrid members at position VI

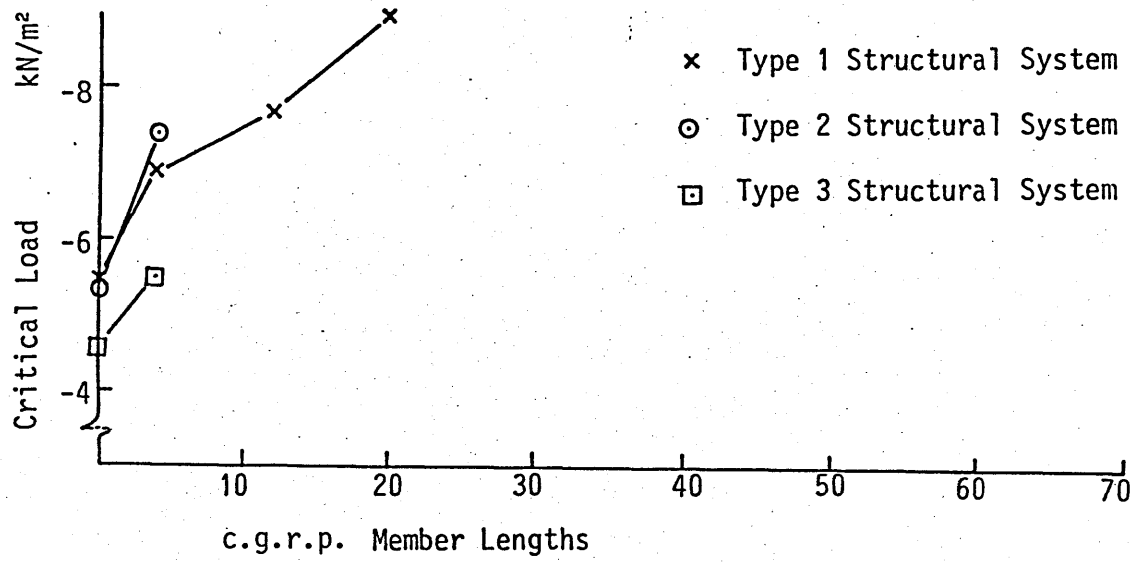

Fig (4.38) Relationship between critical load and hybrid member length

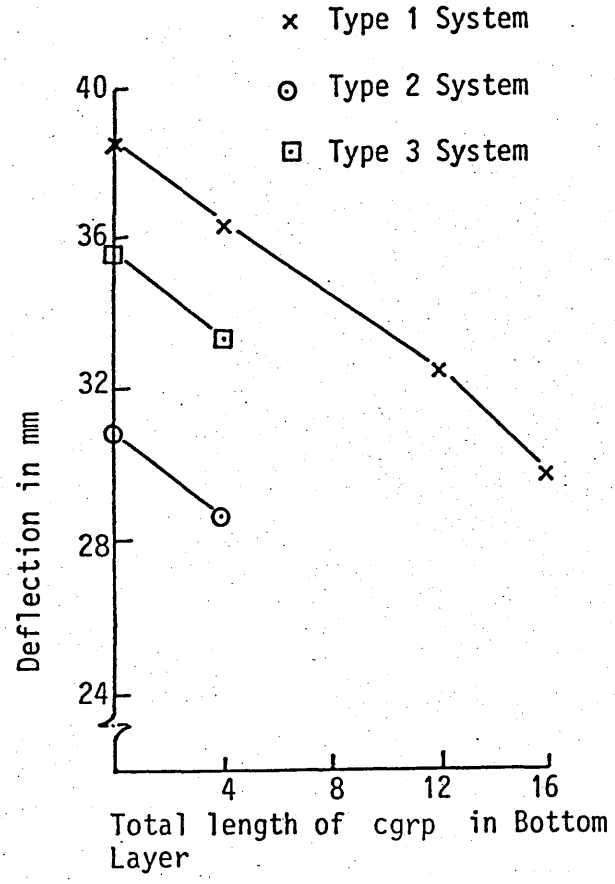

Fig (4.39) Deflection - length of hybrid for node II

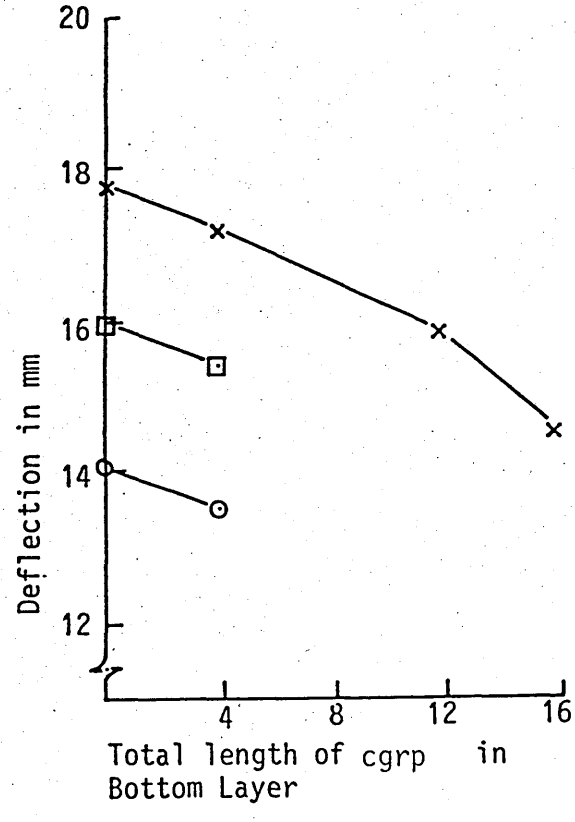

Fig (4.40) Deflection - length of hybrid for node VI

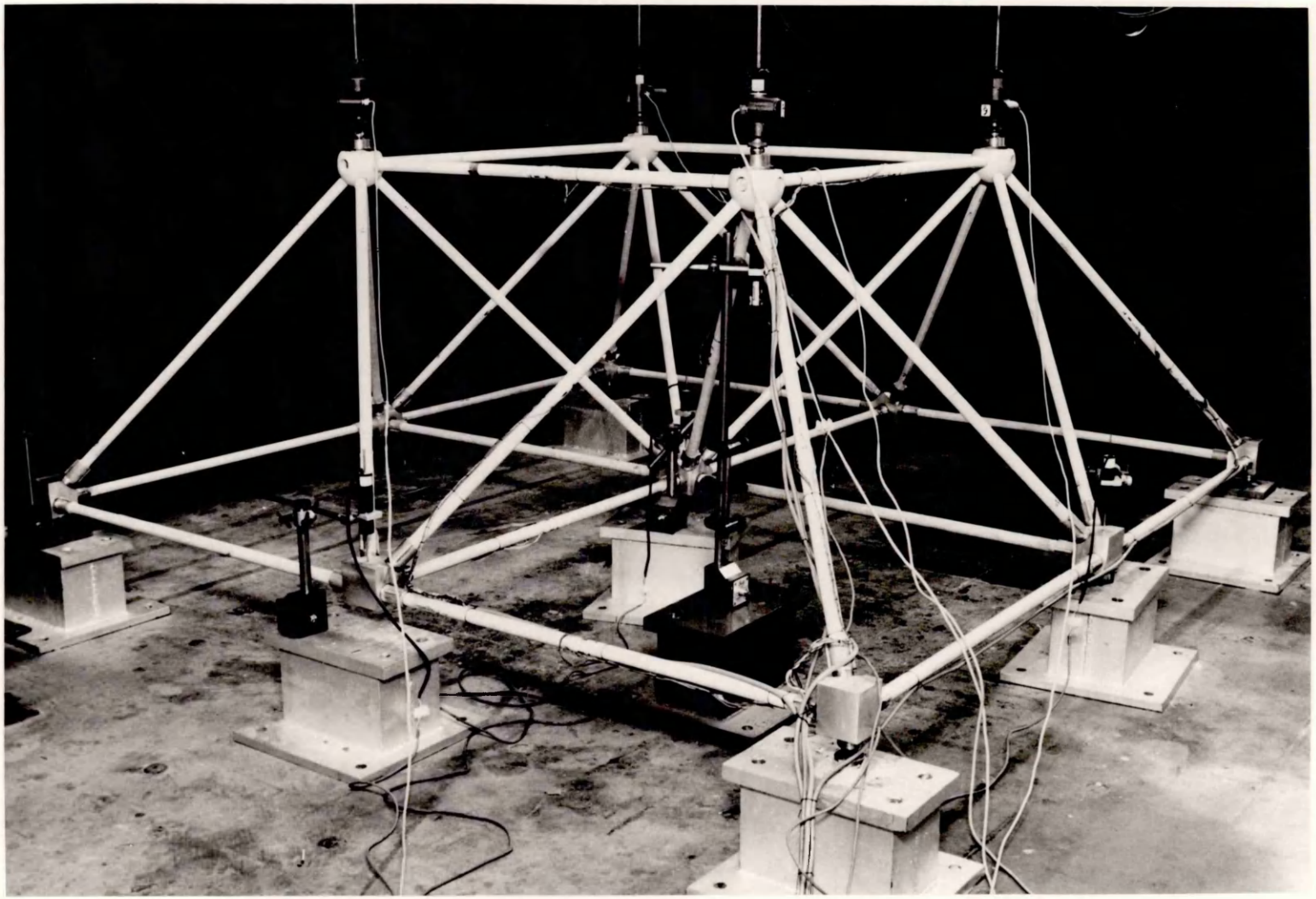

Plate (4.1) The short span double-layer grid model manufactured from pultruded g.r.p.

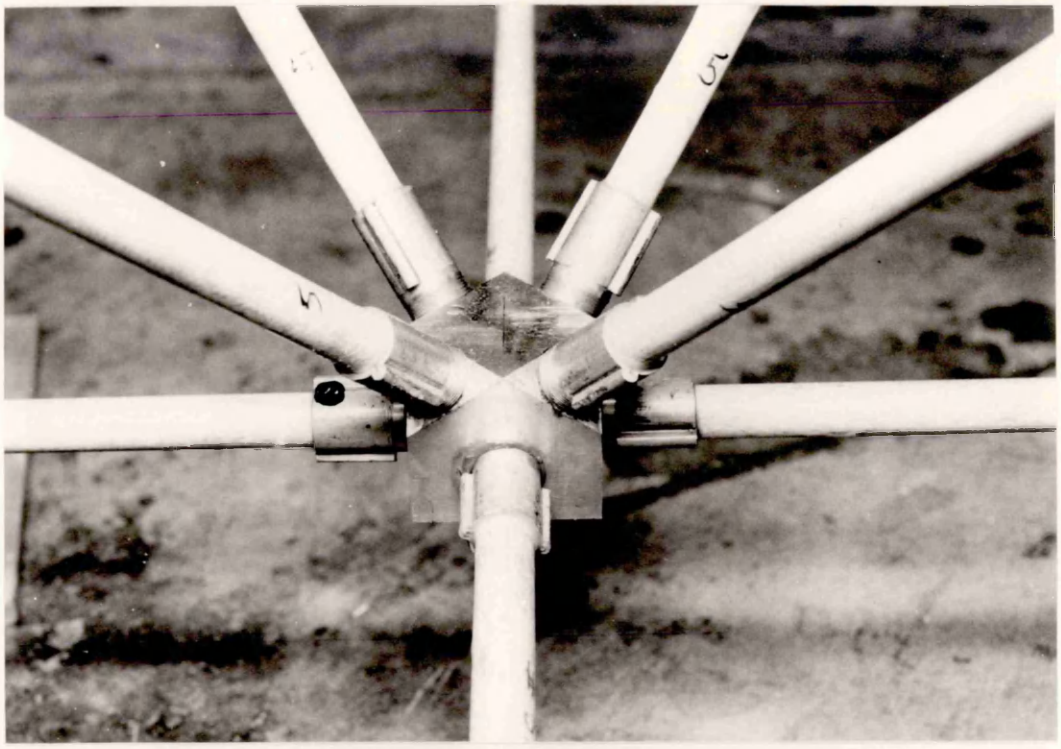

Plate (4.2) Central bottom layer aluminium node

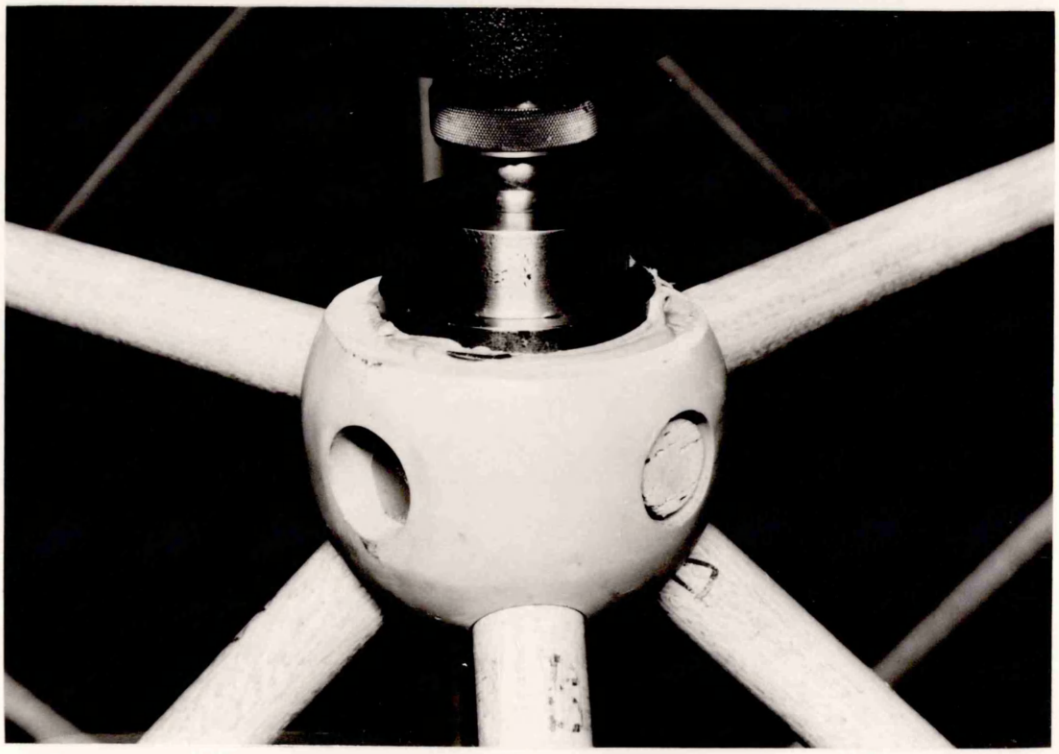

Plate (4.3) Top layer g.r.p. node

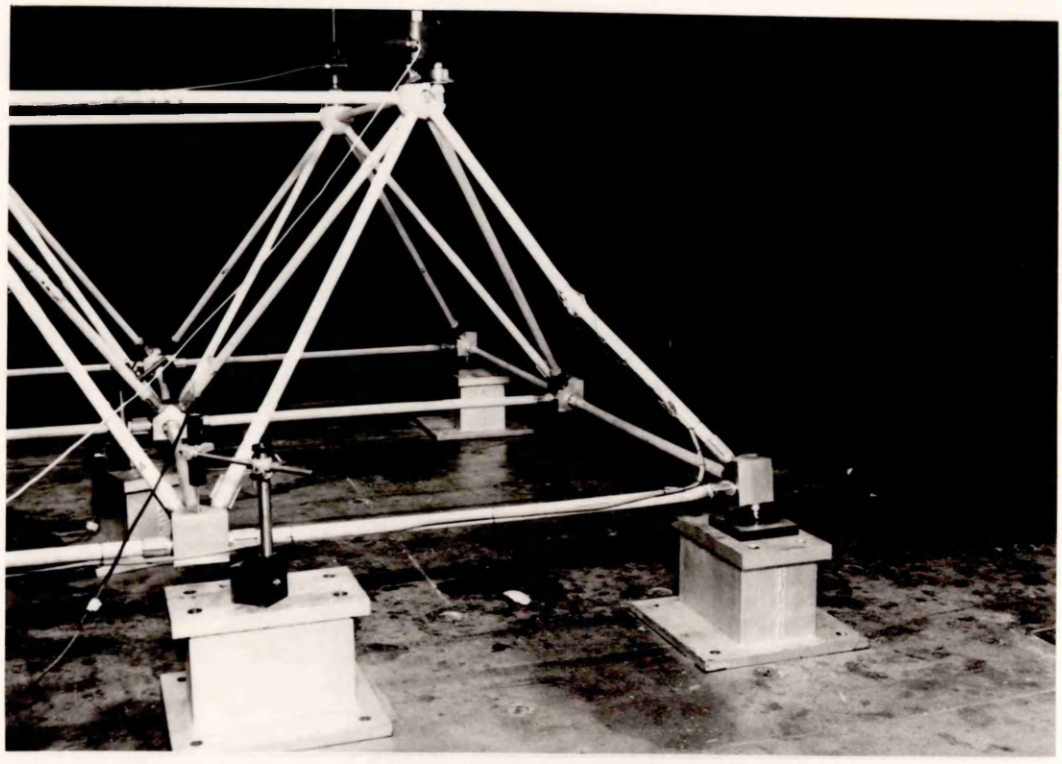

Plate (4.4) The model after final testing showing the failed diagonal member

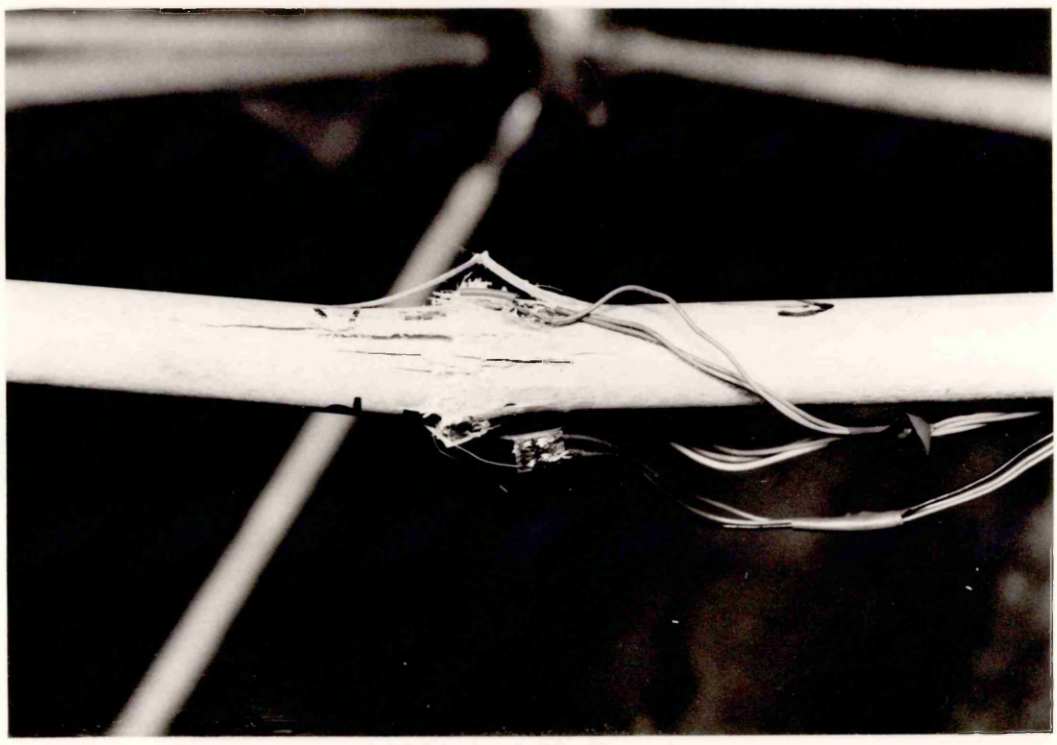

Plate (4.5) Detail of the failed g.r.p. model

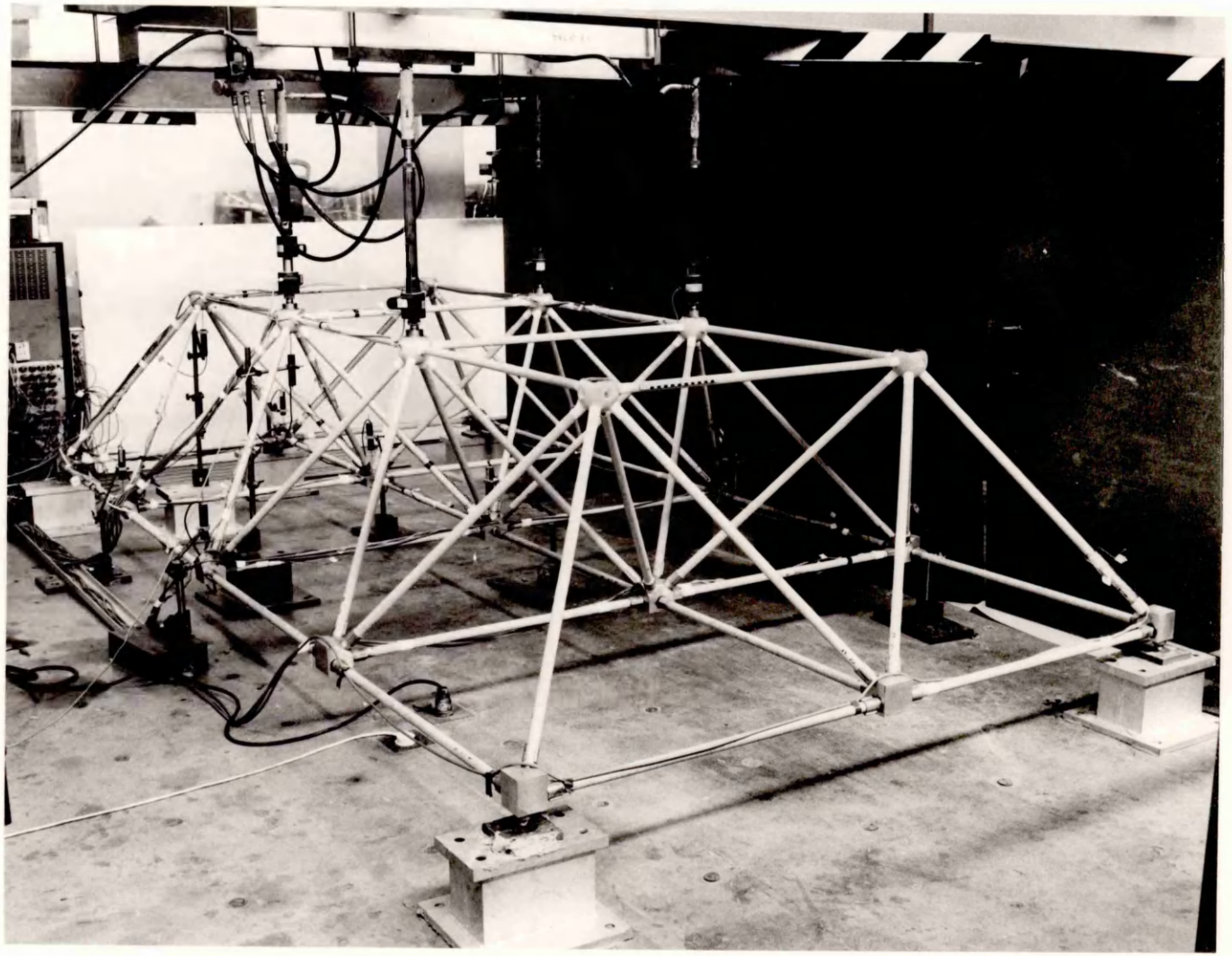

Plate (4.6) The long span double-layer grid manufactured from g.r.p.

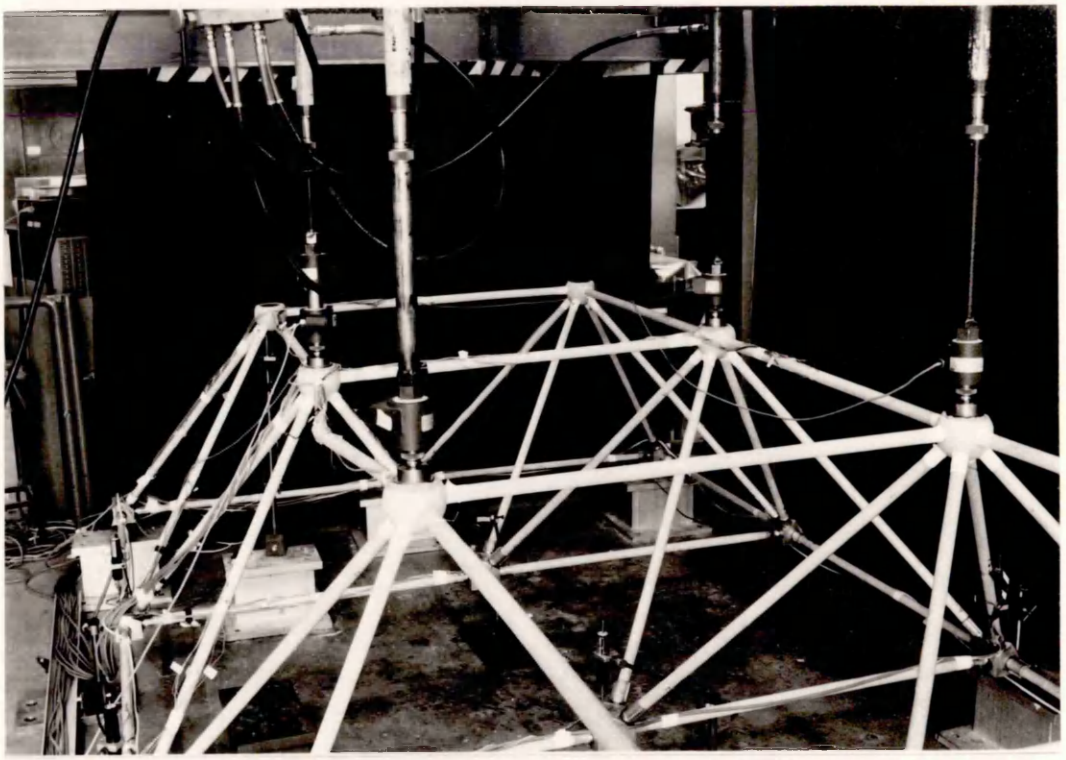

Plate (4.7) Model 2A after final testing showing the failed top central member

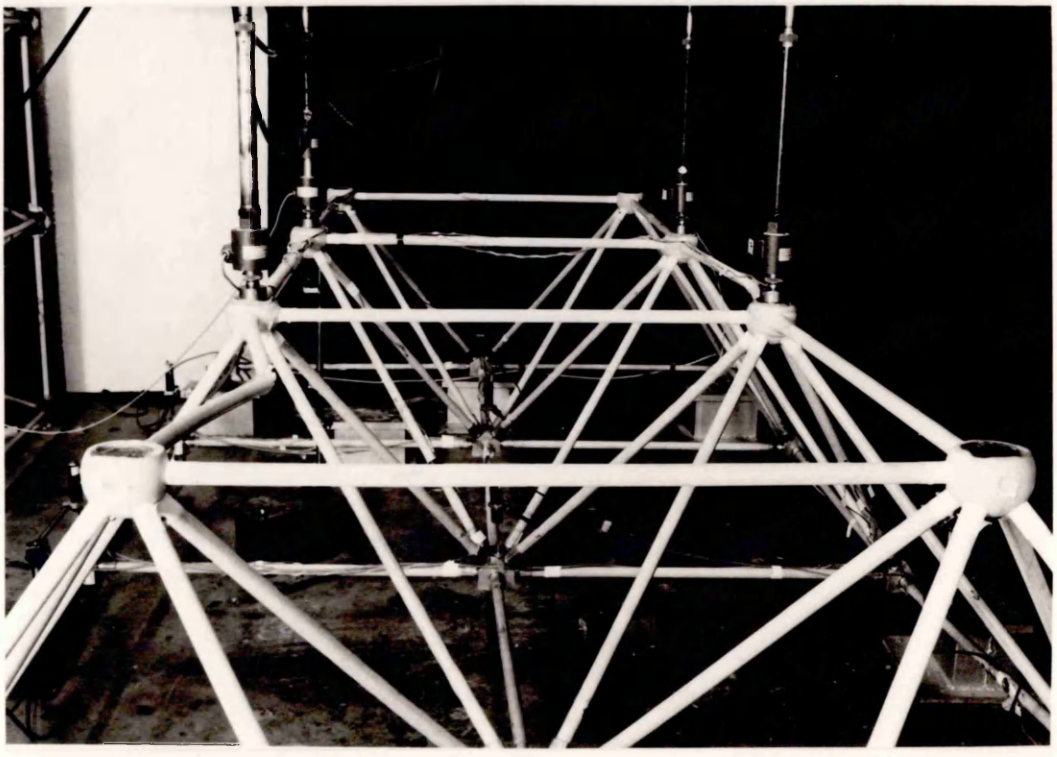

Plate (4.8) Model 2B after final testing showing the failed top longitudinal members

CHAPTER FIVE

FLEXIBLE SKELETAL STRUCTURES IN F.R.P.

5.1 INTRODUCTION

A wide variety of reticulated single layer shell structures have been built over the last few decades using various materials such as steel, aluminium, concrete and timber. Domes and barrel vaults have probably been the most popular of the single layer shell type structures. Both types have curved surfaces composed of members with a wide variety of possible configurations; a detailed description given by Makowski, Ref [62]. Each of these configurations has particular advantages associated with it, however, a consideration should always be given to minimizing the variety of members and connections required. One of the simplest and most efficient configurations is that of the three-way system. This type has been selected for the shallow dome model and the barrel vault configuration used for the parameter study.

These structures are inherently nonlinear, and consequently a linear analysis should be used with caution. When using the linear method of analysis the displacements of the structures would be underestimated when considering downward acting loads, but would be overestimated when the loading is acting upwards. Geometric nonlinearity can be critical, especially with shallow structures and it is essential to check for possible instability that may occur.

The computer nonlinear analysis program, described in Chapter 3, which was used to analyse the structures discussed in this Chapter is also capable of dealing with any type of instability that may occur, whether it is a local snap buckling occuring in one location, or a snap buckling occuring simultaneously in different locations or a general buckling. The program will trace the post-buckling load deflection curve for any degrees of freedom for these structures.

The load deflection curve characteristic of the snap buckling associated with these structures is shown in Fig (5.1). This curve shows the continuous line representing the stable section of the path whilst the dotted line indicates the unstable section. During the loading stage the load deflection curve will follow the section O to A then at the critical point A a dynamic jump occurs from position A to position B. Similarly, when the structure is unloaded it will follow the load deflection curve down to position C where it will swap to position D. If the displacements were controlled, the structure during loading could be forced to follow the whole load deflection curve from the point A to C and then to B. The snap buckling is discussed in more detail in Chapter 3.

In these structures the snap buckling is usually local and occurs when one of the nodes snaps and the local curvature becomes negative; local buckling often leads to general buckling as a result of the structure being unable to resist the shear loads. These loads are transmitted by the buckled unit to the neighbouring members, thus, causing the area of buckling to increase. General buckling and eventual failure could be caused by a series of local bucklings occuring at different locations affecting more than one node. The stability of such structures is affected by several factors such as the geometry, boundary conditions, type of loading and material properties.

This chapter investigates the construction of this type of structure using pultruded glass reinforced members. The main points will concentrate on the general behaviour and its prediction, mode of failure and the possibilities of improving the performance. All this is carried out by means of experimental testing and theoretical analysis.

5.2 SHALLOW DOME MODEL

5.2.1 THE MODEL STRUCTURE

The three way grid dome was fabricated from pultruded glass reinforced polyester composite members of 25.4mm external diameter and 2mm wall thickness. The members chosen for the construction were as free from initial imperfection as possible. The glass

fibre/polyester resin ratio by weight was 60/40 per cent. The dome was a portion of a sphere of diameter 9000mm and had a span of 3000mm and a rise of 280mm to the central node. The dimensions of this test structure were consistent with the laboratory facilities and represented a large scale model.

The members of the domes were cut to size and a special technique was used to manufacture and assemble the nodal joints. Six members met at all internal joints and into each end of the members a milled cylindrical aluminium plug was placed from which flexible metal pins protruded to enter radially another milled cylindrical aluminium disc which formed the centre of the nodal joint. Plates (5.1) to (5.3) shows the operations to form this joint to this stage. The perimeter nodes which connected three or four members were formed in an identical manner. When every joint on the structure was partially made a theodolite and a level were used to adjust the dome to its correct geometry which was readily deformed by the application of a small pressure to the temporary flexible nodal joints. Plate (5.4) shows the dome at this stage of manufacture. An adhesive was then used to fix the temporary nodes and to ensure a degree of rigidity of the structure; pins, made of pultruded g.r.p. rods, are inserted in the end of each member to ensure full connection. Plate (5.5) illustrates this stage of completion of the temporary nodes. A silicone rubber mould, shown in Plate (5.6) was manufactured from an aluminium die and was used to cast a glass reinforced epoxy composite around the temporary nodes to complete the nodal joint. Plate (5.7) shows one of the completed internal nodes and Plate (5.8) shows the assembled moel with all nodal joints completed. The centre of curvature of the bottom of the six peripheral support nodes was coincident with the centre of the node in order to allow rotations to take place about the same point and to avoid any eccentricity. A V-shaped steel channel, with adjustable supports, provided constraints against level displacements as shown in Plate (5.9).

5.2.2 TESTING ARRANGEMENT AND LOADING

The load was applied through a ball bearing and two load cells to the central node only. The first load cell was connected to a monitoring device, to enable a constant check to be made on the applied load level, and the second load cell was connected to a data logging system to record the load readings. To control the displacements at the central node, a manually operated mechanical jack, in series with a load cell and an aligning ball bearing, were placed under the loaded node. This latter load cell was also connected to the data logger. The two ball bearings on both sides of the loaded node were perfectly aligned thus ensuring that no appreciable rotational constraints were imposed. This arrangement was used as a displacement controlled actuator was not available. The displacement of the central node was controlled by the mechanical jack and the actual load applied to the structure was equal to the difference between the readings of the load cells above and below the node point. This arrangement shown in Plate (5.10) allowed the whole load-deflection curve to be traced including the unstable section; it prevented the dynamic snapping from taking place.

5.2.3 INSTRUMENTATION

Electric resistance metal foil strain gauges were used with resistance of 120 Ohms and gauge factor of 2.09. Selected members of the skeletal structure were strain gauged to enable axial and bending strains to be measured. At these points three gauges were used and were spaced equally around the member. Certain symmetric members were gauged to enable a study to be made of imperfections in the system which were unavoidably introduced during the assembly of the model.

Stroke potentiometric transducers were used to measure the vertical displacement of the central node and other selected nodes. All transducers were calibrated by means of a micrometer and their

behaviour was found to be linear. The coefficients of calibration were fed to the computer with the data to be processed.

The load cells used were calibrated in the instron and extra checks on the calibration were obtained by means of a proving ring.

The data obtained from the model testing, which was stored on a punch tape, was transferred to the University main computer to be processed and produced in forms of graphs and tables.

5.2.4 TESTING PROCEDURE

A series of preliminary tests were undertaken for the following reasons:-

(a) To check all instrumentation, the data logging system and the data recording system during testing in order not to lose any important information when testing the structure up to failure.

(b) To adjust the supports and ensure that all six were imposing the same constraints.

Subsequently, the model was loaded twice; during the first test the magnitude of the load was such that snap of the central node took place and during the second test the structure was loaded to failure.

The loading sequence consisted of applying a load of a magnitude slightly higher than the snap load, obtained from the computer analysis through the hydraulic jack. This load was supported by the dome and by the mechanical jack; however, only a small part of it was supported by the dome initially. As the mechanical jack was lowered manually the share of the load taken by the dome was increased until the critical load value was reached. At this point, as the mechanical jack was lowered further, the load taken by the structure decreased until it reached a position of stable equilibrium (equivalent to position C on the curve shown in Figure (5.1) and then commenced to increase its share again.

5.2.5 THE THEORETICAL ANALYSIS

Linear and nonlinear analyses of the shallow dome were carried out by means of the computer program developed for this purpose and fully explained in a previous section of this work. The structure was analysed under three different boundary conditions; however, only one of these conditions represented that of the constraint of the tested model. The three boundary conditions considered were as follows:-

(a) The six support nodes which are shown in Figure (5.2) were position fixed only.

(b) The six support nodes were position fixed in the vertical direction and, in addition, node numbers 1, 127 and 217, shown in Fig (5.2), were position fixed in the horizontal direction.

(c) The six support nodes were position fixed in the vertical direction only.

All assumptions made for the computer program are valid for this structure and in particular there was no need to introduce imperfections as the behaviour was characterized by the limit point (snap buckling) behaviour. In these analyses every member of the structure was discretized into six segments. Two short ones at the end of each member with higher stiffness and with dimensions equal to the distance from the centre of the node to its face. These two segments idealised the physical dimension and the extra stiffness of the nodal joints. A detail of the nodes is shown in Plate (5.7). The other intermediate discretization was required in the case of this structure because of the large deformations involved, especially at higher load level.

5.2.6 RESULTS AND DISCUSSION

The results are divided into two sections; section A deals with the analytical and experimental techniques where only one boundary

condition is considered, section B investigates the analytical solutions only when the structure is under the three boundary conditions discussed in the previous section.

(A) Analytical and Experimental Results for Fully Fixed Boundary Conditions

All supports to the model were constrained against vertical and horizontal displacements and no rotational constraints were imposed. The results of the theoretical analysis are in a graph form and the experimental results are represented by symbols on these graphs. Figure (5.2) shows the configuration and member discretization for the dome.

The sign convention is such that downwards displacements and compressive axial forces are assumed to be negative. Two sets of graphs have been presented, one of load against vertical displacement and the other of load against axial force. Bending moments for the analytical and experimental analyses agree closely as do the axial force and therefore, only the latter graphs will be shown.

The theoretical and experimental load-displacement curves for the central node are shown in Figure (5.3) and excellent agreement is achieved with a percentage difference between the theoretical and experimental snap buckling load, less than 5%. In addition, the experimental and theoretical values of the load displacement relationship for the inner ring nodes, Figure (5.4) agree closely. The difference, however, was that in the pre-buckling state the experimental values were negative. This difference could have been caused by geometric imperfections or ineffective boundary conditions. Figure (5.10) shows the effect different boundary conditions have on the behaviour of this node. From a consideration of the theoretical load deflection curves of the central and the inner ring nodes (viz Figures (5.3) and (5.4)) it may be concluded that the snap buckling affects only the central node.

The experimental strains in members A to K of Figure (5.2) have been converted to axial forces and plotted against the load factor. Figures (5.5) to (5.8) show the results. A symmetrical behaviour was assumed when undertaking the theoretical analysis and all the experimental results for symmetric members have been plotted on these theoretical curves, using different symbols for different members. Figure (5.5) shows the load plotted against the theoretical axial force, as a result of the linear and nonlinear analyses, for the members connected to the central node and superimposed upon this curve are the experimental results for members A, B and C of Figure (5.2). Similarly Figure (5.6) shows the load factor against the theoretical axial force for the inner ring members and superimposed on this graph are the experimental results for members D, E and F. Figure (5.7) shows a similar theoretical curve and experimental results plotted on this graph for members G and H which are on the outer ring of the structure. The experimental relationship between the load factor and force in members I, J and K is shown in Figure (5.8).

In general, the computer nonlinear analysis predicted with a good degree of accuracy the structure's performance but it must be stated that the assumption of symmetric behaviour was unrealistic. The high values of axial force recorded in members C, E, H and K is an indication that the non-symmetric behaviour is the cause of the discrepancies between the analytical and experimental solutions.

The central unit of the model which consists of the central node and the six members connecting it did not sustain any damage during the first loading to snap and a comparison of the initial and final reading at no load condition confirmed this. During the loading cycle to failure and at a load in excess of that causing snap the two members C and L failed at their ends nearest to the central node. From previous investigations on the material and from an observation of the strain gauge readings on the members it was clear that failure was initiated in the compression fibres of the composite. In addition, it was clear that premature failure was caused by imperfections which could have been caused by eccentricities in the central node, due to the members not meeting

at the same point, excessive size and non uniform stiffness of the node and geometric imperfections in the members. It was noticed that the value of force being taken by identical neighbouring members to those that failed, and the compressive stress values in these members from the theoretical investigation, were lower in value.

It was expected that the model would fail suddenly as the material contained a relatively high percentage of glass (60% by weight) and therefore, the composite would follow more closely the stress strain relationship and failure behaviour of the fibre which is a brittle material.

(B) Computer Analysis Results for the Three Boundary Conditions

In this section only the load-displacements curves are considered as they contain all the information required. The effect of the boundary conditions on the internal forces was not considered as it falls outside the scope of the investigation. Figures (5.9) to (5.11) show the load-displacement curves for the central node, the inner ring nodes and the centre ring unrestrained nodes respectively. It should be noted that in the second support boundary case, node point 50, for instance, will behave differently to node point 109 shown in Figure (5.2). Consequently, only the node points in similar locations to that of node point 50 have been considered during the discussions of this support boundary case.

The perimeter members formed a tension ring beam when no horizontal support constraints were provided to the structure and consequently the value of the snap buckling load was sensibly the same for the three boundary conditions; this is shown in Figure (5.9). The general behaviour of the central node was similar in all cases considered here. However, there was a slight difference in the results for the structure with no horizontal constrained supports; these results showed a more flexible behaviour when the structure was under load and the snap buckling resulted after a more severe structural deformation had occured. The load-deflection curves for

these nodes are similar in form but vary in magnitude and direction particularly for the two extreme cases considered, viz for the total horizontal constraint and for the total horizontal freedom.

5.3 PARAMETER STUDY

5.3.1 INTRODUCTION

The reticulated single layer shell structures are extremely flexible and, unlike double layer grids, are more sensitive to local buckling. Consequently, the introduction of stiffer members to improve their performance would not be an efficient method as is the case with double layer grid structures. Local buckling, in the flexible structures, may occur anywhere and the introduction of stiffer members in that location represents a solution for a particular problem and does not normally lead to general improvement of the structural performance. It appears that, in the case of these structures, geometric considerations are more practical and therefore, the investigation was limited to a pure geometric parameter study.

A circular braced barrel vault was selected for the parameter investigation. The span was maintained fixed with a value of 8 metres and the rise was chosen as the variable parameter. The member types considered were of dimensions identical to those used in the parameter investigation of the double layer grids which had a slightly large span.

A preliminary design and analysis of the barrel vault showed that the deformations of the structure, under a relatively small load, were excessively large. Consequently, a set of stiffening skeletal ribs, with spacing of 4 and 6 metres, were introduced to make the structure more practical and to reduce the deformations. Four structures of the same configurations and with four different rises were then studied making use of the linear and nonlinear computer analyses programs.

5.3.2 THE BARREL VAULT STRUCTURES

The barrel vaults considered in this investigation had various span to rise ratios for a constant span of 8000mm and length of 16000mm. They were reticulated of the three way type, a configuration characterized by the small variety of member lengths and connections. All structures have identical topography with an equal number of members and nodes. The four span to rise ratios investigated were 8000/4000, 8000/2000, 8000/1000 and 8000/500 and in this thesis are called types 1, 2, 3 and 4 respectively. Figure (5.12) shows the configurations.

The change of geometry, caused by the difference in the rise, affected only the length of the members. All the nodes of the barrel vaults lay on surfaces of circular cylinders with the larger radii corresponding to the smaller rises and vice versa. These configurations are symmetric about the two vertical planes passing through the longitudinal and transversal centre lines.

The members of the structures were assumed to have been manufactured from 50mm external diameter, 2mm wall thickness pultruded tubes with a glass/polyester matrix percentage ratio by weight of 60/40. Their mechanical properties, required for the analysis, were assumed to be identical to those of the smaller diameter members of the same glass content which were obtained experimentally.

All the configurations have four double layer skeletal curved ribs through their length. For all the configurations the ribs have a constant height of 500mm which means that the nodes of the rib connecting the diagonals are part of circles with centres lying on the axis of the cyclinders associated with the various barrel vaults. Two ribs are at the two ends of the barrel vaults and the other two are spaced 4 metres from the first two with six metres distance between the two central ones. These ribs are to stiffen the overall structural systems; for a single layer braced barrel vault the relatively low modulus material was able to support only a fraction of the working load before deforming excessively.

5.3.3 THE BOUNDARY CONDITIONS

For the analysis, all four barrel vaults were assumed to be position fixed in the x, y and z cartesian coordinate directions at the various nodal joints on the two longitudinal edges. However, when taking advantage of symmetry the nodes on the planes of symmetry have to be constrained such that deformations are conformable with symmetry. Displacements in those planes and rotations represented by vectors normal to the same planes must not be constrained.

5.3.4 THE LOADING OF THE STRUCTURES

The barrel vaults were subjected to a uniformly distributed load over plan area of the structures and, in addition, a uniformly distributed load was applied to half plan area of the span over its full length. The u.d.l. was convered to concentrated loads applied to the nodes. The conversion was based on the plan area of influence of the nodes. The influence areas were computed from the projection of each of the structural configurations on the horizontal plane. In presenting the graphs the snow load of 750 N/m^2 was used to normalize all applied loads. According to the directions of the loads and also whether they were applied on full or half structure, the applied loads were classified as follows:

(a) a uniformly distributed load throughout the structure and acting vertically downwards;

(b) a uniformly distributed load throughout the structure and acting vertically upwards;

(c) a uniformly distributed load on half the structure and acting vertically downwards;

(d) a uniformly distributed load on half the structure and acting vertically upwards.

5.3.5 THE THEORETICAL ANALYSES

A linear and a nonlinear analysis of the barrel vaults were carried out. Symmetry was utilized in these analyses according to the loading condition. For the nonlinear analysis each member of the barrel vault was represented by two elements giving rise to the analysis of a structure containing 424 members and 283 joints in the case of a half of the barrel vault, and 216 members and 147 joints in the case of a quarter of the barrel vault. Limiting the discretization of each member to two members and taking advantage of the symmetry helped in reducing the computing time considerably.

By means of the computer program, described in Chapter 3, each of the four configurations were analysed under four loading conditions; thus, sixteen nonlinear analyses were undertaken. In all the analyses, no member bifurcation buckling occured and, therefore, no imperfections were introduced.

As the nonlinear analysis is extremely expensive, it was stopped when either deformation became excessive or the number of load increments exceeded a specified limit, even if instability did not occur during the analysis.

5.3.6 RESULTS AND DISCUSSION

The nonlinear analysis includes over thirty load increments and to each load level corresponds a set of displacements and internal forces which represent the solution. The results are usually displayed as a set of curves of any of the displacements or internal forces against the load level. As the number of nodal points and members is quite large, only the results of selected nodal points and members are displayed. For the load displacement curves two points on the reinforcing beams (A and C) and the two more flexible nodes (B and D) were selected. Also, the results of the internal forces of the members I to V are shown. The four nodal points A to D and the five members I to V, in the case of loads (c) and (d), are within the part of the structure subjected

to the loading. These nodal points and members are shown in Figure (5.12).

Figures (5.13), (5.14), (5.15) and (5.16) show the linear and nonlinear relationship between the load factor and displacements for the loading case (c), as described in section 5.3.4. The sign convention used in these analyses are that the vertically downward displacements are assumed negative and the upward displacements positive.

Figure (5.17) shows the relationship between the load factor and vertical displacement of nodal point D under load condition (c). The graph enables a comparison to be made between the behaviour and the degree of nonlinearity, associated with the node D, of the four types of structures as the span to rise ratio varies. It is shown that as the rise decreases the structure becomes more flexible and the degree of nonlinearity increases.

The linear and nonlinear load factor against vertical displacement relationship for node point D is shown in Figure (5.18). Three sets of curves are drawn, each giving the behaviour of the node under full and half load (load types (a) and (c)) for barrel vault types 2, 3 and 4. The results of barrel vault type 1 were ommitted because of the partial overlapping of its results and with those of type 2. The curves for barrel vault type 2 show that for both linear and nonlinear analyses, displacement under half load is larger than that under full load. Type 3 barrel vault shows a similar linear behaviour when considering full and half load conditions, whereas under low loads placed on half span only the nonlinear behaviour shows displacements larger than those for full load conditions. However, for the high external load values the situation is reversed with the full load conditions having the larger deflection value for the same applied load. In the type 4 barrel vault, which is a very low rise structure, the displacements under the applied load for both the linear and nonlinear analyses are greater than those under similar loadings applied on only half the span of the structure. For the barrel vaults type 2 and 3, a local snap through instability occurs under full load condition,

whereas under the half loading condition the rate of deformation increases as the higher loads are applied, although no instability is evident. Both the full load and half load investigations of the barrel vault type 4 were stopped after large displacements had been recorded. It was felt that this particular structure at this time did not warrant the large amount of computer time required to cause snap through buckling to occur.

Figure (5.19) shows the relationship between load factor and vertical displacements at positions A, B, C and D in the type 2 barrel vault. The two loading cases considered are a positive and negative half load (load cases (c) and (d)). It may be clearly seen that the linear analysis underestimates deformation when analysing a positive loading condition and overestimates it when analysing a negative loading condition. Figures (5.20) and (5.21) show the load factor plotted against displacement of nodal point D for the barrel vault types 2 and 3. The graphs compare the results for one position on the vault (node D) under loading cases (a), (b), (c) and (d). It may be seen that for the linear curves of both graphs and the nonlinear curves of the first graph, the displacements under half load are larger than those under full load. However, this is not so for the nonlinear behaviour shown in Figure (5.21).

The criterion for the design of fibre/matrix skeletal systems is invariably the deflection and to gain an appreciation of the general behaviour of the overall structure, especially on the nonlinear region, an investigation of the deformation of the entire structure is generally undertaken. From these, all information regarding the elastic stability is readily obtained. The internal forces, however, are obtained and checked against failure. Their nonlinear behaviour is a direct consequence of the geometric nonlinearity, if the behaviour of the material is linear elastic. The few members, I to V, selected from different locations were used to show the effects of nonlinearity and the change of geometry on their internal forces. Figures (5.22) to (5.25) show the relationship between the internal applied load, in terms of load

factor, and the axial forces for the five members of barrel vault types 1 to 4 under load case (c).

The two main points to be noted from the four figures are, firstly the degree of nonlinearity of the axial forces increases as the span to rise ratio of the barrel vault increases (ie, the height of the barrel vault decreases). Secondly, the effect that the geometry of the barrel vault has on the axial forces. It will be seen that as the rise of the structure decreases, axial forces increase in certain members and decrease in others. The general trend is that an increase occurs in the members which are highly stressed. The results also show that the divergence of the axial forces between the high stressed members and the low stressed members in the barrel vaults become larger and the rise decreases; this is clearly shown in Figure (5.26).

Although internal forces are not of the main interest in this study, a set of bending and torsional moments for members I to V is given for completeness. Only barrel vaults type 1 to 3 are included, type 4 being uncapable of carrying significant loads. The results are displayed for one loading level of 600 N/mm^2. The bending moments are given for the member ends furthest from the centre line. Four values are given for each member of a particular configuration. These are the linear and nonlinear results for the two loading conditions (a) and (c).

The general trend for the torsional moment which is generally expected in these types of structures, is that torsional moments are higher in the case of a uniformly distributed load acting on half the barrel vaults than is the case for a uniformly distributed load on all span. However, for the bending moments it depends on the location of members. Another point shown in this table is the difference between the linear and nonlinear results.

5.4 OBSERVATIONS

Single layer reticulated structures manufactured from pultruded

g.r.p. composites are sensitive to the change of geometry resulting from deformation and the shallower the structure the larger the nonlinear effects. Consequently, most of the time, a nonlinear analysis is required to obtain the exact state of deformation. Instability, however, is the main problem in these types of structures. Fortunately, the nonlinear method of analysis can predict their occurance with good accuracy. Local snap through represents the more common type of instability in these structures.

The geometry is quite an important factor with this type of material as shown by the parameter study. The change of geometry may result in improving the overall stiffness of the structure. However, these particular configurations (ie, the single layer reticulated structures) could not be used for large spans, when manufactured from g.r.p. A combination with the stiffer type of structure, such as the double layer arches used with the barrel vaults, can result in more practical types of structures.

It has been shown that pultruded glass reinforced polyester tubes have a good recovery characteristic after they have undergone large deformations and without sustaining any apparent damage. It is to be emphasised that this was the case with members of these flexible structures, when internal stresses were not large. Because of the brittleness of these members the structure tends to collapse without warning.

Imperfection in these structures can be caused by several factors and any combination of these can be incorporated into the computer analysis. However, to be able to understand the effects of particular imperfections it is necessary to be able to study them independently of other imperfections. No particular imperfections were considered in this section except for the analysis of the shallow dome model under different support conditions. The results obtained, related to the effects of imperfections to the lack of horizontal constraints of the structure and thus enabled a greater understanding of the problem.

Member		I		II		III		IV		V	
Method of analysis		Linear	Non Linear	Linear	Non Linear	Linear	Non Linear	Linear	Non Linear	Linear	Non Linear
B.V. Type	Load Case	Bending Moment in N.mm									
1	(a)	11872	12766	12041	14613	27265	36176	73918	88922	93295	108414
	(c)	6790	7782	57313	79359	11939	15247	81784	95270	97990	117308
2	(a)	36000	40720	20142	22929	9799	12025	44510	73560	57170	78734
	(c)	18170	21996	62502	87778	16982	25795	32048	41625	30181	36868
3	(a)	30733	43501	24956	27239	22012	30621	17683	65405	50988	84974
	(c)	15551	32868	81640	144773	19745	54990	46033	35661	21445	23494
		Torsional Moment in N.mm									
1	(a)	0	0	495	689	588	349	14864	19425	12848	15868
	(c)	5754	7942	10949	13485	5522	10346	15664	19877	13806	16588
2	(a)	0	0	3555	4558	1888	1465	9329	19066	14787	20029
	(c)	5753	8952	9689	13570	4112	9137	5851	9084	9547	11054
3	(a)	0	0	502	4638	1063	1037	42	17810	17968	31400
	(c)	10188	23560	12966	12431	2608	3585	6080	524	9248	11237

Table (5.1) Bending and torsional moments of members I to V of the barrel vault types 1 to 3 under a load intensity of 600 N/m²

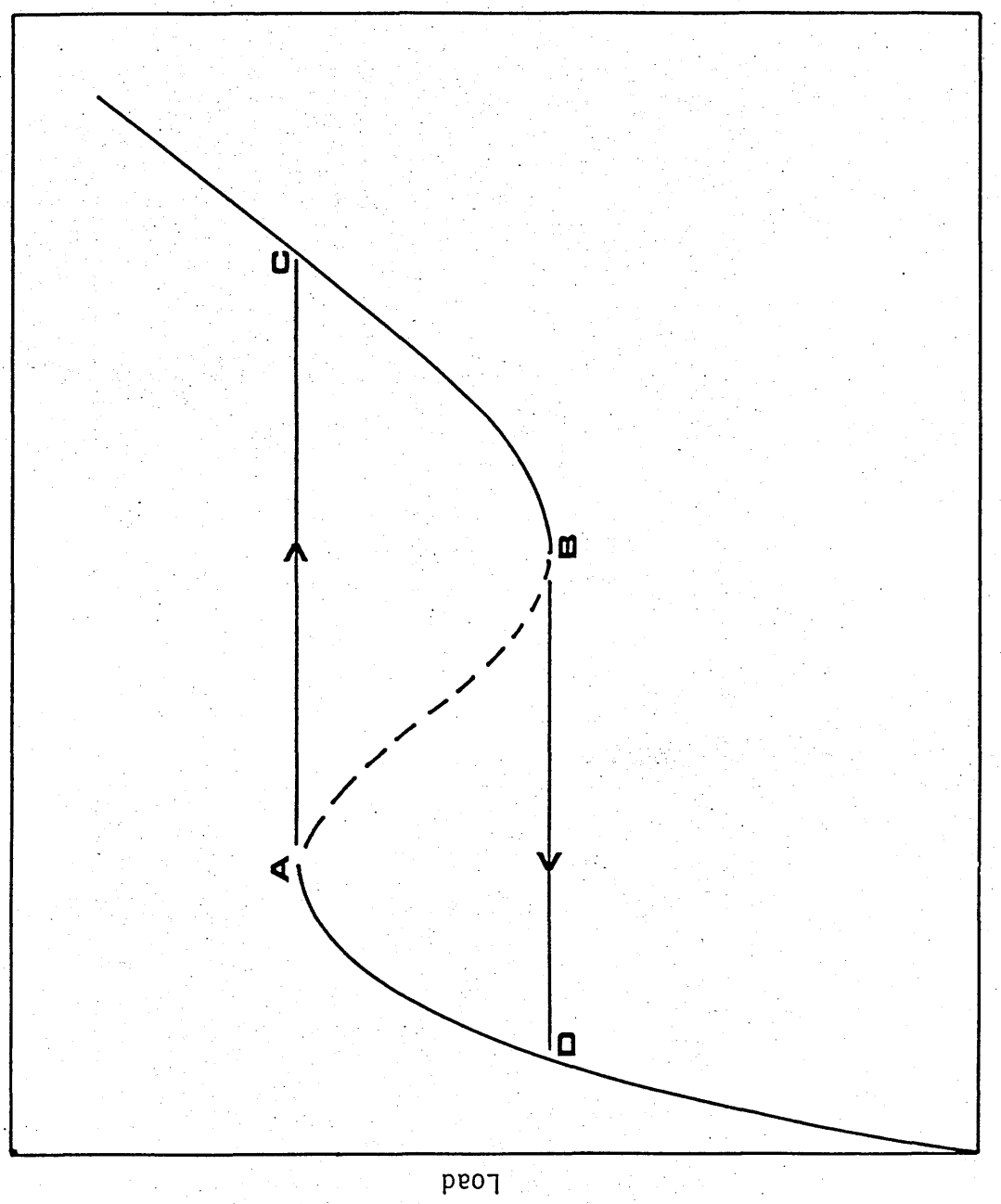

Figure (5.1) Load-displacement relationship for the snap buckling

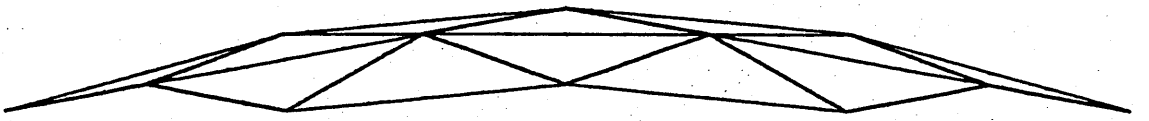

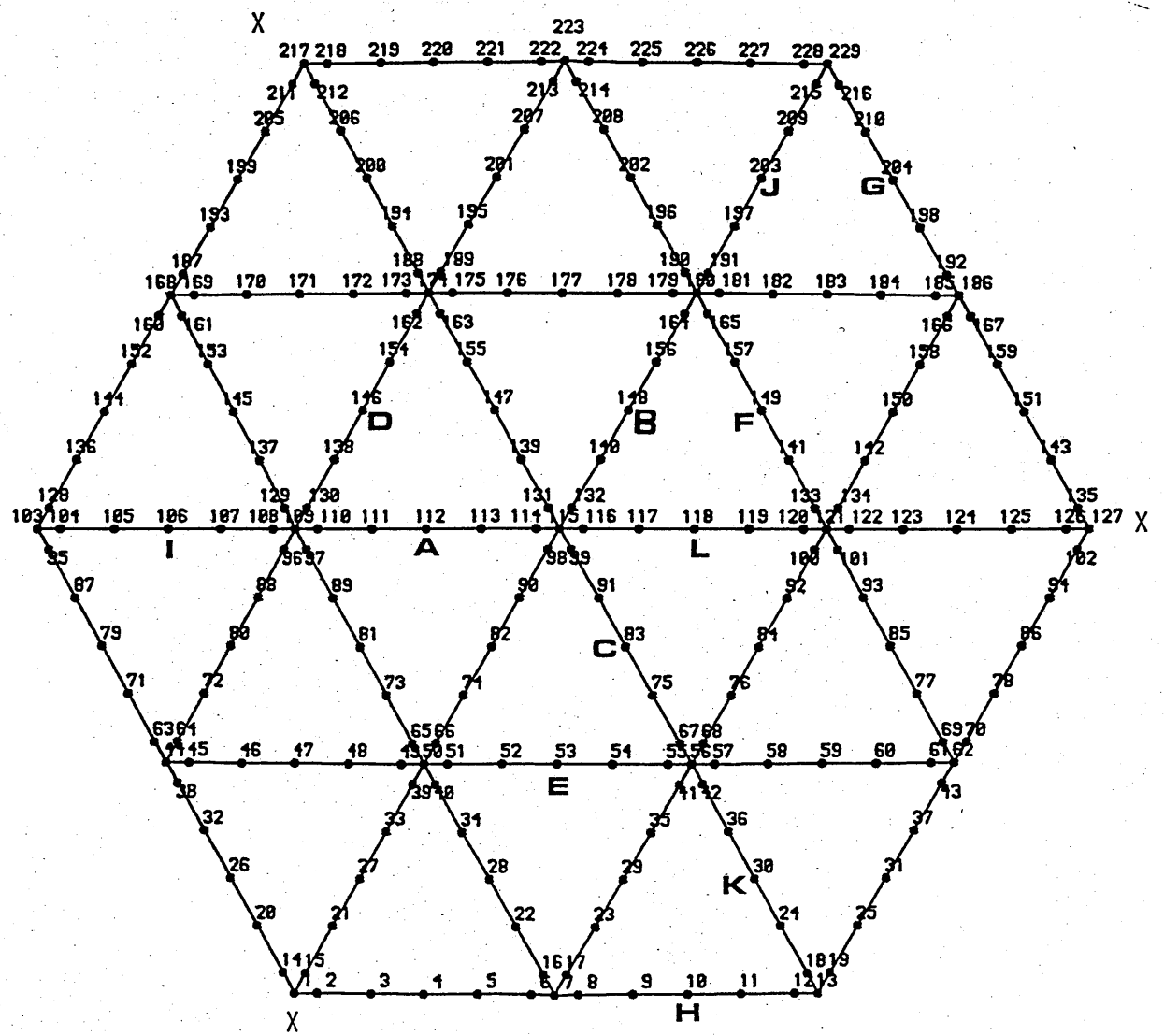

Figure (5.2) Configuration and Member Discretization for the Dome

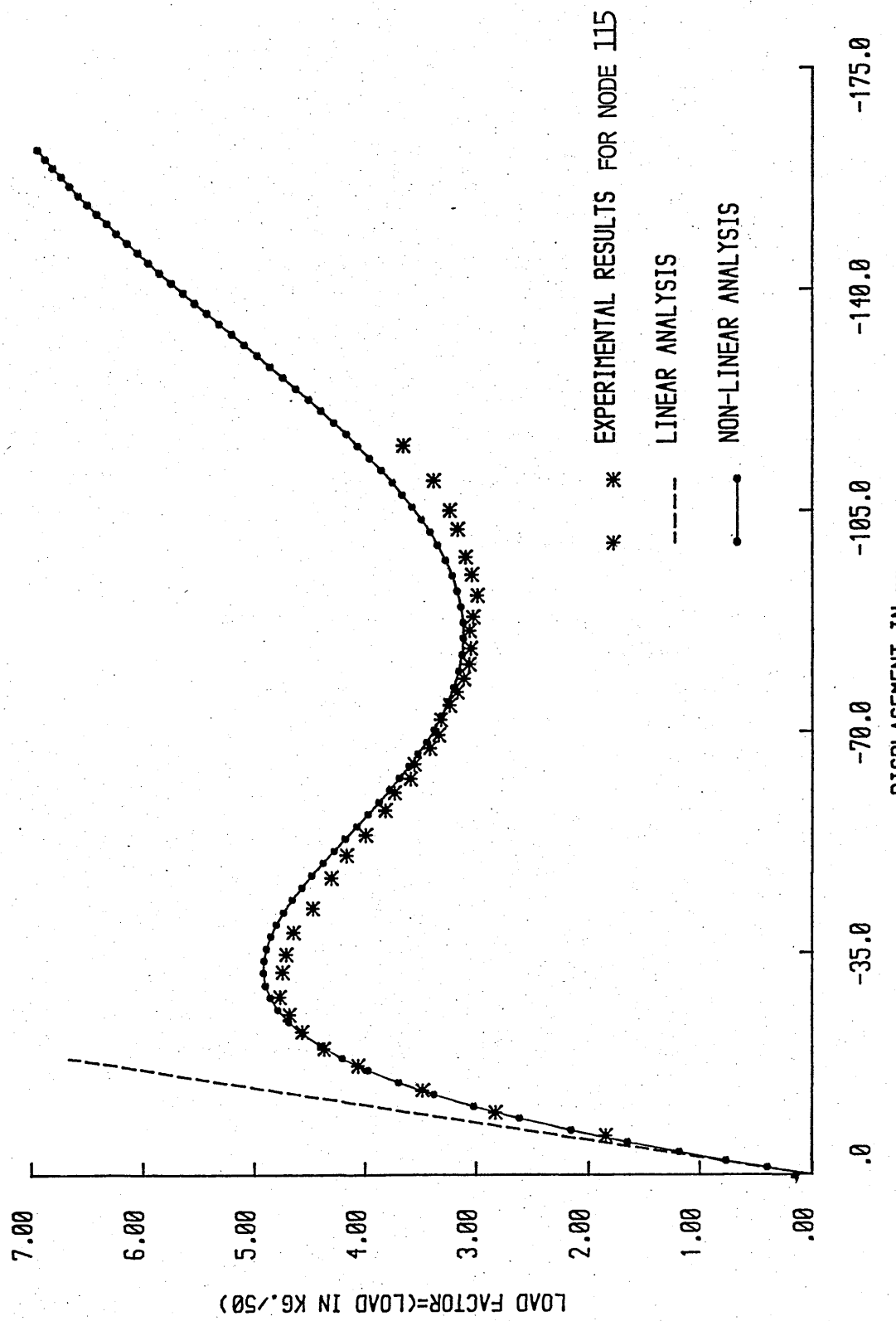

Fig (5.3) Load-displacement curve for central node

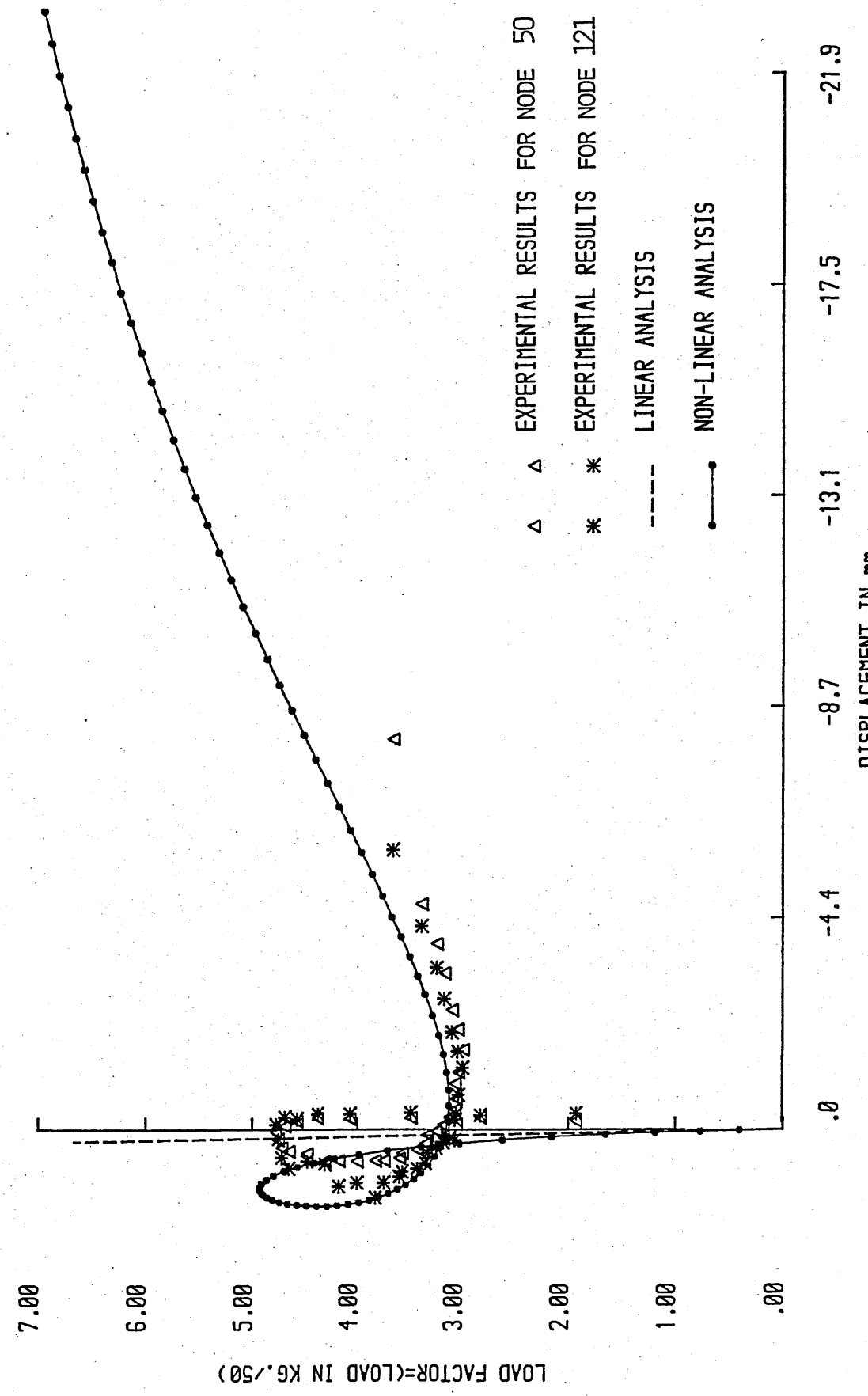

Fig (5.4) Load-displacement curve for inner ring nodes

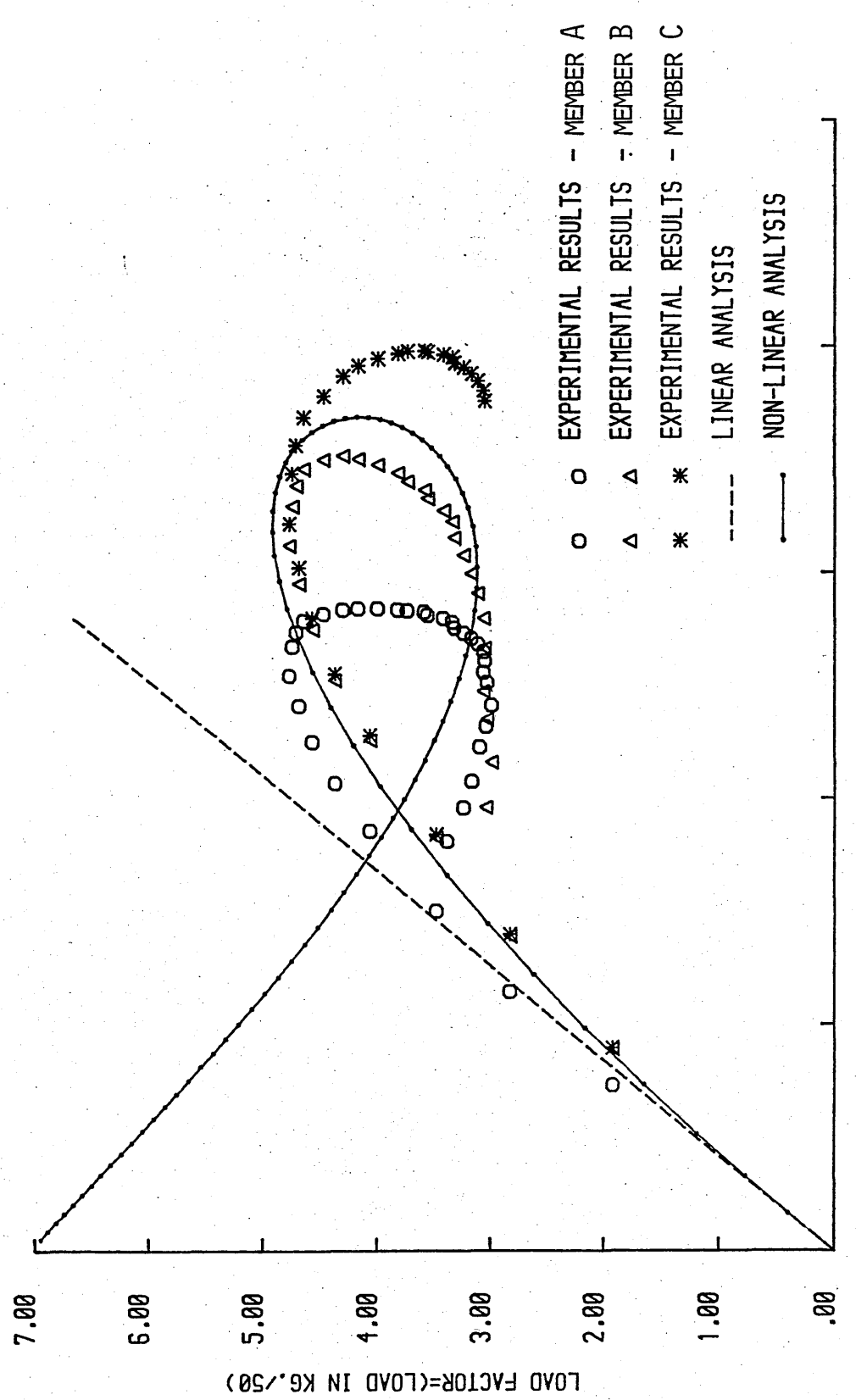

Fig (5.5) Load Factor - theoretical axial force for members connected to central node with superimposed experimental results

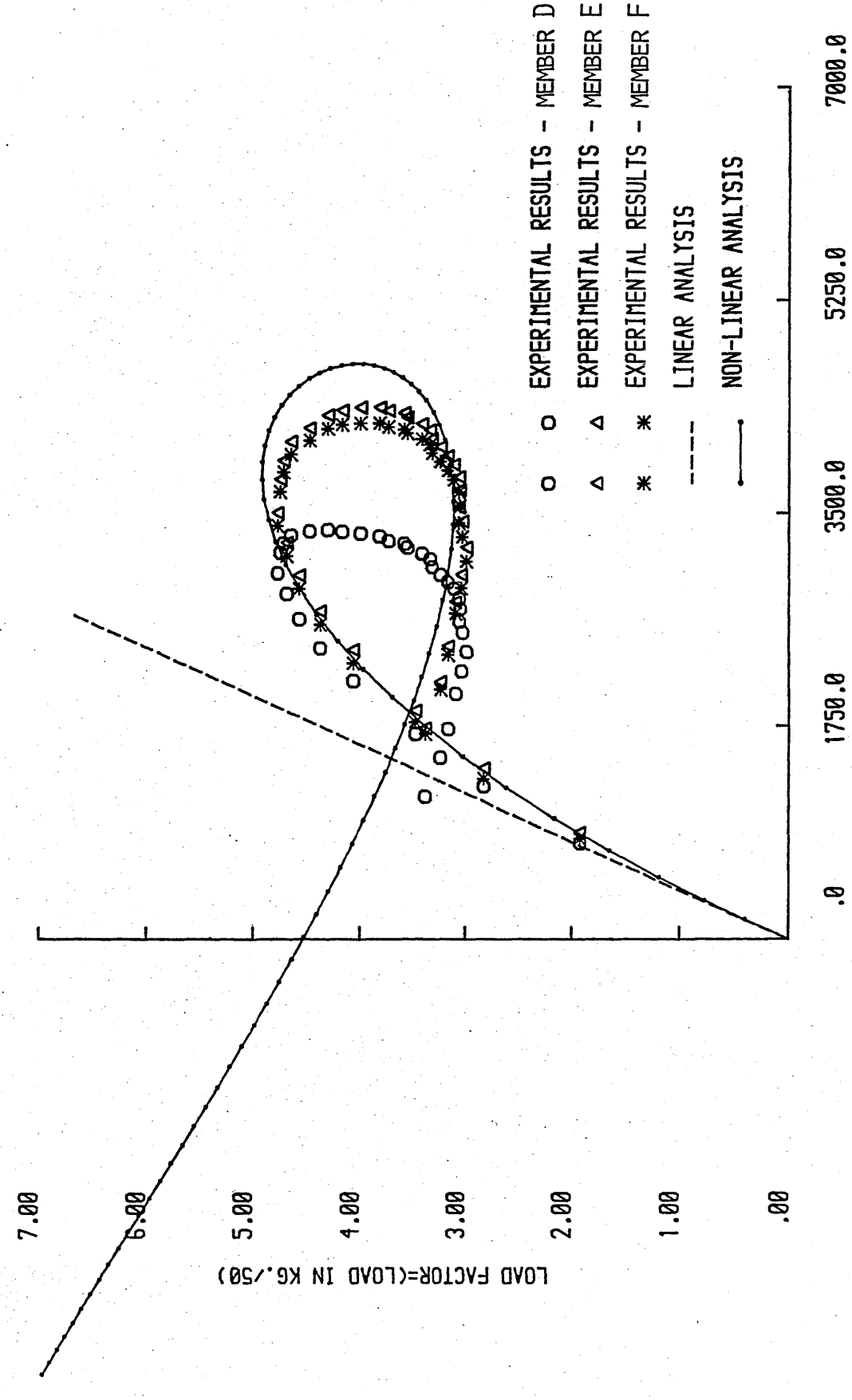

Fig.(5.6) Load Factor - Theoretical axial force for inner ring beam with superimposed experimental results

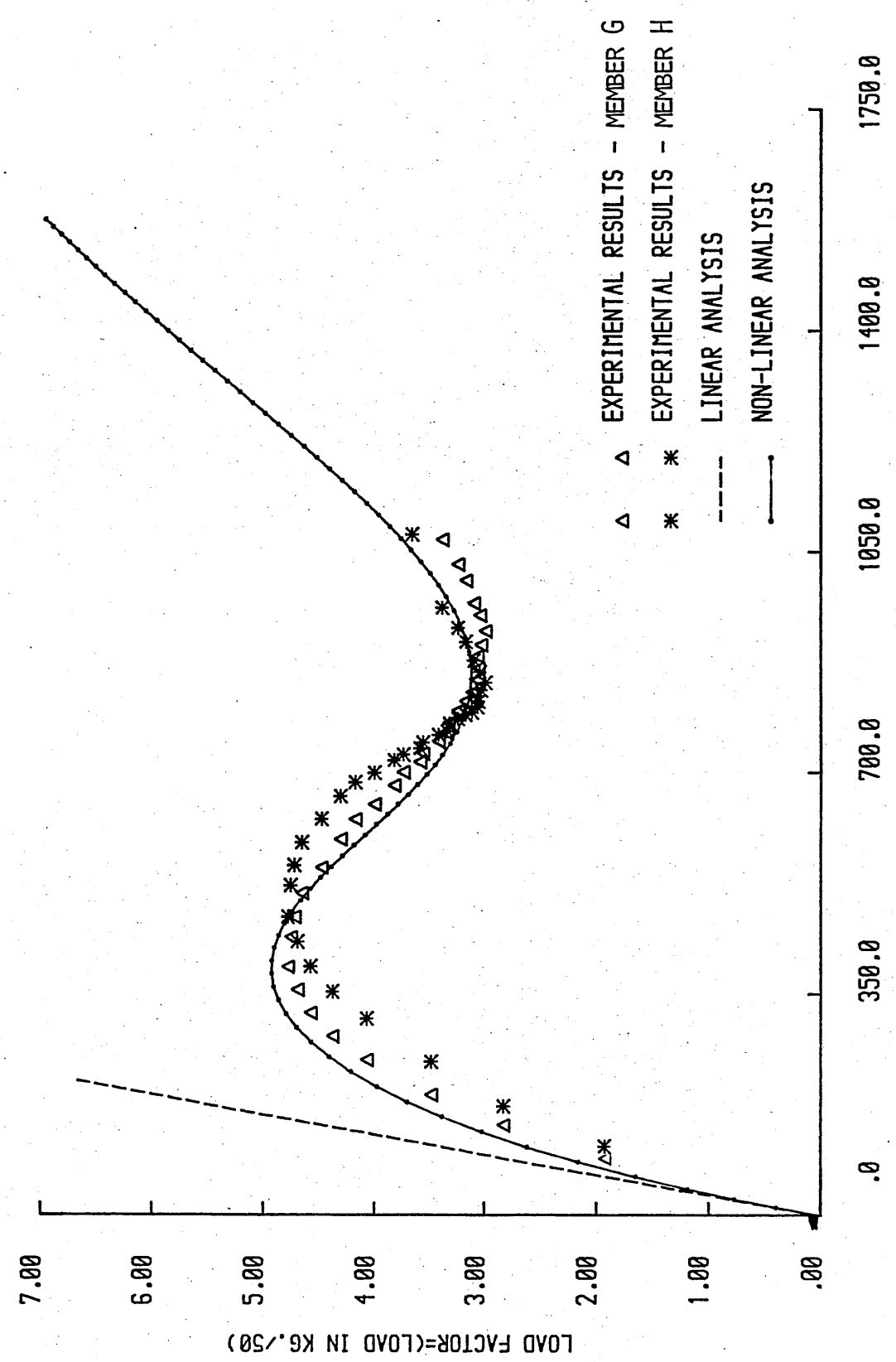

Fig (5.7) Load Factor - Axial force for members G and H with superimposed experimental results

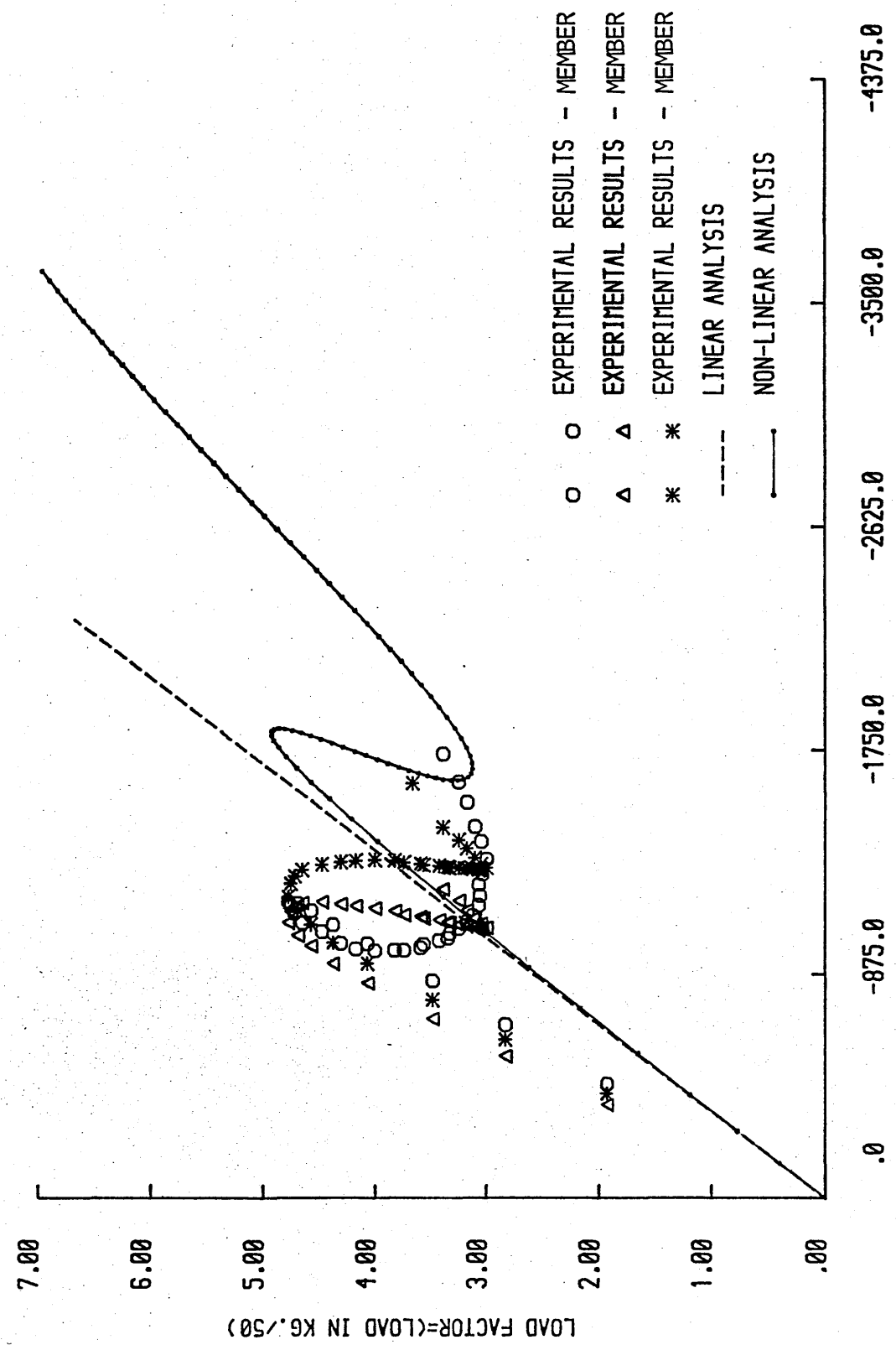

Fig (5.8) Load Factor - Axial force for members I, J and K with superimposed experimental results

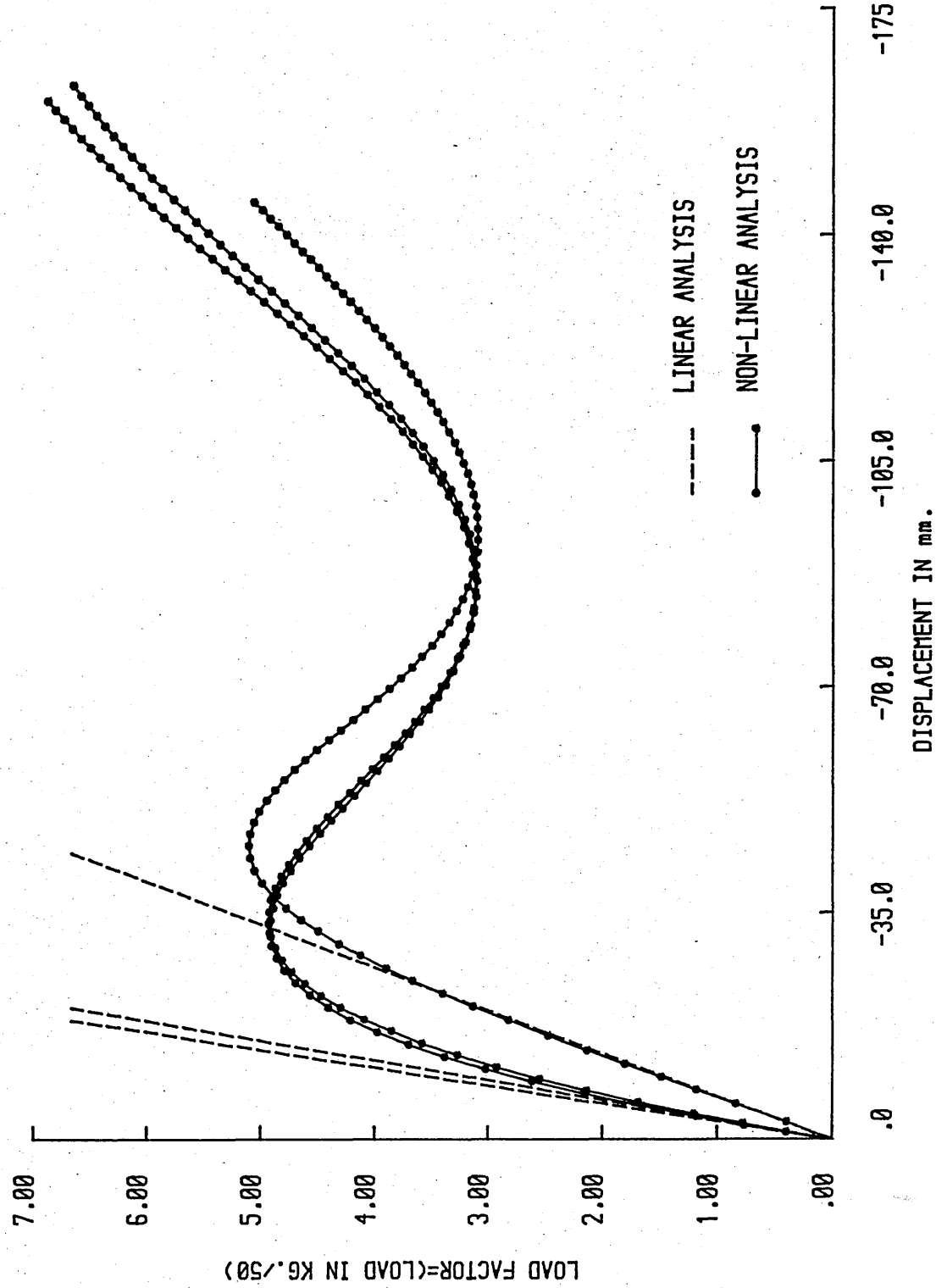

Fig (5.9) Load Factor - Displacement curves for central node point

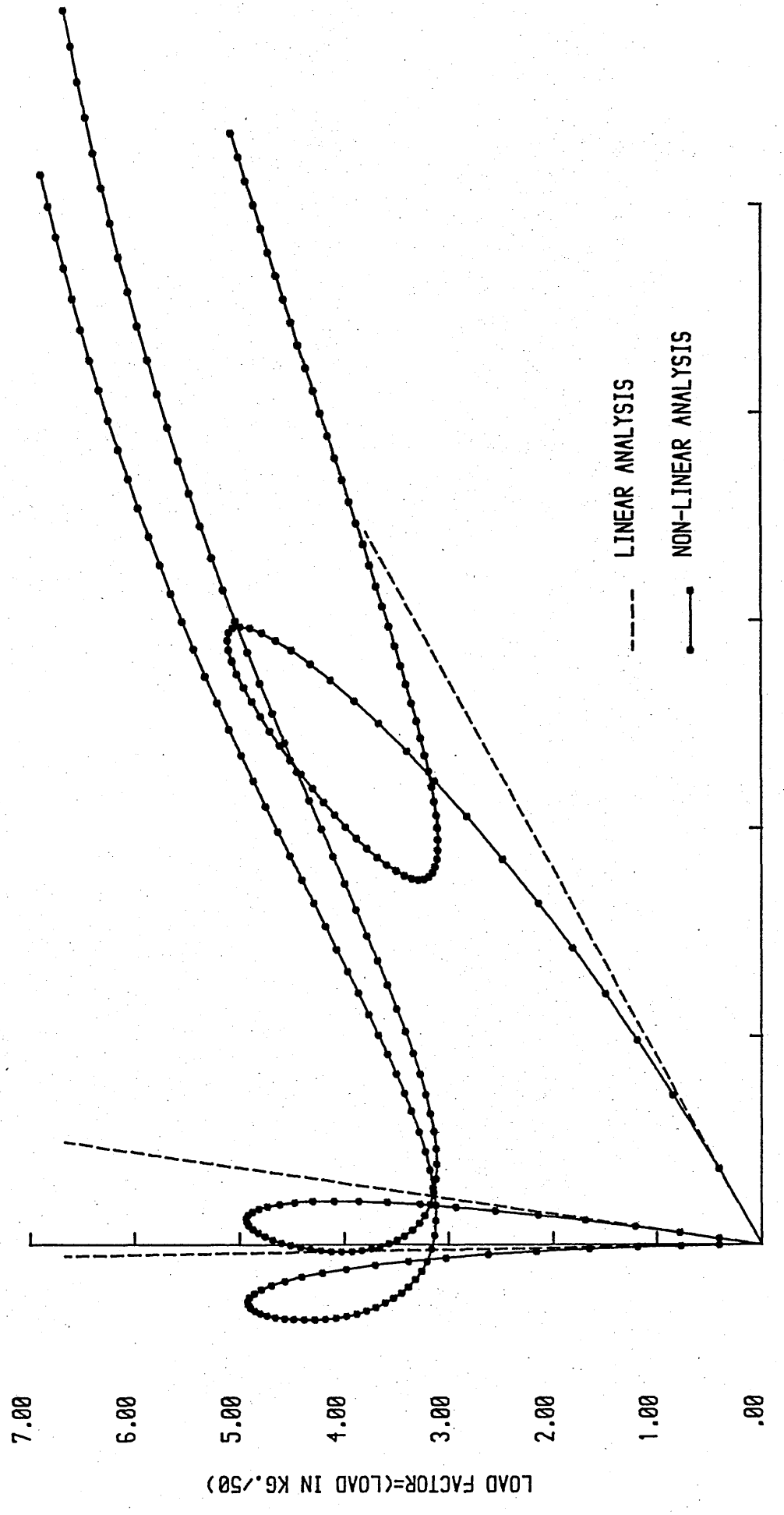

Fig (5.10) Load Factor - Displacement for the inner ring nodes

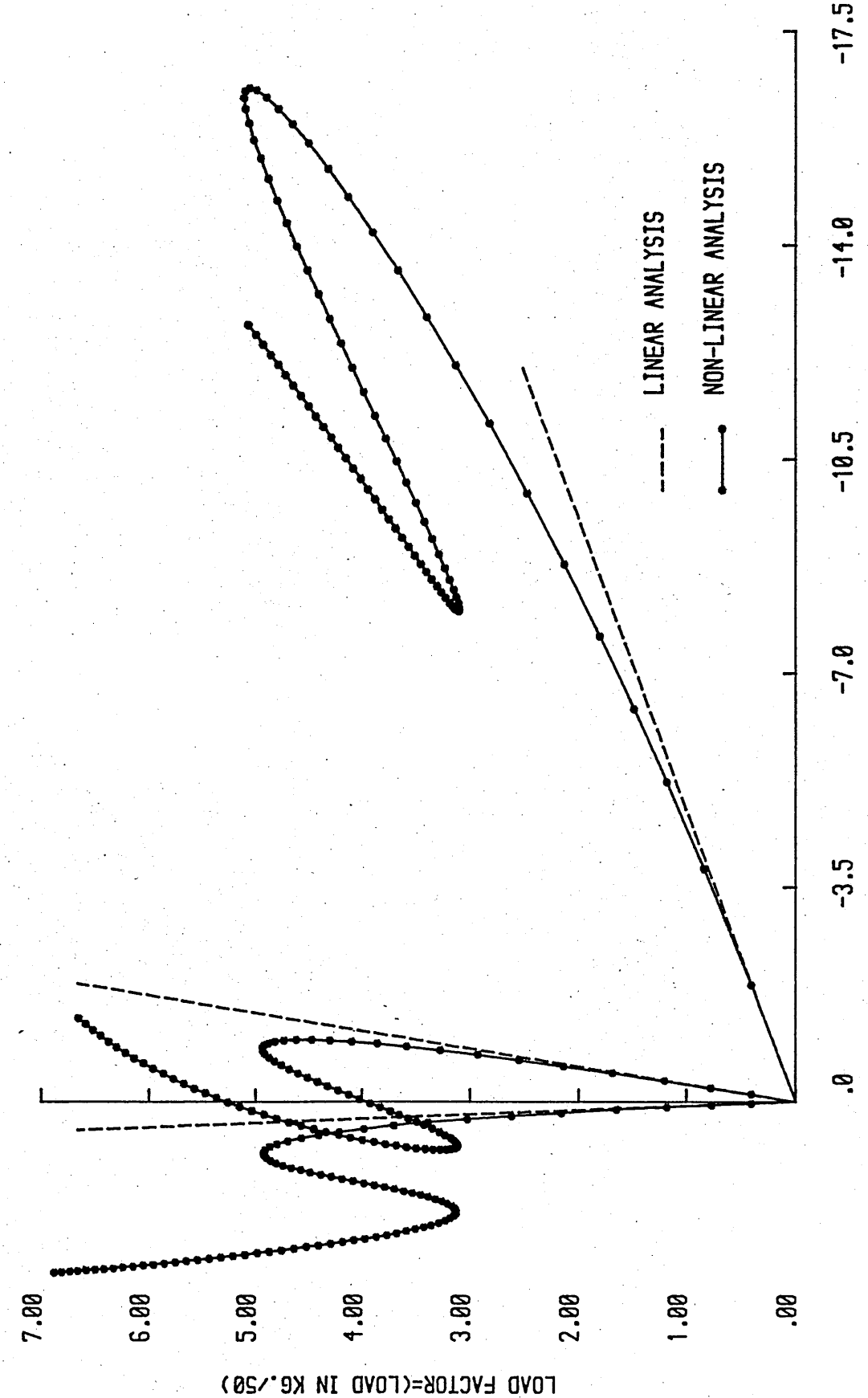

Fig (5.11) Load Factor - Displacement curves of analytical results for outer ring nodes

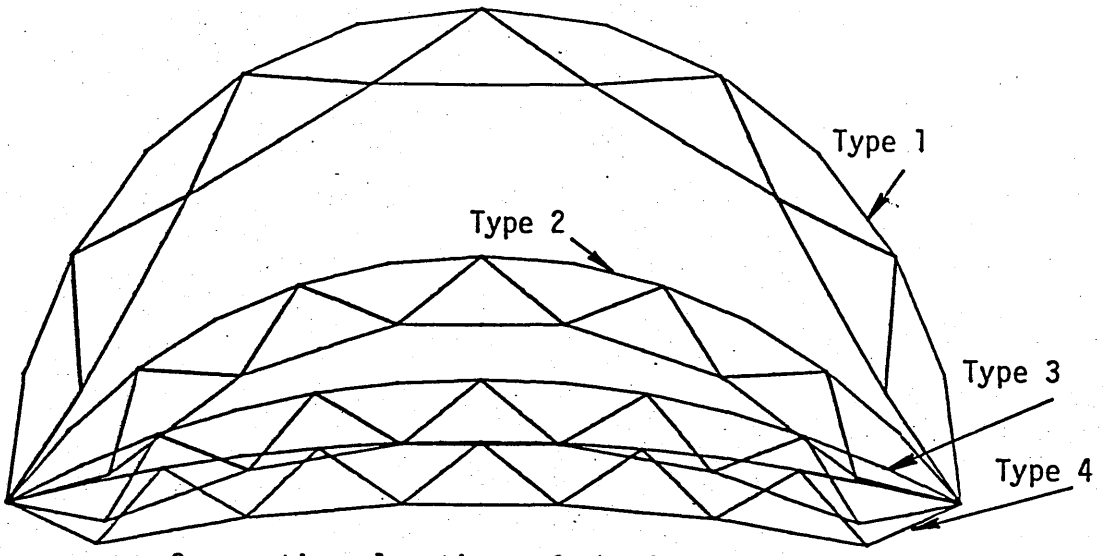

Comparative elevations of the four types of Barrel Vaults.

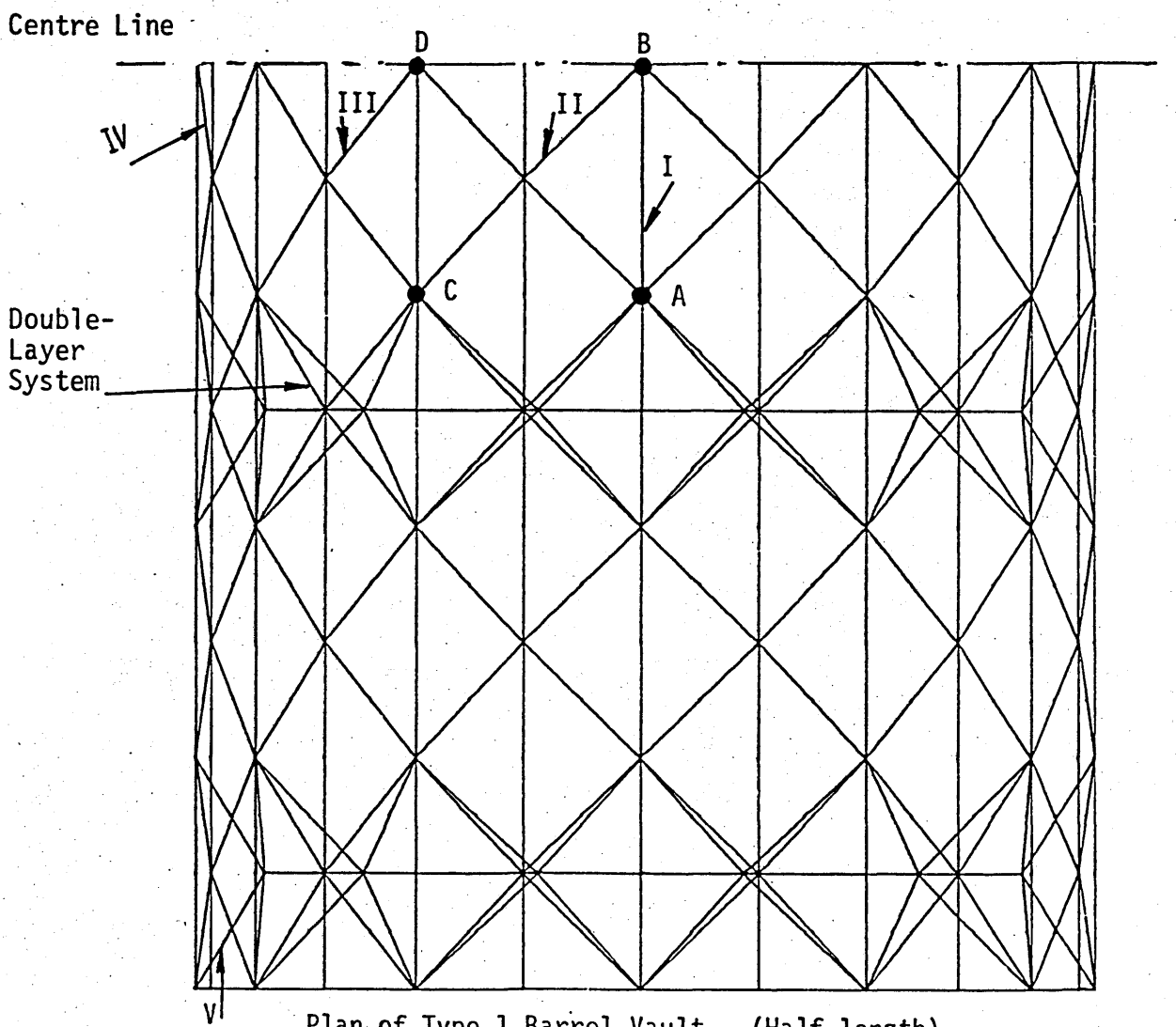

Plan of Type 1 Barrel Vault. (Half length).

Fig (5.12) Plan and Elevations of Types 1, 2, 3 and 4 Braced Barrel Vaults.

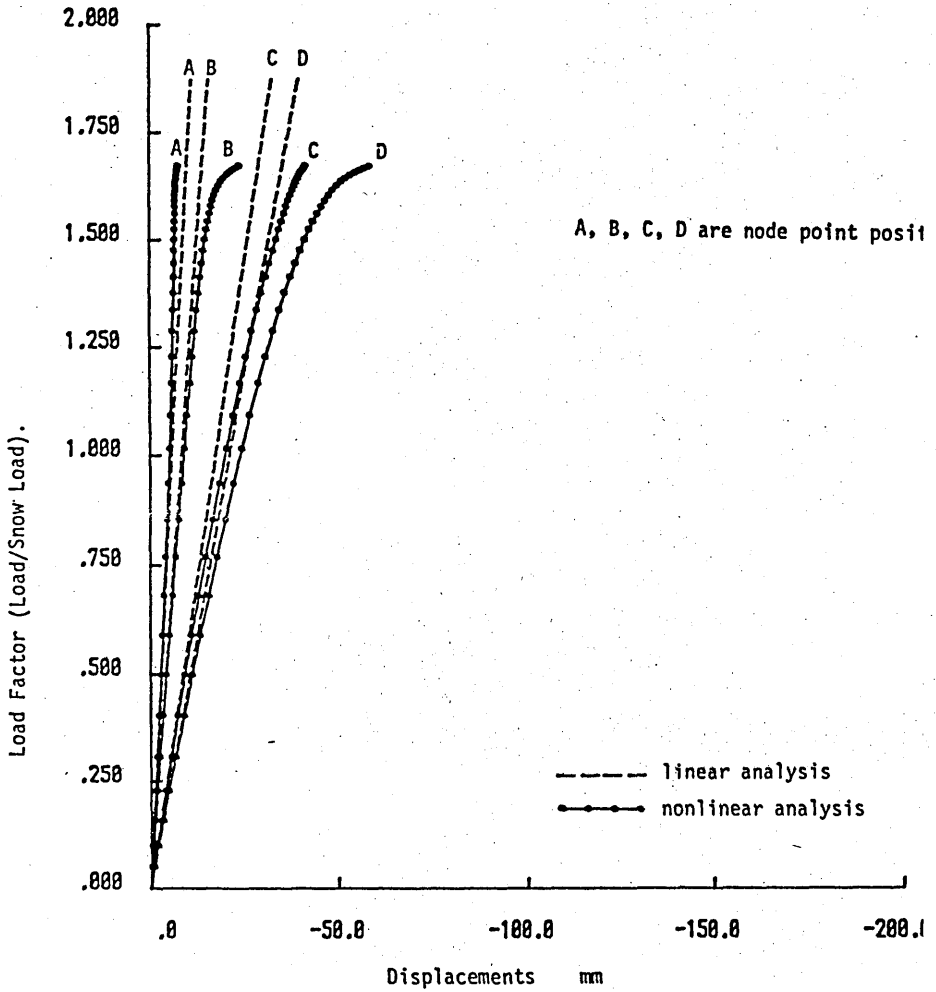

Fig (5.13) Load factor— displacement of node points ABCD for type 1 barrel vault. (Load case (c)).

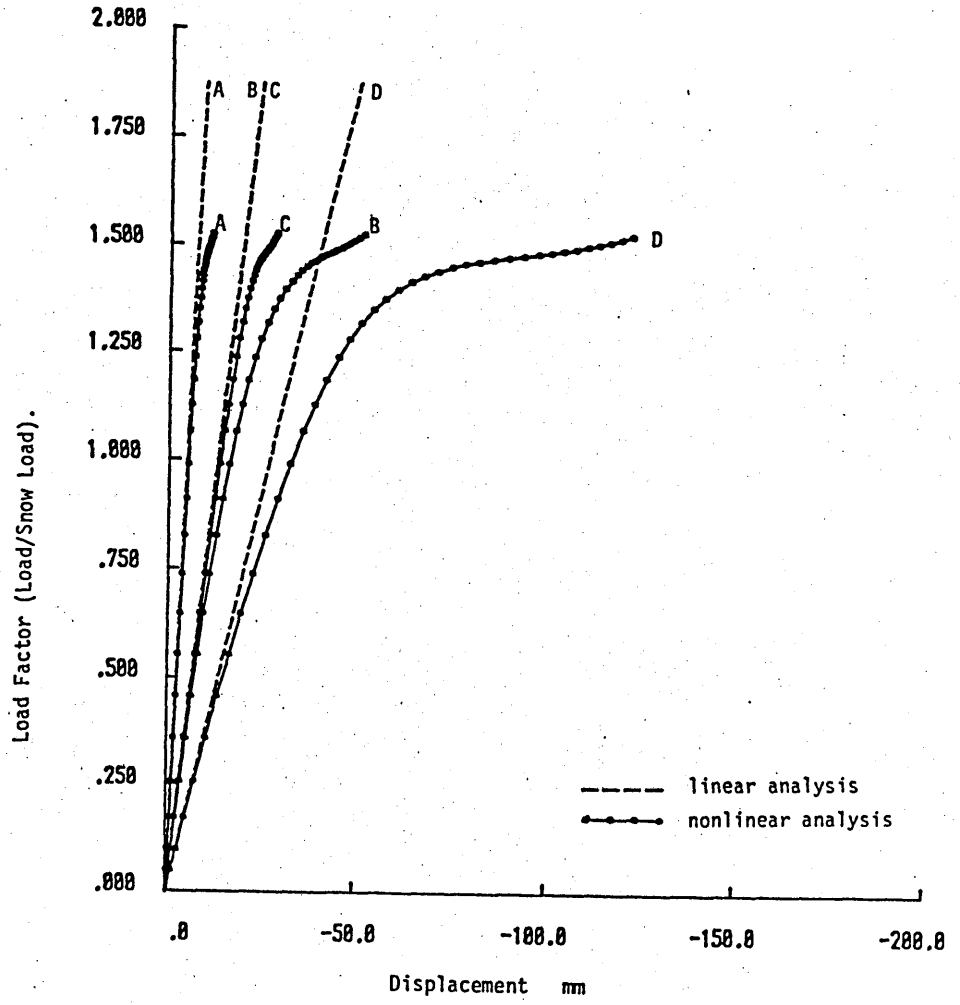

Fig (5.14) Load factor— displacement of node points ABCD for type 2 barrel vault. (Load case (c)).

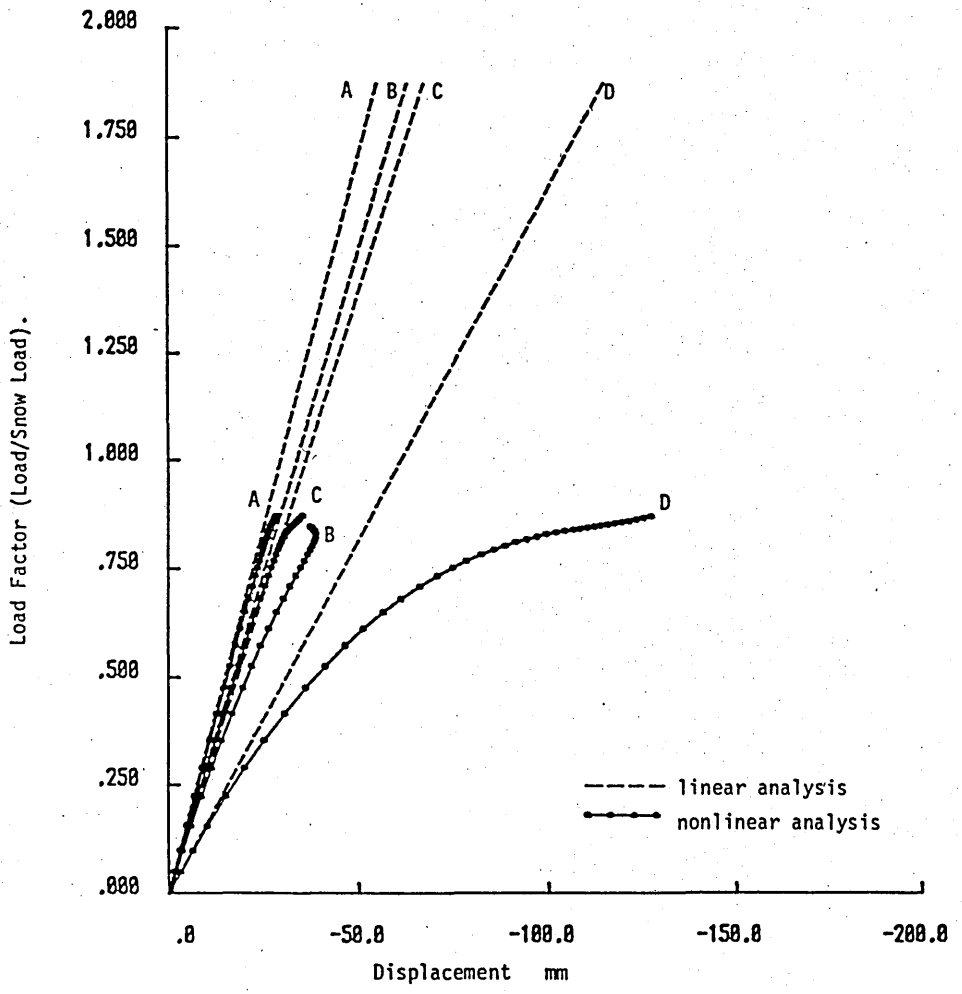

Fig (5.15) Load factor – displacement of node points ABCD for type 3 barrel vault. (Load case (c)).

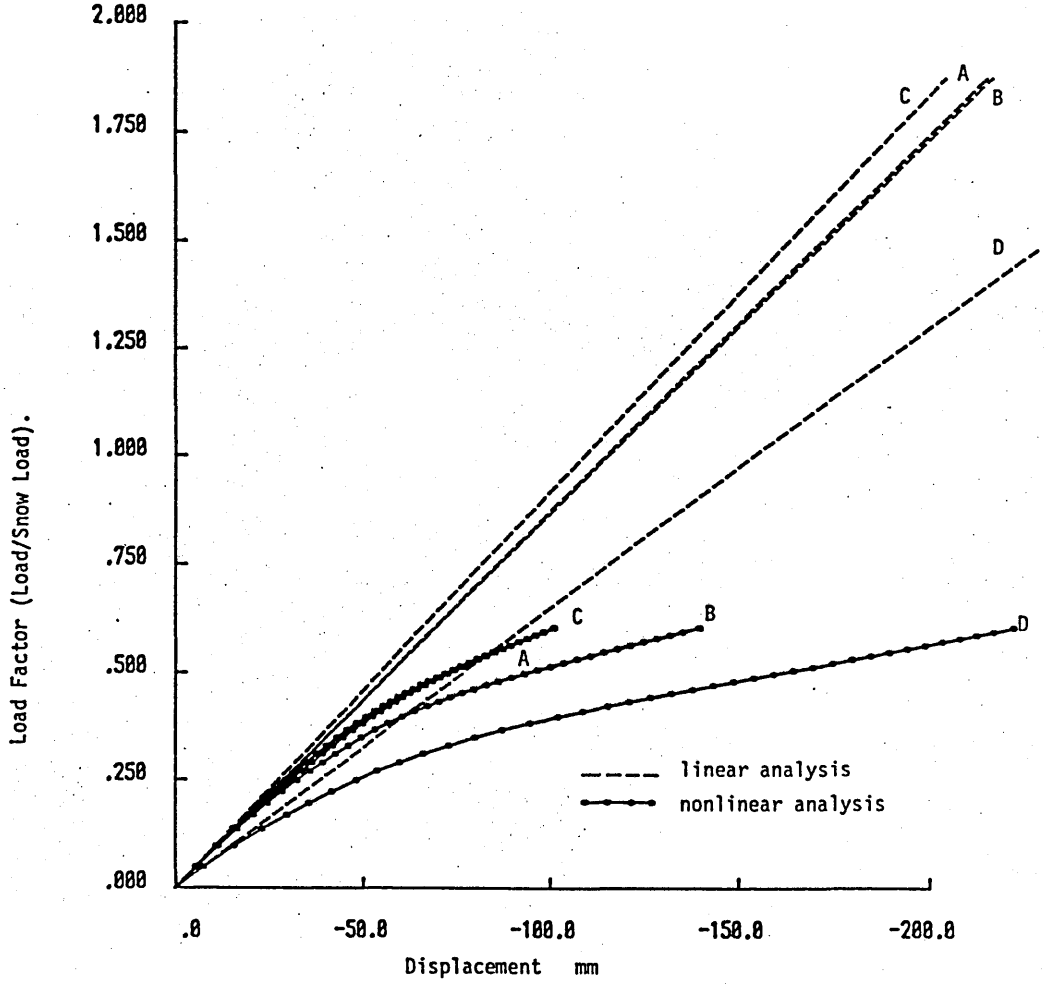

Fig (5.16) Load factor displacement of node points ABCD for type 4 barrel vault. (Load case (c)).

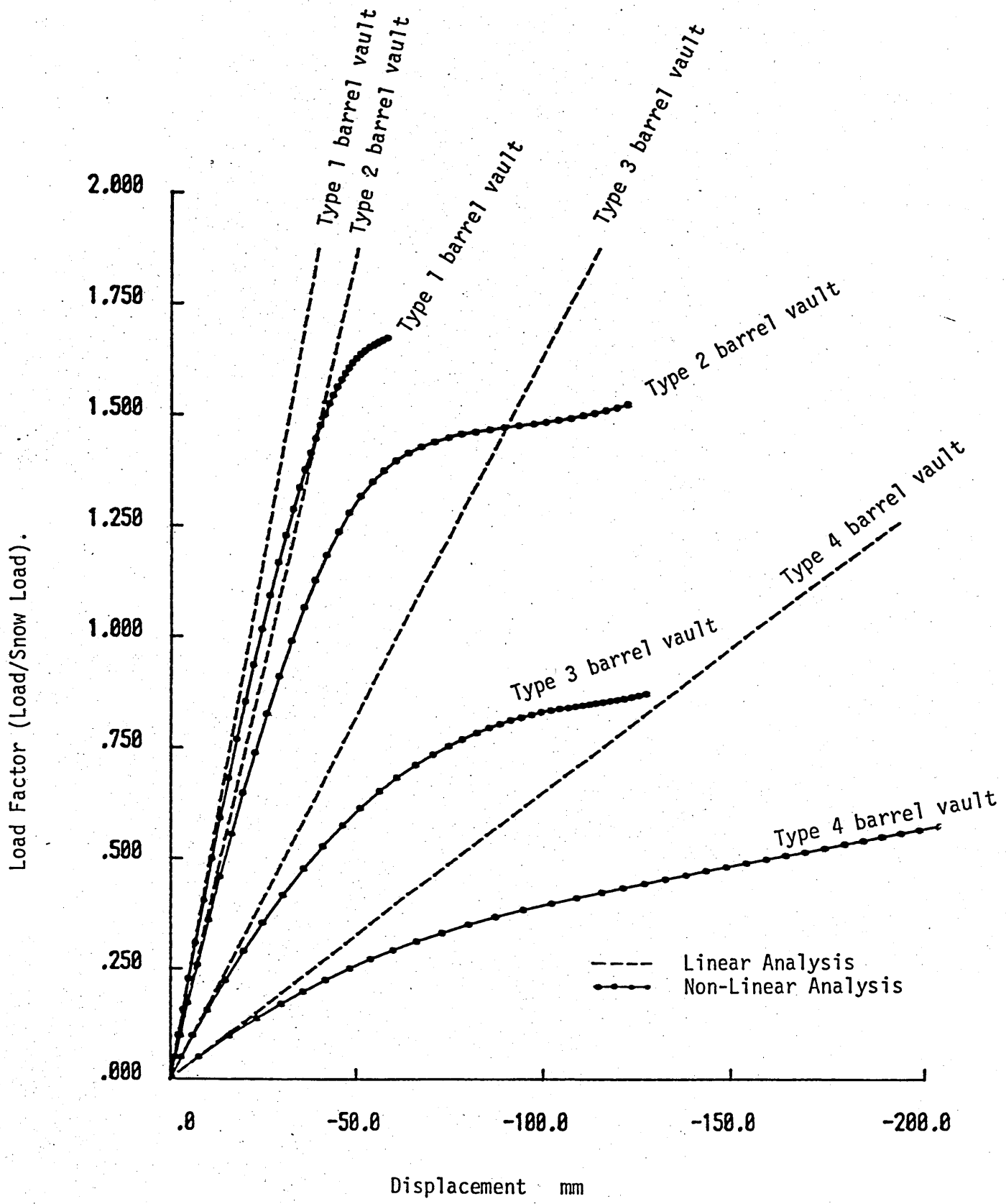

Fig (5.17) Load factor — displacement of node point D for types 1, 2, 3 and 4 barrel vaults. (Load case (c)).

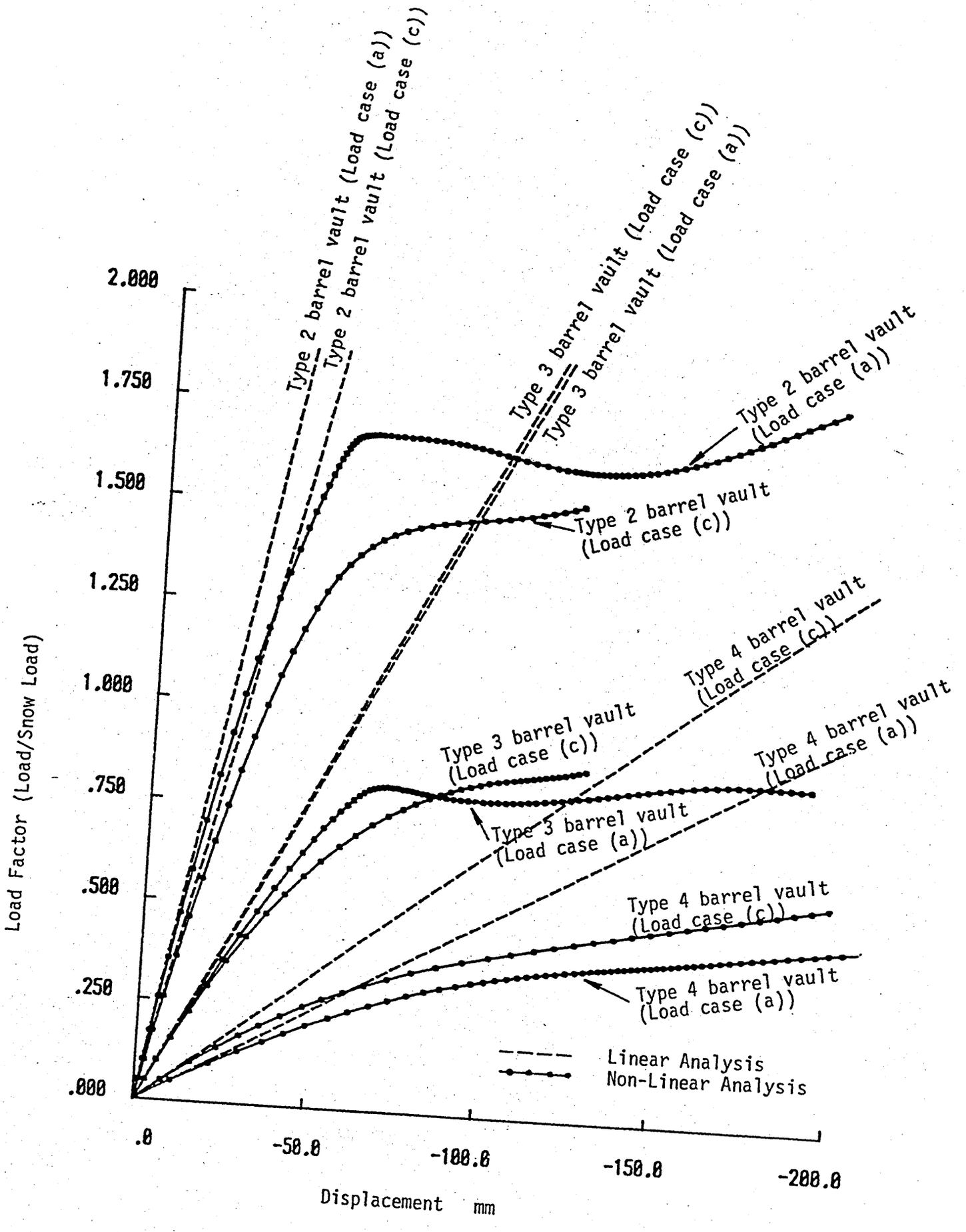

Fig (5.18) Load factor — displacement of node point D for barrel vaults types 2, 3 and 4. (Load cases (a) and (c)).

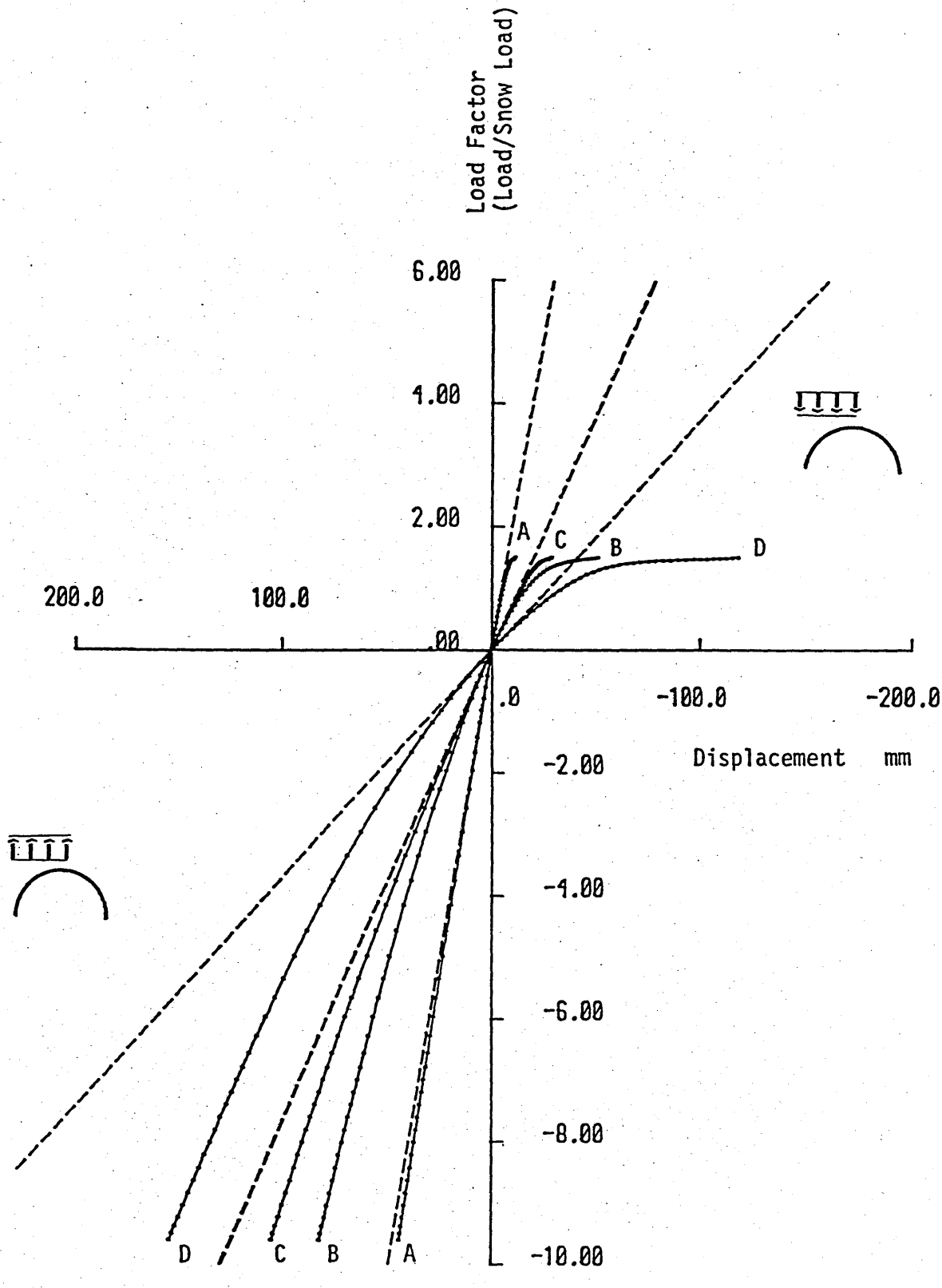

Fig (5.19) Load factor — displacement of node ABC and D for type 2 barrel vault. (Load cases (c) adn (d)).

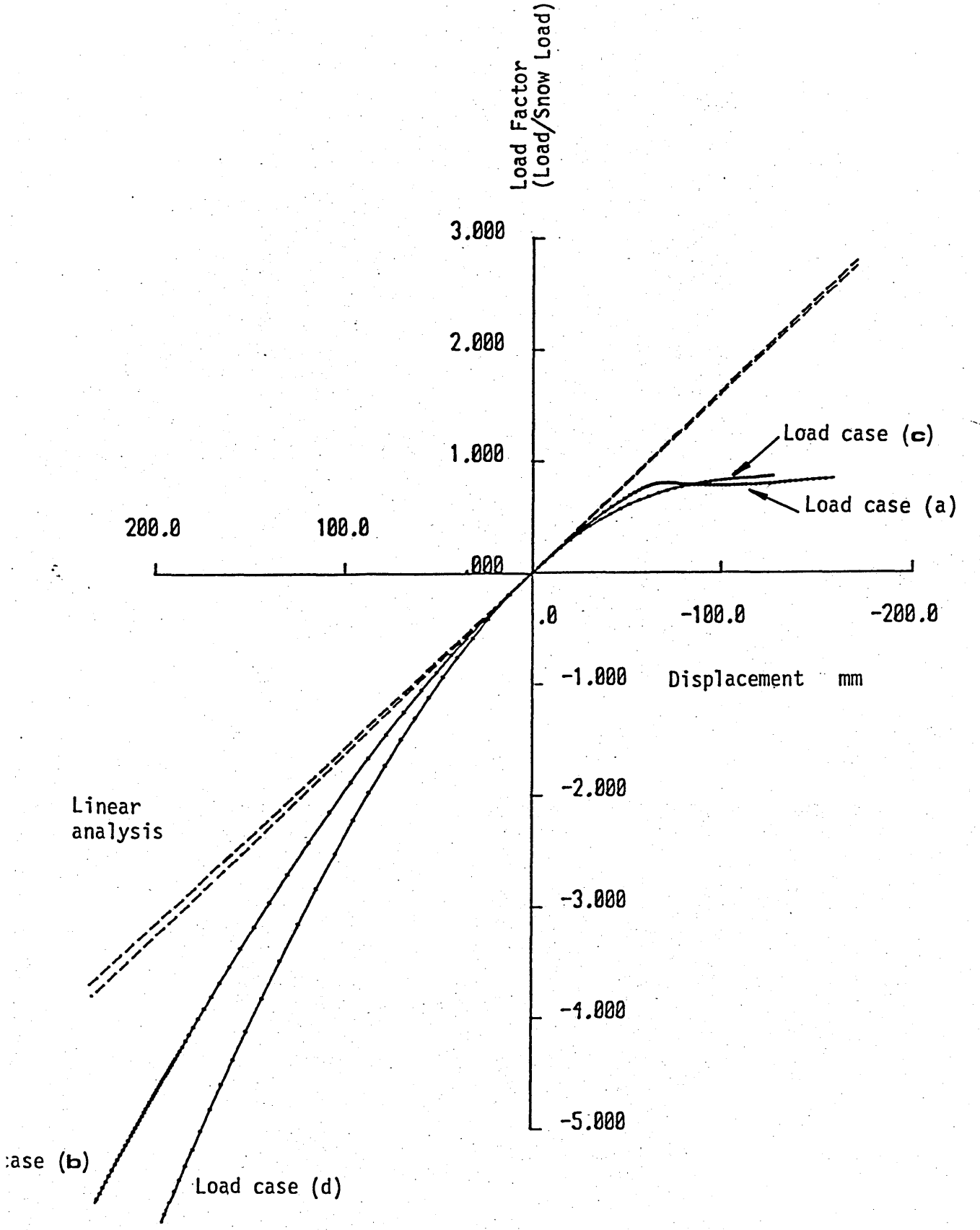

Fig (5.20) Load factor— displacement of node D for type 3 barrel vault. (Loading cases (a), (b), (c) and (d)).

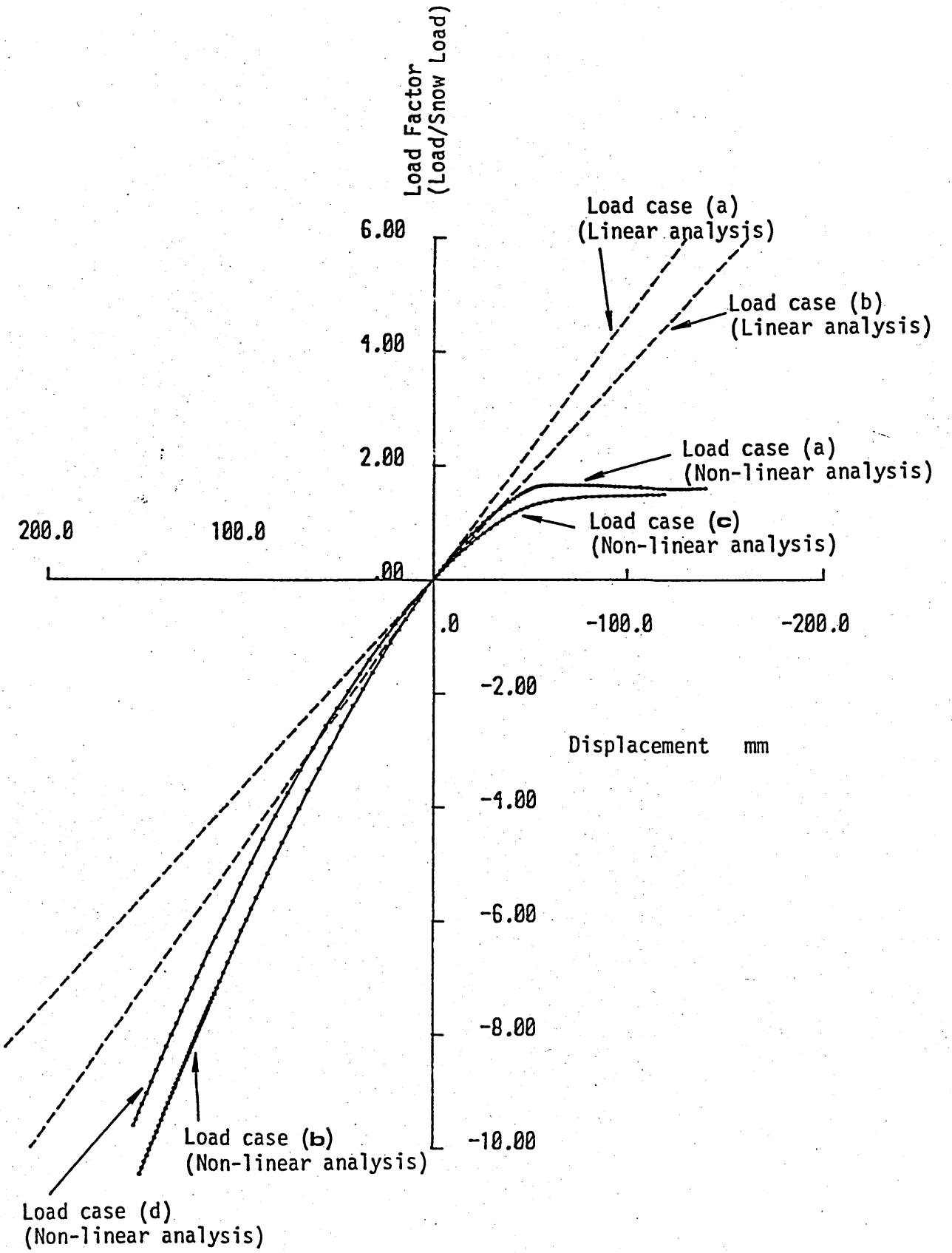

Fig (5.21) Load factor — displacement of node D for type 2 barrel vault. (Loading cases (a), (b), (c) and (d)).

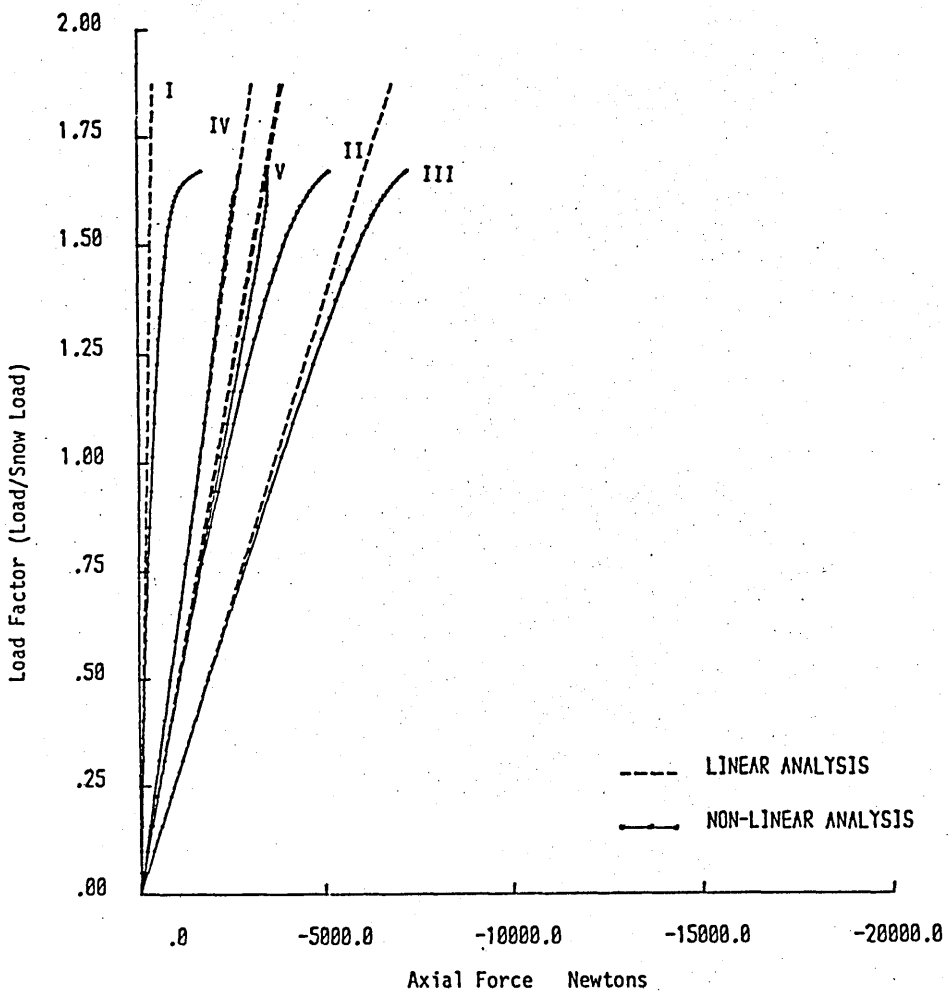

Fig (5.22) Load factor — Axial forces for type 1 barrel vault. (Members I to V. Load case (c)).

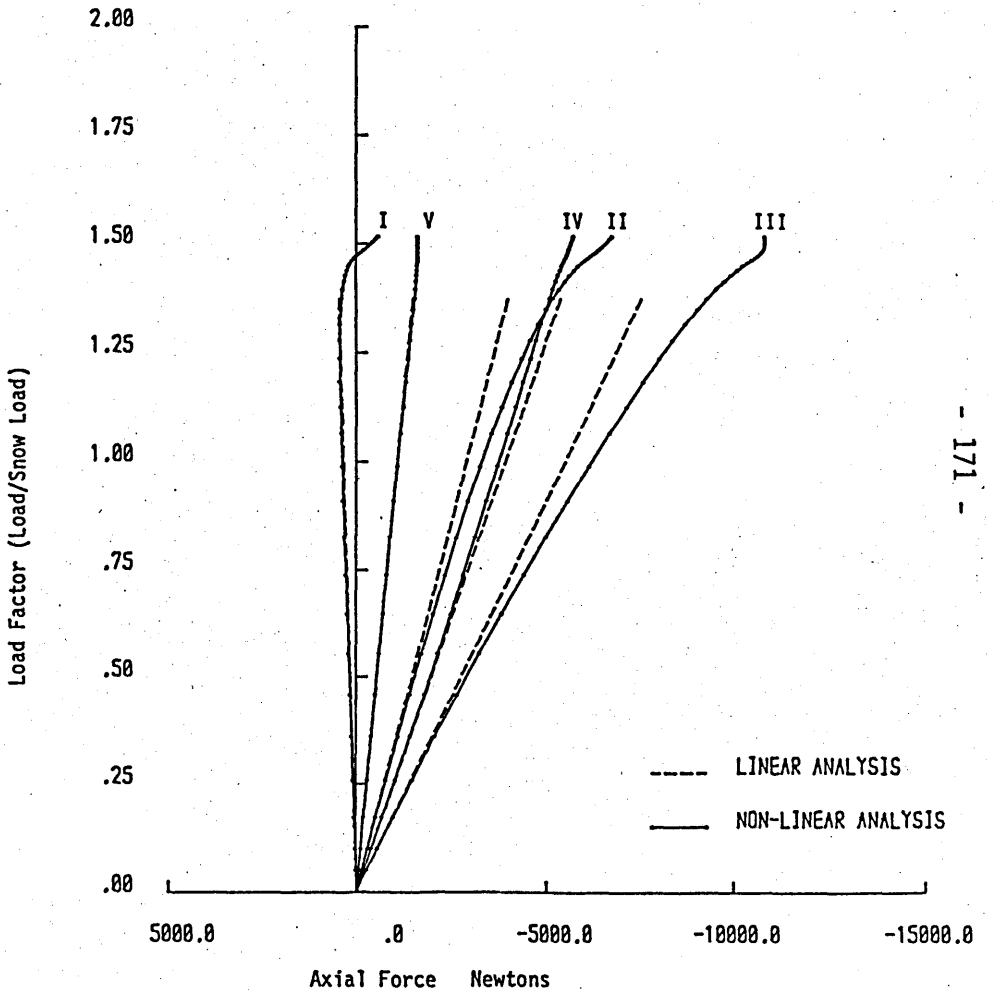

Fig (5.23) Load factor — Axial forces for type 2 barrel vault. (Members I to V. Load case (c)).

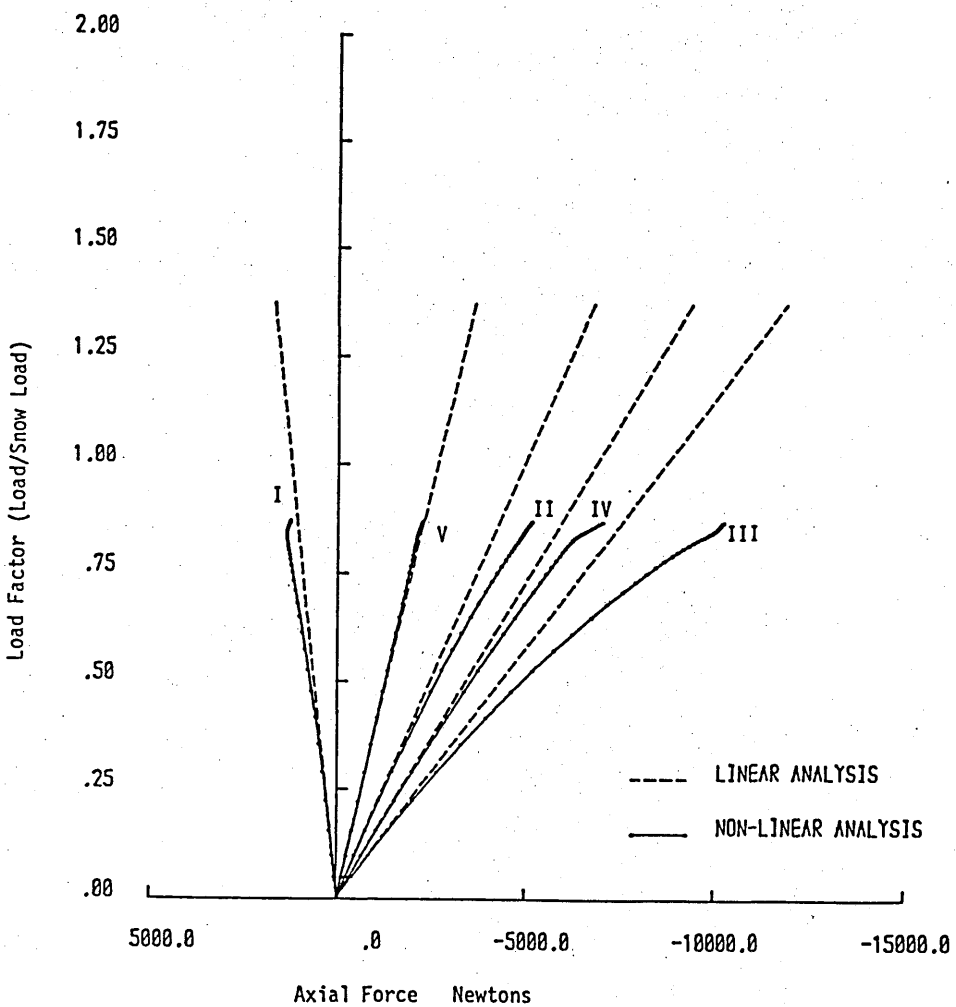

Fig (5.24) Load factor — Axial forces for type 3 barrel vault. (Members I to V. Load case (c)).

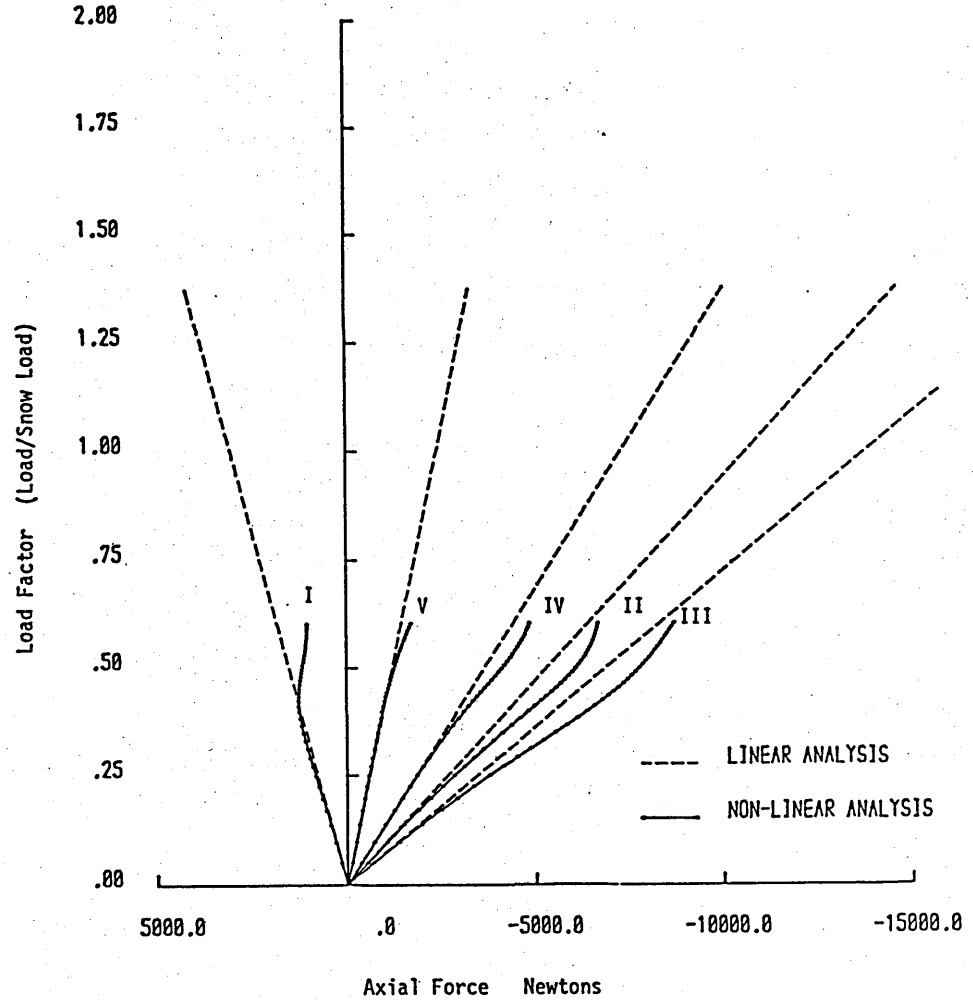

Fig (5.25) Load factor— Axial forces for type 4 barrel vault. (Members I to V. Load case (c)).

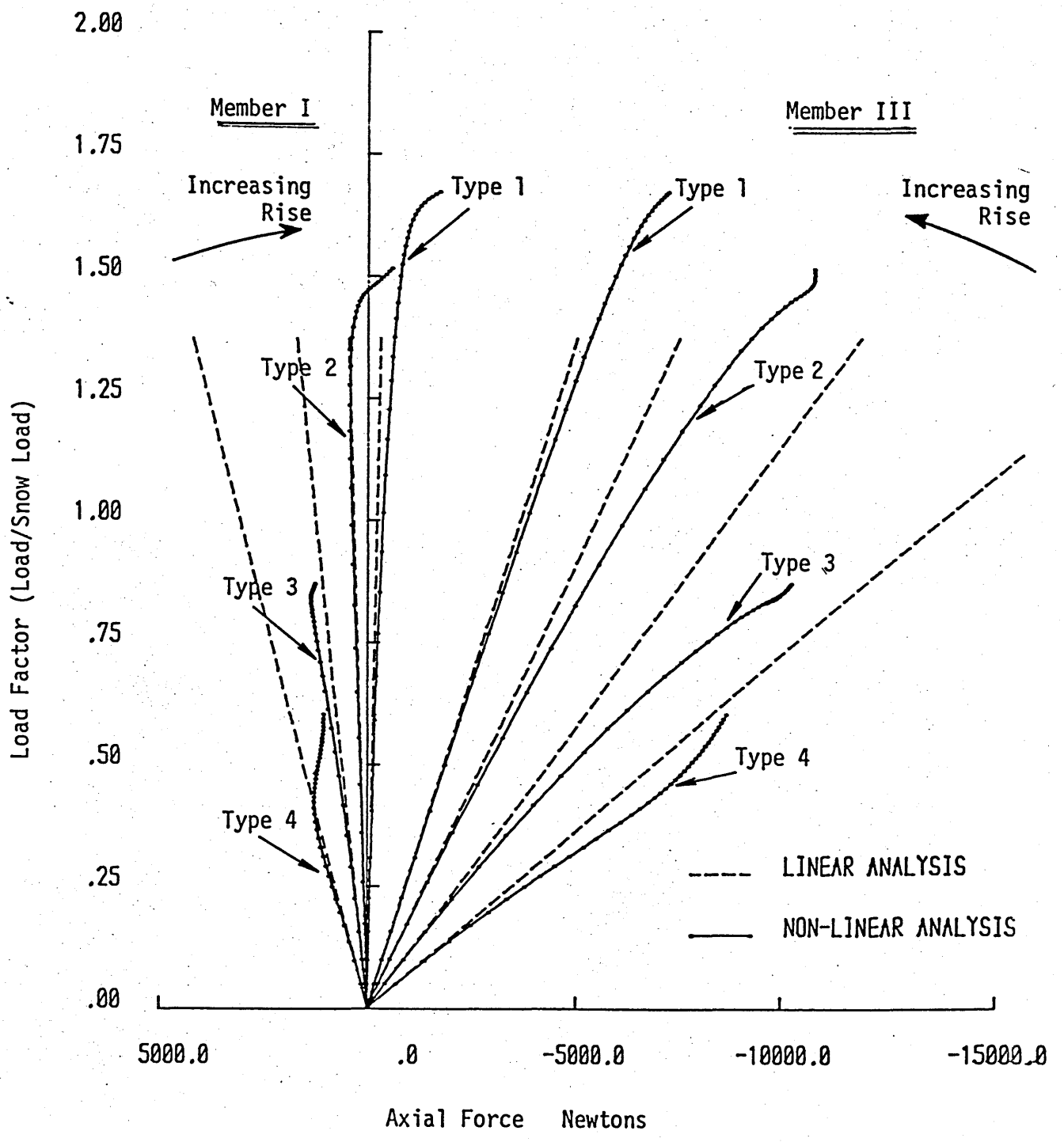

Fig (5.26) Load factor— Axial force for types 1, 2, 3 and 4 barrel vaults. (Members I and II. Load case (c)).

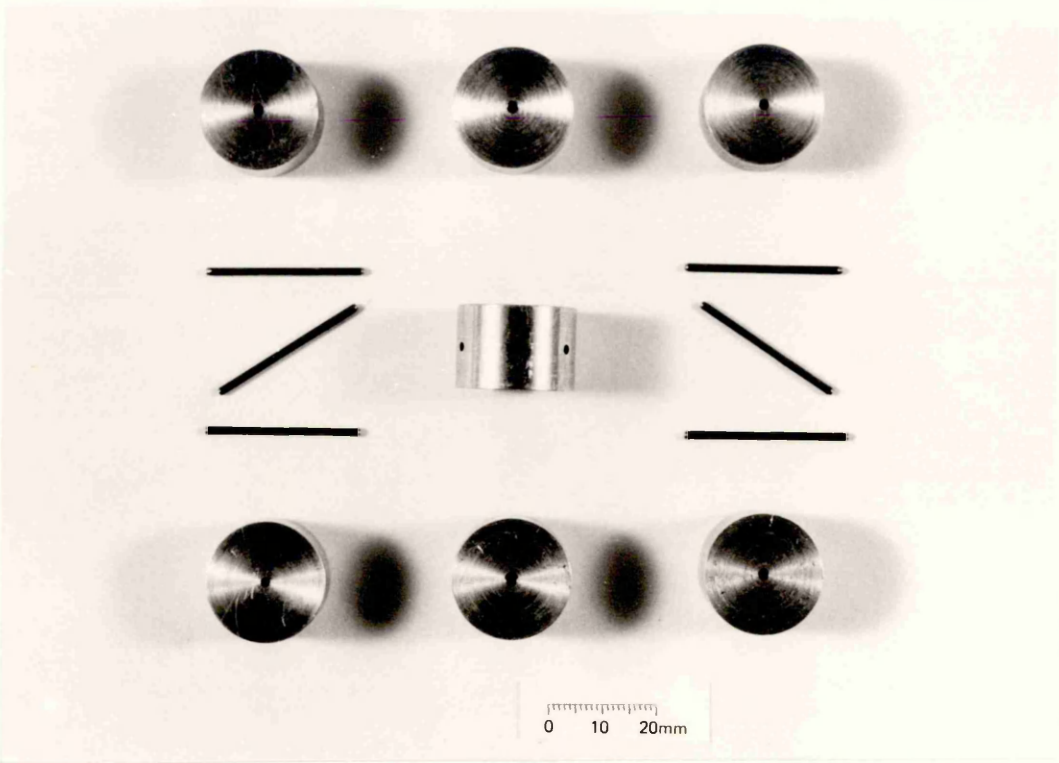

Plate (5.1) The components of the temporary node

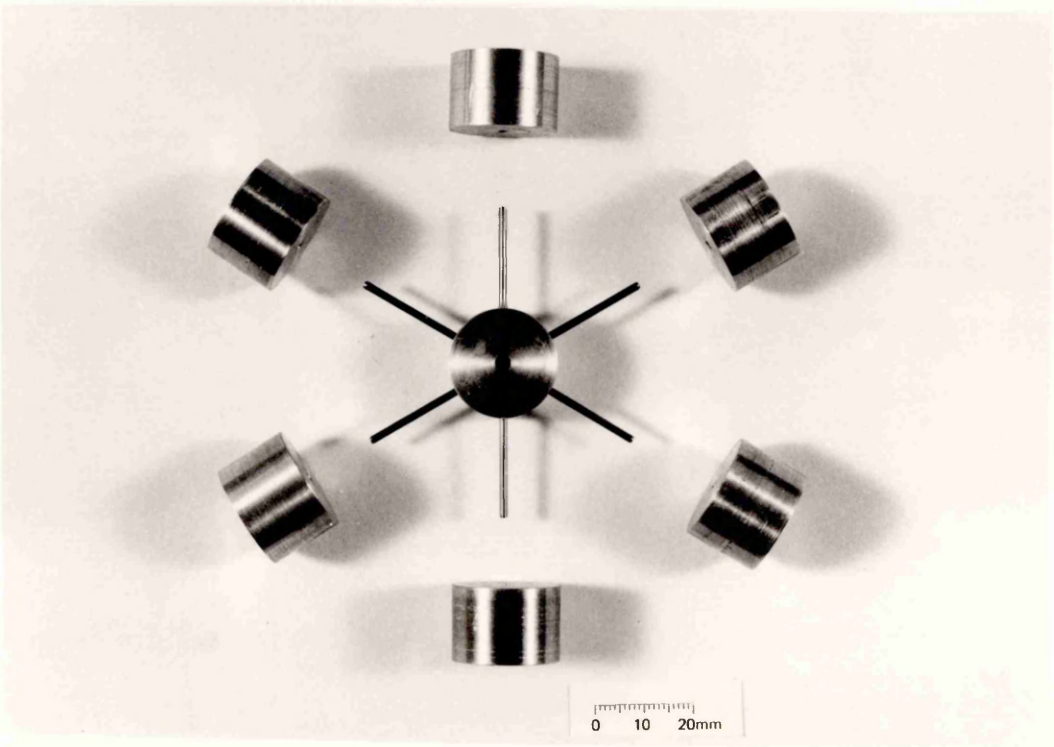

Plate (5.2) Position for connection of components

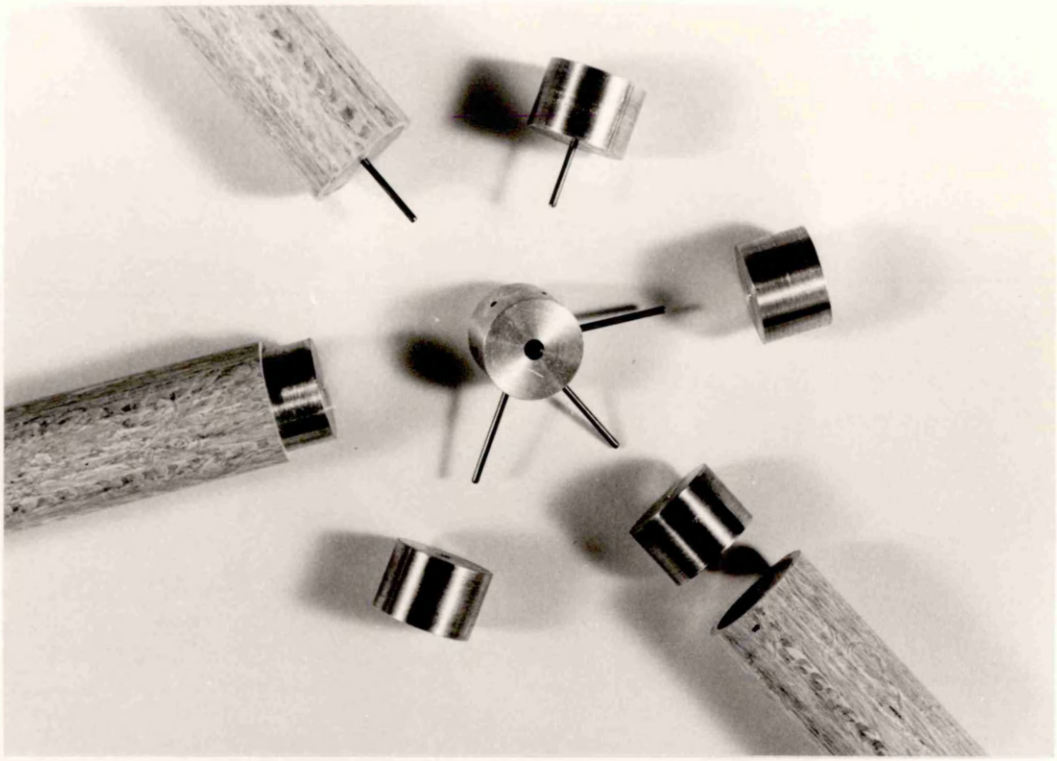

Plate (5.3) First members connected

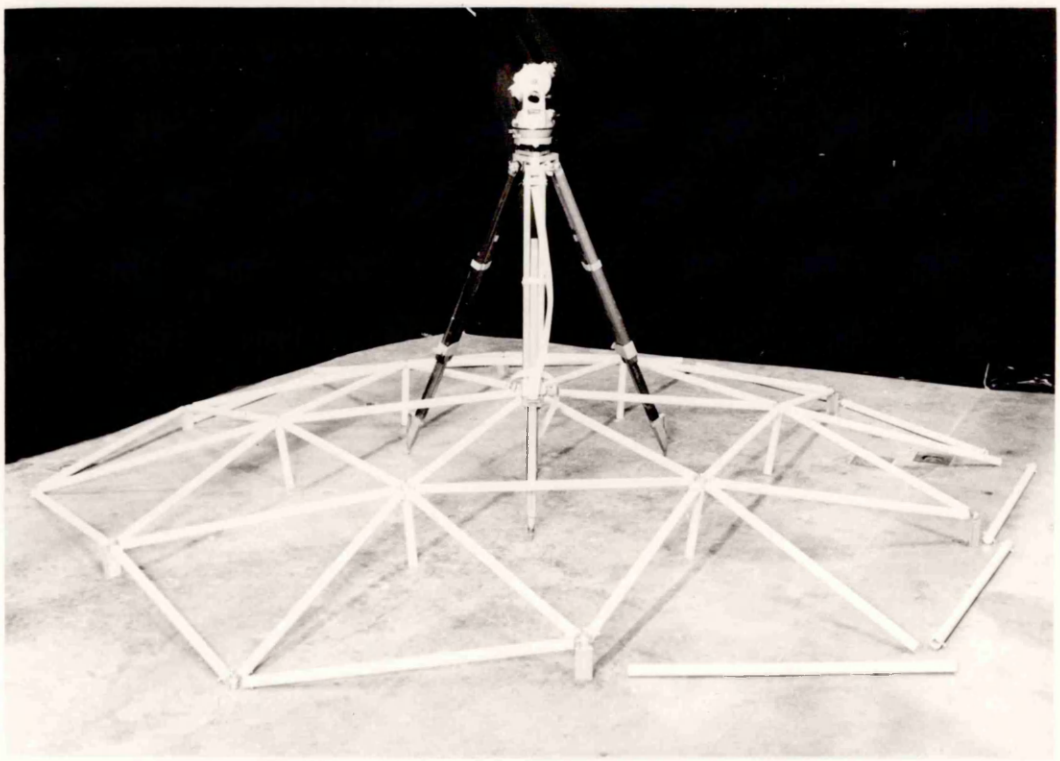

Plate (5.4) Assembly of the dome

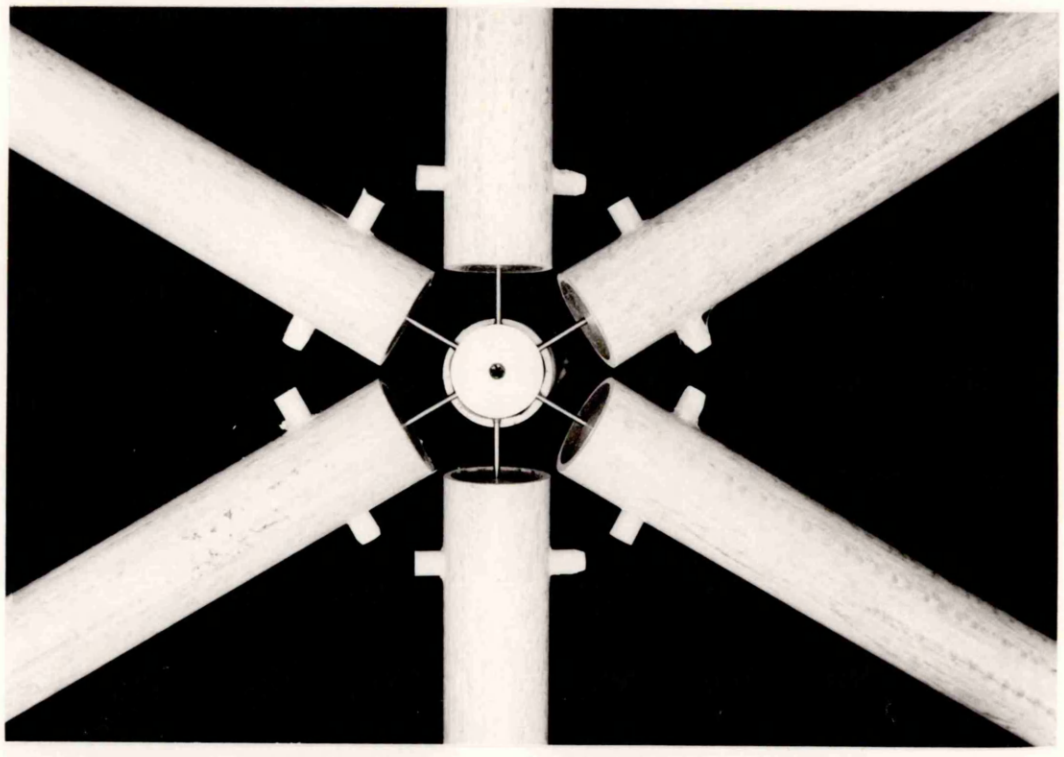

Plate (5.5) Completed temporary node

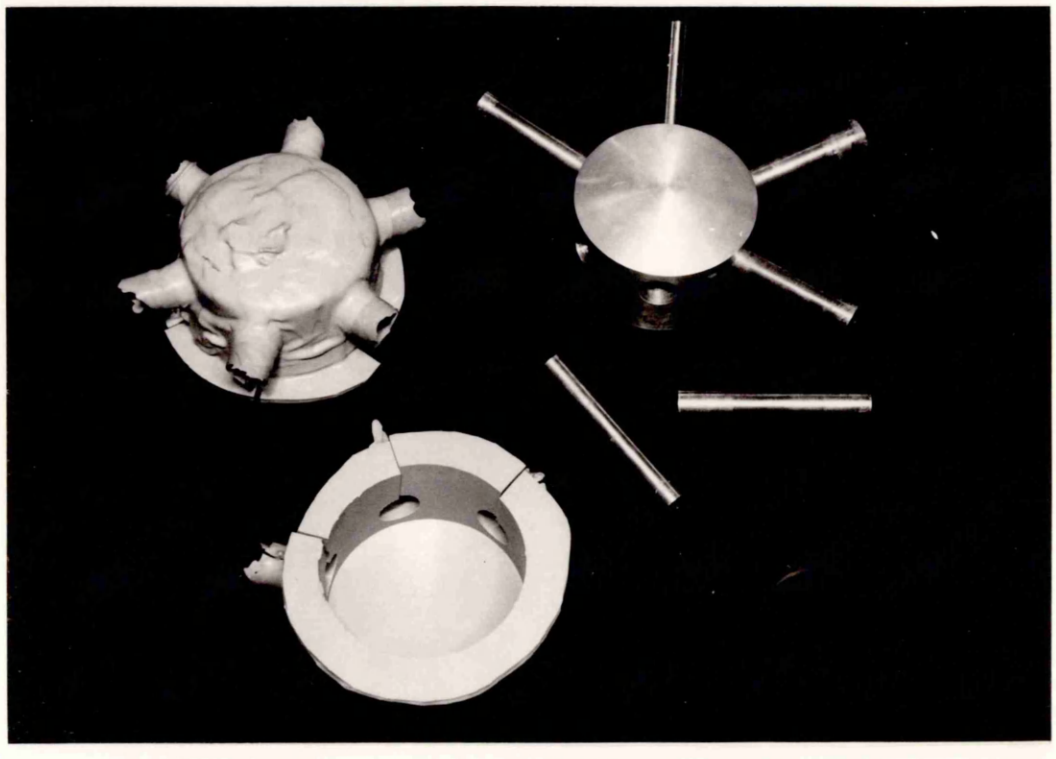

Plate (5.6) The aluminium die and the silicon rubber mould

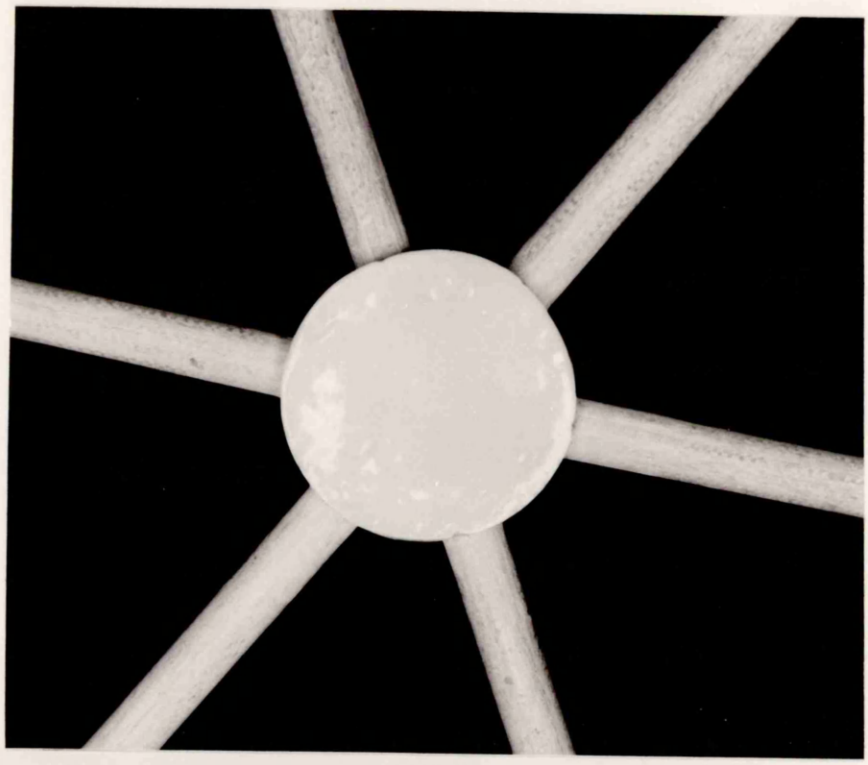

Plate (5.7) Completed glass reinforced epoxy node

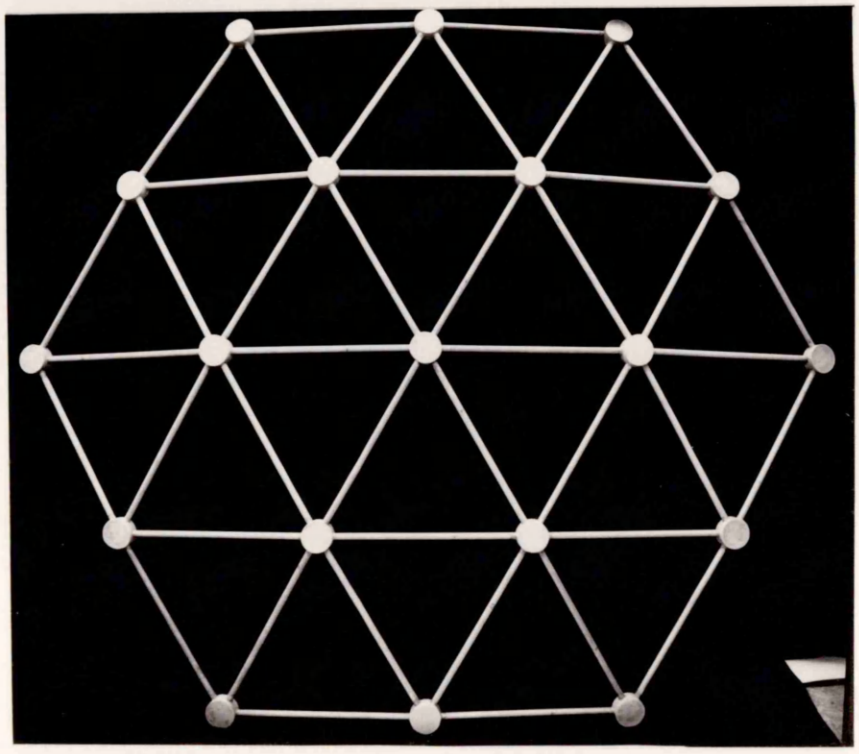

Plate (5.8) The completed dome

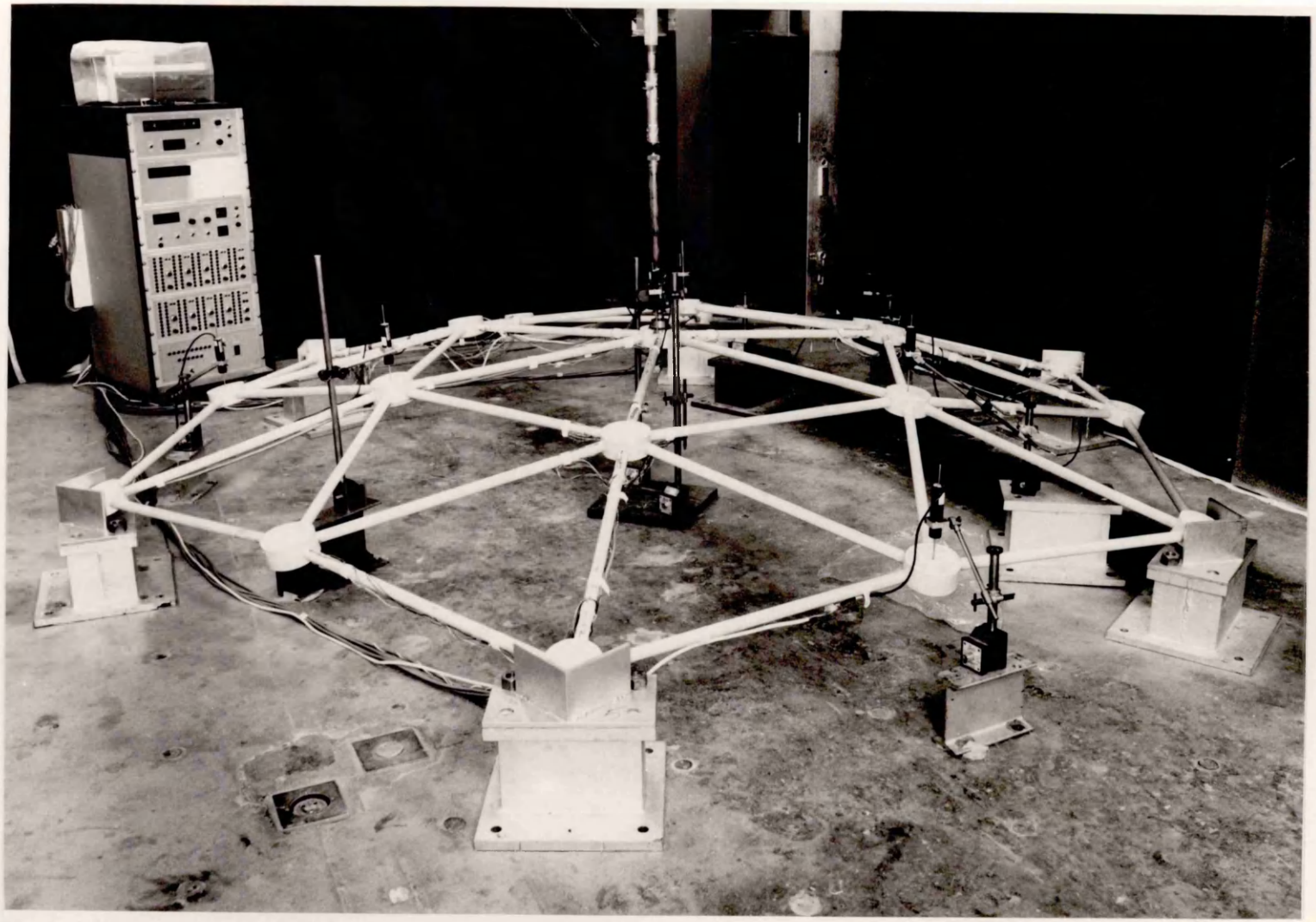

Plate (5.9) The dome test arrangement

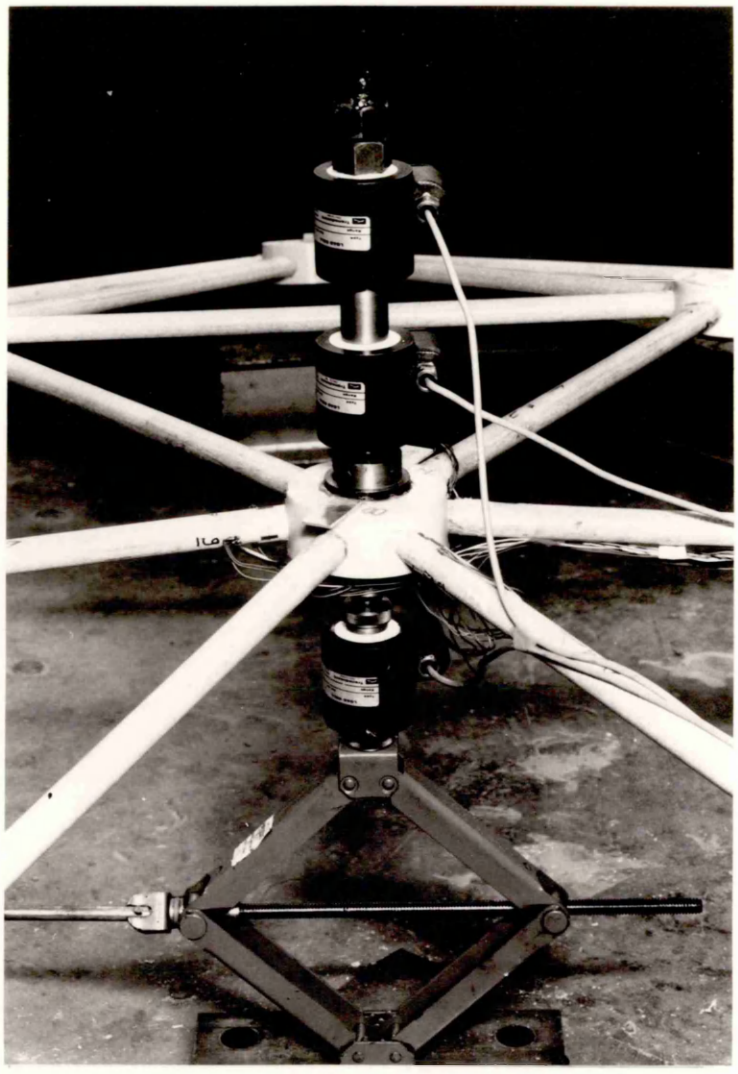

Plate (5.10) The displacement controlled testing arrangement

CHAPTER SIX

CONCLUSIONS AND RECOMMENDATIONS

In conclusion only a general observation on the research project will be made. Specific observations dealing with the theoretical and experimental analysis of single members and skeletal structural assemblies are given at the end of each chapter dealing with particular fundamental points. Of specific interest was the study of structural assemblies from both an experimental and analytical viewpoint; the theoretical analysis included the development of a nonlinear analysis computer program suitable for low modulus linear materials. By using this program it was possible to perform parameter investigations. The following points represent the concluding remarks concerning the structural assemblies:

i) METHOD OF ANALYSIS

The nonlinear analysis technique derived from the fundamental energy principles and the computer implementation proved to be a feasible method to predict the behaviour of both the stiff type and the flexible type of the f.r.p. skeletal structural systems with good accuracy; the excellent agreement between the results of the computer analysis and those obtained experimentally for all the models verified this conclusion. However, it was found that the stiff type of structure can be analysed by means of the simple linear method, if the applied load does not exceed the first buckling load, whilst for the flexible type, the linear method can only be used if low external loads are applied to the structure. If the structure is of the shallow type the linear method of analysis must not be used.

ii) THE STRUCTURAL PERFORMANCE

The stiff type double-layer structures in f.r.p. showed better behaviour than the flexible type with respect to the load carrying capacity and deflections. This is because the pultruded

f.r.p. members have their main reinforcement oriented in the longitudinal direction and, therefore, are more suited to skeletal structures in which the internal forces are mainly axial ones.

The single-layer flexible type structures must be used for either the smaller span systems or in composite constructions of single and double-layer structures.

iii) DEFORMATION AND RECOVERY

The g.r.p. members which were tested as single elements and as components of structures, of varying degrees of stiffness under a small number of loading cycles, showed complete recovery after buckling or bending deformation. The amount of elastic deformation which occured in buckled members was relatively small in the stiff structures compared to that in the flexible ones. In the latter structures large member deformations occured; however, these were caused by bending action (no member buckling was involved).

The deflections of the stiff structures were not particularly large, and considerable reduction can be achieved by replacing the highly loaded members with the stiffer hybrid ones.

iv) MODE OF STRUCTURAL FAILURE

The failure of all types of structures tested (stiff and flexible) was abrupt and highly stressed members failed in a brittle manner, as did the single members.

v) EFFECT OF IMPERFECTIONS

No attempt was made to study fully the effect of various imperfections on the performance of the f.r.p. space structures. However, in the case of the stiff structures, imperfections in the form of initially curved members, were introduced to deteriorate the bifurcation points behaviour to limit points. The larger the imperfections the larger the degree of nonlinearity and the lower the ultimate load became.

The effectiveness of the constraints of the flexible model focussed the attention on the importance of the equivalence of the theoretical model and the real existing conditions of the structure.

vi) IMPROVEMENT OF THE STRUCTURAL PERFORMANCE

The combination of the g.r.p. and the c.g.r.p. members proved to be a very efficient and an economical approach to improve the structural performance of the double-layer grids. The improvement included the stiffening of the structure and the increase of the critical load.

vii) RECOMMENDATION FOR EXTENSION

The nonlinear analysis program proved to be very useful for this research; however, few modifications which could not be implemented because of the time factor but which would improve its efficiency and utility considerably are:

a) The introduction of substructuring, where each discretized member is considered as a substructure, could save on computing time.

b) A criteria for failure incorporated in the computer program, in addition to the existing criteria of maximum number of load increments, would be useful in case of failure occuring before the completion of the maximum number of load increments specified.

c) The addition of a plate bending element within the framework of the computer program would increase its utility.

The next logical extension to this research work is to study the long term behaviour, the fatigue characteristics of these structures and the effect of impact loading.

A study on the effect of imperfections on the behaviour of these structures would be useful to determine the critical imperfections and draw the attention of designers to them.

Another area of research would be the investigation of the skeletal continuum systems. The study of these systems up to first buckling was undertaken in the past. However, the study of the post-buckling behaviour and the problems associated with it can follow the same line of work undertaken in this investigation.

REFERENCES

1) Green, A.K., and Phillips, L.N., "Crimp-bonded end fitting for use of pultruded composite sections", Composites, Vol.13, No.3 (July 1982), pp.219-224.

2) Collings, D.A., and Steinlein, F.R., "The design of composite compression tubes", AIAA Paper No.70-898, (1970).

3) Baker, A.A., Ellis, R., and Hutchison, M.M., "Construction of an experimental carbon fibre reinforced plastic bipod leg for an 81mm Mortar Unit", Aeronautical Defence Scientific Service (October 1974).

4) Fager, F.A., "Application of graphite composites to future spacecraft antennas", Proc. AIAA/CASI 6th Communication satellite systems conference, Montreal, Canada, (April 1976), Paper 76-238, pp.21-33.

5) Hollaway, L. and Ishakian, V.G., "Analysis of a pultruded carbon fibre/epoxy skeletal structure", I.Mech.E. Conf. Publications, (September 1977), Paper C 235-77, pp.63-66.

6) Preedy, J.E., "Composite structures", Engineering (April 1981), pp.314-318.

7) Morrison, A., "Structural plastics for the 80's", Civil Engineering, ASCE, Vol.8, (August 1981), pp.58-61.

8) Oplinger, D.W., Plumer, J. and Ghandi, K.R., "Design, fabrication and testing of a pultruded framework for tent applications", 28th National SAMPLE symposium, Anaheim, California, (April 1983), pp.1478-1491.

9) Makowski, Z.S., "Symbiosis of the architecture and engineering in the development of structural uses of plastics", Proc. ICP/RILEM/IBK, International symposium, Prague, (June 1981), pp.59-72.

10) Einsfeld, U., "Experiences about the application of GRP - structural members", Proc. ICP/RILEM/IBK, International sympsium, Prague, (June 1981), pp.167-170.

11) Pickett, A.K., "Stress analysis of adhesive bonded lap joints", Ph.D. Thesis, University of Surrey, (1983).

12) Tennyson, R.C., "Buckling of laminated composite cylinders: a review", Composites, (January 1975), pp.17-24.

13) Norris, F.D. and Rosen, B.W., "Structural efficiency of orthotropic cylindrical shells subjected to axial compression", AIAA Journal, Vol.4, No.3, (March 1966), pp.481-485.

14) Timoshenko, S.P. and Gere, J.M., "Theory of elastic stability", McGraw Hill Book Co. Ltd., New York, N.Y. (1961).

15) Zienkiewicz, O.C. and Cheung, Y.K. "Finite element method in structural and continuum mechanics", McGraw Hill, (1967).

16) Brebbia, C.A., "Finite element systems - A handbook", A computational Mechanics Centre publication, Springer-Verlag, 2nd Ed., (1982).

17) Thompson, J.M.T., "Basic principles in the general theory of elastic stability", J. Mech. Phys. Solids, Vol.11, (1963), pp.13-20.

18) Sewell, M.J., "A method of post-buckling analysis", J. Mech. Phys. Solids, Vol.17, (1969), pp.219-233.

19) Martin, H.C., "Finite element and the analysis of geometrically nonlinear problems", U.S. - Japan seminar on matrix methods in structural analysis and design, Tokyo, Alabama University Press, (1970).

20) Stricklin, J.A., Heisler, W.E. and Von Reisemann, W.A., "Evaluation of solution procedures for material and/or geometrically nonlinear structural analysis", AIAA Journal, Vol.11, No.3, (March 1973), pp.292-299.

21) Turner, M.J., Dill, E.H., Martin, H.C. and Melosh, R.J., "Large deflections of structures subjected to heating and external load", J. Aerospace Sci., Vol.27, No.2, (1960), pp.97-106.

22) Renton, J.D., "Stability of space frames by computer analysis", Journal of the structural division, ASCE, Vol.88, No.ST4, (August 1962), pp.81-103.

23) Livesley, R.K. and Chandler, D.B., "Stability functions for structural frameworks", Manchester University Press, (1965).

24) Gallagher, R.H. and Padlog, J., "Discrete element approach to structural instability analysis", AIAA Journal, Vol.1, No.6, (June 1963), pp.1437-1439.

25) Saafan, S.A., "Nonlinear behaviour of structural plane frames, "Journal of the structural division, ASCE, Vol.89, No.ST4, (August 1963), pp.557-579.

26) Argyris, J.H., "Recent advances in matrix methods of structural analysis", Progress in aeronauticasl sciences, Vol.4, MacMillan, (1975), New York.

27) Martin, H.C., "On derivation of stiffness matrices for the analysis of large deflection and stability problems", Proceedings, Conference on matrix methods in structural mechanics, Wright Patterson Base, Ohio, (October 1965), pp.697-716.

28) Oden, J.T., "Calculation of geometric stiffness matrices for complex structures", AIAA Journal, Vol.4, No.8, (August 1966), pp.1480-1481.

29) Mallett, R.H. and Berke, L., "Automated method for the large deflection and instability of three dimensional truss and frame assemblies", Technical report AFFDL-TR-66-102, Air Force Flight Dynamics laboratory, Research and technology division, Air Force systems commands, Wright Patterson Air Force Base, Ohio, (December 1966).

30) Mallett, R.H. and Schmit, Jr. L.A., "Nonlinear structural analysis by energy search, " Journal of the structural division, ASCE, Vol.93, No.ST3, (June 1967), pp.221-133.

31) Oden, J.T., "Numerical formulation of nonlinear elasticity problems, "Journal of the structural division, ASCE, Vol.93, No.ST3, (June 1967), pp.235-255.

32) Berke, L. and Mallett, R.H., "Automated large deflection and stability analysis of three dimensional bar structures", Proceedings, International symposium on structures technology for large radio and radar telescope systems, Massachusetts Institute of Technology, (October 1967), pp.381-419.

33) Connor, J.J., Logcher, R.D. and Chan, S., "Nonlinear analysis of elastic framed structures", Journal of the structural division, ASCE, Vol.94, No.ST6, (June 1968), pp.1525-1547).

34) Mallett, R.H. and Marcal, P.V., "Finite element analysis of nonlinear structures", Journal of the structural division, ASCE, Vol.94, No.ST9, (September 1968), pp.2081-2105.

35) Jennings, A., "Frame analysis including change of geometry", Journal of the structural division, ASCE, Vol.94, No.ST3, (March 1968), pp.627-644.

36) Powell, G.H., "Theory of nonlinear elastic structures", Journal of the structural division, ASCE, Vol.95, No.ST12, (December 1969), pp.2687-2701.

37) Hibbitt, H.D., Marcal, P.V. and Rice, J.R., "A finite element formulation for problems of large strain and large displacement", Int. J. Solids and Struts, Vol.6, (1970), pp.1069-1086.

38) Zienkiewicz, O.C. and Nayak, G.C., "A general approach to problems of elasticity and large deformation using isoparametric elements", Proceedings, 3rd conf on matrix methods in structural mechanics, Wright Patterson Air Force Base, (October 1971), pp.881-928.

39) Stricklin, J.A. and Haisler, W.E., "Self-correcting initial value formulations in nonlinear structural mechanics", AIAA Journal, Vol.9, No.10, (October 1971), pp.2066-2067.

40) Stricklin, J.A., Haisler, W.E. and Von Raisemann, W.A., "Geometrically nonlinear structural analysis by direct stiffness method", Journal of the structural division, ASCE, Vol.97, No.ST9, pp.2299-2314.

41) Haisler, W.E. and Stricklin, J.A., "Development and evaluation of solution procedures for geometrically nonlinear structural analysis", AIAA Journal, (March 1972), pp.264-272.

42) The subcommittee on latticed structures, "Bibliography on latticed structures", Journal of the structural division, ASCE, Vol.99, No.ST7, (July 1972), pp.1545-1566.

43) Ebner, A.M. and Ucciferro, J.J., "A theoretical and numerical comparison of elastic nonlinear finite elememnt methods", Computers and structures, Vol.2, (1972), pp.1043-1061.

44) Hollaway, L. and Baker, S., "The development of nodal joints suitable for double-layer skeletal systems made from fibre/matrix composites", To be presented at the 3rd International conference on space structures, University of Surrey, UK (September 1984).

45) Oran, C., "Tangent stiffness in space frames", Journal of the structural division, ASCE, Vol.99, No.ST6, (June 1973), pp.987-1001.

46) Noor, A.K., "Nonlinear analysis of space trusses", Journal of the structural division, ASCE, Vol.100, No.ST3, (March 1974), pp.533-546.

47) Jagannathan, D.S., Epstein, H.I. and Christiano, P., "Nonlinear analysis of reticulated space trusses", Journal of the structural division, ASCE, Vol.101, No.ST12, (December 1975), pp.2641-2658.

48) Oran, C. and Kassimali, A., "Large deformations of framed structures under static and dynamic loads", Computers and Structures, Vol.6, (1976), pp.539-547.

49) Wood, R.D. and Zienkiewicz, O.C., "Geometrically nonlinear finite element analysis of beams, frames, arches and axisymmetric shells", Computers and Structures, Vol.7, (1977), pp.725-735.

50) Kiciman, O.K. and Popor, E.P., "Post-buckling analysis of cylindrical shells", Journal of the engineering mechanics division, ASME, Vol.104, No.EM4, (August 1978), pp.751-762.

51) Riks, A., "An incremental approach to the solution of snapping and buckling problems", Int. J. Solids Structures, Vol.15, (1979), pp.529-551.

52) Crisfield, M.A., "A fast incremental/iterative solution procedure that handles 'snap-through'", Computers and Structures, Vol.13, (1981), pp.55-62.

53) Mohr, G.A. and Milner, H.R., "Finite element analysis of large displacements in flexural systems", Computers and Structures, Vol.13, (1981), pp.533-536.

54) Papadrakakis, M., "Post-buckling analysis of spatial structures by vector iteration methods", Computers and Structures", Vol.14 (1981), pp.393-402.

55) Brebbia, C.A. and Ferrante, A.J., "Computational methods for the solution of engineering problems", 2nd ed., Pentech press, London, (1979).

56) Coates, R.C., Coutie, M.G. and Kong, F.K., "Structural analysis", 2nd Ed., Nelson, (1980).

57) Felippa, C.A., "Solution of linear equations with skyline-stored symmetric meatrix", Computers and Structures, Vol.15, (1975), pp.55-62.

58) Wilson, E.L. and Dovey, H.H., "Solution or reduction of equilibrium equations for large complex structural systems", Advances in engineering software, Vol.1, No.1, (1978), pp.19-25.

59) Makowski, Z.S., "Review of the development of various types of double-layer grids", course on the analysis, design and construction of double-layer grids, University of Surrey, (1980).

BIBLIOGRAPHY

1. Thompson, J.M.T. and Hunt, G.W., "A general theory of elastic stability", John Wiley & Sons Ltd, London, (1973).

2. Ziegler, H., "Principles of structural stability", MacMillan, London, (1972).

3. Supple, W.J. (Ed), "Structural stability", IPC Science and Technology Press Ltd, Guildford, Surrey, UK, (1973).

4. Le-Wu Lu, A.M., "Stability of frames under primary bending moments", Journal of the structural division, ASCE, Vol.89, No.ST3, (June 1963), pp.35-62.

5. Simitses, G.J. and Kounadis, A.N., "Buckling of imperfect rigid-jointing frames", Journal of the engineering mechanics division, ASCE, Vol.104, No.EM3, (June 1978), pp.569-586.

6. Hollaway, L. and Rustum, A., "Buckling analysis of a shallow dome manufactured from pultruded fibre/matrix composites", to be presented at the 3rd International Conference on Space Structures, University of Surrey, UK (1984).

7. Brebbia, C. and Connor, J., "Geometrically non-linear finite element analysis", Journal of the engineering mechanics division, ASCE, Vol.95, No.EM2, (April 1969), pp.463-483.

8. Zienkiewicz, O.C. and Cheung, Y.K., "Finite element method in structural and continuum mechanics", McGraw-Hill, (1967).

9. Gallagher, R.H., "Finite element analysis, Fundamentals", Prentice-Hall, Inc., Englewood Cliffs, New Jersey, (1975).

10. Faddeeva, V.N., "Computational methods of linear algebra", Dover Publications, Inc, New York, (1959).

11. Gere, J.M. and Weaver, Jr. W., "Analysis of framed structures", D. Van Nostrand Co., Inc., (1965).

12. Brockman, R.A., "Economical stiffness formulations for non-linear finite elements", Computers and structures, Vol.18, (1984), pp.15-22.

13. Mondtar, D.P. and Powell, G.H., "Towards optimal in-core equation solving", Computers and structures, Vol.4, (1974), pp.531-548.

14. Wilson, E.L., Bath, K. and Doherty, W.P., "Direct solution of large systems of linear equations", Computers and structures", Vol.4, (1974), pp.363-372.

15. Hollaway, L. (Ed), "Design and specification of GRP cladding", Manning Rapley Publishing Ltd, Croydon, Surrey, UK, (1978).

16. Hollaway, L., "Glass reinforced plastics in constructions: engineering aspects", Surrey University Press, (1978).

17. Paton, W.L. and Lockhart, A.H., "The structural use of carbon fibre composites", N.E.L. Report No.555, (December 1973).

18. Zweben, C., "Advanced composites for aerospace applications", Composites, (October 1981), pp.235-240.

19. Hollaway, L. and Rustum, A., "Structural charateristics of pultruded glass fibre reinforced polymer double layer skeletal systems", International symposium, Future for plastics in building and in Civil Engineering, Liege, Belgium, (1984).

20. Rustum, A. and Hollaway, L., "The use of fibre/matrix hybrid members in improving the stability of glass reinforced polyester double layer skeletal structure", to be presented at the reinforced plastics congress, Britain, UK, (1984).

21. Hollaway, L. and Rustum, A., "The elastic and post-buckling analysis of Braced Barrel Vaults manufactured from fibre/matrix composite materials", Course on the analysis, design and construction of Braced Barrel Vaults, University of Surrey, (1983).